Development of a novel test setup for the determination of the content and orientation of steel fibres in concrete based on electrical resistivity

Von der Fakultät für Bauingenieurwesen der Rheinisch-Westfälischen Technischen Hochschule Aachen zur Erlangung des akademischen Grades eines Doktors der Ingenieurwissenschaften genehmigte Dissertation

vorgelegt von

Simon Cleven

Berichter: Univ.-Prof. Dr.-Ing. Thomas Matschei

Univ.-Prof. Dr.-Ing. Frank Dehn

Tag der mündlichen Prüfung: 11. Juli 2023

I. Preface

This doctoral thesis is submitted to the RWTH Aachen University for the degree of Dr.-Ing (Doctor of Engineering). The research was conducted at the Institute of Building Materials Research of the RWTH Aachen University (ibac) in Aachen, Germany. The supervisors of the thesis have been Professor Thomas Matschei and Professor Michael Raupach.

The work of the research was started in 2020 and the thesis was submitted in 2022. It consists of an extended summary, the theoretical background, four appended papers (published in international scientific journals) and an overall discussion of the results as well as an outlook.

The author, Simon Cleven, declares that the thesis and the work presented in it are his own and have been generated by him as the result of original research while in candidature for the degree of Dr.-Ing. at RWTH Aachen University. The thesis contains no material previously submitted for a degree at this University or any other institution.

Simon Cleven

II. Acknowledgement

This thesis was written in my time as research assistant at the Institute of Building Materials Research at RWTH Aachen University (ibac). A major part of the thesis was developed and performed without any additional fundings but in agreement with the heads of the institute, Univ.-Prof. Dr.-Ing. Michael Raupach and Univ.-Prof. Dr.-Ing. Thomas Matschei, which also worked as my supervisors. Thus, I would like to express my gratitude to both for their support, the interesting and very helpful discussions, and the opportunity to learn and conduct research at the institute. I am also extremely thankful to Univ.-Prof. Dr.-Ing. Wolfgang Brameshuber for giving me the opportunity to work at the ibac and being able to perform interesting research on my favourite topic steel fibre reinforced concrete (SFRC). Additional thanks go to Prof. Dr.-Ing. Frank Dehn from Karlsruhe Institute of Technology for his advice and critical review of my research and thesis.

In the second step I have to say thanks to all my colleagues at the ibac, especially the ones of my working group “Innovative Concrete Technology” for the great support of my work and team spirit, that was necessary to push me through the phases of writing and gave me the support I needed. Those scientific colleagues are Marcus Hinzen, Christian Neunzig, Joachim Hannawald, Thomas Heiermann, Matthias Kalthoff, Lisa Janissen, Denise Maday and Selina Vaculik. Without a great staff inside the laboratory, that gave me much support in the beginning of my research and has performed every test very accurate and with high effort, even if the test methods didn’t work perfectly sometimes, my work wouldn’t have been possible. Thank you very much Thomas Apweiler, Hans Streb, Frank Engelmann, Wolfgang Föller, Günter Wiwianka and Lars Formanns. But thanks are also due to all other ibac staff members for the great team play and support for every question that came up during my work. Here I have to mention Christian Helm in special, who was an essential support for me in the whole thematic of electrical resistivity and conductivity. Special thanks also to my first reader, Matthias Kalthoff, and my last-minute-reader, Cynthia Morales Cruz, who gave me very helpful input for the fine adjustment of this thesis. Additional thanks also to all my student workers, both research assistants and Bachelor and Master workers Hassan Adewunmi, Kirsten Baumann, Frederic Brassinne, Maike Bröskamp, Andreas Carls, Laura Cremer, Dave Dörfer, Klaudia Drensla, Sophie Escherich, Felix Eyben, Lucas Feldhues, Timo Gansen, Carina Hartig, Max Huwe, Helena Kerkhoff, Lukas Killen, Maira Kryschewski, Marina Licht, Denise Maday, Matthias Post, Helen Weinert and Valbone Gerguri. All of you were a big help for my research work and have contributed significantly to the success of this thesis.

Last but not least such a process as the study and the PhD work are not possible without the support of my family, who always stood behind me. My parents as well as my sisters were always there if I needed advice or just a break from studying. My biggest thanks, however, go to my wife, Julia. You always gave me the necessary motivation for the writing that were essential for the success of this thesis. Without you and the possibility to work on my thesis, while you do all the things for our family, this thesis wouldn’t have been possible. In the future, the family will come first, and I am very much looking forward to having more time for you.

Simon

III. Abstract

Steel fibre reinforced concrete (SFRC) has the potential to be used for versatile applications in a cost-efficient and resource-saving way. One of the biggest obstacles for further application at present is that the fibre content, fibre distribution and fibre orientation cannot be determined exactly. Although the global fibre content can be calculated from total fibre addition in the manufacturing plant, local differences regarding the fibre content within the material arising from formwork geometry or other factors remain difficult to quantify. Moreover, only assumptions can be made regarding the distribution and orientation of fibres. As a consequence, high partial safety factors have to be applied for the static design of structural elements, which prevents an economic use of steel fibre concrete in many cases.

To address this challenge, the main objective of this thesis was the development of an easy-to-use measurement approach that enables the determination of the above-mentioned parameters. Based on an in-depth literature review, the electrical resistivity measurement was identified as a promising approach for the measurement methodology. After identifying the decisive influencing factors from the measurement principle and the material SFRC, a prototype test setup for cubic specimens was developed and tested. Following an extensive parameter study to optimize the measurement system, the setup was extended to include cylindrical specimens, allowing for the examination of drilling cores.

Using a two-electrode setup with an alternating current application in a frequency range of 1 to 10 kHz, the electrical resistance measurements yielded positive outcomes. Lower frequencies led to time-dependent measurement errors, which can be attributed to a polarisation at the electrodes. To analyse the measurement results, it is necessary to convert the measured electrical resistances into geometry-independent electrical resistivities. Geometry factors for specific electrode arrangements can be obtained with help of FEM simulations, coupled to a multiphysics-software. By comparing the electrical resistivities of the SFRC with a plain reference concrete, the steel fibre content can be determined with sufficient accuracy. The estimation of the fibre orientation was possible by the relation of different measuring directions of a sample.

The greatest challenge for the further development of the measurement system was identified with the need for a reference concrete or knowledge of its electrical resistivity. The focus of future investigations must therefore be on the creation of a material parameter-dependent database so that an analysis of structural concretes can be realised. In addition, it is necessary to transfer the prototype measuring system into a system with well-defined coupling and measuring conditions. After the successful development and adaptation of these factors, the measurement methodology may be transferred to a general guideline and/or standard in order to be able to realise new static design principles with lower partial safety factors. This will enable material-efficient design principles for steel fibre reinforced concrete in the future.

IV. Kurzfassung

Stahlfaserbeton weist das Potential auf, kosteneffizient und recourcenschonend für vielseitige Anwendungen eingesetzt zu werden. Eines der größten Hindernisse für die weitere Anwendung besteht zurzeit darin, dass der Fasergehalt, die Faserverteilung und die Faserorientierung nicht exakt bestimmt werden können. Zwar lässt sich der globale Fasergehalt aus der gesamten Faserzugabe im Herstellwerk berechnen, aber lokale Unterschiede im Material, die aus der Schalungsgeometrie oder anderen Faktoren resultieren, sind jedoch nicht messbar. Bezüglich der Verteilung und Orientierung können zudem nur Annahmen getroffen werden. Dies hat zur Folge, dass für die statische Bemessung hohe Teilsicherheitswerte angesetzt werden müssen, was den effizienten Einsatz von Stahlfaserbeton in vielen Fällen nicht ermöglicht.

Um dieser Herausforderung in Zukunft zu begegnen, war das Hauptziel dieser Dissertation die Entwicklung eines einfach zu handhabenden Messverfahrens, was die Bestimmung der oben genannten Parameter ermöglicht. Hierzu erfolgte aufbauend auf einer umfangreichen Literaturrecherche die Auswahl der elektrischen Widerstandsmessung als vielversprechender Ansatz der Messmethodik. Nach der Identifizierung der maßgebenden Einflussfaktoren aus dem Messprinzip und dem Werkstoff Stahlfaserbeton wurde ein prototypischer Messaufbau für würfelförmige Prüfkörper entwickelt und erprobt. Nach der Optimierung des Messsystems durch eine umfangreiche Parameterstudie wurde der Aufbau für zylindrische Proben erweitert, um die Analyse von Bohrkernen zu ermöglichen.

Die Messung der elektrischen Widerstände zeigte gute Resultate bei der Nutzung eines Zwei-Elektroden-Aufbaus mit einer Wechselstrombeaufschlagung in einem Frequenzbereich von 1 bis 10 kHz. Geringere Frequenzen führten zu zeitabhängigen Messfehlern, die auf eine Polarisation an den Elektroden zurückgeführt werden können. Zur Analyse der Messergebnisse ist die Umrechnung der gemessenen elektrischen Widerstände in geometrieunabhängige spezifische Widerstände notwendig. Die hierzu benötigten Geometriefaktoren für definierte Elektrodenanordnungen könnten mit Hilfe einer FEM-Simulation in Kombination mit einer Multiphysik-Software durchgeführt werden. Über den Vergleich der ermittelten spezifischen Widerstände des Stahlfaserbetons mit einem unbewehrten Referenzbeton kann der Stahlfasergehalt ausreichend genau ermittelt werden. Die Abschätzung der Faserorientierung war durch die Relation unterschiedlicher Messrichtung einer Probe möglich.

Als größte Herausforderung für die Weiterentwicklung des Messystems wurde das Erfordernis eines Referenzbetons bzw. die Kenntnis dessen spezifischen Widerstands identifiziert. Der Fokus zukünftiger Untersuchungen muss daher auf der Erstellung einer materialparameter-abhängigen Datenbank liegen, damit eine Analyse von Bauwerksbetonen realisiert werden kann. Zudem ist die Überführung des prototypischen Messsystems in ein System mit definierten Ankopplungsbedingungen und Messbedingungen notwendig. Nach der erfolgreichen Entwicklung und Adaptierung dieser Faktoren kann die Messmethodik in eine allgemeine Richtlinie oder Norm überführt werden, um neue statische Bemessungsprinzipien mit geringeren Teilsicherheitsbeiwerten realisieren zu können. Dies wird in Zukunft eine Material-effizientere Bemessung ermöglichen.

V. Table of Contents

VI. List of Papers

The thesis contains four published papers, which are listed below and presented in sections 4 to 6.

1.) Cleven S, Raupach M, Matschei T. Electrical Resistivity of Steel Fibre-Reinforced Concrete - Influencing Parameters. Materials. 2021; 14(12):3408 https://doi.org/10.3390/ma14123408

2.) Cleven S, Raupach M, Matschei T. Electrical resistivity measurements to determine the steel fiber content of concrete. Structural Concrete. 2022; 23(3):1704-1717 https://doi.org/10.1002/suco.202100832

3.) Cleven S, Raupach M, Matschei T. A New Method to Determine the Steel Fibre Content of Existing Structures — Test Setup and Numerical Simulation. Applied Sciences. 2022; 12(2):561 https://doi.org/10.3390/app12020561

4.) Cleven S, Raupach M, Matschei T. A New Method to Determine the Steel Fibre Content of Existing Structures—Evaluation and Validation. Applied Sciences. 2022; 12(1):454 https://doi.org/10.3390/app12010454

Further relevant Publications by the author

5.) Brameshuber W, Cleven S, Uebachs S, Kerkhoff H. Stahlfaserbeton für Tübbings: Eine Alternative zur Stahlbewehrung? BFT international. 2015; 81(2):188-189

6.) Cleven S, Raupach M, Gerguri V. Prüfmethoden zur Beurteilung der Leistungsfähigkeit von Stahlfaserbeton - Beurteilung der gängigen Verfahren und vergleichende Untersuchungen. Beton, Verlag Bau + Technik GmbH, Erkrath. 2018; 68(6):220-224

7.) Cleven S, Janissen L, Raupach M. Prüfmethoden zur Beurteilung der Leistungsfähigkeit von Stahlfaserbeton - Beurteilung der gängigen Verfahren und vergleichende Untersuchungen. FSKB: Am Puls der Betontechnologie – aktuelle Erkenntnisse, 2019:3:1-26

8.) Wolf S, Cleven S, Vlasak O. Early age shrinkage crack distribution in concrete plates reinforced with different steel fibre types. Fibre reinforced concrete: improvements and innovations: RILEM-fib International Symposium on FRC (BEFIB). Serna P, Llano-Torre A, Navarro-Gregori J. 2020; 24-34 https://doi.org/10.1007/978-3-030-58482-5_3

9.) Hunger M, Bokern J, Cleven S, Vrijdaghs R. Creep in FRC: from material properties to composite behavior. Fibre reinforced concrete: improvements and innovations: RILEM-fib International Symposium on FRC (BEFIB). Serna P, Llano-Torre A, Navarro-Gregori J. 2020; 402-413 https://doi.org/10.1007/978-3-030-58482-5_37

VII. List of Tables

VIII. List of Figures

1 Introduction

1.1 Motivation

Concrete can be described as easy to use and free mouldable material for many applications. With an annual production of more than 32 billion tons it is the most used building material in the world (de Brito & Saikia, 2013). In combination with short fibre reinforcement, commonly by use of steel fibres, a ductile composite material can be created, which is able to resist compressive as well as tensile stresses (Di Prisco et al., 2009, Ding et al., 2019, Ferdosian & Camões, 2021, Kachouh et al., 2019, Lehner et al., 2020, Shan & Zhang, 2014). In order to use the material, some limitations still apply due to the inhomogeneity and possible anisotropy of the material itself as well as the handling process. In ordinary steel reinforced concrete (SRC) the reinforcement is placed before the casting process of the concrete and thus can be monitored by structural engineers. In contrast to SRC, the local fibre content and orientation of fibres in steel fibre reinforced concrete (SFRC) are hard to determine and only the total added fibre content can be assessed easily. For this reason, the monitoring mechanisms for SFRC are more complicated than for SRC and larger safety factors must be applied for static calculations (Cugat et al., 2020, Herrmann et al., 2019, Molins et al., 2009, Tarawneh et al., 2021).

The objective of this thesis is the development of an easy-to-use test to determine the steel fibre content as well as the fibre orientation of SFRC. This test should be applicable in a non-destructive way. It is based on electrical conductivity and an adjusted prediction model to analyse freshly casted SFRC structures as well as precast elements and existing structures in case of rehabilitation processes. This way, it presents a good alternative to common alternative testing approach e.g., analysing drilling cores via crushing or specialised, expensive CT-scanning tests. In order to achieve meaningful results a wide range of concrete compositions has been investigated in the course of this study. The proposed test setup covers laboratory and field applications and is inexpensive to install.

1.2 Structure of this Thesis

The thesis is structured in seven sections. After the introduction, the second section summarises the state of the art concerning the impact of fibre content and orientation on the performance of SFRC. In addition, relations to the mechanical behaviour of SFRC are derived. Different known test-setups for the determination of those parameters are presented and discussed.

A schematic summarising of the experimental investigations is presented in Figure 1.1. In total 4 scientific papers, presented by sections 3 to 6 and supplementary investigations were prepared and serve as base for the development of a test procedure for SFRC.

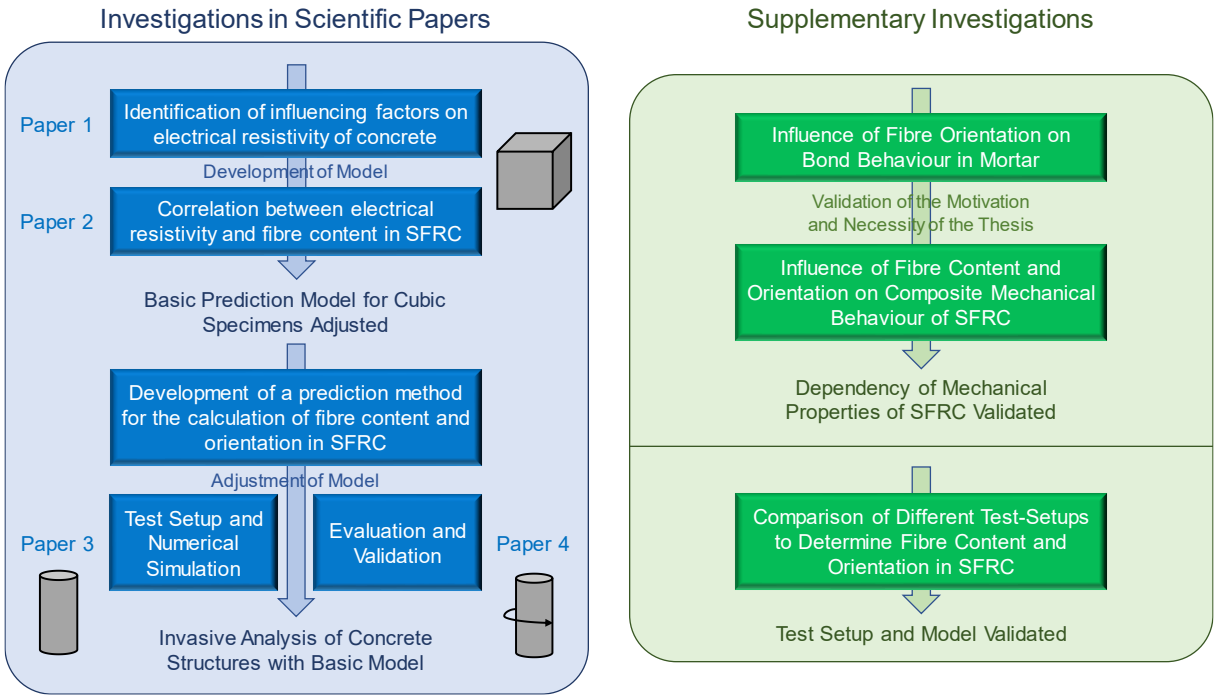

Figure 1.1 Structure of the investigations inside this thesis

Paper 1 (section 3) identifies relevant test parameters and assesses the influence of the concrete composition on the electrical resistivity of SFRC. For this purpose, various SFRC compositions have been evaluated by variation of single parameters, like w/c ratio, cement content, use of ground granulated blast-furnace slag, and fineness of cement. The tests were performed with a simple and easy-to-use test setup on cubic concrete specimens, to achieve reproducible results.

Paper 2 (section 4) deals with an in-depth evaluation of the electrical resistivity to identify a prediction method for the fibre content based on electrical resistivity measurements. The prediction method was deduced by the analysis of six series of cubic specimens, produced with the same concrete composition and varying fibre content. Additional factors like the amplitude of the alternating current, the frequency, and the age of the specimens were considered.

In **papers 3 and 4** (sections 5 and 6) the prediction method has been compared to a literature model and was further optimized for different geometries like cylindrical specimens (paper 3) and drilling cores (paper 4). Therefore, a FEM-model of the current flow in different directions has been set up and further optimized. This enables the calculation of the electrical resistivity of concrete in more complex geometries by use of the adopted easy-to-use test setup. It has been shown, that with the model a statistically satisfying estimation of the fibre content and the orientation of concrete structures is possible with some limitations.

Section 7 summarises and discusses the main results of the four papers to identify open questions concerning necessary supplementary investigations. Subsequently some overall conclusions were derived and an outlook towards further research needs is given.

All investigations were performed using the same steel fibres. Based on the applied use cases the range of fibres will vary throughout the thesis. In most of the investigations an ordinary steel macrofibre with a length of 60 mm was used. Additionally, in paper 1 (section 3), shorter micro- and macrofibres with a length of 8 mm and 35 mm, respectively, were used.

Similar to the fibres, also the concrete compositions differ in agreement with the focus of the investigations. Concretes with only ordinary Portland Cements with strength classes of 32.5 R, 42.5 R and 52.5 R, all from the same cement plant, were used in combination with different water/cement ratios and partially combined with supplementary cementitious materials and hence different mechanical properties were produced.

2 Theoretical Background

2.1 Electrical Resistivity

2.1.1 General

While electrical resistance measurement methods are widely used in electrical engineering, there is still a need to establish those in the field of cementitious materials (Bürchler, 1996, Reichling et al., 2014). For construction materials, the reliable determination of the electrical resistance is often difficult in practice, as it is influenced by numerous parameters. In the case of reinforced concrete, the electrical properties have therefore been increasingly researched, especially in the field of structural diagnostics during the last decades (Reichling et al., 2014). In the following section state-of-the art concerning the electrochemical methods for civil engineering applications are explained. Furthermore, influencing parameters and test setups related to SFRC are elaborated.

2.1.2 Electrical Resistivity

In a conductor, free electrons form the electric current. The movement of the electrons is restricted by heat movements of the atoms in the crystal lattice (Fischer, 2019). This relationship is called electrical resistance. Under the assumption of the arrangement of a conductive medium between two electrodes, the electrical voltage can be calculated by (eq. *2-1*).

$$U = \int_{P+}^{P-} E * ds = \int_{P+}^{P-} \frac{J}{\sigma} * ds \qquad \text{(eq. 2-1)}$$

with:

E	Electrical field strength in V/m
J	Current density in A/m²
σ	Electrical resistivity in S/m

The boundaries of the integral are formed by any two points on one of the two electrodes. The course of the current lines originates in the positive electrode and ends in the negative one. From this it can be concluded that the electric current I, that is flowing from an enveloping surface A around the two electrodes, must be the opposite direction but equal in value. This fact is shown in (eq. *2-2*).

$$I = \pm \oiint_A J * dA \qquad \text{(eq. 2-2)}$$

Since the current density changes only in terms of magnitude at different voltages, the direct proportionality between U and I can be derived for a fixed electrode geometry. The proportionality constant is commonly referred to as the electrical resistance R with the unit Ω (Leone, 2018). This relationship was already investigated in 1827 by the physicist Georg Simon Ohm (Harriehausen & Schwarzenau, 2020). Accordingly, (eq. *2-3*) is called Ohm's law.

$$R = \frac{U}{I} \qquad \text{(eq. 2-3)}$$

The reciprocal value is known as the conductance G with the unit Siemens (S = 1/Ω). In addition to the electrical resistance, the electrical resistivity ρ, which is a geometry-independent

parameter, has proven helpful. The calculation of the electrical resistivity can be described by (eq. *2-4*).

$$\rho = k * R \qquad \text{(eq. 2-4)}$$

The variable k represents a geometry factor that differs depending on the geometry of the electrodes as well as on the test setup (Layssi et al., 2015). The electrical conductivity σ, which was already used in (eq. 2-1), in the analogue way represents the reciprocal value of the electrical resistivity (Clausert et al., 2014).

The electrical conductivity of a material can be classified into conductors of 1st and 2nd order regarding the electrical charge transport. While the transport of conductors of 1st order is based on electron transport, for example in a metal lattice, the electrolyte conductivity is the decisive factor for conductors of the 2nd order. Here, dissolved ions are transported in a fluid. The special factor of the composite material fibre reinforced concrete is that the combination of concrete and metal fibre covers both conditions. The capillary-porous material concrete belongs to conductors of 2nd order and the metal fibres to conductors of 1st order (Reichling, 2014).

2.1.3 Impedance

Examining the electrical resistance of concrete allows conclusions about its condition. However, Ohm's law, which is the basis for the above explanations, only applies to ideal electrical resistances. Thus, the considerations are always independent of frequency (Reichling, 2014). If an alternating current is considered, the equations for the voltage and the current must be adapted. In this case, the amplitude, the angular frequency, and the phase angle must be considered. A sinusoidal alternating voltage with the frequency $\omega = 2\pi f$ results in a likewise sinusoidal current (see (eq. *2-5*) and (eq. 2-6)) (Funke, 2002).

$$U(t) = U_0 * sin(\omega t + \phi_U) \qquad \text{(eq. 2-5)}$$

$$I(t) = I_0 * sin(\omega t + \phi_I) \qquad \text{(eq. 2-6)}$$

with:

U_0, I_0 Amplitude of voltage respectively current in V, A
ϕ_U, ϕ_I Phase angle in rad

Analogous to Ohm's law, an electrical resistance, the so-called impedance, can be defined, which now is dependent on the frequency (eq. *2-7*).

$$Z(\omega) = \frac{U(t)}{I(t)} \qquad \text{(eq. 2-7)}$$

To reduce the computational effort with this parameter, it has proven helpful to represent it in the complex notation. Through mathematical transformations, the amount of the impedance can be calculated by (eq. *2-8*).

$$Z = \frac{U_0 * e^{i(\omega t + \phi_U)}}{I_0 * e^{i(\omega t + \phi_I)}} = \frac{U_0 * e^{i \cdot \phi_U}}{I_0 * e^{i \cdot \phi_I}} = \frac{U_0}{I_0} * e^{i(\phi_U - \phi_I)} = |Z| * e^{i \cdot \phi} \qquad \text{(eq. 2-8)}$$

In a further step, Euler's formula $e^{i \cdot \varphi} = \cos(\varphi) + i * \sin(\varphi)$ can be applied to (eq. *2-8*), which enables a representation of the impedance as a pointer in the Gaussian plane. The axes are formed by the real and imaginary parts of the impedance (Thannberger, 2002).

$$\underline{Z} = cos(\phi) + i * sin(\phi) = Re(\underline{Z}) + i * Im(\underline{Z}) \quad \text{(eq. 2-9)}$$

$$\Rightarrow \quad |Z| = \sqrt{\left(Re(\underline{Z})\right)^2 + \left(Im(\underline{Z})\right)^2} \quad \text{(eq. 2-10)}$$

$$\Rightarrow \quad \phi = arctan\left(\frac{Re(\underline{Z})}{Im(\underline{Z})}\right) \quad \text{(eq. 2-11)}$$

The amount of the impedance |Z| is called apparent impedance (eq. *2-10*), which can be represented under the phase angle ϕ (eq. *2-11*). The real axis of the complex representation is called active resistance and the imaginary part reactive resistance or reactance (Harriehausen & Schwarzenau, 2020). Figure 2.1 shows these relationships graphically.

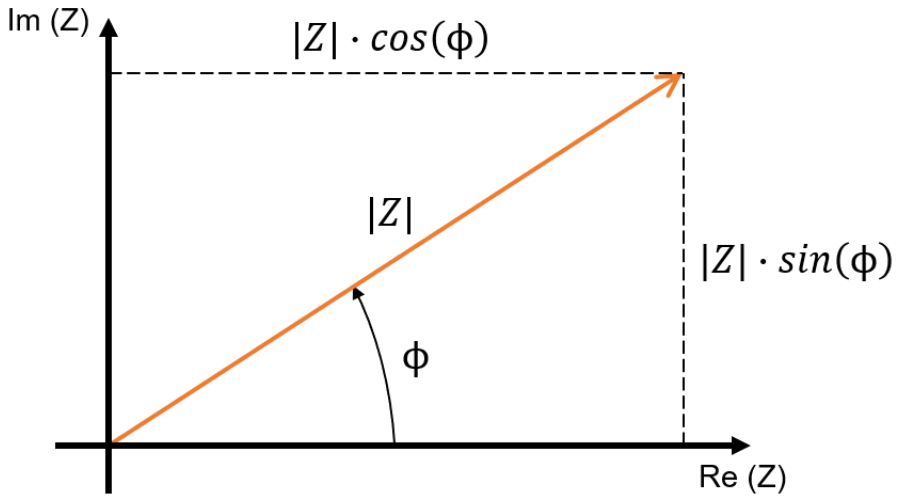

Figure 2.1 Impedance in Gaussian plane (Thannberger, 2002)

The measurement and evaluation of the impedance is called impedance spectroscopy. By applying an alternating current of different frequencies to a substance, it is possible to obtain information about the condition of a substance. The evaluation is usually done in the Nyquist plot, which is based on the pointer diagram mentioned above. The frequency spectrum of a measurement can range from 0.01 Hz to 100 kHz (Heins, 2015, Hoffmann-Walbeck, 2017, Layssi et al., 2015). The procedure as well as the evaluation and interpretation of impedance spectroscopy are explained in more detail in section 2.3.1.7.

2.2 Steel Fibre Reinforced Concrete

2.2.1 Mechanical Properties and Applications

Compared to other building materials, the advantage of concrete is its ability to withstand compression. In contrast, the tensile strength is lacking, which leads to brittle failure of the matrix under load. To prevent concrete from cracking when its ultimate load-bearing capacity is exceeded, fibres are added in the case of fibre reinforced concrete (Müller, 2014). The principle of the crack-bridging effect of fibres is shown in Figure 2.2.

In addition to the avoidance and retardation of macro-cracks, the use of SFRC is associated with further objectives. On the one hand, an improvement of the post-fracture behaviour, accompanied by an increase in ductility and durability, is to be aimed for, on the other hand, an optimisation of the fire resistance (Holschemacher et al., 2006). Influencing parameters for

the composite material behaviour are, in addition to the concrete tensile strength, the bond between fibre and matrix, the fibre geometry, strength, ductility, content, and orientation (Müller, 2014).

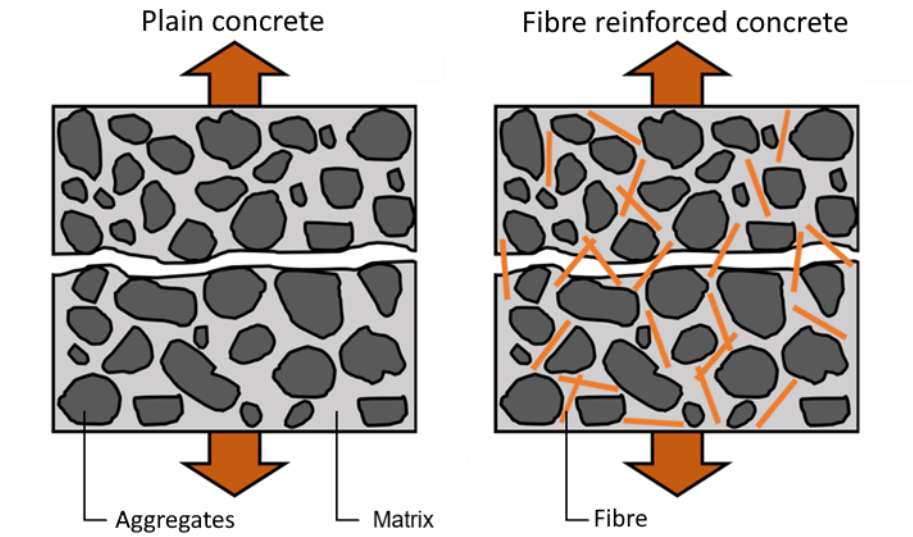

Figure 2.2 Effect of fibre reinforcement in concrete (Holschemacher et al., 2006)

With increasing crack width, fibres must absorb greater tensile forces. In the cracked state, only the fibres must bear these forces. Due to this fact, the decisive failure modes for steel fibre reinforced concrete are the pulling out of the fibre from the matrix or the fracture of the fibre itself (Holschemacher et al., 2006).

The load-bearing capacity of the composite material mainly depends on the bond between fibre and matrix. The interaction of the two components is comparable to conventional construction with reinforcing steel. The higher the bond, the greater the pull-out resistance of the fibre. The composite behaviour can be assigned to a total of three different mechanisms: Adhesion, friction, and form bond (Müller, 2014).

In the case of chemical adhesion, an elastic bond prevails over the entire embedment depth during the so-called fibre activation phase (Leutbecher, 2007). Fibre and concrete form a cohesive body in this phase, which under load is deformed together (Müller, 2014). When the adhesive bond strength is exceeded, the fibre slowly begins to detach from the matrix. In this intermediate phase, the adhesive and frictional bonds are present at the same time (Jungwirth, 2006). The transition between fibre activation and fibre pull-out is called "fibre effectiveness". At the same time, this is the point where the maximum stress between fibre and matrix is transferred (Leutbecher, 2007).

After reaching the highest stress, the fibre gradually detaches relative to the matrix (Müller, 2014). The bond strength at the moment of fibre pull-out is based only on friction in the contact zone and depends on the roughness strength. With increasing fibre extraction, the friction decreases steadily due to the lower bonding depth (Leutbecher, 2007).

The relationship between the stress and the existing crack opening is shown in Figure 2.3. The course of the stress, which is almost exclusively absorbed by the matrix at the beginning, initially increases linearly until the initial crack stress $\sigma_{cf,cr}$ is reached. At this point, the maximum tensile strength of the concrete f_{ct} has already been exceeded. Subsequently, the stress decreases slightly. At the moment when the bond between fibre and matrix carries all

the stress, the crack opening begins. As already explained, the maximum stress σ_{cf0} is measurable at the point between fibre activation and fibre pull-out. After reaching this point, the stress drops continuously. When the fibre is half extended, which is the case for an optimum position of the fibre in a crack, the stress absorption tends towards zero. (Leutbecher, 2007)

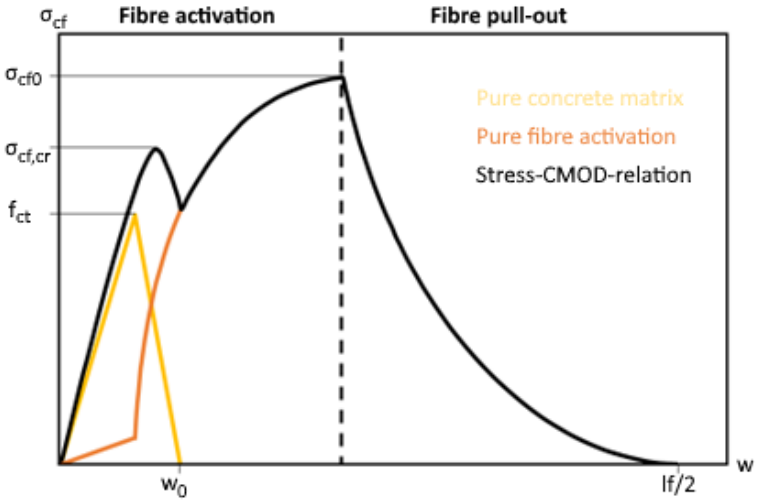

Figure 2.3 Tension-CMOD-curve of fibre reinforced concrete **(**Leutbecher, 2007, Lehmberg, 2018)

2.2.2 Influence of Fibre Content

In general, a variation of the fibre content can positively or negatively influence both the fresh and hardened concrete properties. Regarding the fresh concrete properties, the fibre content affects the consistency, the air content, and the workability of the fresh concrete. The consistency of the plain concrete normally becomes stiffer as a result of the fibre addition and the fresh concrete is therefore more difficult to process or compact (Dahms, 1979). Regarding the fresh concrete consistency, a reduced spread of 10 to 15 cm can be expected, depending on the used fibre content. In practice, SFRC with a very soft consistency and a slump flow of 490 to 550 mm is predominantly used (Breitenbücher, 2012, Müller, 2014, Schulz, 2000a, Schulz, 2000b). The possible maximum fibre content of concrete is largely influenced by the concrete composition. In general, a finer grading curve of the aggregates results in the ability to add more fibres to the concrete. The workability of the fresh concrete behaves anti proportionally to the existing fibre content. At high fibre contents fibre agglomerations can occur. These can impair the strength development of fibre reinforced concrete and already occur depending on the concrete composition and compaction at fibre contents of 1.0 to 1.25 % by vol. For this reason, maximum fibre contents of between 2.0 and 2.5 % by vol. have proven effective in practice for addition to normal concrete by use of suitable SFRC compositions (Müller, 2014). With special methods, such as the so-called SIFCON (slurry infiltrated fibre concrete), higher fibre contents of up to 20 % by vol. can be realised (Müller, 2014, Schulz, 2000a, Schulz, 2000b).

With increasing fibre content, the air content of the concrete also increases, which leads to an increase in the compaction effort. With fibre contents of 3 % by vol. and more, vibro-compaction is therefore no longer sufficient. Above a fibre content of 3.5 % by vol., fibre reinforce concrete is no longer completely compactable (Dahms, 1979, Schulz, 2000a, Schulz, 2000b).

Regarding the influence of the fibre content on the hardened concrete properties, it can be stated that the effectiveness of the steel fibres increases with increasing fibre content. The fibre content therefore has a decisive influence on the deformation behaviour and crack distribution of the concrete, so that SFRC can absorb increasingly higher loads with increasing fibre content in the cracked state. In general, an increase in compressive strength of maximum 20 % and an increase in tensile strength of maximum 50 % can be expected. The elongation at break increases accordingly by a maximum of 30 % (Holschemacher et al., 2006, Müller, 2014, Schulz, 2000a, Schulz, 2000b).

There is a correlation between the fibre content and the transferable tensile stress of the composite. A so-called critical fibre content V_{crit} can be defined according to (eq. 2-12) (Holschemacher et al., 2006), which specifies the fibre content that is at least necessary to maintain the maximum tensile strength of the plain concrete. Lower fibre contents increase the ductility of the material, but do not lead to an increase in the maximum tensile stress that can be absorbed.

$$V_{crit} = \frac{\sigma_{cf,cr} * d_f}{\tau * l_f} \qquad \text{(eq. 2-12)}$$

with:

$\sigma_{cf,cr}$	Transmittable tensile tension in concrete cross-section in N/mm²
d_f	Fibre diameter in mm
τ	Mean compound tension in N/mm²
l_f	Fibre length in mm

Fibre contents can therefore be categorized in the subcritical, critical, or supercritical range. Figure 2.4 shows the effects of the different ranges of fibre content on the load-bearing behaviour of the concrete using the example of the flexural and tensile load-bearing behaviour of fibre reinforced concrete.

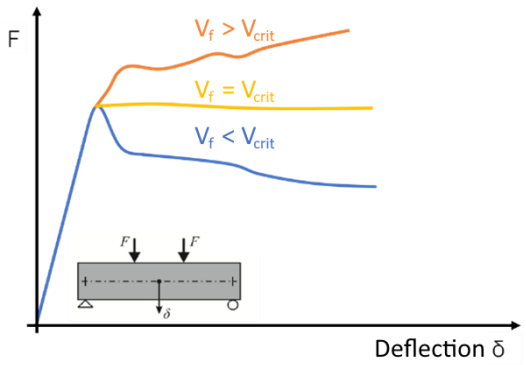

Figure 2.4 Critical fibre content V_{crit} (Müller, 2014)

The critical fibre content V_{crit} is comparable to the minimum reinforcement of steel reinforced concrete construction. The forces released as a result of the formation of an initial crack can still be absorbed by the existing fibres. A further increase in load is not possible. A subcritical fibre content, on the other hand, initially leads to a drop in stress after the formation of an initial crack, which then stabilises depending on the pull-out behaviour of the fibres. With a supercritical fibre content, a direct load increase is already possible after initial crack formation. The fibres can completely absorb the tensile forces released by the cracking of the concrete matrix and enable a further load increase by higher possible deformation (Breitenbücher, 2012,

Holschemacher et al., 2006, Müller, 2014). The critical fibre content can therefore be determined as a function of the existing fibre slenderness λ as well as the transferable bond stress τ_m and the crack energy. With decreasing fibre length or a lower fibre slenderness, a higher critical fibre content can be expected accordingly.

Furthermore, the critical fibre content is also influenced by the strength properties of the concrete matrix and the type of loading (Müller, 2014). Both factors determine the size of the released crack energy. The concrete strength additionally affects the bond. Furthermore, the critical fibre content is also influenced by the existing fibre orientation. In practice, common and easy-to-process fibre contents are usually in the subcritical range with up to 80 kg/m³ or 1.0 % by vol.

2.2.3 Influence of Fibre Orientation

2.2.3.1 General Influences

In addition to the fibre content, their distribution in the matrix also exerts an influence on the properties of the fibre reinforced concrete. The fibre distribution refers to the number of fibres in a specific concrete volume. A homogeneous and uniform concentration per unit (N_i / V_i = constant) is to be aimed for. The fibre distribution is mainly dependent on the production process. More precisely, the direction of concreting, the consistency of the fresh concrete, the compaction process, the mixing process, the geometry of the formwork and, if applicable, the installation parts respectively additional reinforcement have an influence on the distribution. (Ackermann, 2010, Rosenbusch, 2004)

Without external disturbing influences, the fibres theoretically are initially distributed ideally three-dimensional and randomly in space after the mixing process. However, this is not automatically the case after insertion into the formwork. The casting method, the geometry of the formwork, especially the effect of formwork sides and free surfaces, as well as the use of vibration for impaction have an influence on the distribution and orientation of the fibres in the concrete (Figure 2.5). (Edgington & Hannant, 1972, Lin, 1996, Maidl, 1991)

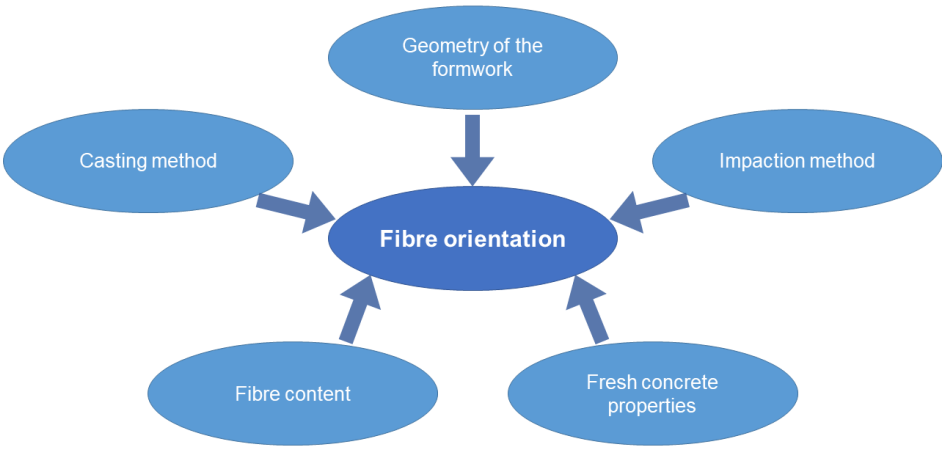

Figure 2.5 Influencing parameters on the fibre orientation in fibre reinforced concrete

However, the arrangement of the fibres is also influenced by the choice of the largest grain within the concrete mixture. Large grain sizes can lead to uneven distribution of fibres between

aggregates. Grain sizes that exceed the average fibre spacing of the material can be seen as an obstacle to the distribution (Holschemacher et al., 2006, Müller, 2014).

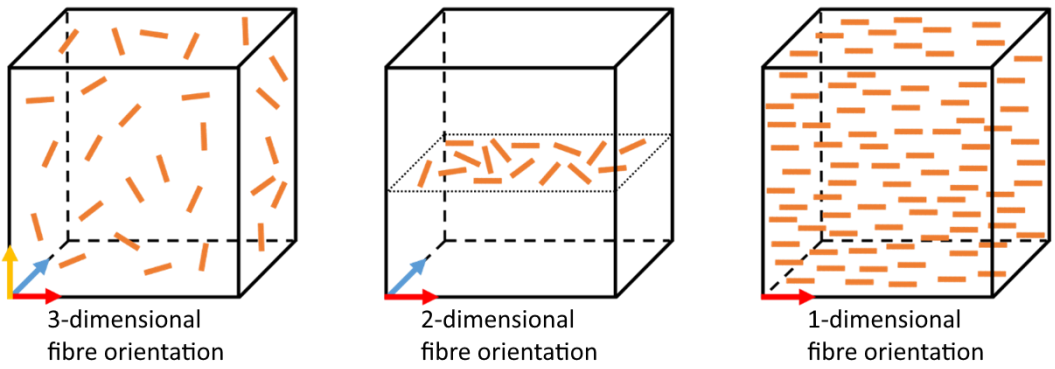

Figure 2.6 Possible orientations of fibres in concrete (Grunert, 2006)

The fibre distribution, however, only has significance regarding the arrangement in the volume element, the fibre orientation, on the other hand, refers to the spatial orientation of the fibres (Hadl & Tue, 2016). As previously explained, fibres are intended to bridge cracks that occur perpendicular to the tensile stress. Consequently, their effectiveness is greatest when the main tensile stress is in the longitudinal direction of the fibre. In space, a distinction is made between different fibre orientations, which are shown in Figure 2.6. In the left cube, the fibres are oriented three-dimensionally. There is a uniform orientation and distribution. This is the aimed condition when using fibre reinforced concrete. In the middle cube, a two-dimensional orientation is shown. Almost all fibres are oriented in one plane and their angles to the horizontal are almost zero. Such an arrangement is found, for example, in the use of fibre reinforced shotcrete. In the last model, a one-dimensional alignment is presented. The fibres are evenly distributed as in the first case. However, their alignment is limited to one axis. Practical examples of this case are extruded concrete products (Ackermann, 2010, Grunert, 2006).

The previously mentioned influences for the fibre distribution can be applied equivalently to the fibre orientation (Rosenbusch, 2004). Studies have shown that fibres prefer to be oriented perpendicular to the direction of compaction. About 40 % are located each on the x- and y-axis at an angle of 90 ° to the compaction direction, while only 20 % are oriented parallel to it (Breitenbücher & Rahm, 2009).

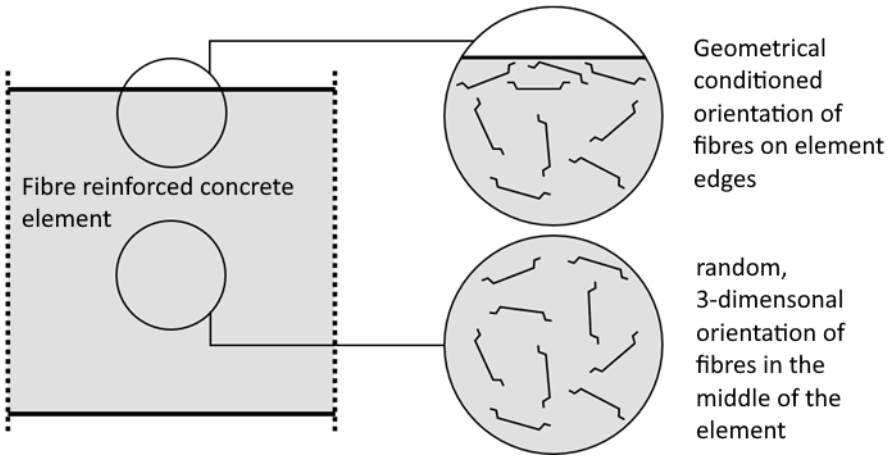

Figure 2.7 Influences of the concrete element itself on the fibre orientation (Müller, 2014)

Geometric constraints, for example due to the formwork or additional reinforcing bars, lead to a disturbance of the three-dimensional orientation. In a zone whose width corresponds to the fibre length, fibres only align two-dimensionally due to the existing barrier. This in turn leads to the compound material properties being disturbed at the edges. This problem plays a decisive role especially for slim components. A schematic representation of the problem can be found in Figure 2.7. (Hadl & Tue, 2016, Leutbecher, 2007, Müller, 2014)

(Bonzel & Schmidt, 1984, Empelmann et al., 2009, Hilsdorf et al., 1985, Teutsch & Empelmann, 2008) investigated the influence of the casting direction on the distribution and orientation of steel fibres in the surrounding concrete matrix. They have produced beams conventionally in the horizontal direction (lying) and vertically (standing). The post-cracking tensile strength of the upright beams was only about 55 % to 65 % (Empelmann et al., 2009) respectively about 2/3 (Bonzel & Schmidt, 1984) of the horizontal beams, because the fibres were mainly oriented perpendicular to the concreting direction, i.e., horizontally.

(Blanco et al., 2015, Hadl et al., 2015, Svec et al., 2013) considered the orientation of the fibres regarding the flow movement of concrete. For slab-like components, they have found out that the fibres align orthogonally to the flow direction under the permission that the orientation is not restricted by formwork surfaces. The fibres are therefore pushed in front of the concrete like a kind of largest grain. (Grünewald & Wallraven, 2004) also detected this behaviour in the investigation of tunnel elements.

For a single fibre, the orientation in relation to the tensile stress direction plays a major role in terms of the maximum transmissible load (Breitenbücher, 2014). Here, a higher embedding angle tends to lead to a higher transmittable load, under the prediction that the fibres have a sufficiently high tensile strength. From an angle of approx. 60 °, the high necessary deformation of the fibres, which leads to a pull-out of the fibre, no longer leads to an increase in the transmissible load, but increasingly to fibre breakage, as can be seen in Figure 2.8. Thus, for a single fibre, an embedding angle of about 45 ° to the tensile stress is ideal to enable high load transmission even over long distances.

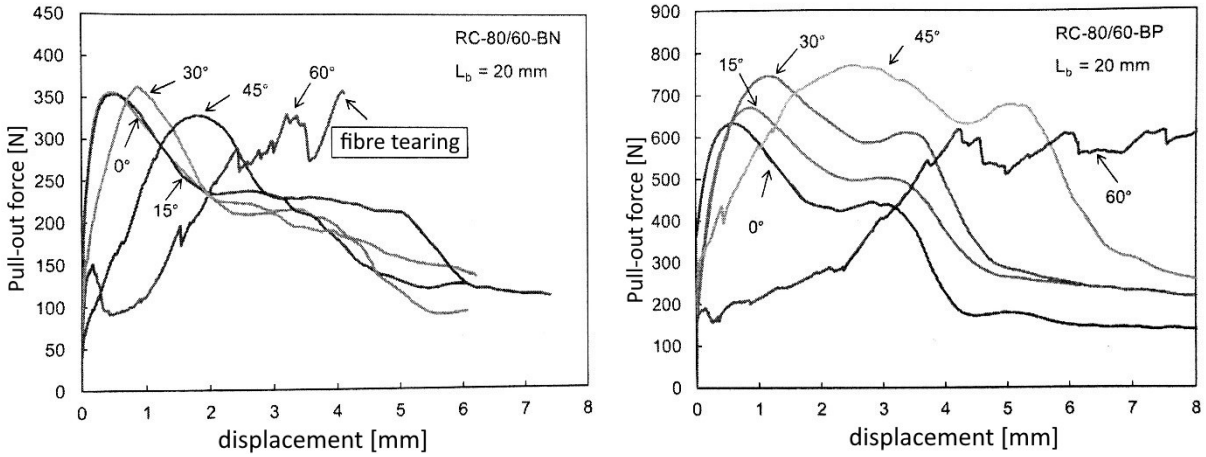

Figure 2.8 Influence of the fibre orientation on transmissible force between concrete and fibres (left: low strength fibre, right: high strength fibre) (Breitenbücher, 2014)

The global fibre orientation in the component in turn leads to other correlations than described above. For example, according to DAfStb, 2015 the mechanical performance is determined on beams and adopted for plate-like components, while for other components (walls, columns) a

lump-sum reduction of 50 % is made. Reduction factors according to Fehling et al., 2013 for prisms and beams manufactured upright compared to those manufactured horizontally are with values 0.662 and 0.796 even higher.

The decisive difference to pure fibre extraction is the globality of the fibres. While a single fibre bridges a defined crack best when it is bound at a 45 ° angle, a multitude of fibres crossing the crack relatively perpendicularly leads to the highest load transfer, since in this case the probability is highest that many fibres simultaneously take up the load. In the case of a deviating fibre orientation, a single fibre can take more load, but fewer fibres don't take part in load transfer and thus the total possible load transfer is lower.

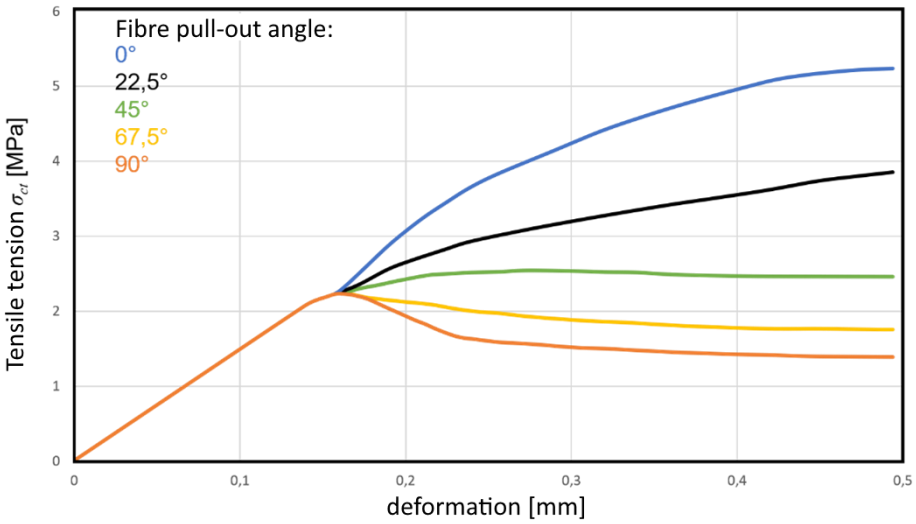

Figure 2.9 Transmissible tensile tension depending on the fibre orientation (Lehmberg, 2018, van Mier, 1991)

In fibre reinforced components, it can be observed that a global fibre orientation in the direction of the tensile stress leads to a significantly increased maximum transmissible tensile stress. Figure 2.9 shows the dependence of the transmissible tensile stress in a uniaxial tensile test on a notched specimen dependent on the fibre pull-out angle. Furthermore, it can be seen that this is no linear relationship. Thus, the difference in tensile stress between 0° and 22.5° is significantly greater than the difference between 67.5° and 90° in view of the maximum deformation (van Mier, 1991).

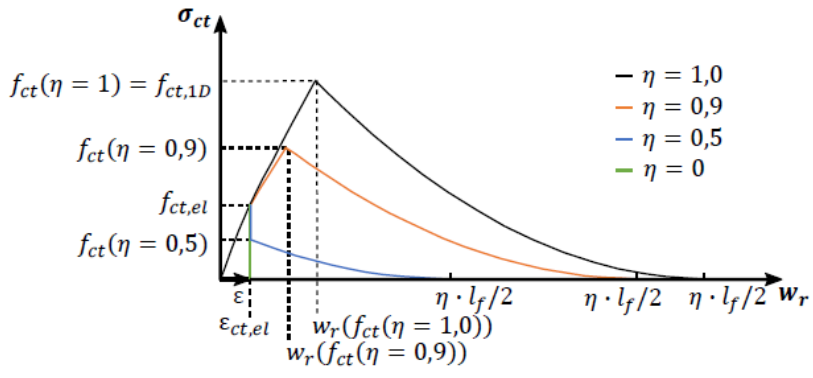

Figure 2.10 Tensile behaviour of fibre reinforced concrete depending on the fibre orientation (Frettlöhr, 2011)

Similar results can also be seen during the tensile stress-crack opening relationship in Figure 2.10 (Lehmberg, 2018).

Zhou investigated the influence of the fibre orientation on the post-crack bending tensile strength in his work. The linear curve describing this behaviour can be seen in Figure 2.11 despite relatively large scatter. He concludes that the load capacity of the material to tensile stress increases with increasing fibre orientation value. (Zhou & Uchida. 2017)

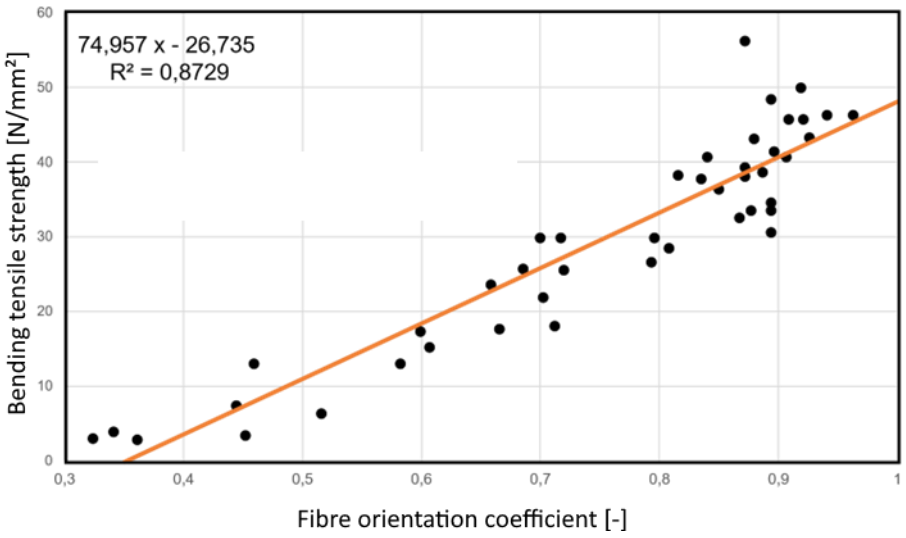

Figure 2.11 Bending tensile strength, after first cracking of concrete, depending on the fibre orientation factor (Zhou & Uchida, 2017)

2.2.3.2 Orientation Factor

Like already seen in Figure 2.11, the fibre orientation best can be described by a so-called orientation factor or orientation coefficient. In literature, there are several ways of calculating, based on different principles.

According to Lin, 1996, the coefficient is defined as the ratio between the actual fibre length and all fibre lengths projected in the tensile stress direction (Thomée, 2005). Accordingly, an orientation value of one corresponds to a one-dimensional alignment of the fibres in the direction of tensile stress. A value of zero, on the other hand, corresponds to the opposite case (Holschemacher et al., 2006). The exact calculation is done according to (eq. 2-13) (Leutbecher, 2007):

$$\eta = \frac{1}{N} * \sum_{i=1}^{N} cos\alpha_i \qquad \text{(eq. 2-13)}$$

with:

N Number of fibres crossing the observed surface
α Angle between fibres and observed area in °

In addition, Pfyl, 2003, derived an approach based on Lin's work. From N parallel fibres on the crack plane A_m, the fibre orientation value for different angles θ can thus be determined with the help of (eq. 2-14) (Leutbecher, 2007).

$$\eta = N * cos\,\theta \qquad \text{(eq. 2-14)}$$

When determining the value according to Markovic, 2006, mainly crack surfaces are examined. Here, the cut surfaces of all fibres crossing the crack are considered. The more perpendicular the fibres run through the crack, the more the sectional view resembles a circle. At shallower angles it becomes an ellipse. The orientation coefficient of a single fibre can be determined according to (eq. 2-15) (Leutbecher, 2007).

$$\eta = cos\alpha = \frac{d_f}{d_{f2}} \qquad \text{(eq. 2-15)}$$

with:

- α Angle between fibres and tensile force in °
- d_f Fibre diameter in mm
- d_{f2} Diameter of the projected fibre in the cross-section of the crack in mm

The sketches illustrating the respective derivation and angular relationships can be found in Figure 2.12.

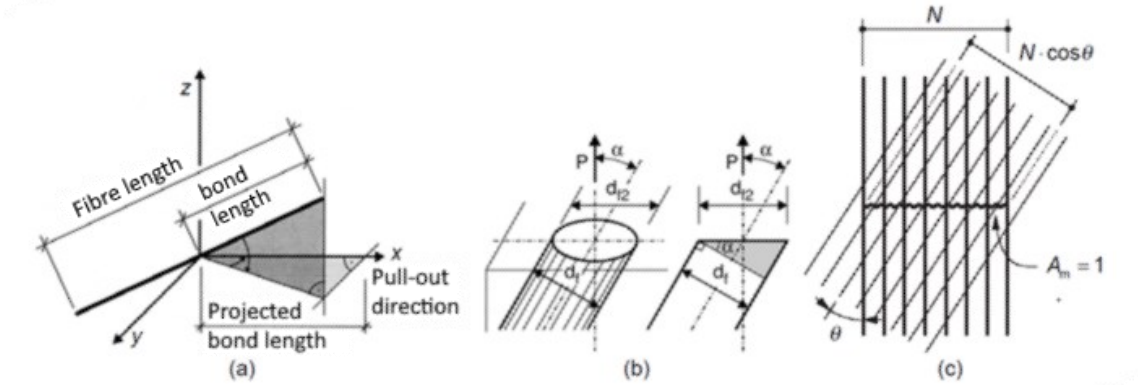

Figure 2.12 Interpretation of the fibre orientation factor (Leutbecher, 2007) according to a) Lin, 1996 b) Markovic, 2006 c) Pfyl, 2003

2.2.4 Influence of Fibre Type

The fibre geometry and tensile strength of the used fibres are decisive for the properties of the concrete. Several geometric parameters are decisive for the composite effect (Holschemacher et al., 2006).

First of all, the surface quality of the fibre should be mentioned. Rough fibres, such as chip fibres, are particularly suitable for low deformations. The roughness leads to a significant increase in the adhesive bond compared to smooth surfaces. However, the fibre pull-out that begins when the fibre activation is overcome can hardly be influenced by profiled surfaces. Thus, in pull-out tests with corresponding materials, there is an abrupt drop in the force that can be absorbed. (Müller, 2014)

Constructively deformed fibre ends such as end anchors help to limit the pull-out of the fibre (Müller, 2014). In the non-cracked state, these do not lead to any significant change in the load-bearing behaviour compared to conventional concrete, but they are activated by even the smallest displacements and lead to a significant increase in the pull-out strength (Holschemacher et al., 2006). This advantage is offset by the often-difficult workability. Due to the end hooks, mixing in of those fibres is significantly more difficult than with smooth fibres (Müller, 2014).

To achieve the necessary strength, the so-called aspect ratio of the fibres must also be considered. This is the ratio of fibre length to fibre diameter, also known as the fibre slenderness. It is well-known that a high fibre slenderness is associated with a high post-crack strength (Schepers, 2008). However, to prevent the tensile strength of the fibre from becoming too low and the failure of the concrete thus occurring through the tearing of the fibre, fibre slenderness's above 65 should be avoided (Brux, 2004).

A tool that allows statements to be made about the type of failure of straight fibres is the critical fibre length l_{crit}. It can be calculated using (eq. 2-16) (Holschemacher et al., 2006).

$$l_{crit} = \frac{f_f * d_f}{2 * \tau} \qquad \text{(eq. 2-16)}$$

with:

f_f Tensile strength of the fibre in N/mm²
d_f Fibre diameter in mm
τ Mean compound strength in N/mm²

The equilibrium state, where the critical fibre length is equal to twice the binding length, separates the two failure modes fibre tearing and fibre pull-out. If the critical length is greater than twice the bonding length, failure occurs due to fibre pull-out. If the opposite is the case, the fibre will tear (Holschemacher et al., 2006, Meyer, 1991).

2.3 Determination of Fibre Content and Orientation

2.3.1 Test-Setups for the Analysis of Steel Fibre Reinforced Concrete

2.3.1.1 Standardized Test Methods

A method for quantifying fibres in concrete is specified in DIN EN 14721, 2007. This destructive method provides the fibre content as a result and requires the extraction of drilling cores out of the construction. Subsequently, the fibres shall be extracted from the fabric by crushing the concrete samples. The loosened fibres are now to be collected and the total mass of the fibres is determined and related to the summed volumes of all specimens taken. Using (eq. 2-17), the calculation of the fibre content C_f is thus made possible (DIN EN 14721, 2007). Alternatively, the method can be applied on fresh concrete samples, where the fibres are washed out of the fresh concrete.

$$C_f = \frac{m}{V} \qquad \text{(eq. 2-17)}$$

with:

m Mass of the fibres in kg
V Volume of the specimen in m³

2.3.1.2 Optoanalytical Investigation based on Cross-Sectional Analysis

The optoanalytical or photo-optical method is based on the optical analysis of a crack plane and is carried out on ground cut surfaces. The local fibre content can be determined by simply counting the number of cut areas of fibres on the cut concrete surface under consideration. The fibre distribution can then be determined with the help of this fibre count. For this purpose, the area under consideration is divided into equally sized sub-areas and a fibre density per sub-area is determined. In addition, a comparison of the fibre densities of orthogonal cut surfaces enables a statement to be made about the isotropy of the material.

Depending on the single fibre orientation, the shapes of the fibres inside the cut surfaces differ, what for round fibres allows a statement on the fibre orientation. Round fibres oriented perpendicular to the considered cut surface appear as a circle, while fibres oriented obliquely to the cut plane have an elliptical cut shape. Based on the geometric relationship between fibre angle and cut shape, the respective orientation of the individual fibre can be determined (Figure 2.13) (Gettu, 2005, Gröger et al., 2011, Schönlin, 1983, Schönlin, 1988, Stähli et al., 2007, Strack, 2007, Tue et al., 2007, Wichmann et al., 2013).

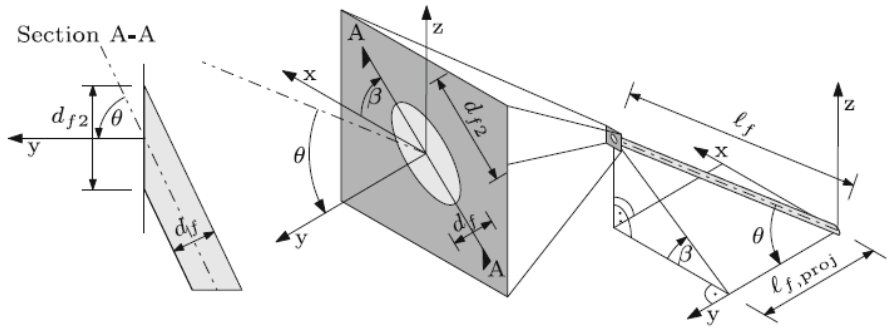

Figure 2.13 Optoanalytical investigation of fibres in concrete (Wille et al., 2014)

2.3.1.3 Inductive Analysis of Fibre Content

The inductive analysis of SFRC, developed at the IBMB at the Technical University of Braunschweig is baes on electromagnetic activation and is applicable to hardened concrete and fresh concrete only on prepared samples (Schnell et al., 2008, Matenco, 2009, Wichmann et al., 2013). In order to obtain the most accurate results, a homogeneous fibre distribution inside the sample must be ensured. (Schnell et al., 2010). A detailed analysis of the distribution inside of one sample thus is not possible.

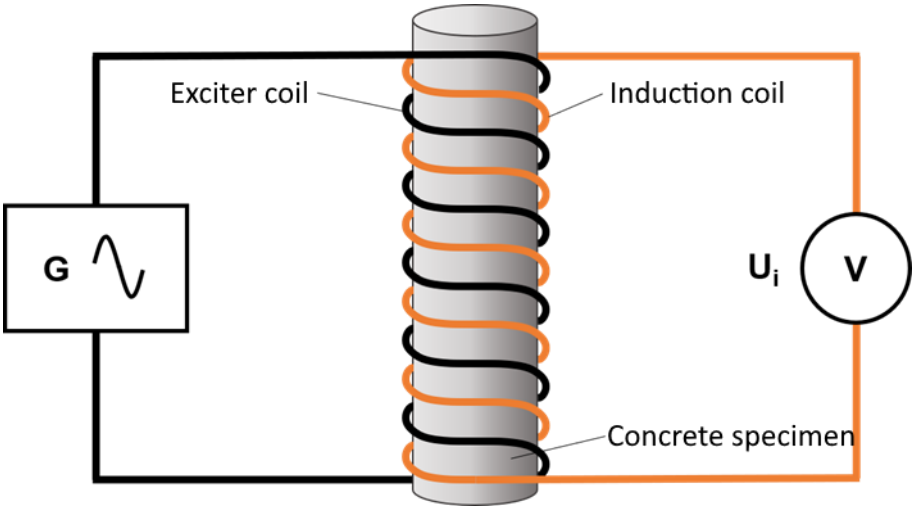

Figure 2.14 Schematic figure of inductive testing (Wichmann et al., 2011)

The set-up of the method is shown in Figure 2.14. In this system, the enclosed specimen can be regarded as the coil core. By generating a sinusoidal alternating current in the exciter coil from a generator, the voltage U_i can be measured in the induction coil (Wichmann et al., 2012).

Because only the fibres as electromagnet material inside the concrete take part in the inductive process, it is possible to draw conclusions about the content and orientation of steel fibres inside the sample via the measurement results, after the examination of calibration measurements (Torrents et al., 2012, Wichmann et al., 2012). Assessments about the orientation of the steel fibres are only made possible by measurements in all three spatial directions (Torrents et al., 2012, Wichmann et al., 2012).

2.3.1.4 Microwave Analysis

Microwaves, which range in the frequency between 300 MHz and 100 GHz, cause polar molecules to start oscillating. The different electronegativities of the oxygen and hydrogen molecules lead to the formation of a dipole. The strength of this dipole can be quantified by its polarizability. In the course of the process, a shift of the charges occurs, which in turn consumes energy. By means of special sensors, it is possible to measure this energy, the so-called permittivity (Dollase, 2019).

In the contactless so-called FSM method (free-space microwave method), two antennas face each other with the sample right in their centre (Figure 2.15 a). This method covers a frequency range of 8 to 12.5 GHz (Jamil et al., 2013), while for the coaxial probe setup (Franchois et al., 2014) lower frequencies up to a maximum of 2 GHz are used (Dollase, 2019, Torrents, 2009, van Damme et al., 2004). Using those methods, the determination of the fibre content is well possible; the applicability regarding the fibre orientation is limited (Wichmann et al., 2013).

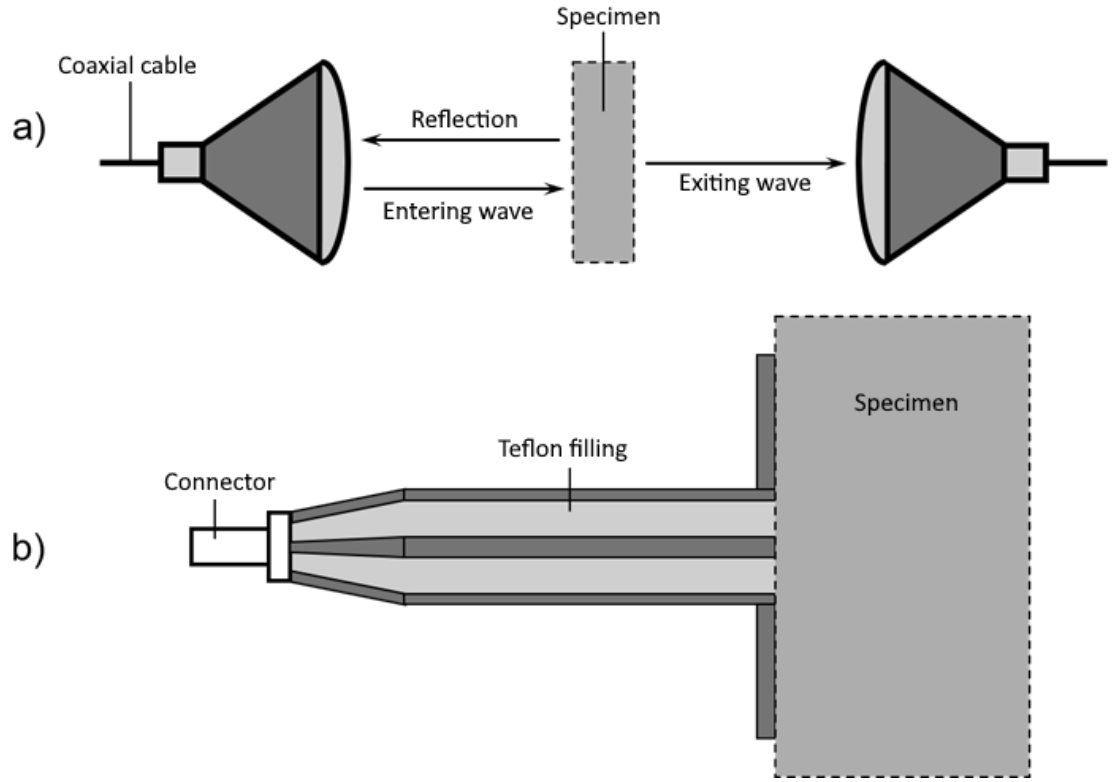

Figure 2.15 Microwave analysis with a) FSM method, b) Coaxial method (Jamil et al., 2013 and Franchois et al., 2004)

2.3.1.5 Computed Tomography (CT)-Scanning

Non-destructive X-ray testing, also called CT-scanning, enables, for example, the reconstruction of concrete components (Schnell et al., 2009). However, the implementation is limited to measurements in the laboratory, which conversely means that in-situ examinations of objects on the construction site are not feasible. Comparing this method with others, on the one hand the great effort, long measuring times and expensive equipment are negative aspects, but on the other hand the high accuracy speaks for the computed tomographic method (Wichmann et al., 2013).

The process of the measurement method can be divided into several sections. (Pittino et al., 2011). The set-up and process are illustrated in Figure 2.16. In the first step the concrete component is recorded (left side), followed by the computer-aided reconstruction (middle) and then finally visualized (right side). (Schuler et al., 2017)

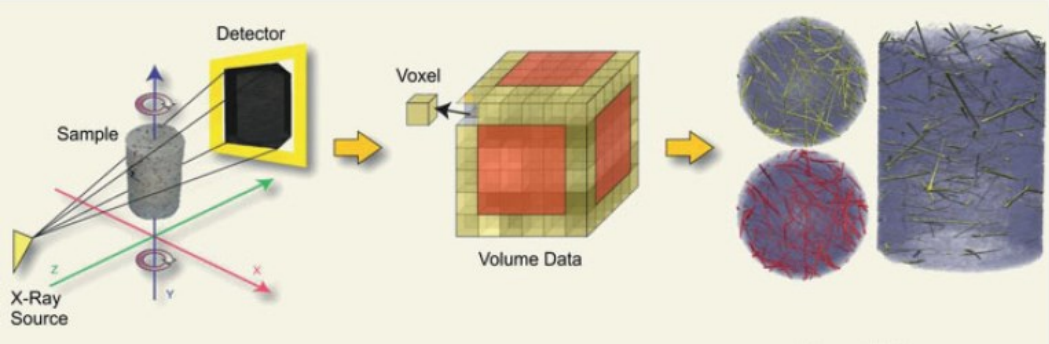

Figure 2.16 Schematic overview of a CT-scanning process (Pittino et al., 2011)

While the body is rotated 360°, hundreds of images of the projection are generated. Based on differences of density and atomic type of the material, a virtual image can be created, and a reconstruction algorithm enables the representation of all obtained points in a voxel model. Those voxels are divided into two groups, based on a certain threshold of grey-scale, receiving either the value 0 (black) or the value 1 (white) in a graphically simple representation (Schuler et al., 2017).

For the evaluation of the experiment, the number of fibres inside the specimens can be determined as well as fibre orientation coefficients η_φ can again be determined. Since the entire volume is examined, the values for all spatial directions are to be calculated separately via (eq. *2-18*).

$$\eta_\varphi = \frac{L_{p,\varphi}}{L_V * V} \qquad \text{(eq. 2-18)}$$

with:

$L_{p,\varphi}$	Projected fibre length per spatial direction in m
L_V	Dense of fibre length (fibres per volume) in m/m³
V	Volume in m³

For the variables obtained, $0 \leq \eta_\varphi \leq 1$. The larger the result, the more strongly the fibres are oriented in the direction considered. For the value 0, all fibres are oriented orthogonal to the reference direction (Schnell et al., 2009).

2.3.1.6 Infrared Thermography

Infrared thermography is a technique that is mainly used for the evaluation and identification of component surfaces. By analysing the thermal radiation of test specimens, this method can also be used to identify inhomogeneities and defects inside of construction elements (DAfStb, 1991). Based on this state of application, Maldague and Fernandes developed a method for the assessment of fibre reinforcement in concrete specimens. It is called Pulsed Thermal Ellipsometry (PTE).

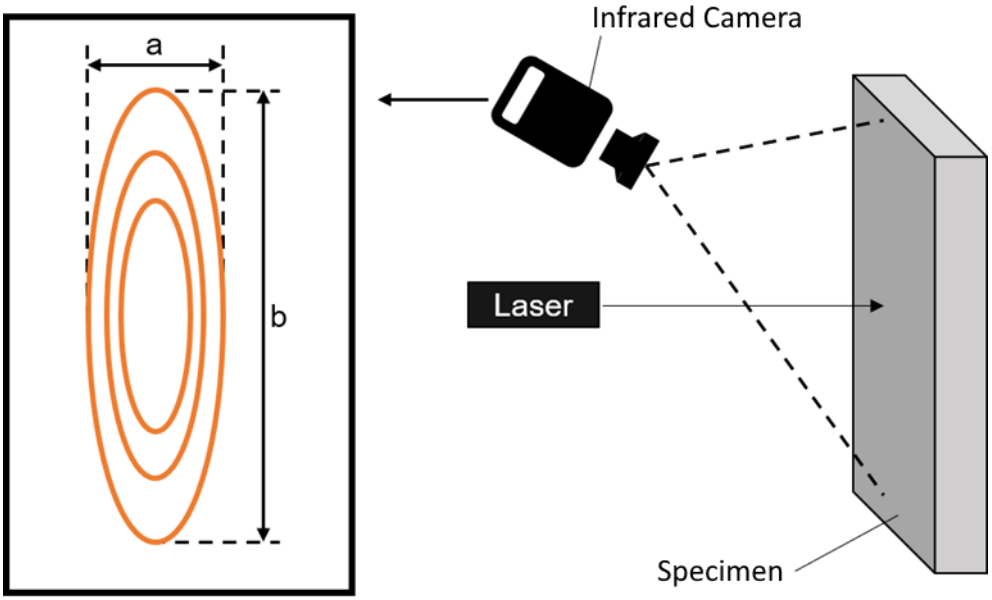

Figure 2.17 Test setup for pulsed thermal ellipsometry(Maldague & Fernandes, 2013)

The experimental setup of the PTE is shown in Figure 2.17. A diode laser is placed perpendicularly in front of the test specimen. It irradiates the concrete surface for 0.1 seconds with a frequency of 805 nm. This heating process and the subsequent cooling are recorded by a camera. A visualisation in the form of an ellipse allows conclusions to be drawn about the presence and orientation of fibres because of material specific differences of the heating and cooling curves.

Although this method, which is still part of research, shows precise measurement results, it has the decisive disadvantage that only very small areas and especially a very small depth of a specimen can be evaluated. In addition, it is, up to now, not possible to determine the fibre content of a concrete element (Maldague & Fernandes, 2013).

2.3.1.7 Electrical Resistivity Measurements

- **Basics**

In contrast to the optoanalytical analysis, electrical resistivity measurements, like inductive or microwave analysis, is a non-destructive testing method for examining steel fibres in concrete (Just et al., 2001). Thereby it can be differentiated between electrical resistance tomography (ERT) and impedance spectroscopy.

In general, the measurement of the material's electrical resistance is based on the measurement principles presented in section 2.1. Here, depending on the electrode configuration, a distinction is made between 2-point, 4-point measuring methods, for example

the Wenner method and further methods (Layssi et al., 2015, Reichling, 2014, Wichmann et al., 2013). Depending on the method, the geometry factor must be determined as a function of the electrode arrangement, resistivity distribution and geometry of the test object. To record horizontal inhomogeneities of a test specimen, it is necessary to carry out the measurements at different positions. Statements about the vertical structure can be made by changing the electrode distances (Reichling et al., 2015). In order to be able to make a statement about the content of steel fibres, reference measurements must first be made on plain concrete samples because both materials, steel and concrete, take part in the electrical conduction. Corresponding conclusions can be drawn from the increase in conductivity (Lataste et al., 2008). To investigate the fibre orientation, measurements in different spatial directions are essential. Subsequently, the resistances of the different directions are to be compared with each other. The lower the measurement results, the more likely the fibres are oriented in the corresponding direction (Hicks, 2015). According to Lataste et al., this method could be used well to answer questions regarding fibre distribution. Even information on orientation seems to be possible (Hicks, 2015, Lataste et al., 2008, Karhunen et al., 2010).

- **Impedance Spectroscopy**

The fundamental difference between the ERT and impedance spectroscopy is that the latter does not consider ideal resistances but impedances, i.e., complex electrical resistivities (Barsoukov & Macdonald, 2005). Since polarisation effects occur at phase boundaries at low frequencies or when direct current is used between electron and ion conductors, the behaviour must be described in the complex. This occurs, for example, when the electrodes or the fibres and the electrolyte come into contact. Using a direct current measurement, it is only possible to determine the sum of the resistances. For further investigations, an alternating current measurement is necessary (Reichling, 2014). Consequently, the frequency of the AC voltage and current must always be considered during the measurement (Barsoukov & Macdonald, 2005).

Impedance spectroscopy is suitable for various applications. For example, it is possible to make statements about cracks in concrete. Furthermore, reinforcement elements can be characterised regarding their type and quantity as well as their state of corrosion (Layssi et al., 2015) and even other areas like electrochemistry or geophysics are covered by similar test methods (Zimmermann, 2011).

The typical frequency range of impedance spectroscopy ranges between 0.01 Hz and 100 kHz. For an examined system, impedances are measured as a function of different frequencies - which are increased step by step. This results in a progression of the complex variable, which allows conclusions to be drawn about the condition of the tested substance (Hoffmann-Walbeck, 2017). The graphical representation of the impedance is usually done in a pointer diagram (cf. Figure 2.1, section 2.1.3), by plotting the real and imaginary part (Müller, 2000). To enable qualitative statements about the system, it must be described by a suitable equivalent circuit. Such a circuit includes the elements resistor, also known as Ohmic resistance, capacitor, and coil, which are connected with each other (Müller, 2000).

For the elements, the respective impedances can be represented in a vector diagram. A visualisation can be seen in Figure 2.18. The interpretation of the impedance measurement results becomes possible through the suitable combination of the components in a series or parallel connection.

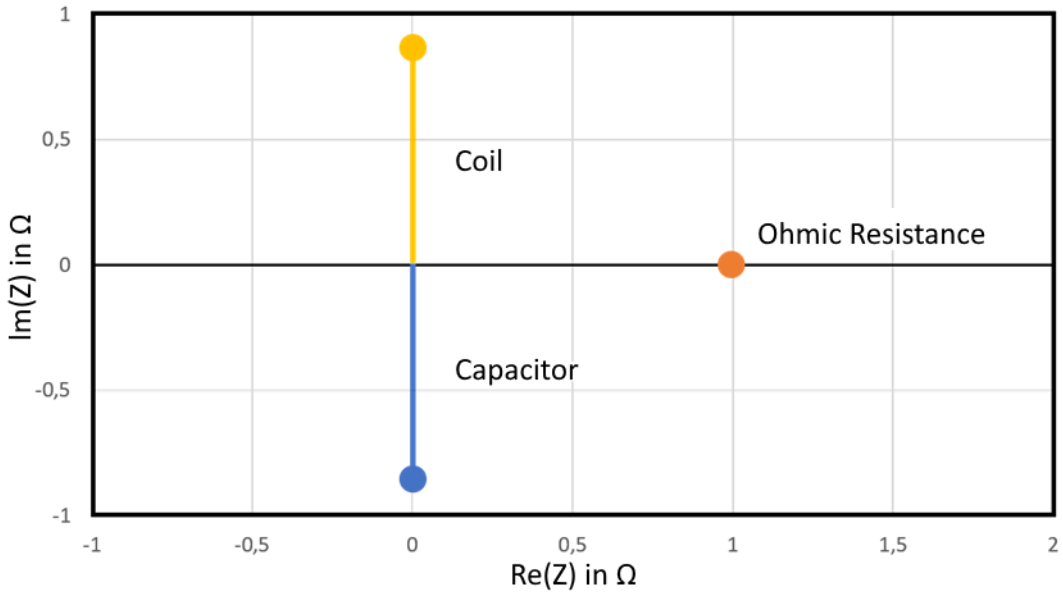

Figure 2.18 Basic elements in the vector diagram (Hoffmann-Walbeck, 2017)

The frequently used parallel circuit of resistor R and capacitor C is called an RC element. The impedance of the circuit is therefore also dependent on the frequency. The plot of the impedances over the entire frequency spectrum is called a Nyquist plot, which has the shape of a semicircle for a RC element (Figure 2.19).

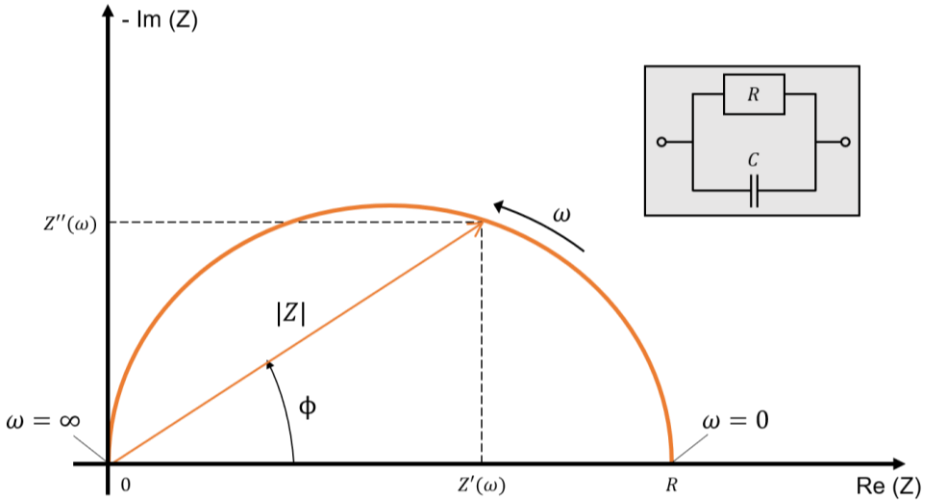

Figure 2.19 Representation of a RC element in the Nyquist plot (Reichling, 2014)

The resulting limit values are calculated by (eq. 2-19) (Heins, 2015).

$$\lim_{\omega \to 0} Z_{RC} = R \quad und \quad \lim_{\omega \to \infty} Z_{RC} = 0 \qquad \text{(eq. 2-19)}$$

Nyquist plots have the advantage that all parameters can be shown in one plot. This makes it easy to compare the results from two different experiments. In addition, the extrapolation of values outside a measured frequency range is possible. A disadvantage of these diagrams, however, is that the frequency cannot be read explicitly. Consequently, the capacity of the system can only be calculated when the frequency at a point is known (Orazem & Tribollet, 2008).

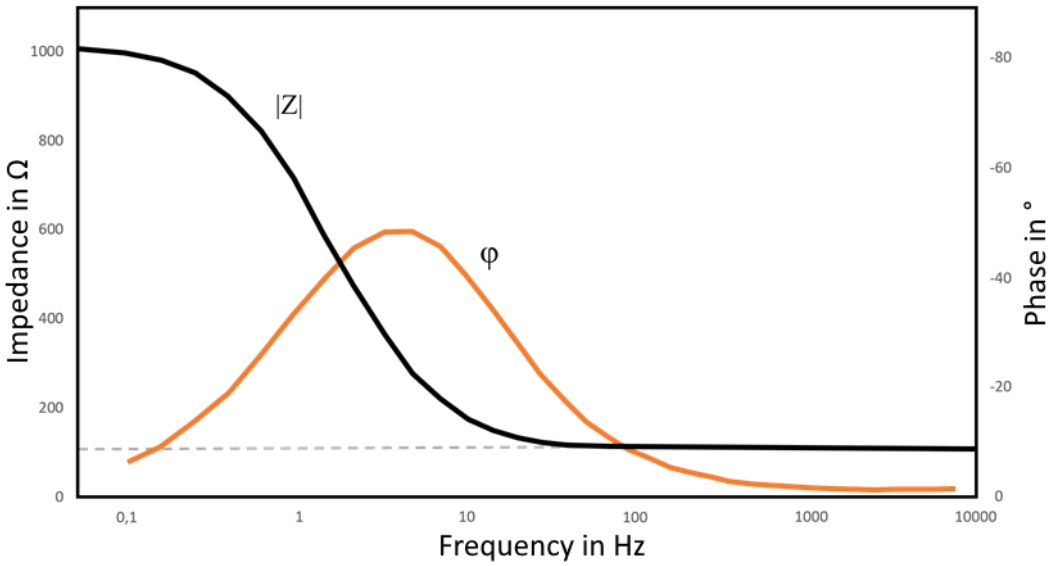

Figure 2.20 Bode plot to present test results (Sauer, 2006)

In contrast to the Nyquist plot, reading of the frequency is well possible in the Bode plot (Figure 2.20), which is also widely used. On two y axes, both the amount of impedance and the phase are visualised as a function of the frequency. (Sauer, 2006). The disadvantage of this plot is that it is often difficult to evaluate and compare two measurements (Lvovich, 2012).

In the meantime, numerous investigations of fibre reinforced concrete using impedance spectroscopy can be found in the literature. Not only the basic suitability of the method is examined. For example, Ozyurt et al. describe the method as an effective technique for analysing the conductivity of cementitious materials (Ozyurt et al., 2006a). In addition, sources can be found in the literature that report a suitability for the observation of fibre orientation and fibre content.

According to Berrocal et al. the presence of fibres is directly evident from the Nyquist plot. While the diagram without fibres consists only of a single arc, the addition of fibres results in another arc, which can be used to make statements about the fibre content (Berrocal et al., 2018, Torrents et al., 2000).

According to Mason et al., there is a linear relationship between the proximity of the fibres in the component and the resistance of the building material. However, if the fibre-to-fibre distance is too small, the resistance drops rapidly (Mason et al., 2002). This relationship can be used to assess the distribution of the fibres in the component.

According to Lataste et al. and Mason et al. and Woo et al. the fibre orientation can also be investigated with sufficient accuracy. According to this, for fibres that are arranged perpendicular to the direction of measurement, only a single arc, like for plain concrete, can be seen in the plot (Lataste et al., 2008, Mason et al., 2002, Woo et al., 2005).

- **2-point method**

In the 2-point method, a test specimen is placed between two parallel metal plates that serve as electrodes. As with the Wenner method, the coupling is carried out by means of moist sponges to establish a sufficient electrical connection. (Layssi et al., 2015)

After adding an alternating current, the potential drop in the concrete can be measured (Whiting & Nagi, 2003). Different test specimens can be chosen for the execution. In addition to cubes,

the use of drilling cores is possible, for example (Reichling, 2014). The structure of the procedure is shown in Figure 2.21.

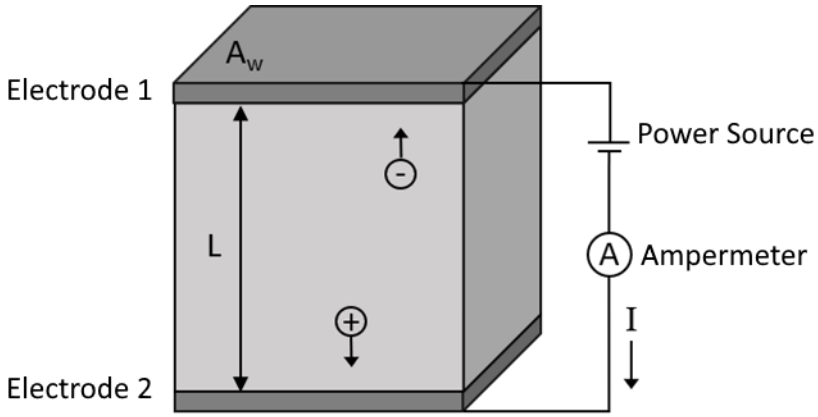

Figure 2.21 Schematic structure of the 2-point method (Rei14)

A geometry factor k (see (eq. 2-20)) can easily be determined for the 2-point method, through which the calculation of the electrical resistivity is possible (Layssi et al., 2015).

$$k = \frac{A_w}{L} \qquad \text{(eq. 2-20)}$$

with:

A_w Effective cross-sectional area in m²
L Distance of electrodes in m

- **Wenner method**

The Wenner method, also called the 4-point method, is the most widely used resistance measurement method (Whiting & Nagi, 2003). Its structure can be seen in Figure 2.22 and consists of four electrodes, arranged equidistantly on a line (Layssi et al., 2015).

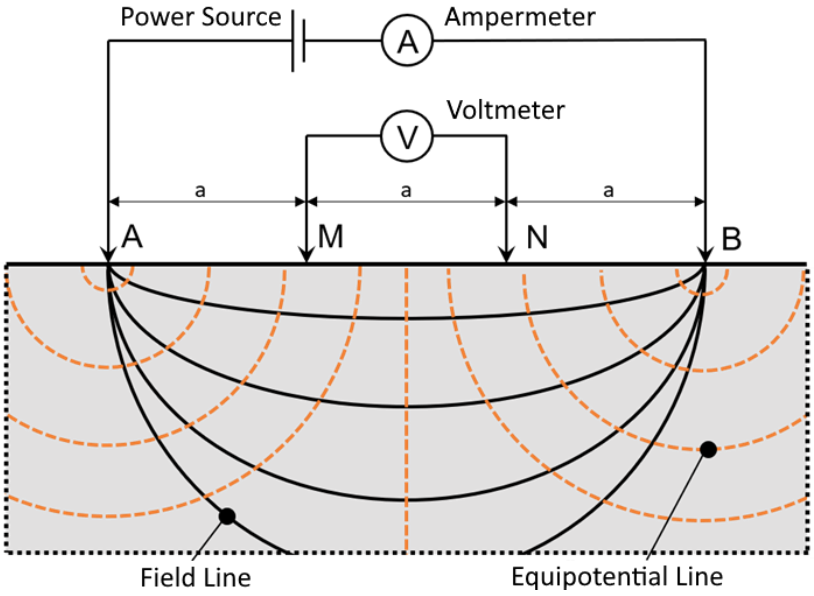

Figure 2.22 Schematic structure of the test method according to Wenner (Reichling, 2014)

As a result of the injection of an alternating current through the two outer electrodes A and B, a radial propagation of the current occurs. The inner electrodes, M and N measure the potential drop in the resulting field (Layssi et al., 2015, Reichling, 2014). This results in the geometry factor k according to (eq. 2-21), which can be simplified due to the equal electrode distances (Reichling, 2014).

$$k = \frac{2 \cdot \pi}{\left(\frac{1}{r_{AM}} - \frac{1}{r_{BM}} - \frac{1}{r_{AN}} + \frac{1}{r_{BN}}\right)} = 2 \cdot \pi \cdot a \qquad \text{(eq. 2-21)}$$

with:

r_{ij} Distance between potential and current electrodes in m

In practice, the method can be applied both on site at the structure and in the laboratory. Sufficient coupling of the brass or stainless steel electrodes to the concrete can be ensured by means of damp sponges. The usual electrode spacing is 50 mm (Reichling, 2014).

Numerous other methods are based on the same principles as the Wenner method. These differ in each case in the electrode arrangement and their spacing. The methods and their geometry factors are shown in Table 2.1 (Reichling, 2014).

Table 2.1 Geometry factors of different electrode configurations (Edwards, 1977, Reichling, 2014)

Electrode configuration	**Formula**	**Geometry factor k in m** [1)]
Schlumberger	k = π*n*(n + 1)*a	4,71 [2)]
Wenner Alpha	k = 2π*a	0,31
Wenner Beta	k = 6π*a	0,94
Wenner Gamma	k = 3π*a	9,47
Dipole-Dipole	k = π*n*(n + 1)*(n + 2)a	32,99 [2)]
Pole-Pole	k = 2π*a	0,31
Pole-Dipole	k = 2π*n*(n + 1)*a	9,43 [2)]

[1)] Exemplary for a = 50 mm; [2)] Exemplary für n = 5

- **Further methods**

Based on the methods listed above, further methods have been developed to measure the resistance of concrete. Feliu et al. use the existing reinforcing steel as a second electrode (Feliu et al., 1996), which is only possible for steel fibre reinforced steel reinforced concrete. By placing a round electrode disc on the concrete surface, it is possible to take measurements in the existing structure. Since an electronic connection to the existing steel must be created, for example by means of a drilled hole, the method is not non-destructive. However, the destruction of the material is significantly less than with drilling core removal. The geometry factor in this method corresponds to twice the diameter of the applied electrode (Reichling, 2014).

A method that is primarily used for long-term monitoring of resistance profiles in concrete is the principle of the multi-ring electrode (MRE). This consists of nine 2.5 mm thick stainless steel rings insulated from each other. These serve as electrodes by applying an alternating voltage to each of the neighbouring rings. The evaluation of the experiment is depth-dependent

from 7 to 42 mm. The experimentally and numerically determined geometry factor k = 0.1 m is used to calculate the resistance. The device is installed either in fresh concrete or in specially provided drilled holes (Raupach et al., 2007).

2.3.2 Evaluation of the Different Test-Setups

The presented methods differ fundamentally in their experimental approach, their suitability for the intended use, their accuracy as well as the costs and the effort involved. Table 2.2 provides an overview of all methods.

Table 2.2 Overview and comparison of the most important test setups for the analysis of fibre content and orientation in concrete (Wichmann et al., 2013)

Test setup	**Standar-dized method**	**Opto-analytical investi-gation**	**Impedance spectro-scopy**	**Microwave analysis**	**Inductive analysis**	**Computed tomo-graphy**	**Infrared thermo-graphy**
Principle	optical	optical	electrical	electrical	electro-magnetic	x-ray	thermal
Fibre content	x	x	x	x	x	x	-
Fibre orientation	-	x	x	x/-	x	x	X
Laboratory specimen	x	x	x	x	x	X	x
Construction side specimen	x	-	x	x	x	-	-
In-situ measurement	-	-	x/-	x/-	-	-	x
Fresh concrete	x	-	x/-	x/-	x	x/-	x/-
Influences / sources of error	Loss of fibres	Preparation of specimen	Concrete composition & temperature	Concrete composition & temperature	Fibre type, magnetic aggregates	Specimen size	Localisation of fibres is necessary

With the normative method as well as the optoanalytical method, the determination of the steel fibre content in particular is possible with a high degree of accuracy, whereby only with the optoanalytical method also the fibre orientation can be detected but both methods use a destructive specimen extraction.

In the case of the electrical methods, the universal application should be emphasised above all. Furthermore, fresh concrete can also be examined using these methods. However, the accuracy of the measurement and evaluation methods available so far are limited compared to methods such as computed tomography and requires further research.

With the induction method, precise determinations of the steel fibre content and orientation are also possible as long as there is a homogenous fibre distribution. Only direct measurements on the structure have to be dispensed with. Since the infrared thermography is limited to very small areas, only the orientation of a specific fibre can be determined.

The most accurate, but also most expensive method is computed tomography. It can be used to create an exact three-dimensional image of a steel fibre reinforced concrete sample. However, since the evaluation time, the costs and the overall effort are significantly higher than with the other methods, tomography is only suitable for special applications. In addition, it is not possible to use the method directly on the structure.

2.3.3 Influencing Parameters for Electrical Resistivity Measurements

2.3.3.1 Boundary Parameters

The electrical resistivity of concrete can show significant differences in different frequency ranges (Bürchler, 1996, McCarter & Garvin, 1989). This influence can mainly be attributed to the polarisation effects and the associated phase shift. These effects mainly occur at very low frequencies. At higher frequencies, however, they are hardly noticeable. According to (Bürchler, 1996, McCarter & Garvin, 1989, Raupach et al., 2006), a suitable range for measuring of the electrical resistance in concrete is between 10 and 1000 Hz.

Another factor that influences the conductivity of a material is temperature. The literature is unanimous in concluding that increasing the temperature lowers the electrical resistance of the material (Hope et al., 1985, Layssi et al., 2015, Malakooti et al., 2019, Zapico, 2015). This is due to the fact that at higher temperatures the mobility of the ions (Na^+, K^+, Ca^{2+}, SO_4^{2-} and OH^-) changes and the ion-ion and ion-solid interactions are influenced. Finally, the temperature causes a change in the ion concentration in the medium (Azarsa & Gupta, 2017).

Formally, this dependence can be represented with the law of Rasch and Hinrichsen from 1908, expressed in (eq. 2-22) according to Arrhenius (Rasch & Hinrichsen, 1908, Zapico, 2015):

$$\rho_2 = \rho_1 * e^{A*\left({}^1/_{T_2} - {}^1/_{T_1}\right)} \qquad \text{(eq. 2-22)}$$

with:

ρ_i	Electrical resistance in Ω
T_i	Temperature in K
A	Activation energy in K

An approach for calculating the activation energy can be taken from Frenkel (Frenkel, 1946). Typical values for concrete here are between 2200 and 5000 K. Mostly an average value of 3000 K is assumed. Since the exponent of this equation always becomes negative with an increase in temperature, this results in a decrease in electrical resistance. (Elkey & Sellevold, 1995)

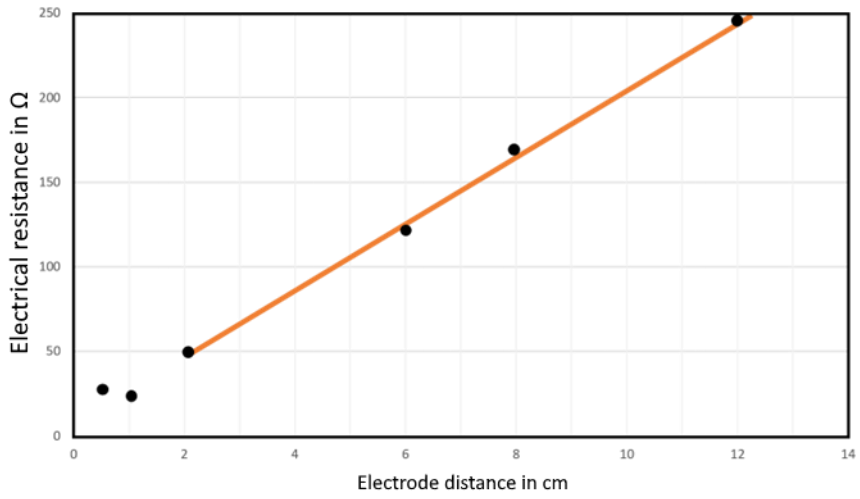

Figure 2.23 Influence of the electrode distance on the electrical resistance (Banthia, 1992)

When evaluating the electrical resistances, it is important to consider not only the material-specific parameters but also the test setup and the specimen geometry. In the 2-point method, the material-independent electrical resistivity is calculated from the product of resistance and geometry factor. Due to the fact that the specific value only changes with the material and not with the geometry, small geometry factors are inevitably followed by large resistances. The dependence between electrode distance and resistance could be proven in experiments by Banthia et al. and is visualised in Figure 2.23 (Banthia et al., 1992).

The coupling of the electrodes to the medium is also of great importance. Lack of contact between the test specimen and the metal plates results in higher measurable resistances (Azarsa & Gupta, 2017). One way to avoid this problem is to use flexible electrodes on very flat surfaces. This optimisation ensures that the concrete resistance can be determined more accurately (Morris et al., 1996). Alternatively, the use of a conductive gel has proven to be practical (Henkensiefken et al., 2009). Furthermore, there are experiments with water-soaked sponges or cloths in the interstitial space. Here, however, the uniform saturation of the coupling medium must be ensured over several trials (Newlands et al., 2008).

2.3.3.2 Concrete Related Parameters

As previously explained, the electrical conductivity of materials can be distinguished between conductors of the I. and II. order. In concrete, the electrons are transported through the pore solution (Reichling, 2014). Accordingly, the decisive factor for the conductivity of the material is how this pore system is formed. The structure of the pore system is in turn significantly dependent on the hydration and the concrete composition (Mouhasseb, 2007, Zapico, 2015). Furthermore, the concrete pore solution and the saturation of the pores also exert an influence on the electrical conductivity of the concrete (Andrade, 2005, Layssi et al., 2015). In addition, the number of fibres added as well as their geometry and orientation control the conductivity of the composite material in case of SFRC (Chen et al., 2004, Holschemacher et al., 2006, Lataste et al., 2008). How exactly these and other parameters influence the electrical conductivity will be shown in the following.

- **Porosity**

In principle, it can be assumed that the conductivity of the pore solution exceeds that of the matrix by far. Accordingly, the electrical resistance decreases with increasing porosity (Müller, 2000). This is since in concrete the pore solution is mainly responsible for ion transport (Reichling, 2014). Within the concrete, continuous conduction channels ensure high conductivity. Conversely, closed, or ink bottle pores only contribute to a limited extent to increasing this parameter (Müller, 2000).

One tool for evaluating porosity is the so-called formation factor. It is formed from the quotient of the resistances of the electrolyte solution and the sample with complete pore filling. This relationship forms the basis for Archie's 1st law. This is often used in the evaluation of electronic measurements and is formulated in (eq. *2-23*) (Archie, 1942, Müller, 2000).

$$F = \frac{R_{Sw=100\%}}{R_{Lsg}} = P^{-m} \qquad \text{(eq. 2-23)}$$

with:

$R_{Sw=100\%}$	Electrical resistance with complete pore filling in Ω
R_{Lsg}	Electrical resistance of the electrolytic solution in Ω

P Porosity in %
m Material specific exponent

In addition to the formation factor, tortuosity offers a suitable approach for making qualitative statements about porosity. This describes the lengthening of the path, which is associated with the fact that in porous materials there is no straight path between the two electrodes. The path through the capillaries is rather tortuous or interrupted (Müller, 2000). There are several different formulas for quantifying the tortuosity, Winsauer et al. for example propose (eq. *2-24*) (Winsauer et al., 1952):

$$T = \left(\frac{l_{eff}}{l_{Specimen}}\right)^2 \qquad \text{(eq. 2-24)}$$

with:

l_{eff} Effective length of the capillaries in mm
$l_{Specimen}$ Length of the specimen in mm

In his work, Müller investigated the usability of the formatting factor and tortuosity for conductivity measurements of building materials. According to this, the formation factor is only suitable to a limited extent for making a statement about the rock conductivity. It makes more sense to determine the tortuosity. A low tortuosity value is associated with a high porosity (Müller, 2000).

The previously mentioned parameters have the disadvantage that only the pore system of the materials is considered. However, cracks in the concrete can be significant sources of error in the measurement of conductivity. Azarsa & Gupta describe that the conductivity of a cracked concrete can contain an error of about 200 % in contrast to the actual resistivity. This is since the crack represents a continuous channel for ion transport in the pore solution (Azarsa & Gupta, 2017).

- **Water Saturation**

Numerous studies have been carried out in the literature on the interaction between the amount of pore solution and electrical resistance. The result of the investigations is unanimous: as the amount of pore solution decreases, the electrical resistance increases (Bürchler, 1996, Elkey & Sellevold, 1995, Jamil et al., 2013, Presuel-Moreno & Liu, 2012, Zapico, 2015). The conductivity of the pore solution is even the parameter that makes the greatest contribution to the conductivity of the concrete (Müller, 2000). In a hydrated and water-saturated concrete, the electrical resistivity is approximately between 10 and 500 Ωm. With increasing drying, the resistivity increases rapidly, especially in edge areas. Interior components, for example, can reach an electrical resistivity of up to 10 MΩm after a few years (Raupach et al., 2007).

These results are mainly explained by the fact that at low saturations there is also little water in the pores. However, since the pore solution is the carrier of the ions, this is equivalent to a low conductivity due to the inhibited ion flow (Zapico, 2015).

The relationship between water saturation and resistivity is visualised in Figure 2.24. Although the test set-ups and test specimens with different water/cement ratios are different, the curves can be compared well. It can be seen that the resistivity increases exponentially with decreasing water content (Gjørv et al., 1977).

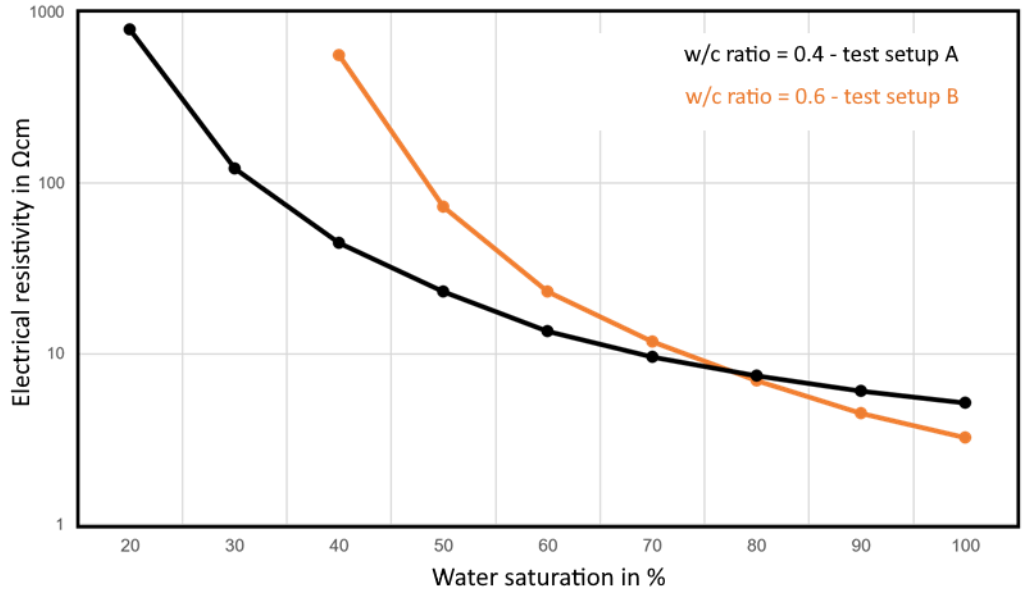

Figure 2.24 Influence of water saturation on electrical resistivity (Gjørv et al., 1977)

- **Pore Solution**

In the pore solution, the current flow takes place mainly through anions and cations. The conductivity is thus dependent on the type and number of ions contained in the solution (Müller, 2000, Reichling, 2014).

Formally, the electric current I of an electrolyte can be described with the help of (eq. *2-25*). Applied to Ohm's law, the electrical conductivity of a solution with a known composition can be calculated (Bürchler, 1996).

$$I = F * A_Q * E * \sum_{i=1}^{n} c_i * u_i * |z_i| \qquad \text{(eq. 2-25)}$$

with:

F	Faraday constant in A*s/mol
A_Q	Cross-sectional area in m²
E	Electric field strength in V/m
n	Number of ions
c_i	Concentration of the ion type i in mol/m³
u_i	Mobility of the ion type i in m²/(V*s)
z_i	Valence of the ion i

According to this, the conductivity of a concrete pore solution is mainly dependent on the concentration of the ions, their valence, and their mobility, in addition to its composition. An increase in these values accordingly causes an increase in conductivity (Müller, 2000).

Overall, however, the influence of the pore solution is small as long as an alkaline environment remains. At high pH values, the electrical resistivity is between 30 and 100 Ωcm. If the concrete is carbonated, however, the resistivity increases, making the influence of this parameter more significant (Andrade, 2005).

- **Concrete Composition**

The conductivity of a concrete depends, as described, on the pore system of the material. The structural formation of the material is influenced by several factors. In addition to the water-cement ratio (w/c ratio), all ingredients such as the aggregate, the cement and any additives should be mentioned (Azarsa & Gupta, 2017, Lübeck et al., 2012, Ramezanianpour et al., 2014, Zapico, 2015). The effects on the structure of the concrete - with regard to conductivity - will be explained in this section.

The w/c ratio is one of the main factors determining the permeability of a concrete. In his dissertation, Reichling was able to establish not only a correlation of the porosity via the formation factor with the tortuosity, but also with the w/c ratio. (Reichling, 2014)

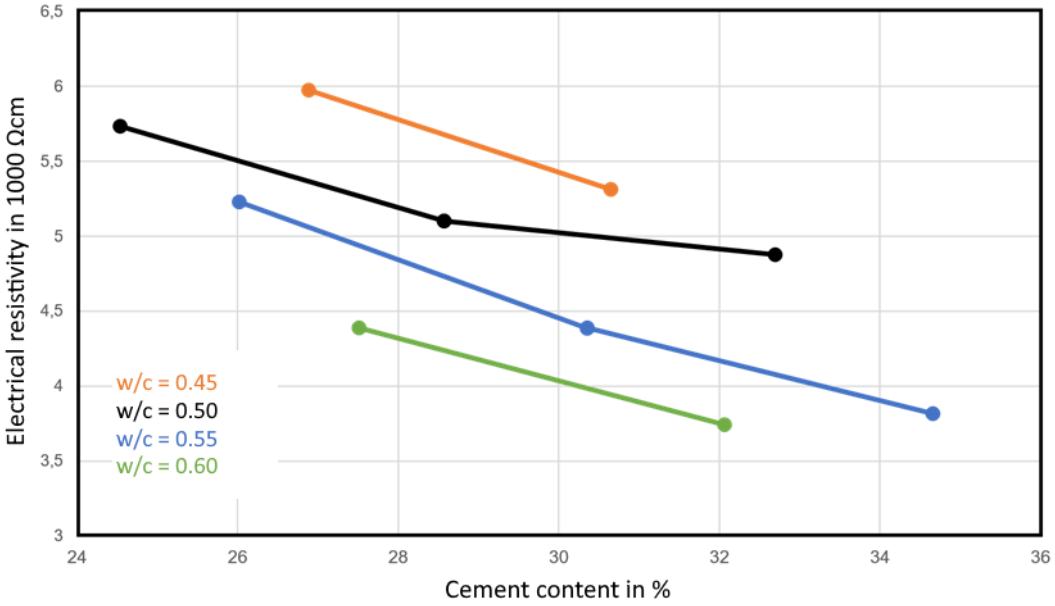

Figure 2.25 Influence of the cement on the electrical resistivity (Elkey & Sellevold, 1995)

High w/c ratios lead to a high porosity, i.e., a pronounced pore system that can absorb more water. Thus, the conductivity also increases with an increasing ratio of liquid to cement, which can be seen in Figure 2.25 (Azarsa & Gupta, 2017). A study carried out by Monfore in this context concludes that an increase in the w/c ratio from 0.4 to 0.6 is accompanied by a halving of the resistivity. The relationship can be assumed to be approximately linear (Monfore, 1968, Whiting & Nagi, 2003).

Also cement type and content exert an influence on conductivity. The reduction of the cement content at the same w/c ratio causes an increase of the electrical resistivity. The more cement paste is present, the more channels for the concrete pore solution are created in the hardened product. As can be seen in Figure 2.25, there seems to be no interaction between the w/c ratio and the cement content. The slopes of the curves are almost identical regardless of the w/c ratio considered. (Elkey & Sellevold, 1995, Hughes et al., 1985).

In addition to the cement content, different cement compositions also cause different conductivities. According to Malakooti et al., cements differ depending on their chemical composition and the associated number of ions (Malakooti et al., 2019). In principle, it should be noted that the resistivities of Portland cements are lower than those of cements with other constituents, such as trass or ground granulated blast-furnace slag. These additives can lead

to a change in tortuosity, which in turn influences the conductivity (Banea, 2015, Weigler & Karl, 1989).

The pozzolanic substance silica fume is a by-product of the condensation of evaporating silicic acid. The grains are spherical with a diameter of between 0.05 and 0.5 µm and a specific surface area of around 22 m²/g and thus, much finer than cement grains. Silica fume is mainly used to increase the concrete resistance or to create an impermeability against chlorides, chemicals or similar (Weigler & Karl, 1989). Mixing in silica fume results in higher resistances. Although the electrical resistances are lower in the first seven days after production, they increase even more rapidly thereafter (Tumidajski, 2005). Silica dust leads to a finer pore structure with a simultaneous decrease in ion concentration. The larger the proportion of dust, the greater the changes to be expected (Berke et al., 1992, Elkey & Sellevold, 1995, Hauck, 1993). According to Mazloom et al. the use of 5 and 10 % silica dust leads to an increase in electrical resistance of 43 and 139 % respectively compared to the control mixture (Mazloom et al., 2017).

Fly ash is produced during the combustion of ground or pulverised materials in coal-fired power plants. These fuels contain mineral fractions that melt and solidify to a glassy consistency during the processing procedure. This creates smooth and spherical structures. The chemical composition of fly ash varies greatly, as does its grain size. Fly ash is mostly used to optimise workability and water demand of the concrete (Weigler & Karl, 1989). Studies by Montemor et al. show that fly ash contributes to a reduction in concrete porosity. Less porous structures lead to lower tortuosity. Thus, substitution with fly ash in a mix results in an increase in resistance by a factor of ten (Montemor et al., 2000). Naik et al. came to the same conclusion in their study. Concretes with fly ash show lower electrical resistivities across all mixtures. The spectrum of the electrical resistance of the test specimens with fly ash ranges from 173 to 60,000 Ωcm, whereas that of the specimens without fly ash only ranges from 131 to 50,000 Ωcm (Naik et al., 2010).

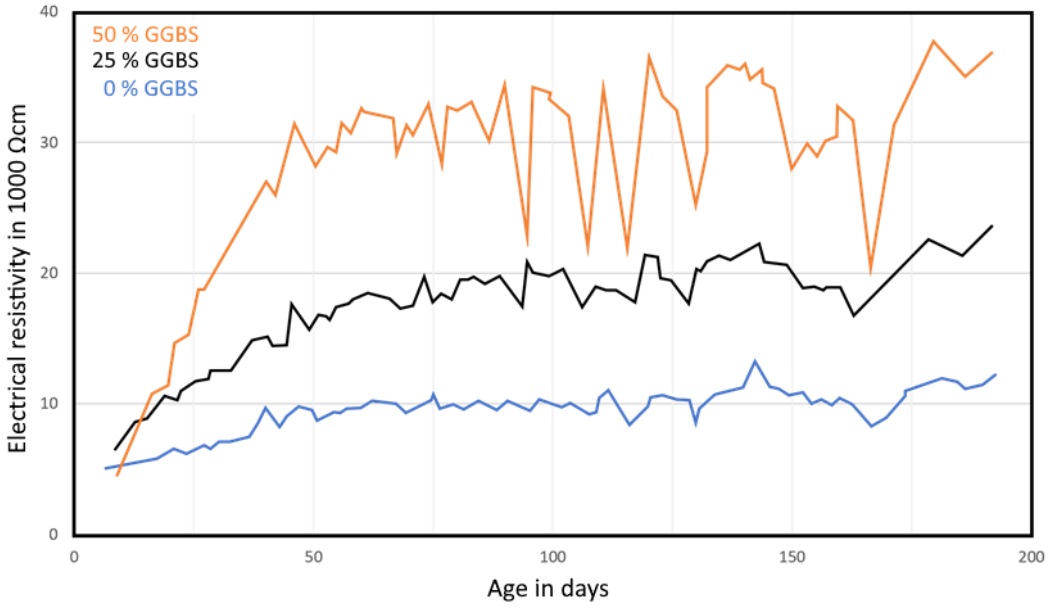

Figure 2.26 Influence of granulated blast-furnace slag on electrical resistivity (Hope & Ip, 1987, Whiting & Nagi, 2003)

Unlike the previously mentioned additives, ground granulated blast-furnace slag is not a pozzolanic but a latent hydraulic substance consisting of calcium silicate aluminate compounds. GGBS is produced during pig iron production in the blast-furnace, more precisely during the rapid cooling of slag melt. The hydrated lime split off from the Portland cement during hydration serves as an exciter for the hydraulic reaction of the material (Weigler & Karl, 1989). Hope and Ip investigated the effects of GGBS on the electrical resistance. Three different concretes, each with 0 %, 25 % and 50 % GGBS, were measured over 200 days. After only a few days, it can be seen that a high proportion of ground granulated blast-furnace slag results in a higher resistivity due to the denser structure. The exact curves can be seen in Figure 2.26 (Hope & Ip, 1987, Whiting & Nagi, 2003).

With trass, limestone and metakaolin, further additives were investigated by Ramezanianpour et al. While the electrical resistivity of concrete with limestone deviates only insignificantly from normal concrete at the beginning of the measurements, after 90 days a 14 % lower value can be observed in the mixture without limestone. The measured resistivities of concretes with metakaolin are again 68.2 % and 15.3 % higher than those of concretes with limestone and trass. This can be explained by the fact that metakaolin is better able to fill the capillary pores, which results in reduced permeability (Ramezanianpour et al., 2014).

In summary, the fine additives result in a lowered conductivity of the concrete. They ensure that the pore structure is refined. As a result, less conductive pore solution can penetrate the material. This finding can be taken from numerous other studies. The works of Liu and Presuel-Moreno, Lübeck et al., Topçu et al., Gastaldini et al. and many others (Gastaldini et al., 2009, Liu & Presuel-Moreno, 2014; Lübeck et al., 2012; Topçu et al., 2012) should be mentioned here.

Basically, the aggregate has a significantly lower conductivity than the hardened cement paste. This is since most aggregates are less porous. In addition to the amount of aggregate used, its size and type also have an influence on the conductivity of the material (Azarsa & Gupta, 2017). Increasing the proportion of aggregate leads to an increase in resistance because the pore space becomes smaller. A similar result is obtained when using large aggregates. The larger the aggregate, the less conductive the material.

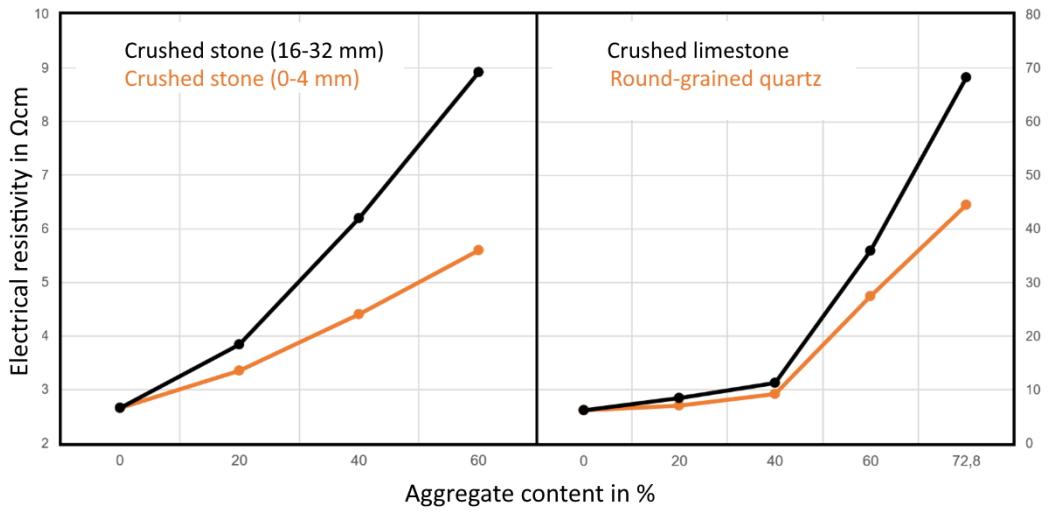

Figure 2.27 Influence of aggregate size on resistivity (Sengul, 2014)

Further investigations into the type of rock revealed that a higher resistance is always measured for broken grains than for round grains (Azarsa & Gupta, 2017, Sengul, 2014). To illustrate these facts, Figure 2.27 shows the relationship between grain size, proportion and shape and resistivity.

The influences described so far are mostly based on charge transport in the concrete pore solution. However, steel fibres are a second-order conductor in which the transport is performed due to the mobilisation of electrons in a metal lattice (Reichling, 2014). Therefore, the choice of fibre is relevant to the results of the resistance measurement. In the literature, work can be found regarding fibre type, fibre content and orientation.

Significant differences can be seen in the resistivity of carbon and steel fibres (in Table 2.3). In the measurements carried out by Banthia et al., significantly lower resistances can be seen in the fibre reinforced concrete after just one day. Adding one percent of steel fibres reduces the resistance of the concrete by about half. This tendency is even more pronounced with carbon fibres. In addition, increasing the fibre content is accompanied by a reduction in resistance. (Banthia et al., 1992).

Table 2.3 Electrical resistivities of different fibre materials (Banthia et al., 1992)

Fibre type	**Fibre volume fraction in %**	**Electrical resistivity in Ωcm at age of concrete of**		
		1 day	**7 days**	**28 days**
No fibre	-	1.594	11.638	66.117
Carbon fibre	1	83	249	820
	3	34	101	349
	5	17	35	78
Steel fibre	1	769	4.886	31.921
	3	585	2712	14.860
	5	251	1404	7.439

A comparison of carbon and steel fibres shows that the conductivity of the former is lower. Nevertheless, higher conductivities can be recorded for carbon fibre reinforced concrete than for steel fibre reinforced concrete, which indicates that the distribution and dimensions play a decisive role (Holschemacher et al., 2006).

Also of importance for the conductivity is the fibre length. Longer fibres have a positive effect on the conductivity of the material. Longer fibres are more likely to form a continuous fibre-to-fibre contact throughout the specimen than short ones. However, this only applies to low fibre contents (Chen et al., 2004).

In addition to the content and length, the orientation of the fibres is also relevant. Maximum conductivity is achieved when the fibres run parallel to the direction of measurement. This orientation creates conduction channels that favour electron transport between the poles. At the same time, measured resistances are always higher with fibres perpendicular to the direction of measurement than with the previously described orientation (Lataste et al., 2008, Zapico, 2015).

- **Age of Concrete**

In general, it can be stated in this context that the electrical resistance of a concrete increases with time (Zapico, 2015). The reason for this is a combination of the processes of hydration (Daniel et al., 2001, Gjørv et al., 1977, Liu & Presuel-Moreno, 2014), leaching (Spragg et al., 2017) and evaporation (Daniel et al., 2001). Additionally, a water storage leads to a significant reduction in electrical resistance over time (Wedding et al., 1979).

2.4 Summary of Literature

The literature analysed the necessity and applicability of the development of a test method, based on electrical resistivity measurements in order to determine the fibre content and orientation of SFRC specimens. Herein the influences of fibre content and orientation on the mechanical properties are analysed. Both parameters show significant effect on the transmittable tensions in the compound material. Hence, for the fibre content a critical value can be determined, which enables an estimation of the necessary fibre content for an optimum design of SFRC. Analysing the fibre orientation, it is visible that in SFRC fibres oriented parallel to the tensile forces show the best crack bridging properties. Thus, the determination of both parameters has to be enabled to economically calculate the statics of an SFRC element without using rough estimations that lead to high safety parameters and thus lower design parameters.

In addition, common and experimental test methods for the determination of fibre content and orientation of SFRC are presented and discussed. While there a plenty of test methods for laboratory applications, only two methods are standardized so far for construction side application, which both are based on manually counting of fibres after eliminating the concrete matrix. Besides these methods an excellent method for a detailed analysis of fibre content and orientation is CT-scanning. Nevertheless, this method needs a significantly higher investment and know-how and is limited to small specimens only. Other methods like inductive measurements or microwave analysis are used in laboratory tests of several researchers but are not usable as standard test method because of their state of development. Electrical resistivity measurements on the other hand are to be used for material analysis in lab scale as well as for structural diagnostics (multi ring electrodes), but the application for the analysis of SFRC is still lacking.

To look on this method in more detail, the fundamentals of electrical resistivity and especially measurement principles were shown, supplemented by influencing parameters of the electrical resistivity of concrete and SFRC. These parameters have to be considered for the development of a test setup to ensure that the test method is applicable and sufficiently accurate.

For these reasons, in the four scientific publications presented below the development, testing and verification of a novel test based on electrical resistivity measurements is demonstrated and discussed. Hereby the focus was set of an easy-to-use setup to measure fibre content and orientation that is applicable for lab and construction side conditions.

3 Initial Investigations on Concrete Cubes

This section was published as scientific paper under the title “Electrical Resistivity of Steel Fibre-Reinforced Concrete — Influencing Parameters” in the journal Materials in 2021 (Cleven et al., 2021).

3.1 Abstract

This paper presents a systematic study of the electrical resistivity of different steel fibre-reinforced concretes with fibre contents from 0 kg/m³ to 80 kg/m³ in order to identify possible effects of interactions among concrete composition and fibre type and content regarding electrical resistivity. Based on a literature review, four parameters, w/c ratio, binder content, ground granulated blast-furnace slag (GGBS) and fineness of cement, which show a significant influence on the electrical resistivity of plain concrete, were identified, and their influence on the electrical resistivity as well as interaction effects were investigated. The results of the experiments highlight that the addition of fibres leads to a significant decrease in electrical resistivity, independent of all additional parameters of the concrete composition. Additionally, it was shown that a higher porosity of the concrete, e.g., due to a higher w/c ratio, also results in a lower electrical resistivity. These results are in agreement with the literature review on plain concrete, while the influence of the concrete composition on the electrical resistivity is weaker with the increase in fibre content. The influence of fibre reinforcement is thus not affected by changes in the concrete composition. In general, a higher fibre dosage leads to a decrease in electrical resistivity, but the impact on the electrical resistivity varies slightly with different types of steel fibres. Based on this study, the potential of determining the fibre content using electrical resistivity measurements could be clearly presented.

3.2 Introduction

As a commonly used composite material for civil construction steel fibre-reinforced concrete (SFRC) combines the positive aspects of both basic materials with respect to its load bearing behaviour (see e.g., Di Prisco et al., 2009; Ding et al., 2019; Ferdosian & Camões, 2021; Kachouh et al., 2019; Lehner et al., 2020; Shan & Zhang, 2014). Since the plain concrete has excellent resistance to compressive forces but has almost no ability to withstand tensile stresses, the fibre fraction takes up the remaining tensile forces. With this material, one can produce elements in almost every shape, with sufficient durability and improved mechanical characteristics (see e.g., Hedjazi & Castillo, 2020; Kobaka et al., 2019; Luo et al., 2020; Song & Hwang, 2014; Zhang et al., 2019). Principal applications of SFRC include industrial floorings, structures in seismic zones or underground construction and applications where structures are exposed to torsion, impact, or fatigue (see e.g., Brandt, 2008; Facconi et al., 2021; Li et al., 2019). One disadvantage of this type of construction material is the huge influence of fibre content, distribution, and orientation on its mechanic properties (see e.g., Barnett et al., 2010; Gettu et al., 2005; Li et al., 2018; Martinelli et al., 2021a; Martinelli et al., 2021b). There are studies which show that the mechanical parameters of identical concrete specimens can differ up to 20 % (see e.g., Molins et al., 2009) due to a lack of control of the fibre fraction of the concrete. For this reason, large safety factors must be used for static calculations.

While the fibre content in new construction projects can easily be determined by washing fibres out of a defined fresh concrete sample or by checking the weighing protocols, in hardened concrete or existing constructions, to date, there is no easy method to calculate the exact fibre content. One non-destructive test method that seems to be suitable for the determination of

fibre content and orientation in concrete is to measure the electrical resistance of the concrete (see e.g., Berrocal et al., 2018; Karhunen et al., 2010; Lataste et al., 2008; Lataste et al., 2010; Layssi et al., 2015; Mason et al., 2002; Ozyurt et al., 2006a; Ozyurt et al., 2006b; Torrents et al., 2000; Walsh et al., 2018; Woo et al., 2005). Resistance measurements with so called multiring-electrodes are well known to monitor the durability of concrete, with respect to potential corrosion processes of steel rebars (see e.g., Raupach et al., 2006; Raupach et al., 2013; Reichling, 2014; Reichling & Raupach, 2012).

The degree of water saturation of the pore structure of the concrete, the porosity and the conductivity of the pore solution are the most relevant influencing factors for the electrical resistivity of concrete (see e.g., Andrade, 2005; Bürchler, 1996; Layssi et al., 2015; Reichling et al., 2015). Nevertheless, it should be considered, that the influence of the pore solution chemistry is relatively small, unless extreme drying and carbonating effects take place. In general, the composition of the pore solution changes with the ongoing hydration process due to hydration reactions and related dissolution processes of ions, especially during early age until 28 days of hydration. Typically, the chemical composition stabilises afterwards and shows an electrical resistivity in a range between 0.3 and 1 Ωm (see e.g., Andrade, 2005; Bürchler, 1996).

For SFRC, the fibres have a significant influence on the conductivity of the material due to their ability to function as metallic conductor in contrast to the pore solution which only conducts electricity via ionic transfer (see e.g., Chen et al., 2004; Hedjazi & Castillo, 2020; Lataste et al., 2008; Reichling & Raupach, 2012). Therefore, for the concrete, if investigated under controlled humidity, especially the pore structure influences the resistivity and in turn is influenced by the process of hydration and the concrete composition (see e.g., Mouhasseb, 2007). By screening the literature several other parameters become apparent, which affect the pore structure of concrete, such as water/cement ratio, cement content and the concrete ingredients, e.g., type of cement or applied supplementary cementitious materials and aggregates (see e.g., Azarsa & Gupta, 2017; Chen & Brouwers, 2006; Cosoli et al., 2020; Elkey & Sellevold, 1995; Hughes et al., 1985; Liu et al., 2014; Lübeck et al., 2012; Monfore, 1968; Polder & Ketelaars, 1991; Ramezanianpour et al., 2014; van Beek & Stenfert Kroese, 2019).

The most influencing parameters on the porosity and, therefore, on the electrical resistivity of concrete are the water/cement ratio and the cement content. An increasing water/cement ratio is paired with an increase in porosity; therefore, a decrease in electrical resistivity due to an enlarged capillary network is observed. The total amount of water, at a constant w/c ratio, is influenced by the cement content, which also influences the total porosity. At constant cement content, an almost linear decrease in electrical resistivity is visible with increasing water/cement ratios between 0.4 and 0.6, while higher cement contents at a constant w/c ratio also lead to decreasing electrical conductivity. Both parameters are independent of each other and showed no interactions (see e.g., Azarsa & Gupta, 2017; Chen & Brouwers, 2006; Cosoli et al., 2020; Elkey & Sellevold, 1995; Hughes et al., 1985; Liu et al., 2014; Monfore, 1968; Polder & Ketelaars, 1991; van Beek & Stenfert Kroese, 2019).

Different types of cement as well as the use of SCM significantly affect the conductivity of the pore solution as well as the resulting pore structure of the concrete. In general, ordinary Portland cements show the lowest electrical resistivity, while the use of different cement types or the addition of silica fume, fly ash or ground granulated blast-furnace slag (GGBS) significantly decreases the porosity of the concrete, thus leading to an increase in electrical

resistivity. Mainly due to the pozzolanic or latent-hydraulic reaction of SCMs, such as GGBS, silica fume or fly ash the pore structure becomes finer and less permeable, and thus the conductivity of the pore solution is reduced. The same phenomenon can be observed using finer cements, such as cements with higher strength classes (see e.g., Cosoli et al., 2020; Gastaldini et al., 2009; Hauck, 1993; Hope & Ip, 1987; Liu & Presuel-Moreno, 2014; Lübeck et al., 2012; Mazloom et al., 2017; Montemor et al., 2000; Naik et al., 2010; Topçu et al., 2012; Tumidajski, 2005).

Additionally, aggregates may influence the conductivity of concrete, since different grain size distributions or water absorption capacities of these concrete components can influence the total porosity of the concrete. For example, the use of crushed aggregates leads to a higher electrical resistivity than round grain shapes. Additionally, a greater maximum grain size increases the electrical resistivity as large grains are non-conducting and increase the tortuosity of the concrete (see e.g., Azarsa & Gupta, 2017; Sengul, 2014). It must be mentioned that in some cases conductive aggregates are also used for concrete, which leads to a significant decrease in the electrical resistivity.

One additional parameter that may have a large effect on the electrical resistivity independent of the concrete composition is the aging of the concrete as a function of service exposure, which is paired with changes in the pore structure and also impacts leaching and drying processes. Furthermore, the continuing hydration process leads to a refinement and densification of the pore structure, thus increasing electrical resistivity. The same effect occurs due to ion leaching effects (see e.g., Daniel et al., 2001; Gjørv et al., 1977; Liu & Presuel-Moreno, 2014; Spragg et al., 2017).

When studying SFRC, the use of conductible fibres, e.g., steel, also contributes to electric conduction processes and thus significantly affects the electrical resistivity of the composite material. Since steel is a metallic conductor, the fibres have a substantially higher conductivity than the concrete. Therefore, by the addition of steel fibres, a composite is formed, which includes a combination of parallel and serial electrical connections. Thus, the electrical resistivity of the composite is dependent on the amount of fibre and orientation in the structure. A high fibre content leads to a significant decrease in electrical resistivity, and fibres with a parallel orientation to the electrical transport direction reduce resistivity. In addition, the geometry of the fibres influences conductivity. Small fibres, in general, tend to show an even distribution and orientation, whereas the use of longer fibres increases the probability of direct fibre to fibre contacts, which leads to a short circuit and, therefore, to almost no influence of the concrete on the electrical conductivity. These effects of fibre length, however, only take place at low fibre dosages (see e.g., Banthia et al., 1992; Chen et al., 2004; Lataste et al., 2008).

Measurements of the electrical resistivity of the concrete show a high potential for use as non-destructive test method for the determination of the fibre content of SFRC, and thus possible negative effects of other parameters have been known to enable sufficient and accurate results by the use of an easy test setup. Even though, in the past, investigations have been performed to show the influence of fibres on the electrical resistivity (see e.g., Berrocal et al., 2018; Karhunen et al., 2010; Lataste et al., 2008; Lataste et al., 2010; Layssi et al., 2015; Mason et al., 2002; Ozyurt et al., 2006a; Ozyurt et al., 2006b; Torrents et al., 2000; Walsh et al., 2018; Woo et al., 2005) or to analyse effects of the concrete composition on the permeability or electrical resistivity of concrete (see e.g., Andrade, 2005; Banthia et al., 1992; Bürchler, 1996; Chen et al., 2004; Chen & Brouwers, 2006; Elkey & Sellevold, 1995; Hughes et al., 1985; Liu

et al., 2014; Monfore, 1968; Mouhasseb, 2007; Polder & Ketelaars, 1991; van Beek & Stenfert Kroese, 2019), a systematic study that combines the effects of SFRC and different parameters of the concrete composition is lacking.

In this study, the effects of concrete composition in combination with the addition of fibres on the electrical conductivity are studied. The aim of this paper is to identify single effects and interactions which allow a model to be constructed and/or represent an important dataset for the future development of a test method for the determination of fibre content and orientation on fresh and hardened concrete based on electrical resistivity measurements. With the help of such a novel test method, it is possible to simplify monitoring processes for SFRC and to allow a more precise prediction of the mechanical characteristics of SFRC, which could lead to static calculations with lower safety factors and thus to a higher acceptance of SFRC in fields of construction.

3.3 Materials and Methods

3.3.1 Materials

3.3.1.1 Characterisation of Materials

For the experiments presented in this paper, we decided to use three different ordinary Portland cements originating from the same cement plant with strength classes of 32.5 N/mm², 42.5 N/mm² and 52.5 N/mm², as these types are commonly used, and neither negative interactions based on chemical reactions in combination with ground granulated blast-furnace slag (GGBS) nor changes in clinker composition for the different cements should take place. Additionally, the use of GGBS was investigated in different mixtures. Quartzite gravel with a grain size distribution of A/B 16 in accordance with DIN 1045-2, 2008 was the used aggregate.

The binder components, cements and GGBS, were analysed regarding density and fineness to consider these factors in the evaluation of the measurements of the electrical resistivity. The results are presented in Table 3.1.

Table 3.1 Characterisation of the cements and supplementary cementitious materials.

Binder	Density in g/cm³	Specific surface in cm²/g
CEM I 32.5 R	3.15	3000
CEM I 42.5 R	3.14	3670
CEM I 52.5 R	3.15	4320
GGBS	2.91	4240

All three cements showed almost the same density, while the GGBS had an 8 % lower density. This difference was taken into account for the concrete mix design. The cements were selected to differ in fineness, so the results of specific surface according to Blaine optimally fulfilled this requirement. The specific surface of the CEM I 52.5 R exceeded that of the CEM I 32.5 R by 44 %, and the specific surface of CEM I 42.5 R, which is 22 % higher than that of the CEM I 32.5 R, almost presented the mean value of the two other cements. The specific surface of the GGBS, as expected, exceeded that of the less fine cements and was in the same range as the CEM I 52.5 R.

Table 3.2 Parameters of the used fibres

Parameter	Unit	Fibre 1	Fibre 2	Fibre 3
Fibre type	-	Macrofibre	Macrofibre	Microfibre
Material	-	steel wire	steel wire	steel wire
Coating	-	-	-	brass
Length	mm	60	35	8
Diameter		1	0.75	0.175
l/d ratio	-	60	46.7	45.7
Fibre quantity	pieces/kg	2600	8200	662000

Three different steel fibres were used as the reinforcement materials for the experiments. While fibre 1 and fibre 2 are hooked-end macro steel fibres, produced as wired fibres, fibre 3 is a straight micro steel fibre with a brass coating. Fibre 1 represents a type of steel fibre that is commonly used in Europe for SFRC. In contrast, fibre 3 is recommended for use in UHPC, as presented in Kalthoff & Raupach, 2021. Fibre 2 was chosen due to its geometry, which is directly in between those of the other fibres. The fibres differ in length, diameter and aspect ratio, but the greatest difference is the fibre quantity. While there are 2600 fibres of type 1 per kg, the quantity of fibre 3 with 662,000 fibres is almost 250 times higher. A characterisation of the fibres is given in Table 3.2, and a graphical presentation of the fibres is presented in Figure 3.1.

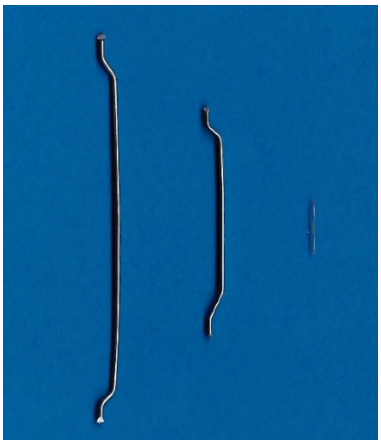

Figure 3.1 Shapes of the used fibres (left: fibre 1; middle: fibre 2; right: fibre 3)

3.3.1.2 Basic Concrete Mix Design

The electrical conductivity of both plain concrete (PC) and steel fibre-reinforced concrete (SFRC) was investigated on various concrete mixtures to identify the effects of different parameters of the concrete composition on electrical resistivity. For this purpose, a basic concrete mixture according to EN 206, 2017 in combination with DIN 1045-2, 2008 was chosen and investigated.

The basic concrete composition is given in Table 3.3. A cement content of 300 kg/m³ of CEM I 32.5 R in combination with a water/cement ratio of 0.60 was used to obtain a sufficient workability with the use of a high amount of steel fibres. For the reinforcement, fibre 1 (Table 3.2) was chosen, and fibre contents from 0 kg/m³ to 80 kg/m³ were applied. No superplasticizer was used.

Table 3.3 Concrete mix design of the basic concrete

Parameter	Unit	Content
CEM I 32.5 R	kg/m³	300.0
GGBS		-
Water		180.0
Aggregates		1849.5
Water/cement ratio		0.60
Grain size distribution	-	A/B16
Steel fibre type	kg/m³	Macrofibre 60 mm
Steel fibre content		0 to 80

Every concrete batch within this study was produced according to the following scheme with a material volume of 60 L. The homogenisation of the solid materials, such as cement, GGBS and aggregates, was performed in a compulsory mixer with a nominal volume of 160 L for 30 s. In the next step, the water was added during the ongoing mix process, and the concrete was mixed for at least two minutes. After a visual inspection of the homogeneity of the concrete, adhering components were removed from the mixer wall, followed by an additional mixing time of one minute.

Directly after the mixing process, the consistency of the concrete was determined via a flow table test in accordance with EN 12350-5, 2019. Additionally, the air content and fresh concrete density in accordance with EN 12350-6, 2019 and EN 12350-7, 2019, respectively, were determined. After the execution of the fresh concrete tests, samples of 4 L of concrete were placed in a small bucket mixer with a mixing volume of a maximum of 10 L. Defined amounts (between 10 kg/m³ to 80 kg/m³) of steel fibres were added into the bucket mixer, and the fresh concrete was mixed for approximately one minute to ensure the correct fibre amounts. Then, cubical steel formworks with dimensions of 150 mm³ were filled with the SFRC. One additional reference specimen was produced using the plain concrete without fibres.

After the production, the specimens were left in the formworks for approximately 24 h and covered with foil to prevent drying of the surfaces. The upper surfaces of the demoulded specimen were removed by grinding since a flat surface was recommended to reach optimal conditions for the electric connection. Afterwards, the dimensions of the specimens were determined, and they were stored in 2.7 L of regular water each at a temperature of 20 °C in separate storage boxes till testing.

In total, 180 specimens were investigated, including the basic concrete mixture, ten additional mixtures for the single parameter variation and eight mixtures for the multiple parameter variation with nine specimens each and nine specimens for the investigations of possible leaching effects.

3.3.2 Experimental Methods

3.3.2.1 Design of Experiments—Single Parameter Variation

For the identification of changes in single parameters of the concrete mix design, several mixtures with one varying parameter were produced and investigated. The following parameters were varied individually in order to prevent interactions based on combined variations:

- Cement type (CEM I 32.5 R, CEM I 42.5 R and CEM I 52.5 R) (all from the same plant);
- Water/cement ratio (0.55, 0.60 and 0.65);
- Binder content (270 kg/m³, 300 kg/m³ and 330 kg/m³);
- Content of GGBS (replacement of 0 %, 35 % and 65 % of total binder);
- Fibre type/geometry (macro steel fibre 60 mm, macro steel fibre 35 mm and micro steel fibre 8 mm).

In total, based on the basic concrete mix design, ten additional concrete mixtures were produced and investigated with fibre contents from 0 kg/m³ to 80 kg/m³, so each of the 5 parameters could be observed at three levels to identify possible effects and evaluate if there is a linear or non-linear correlation. The mix designs of the additional concretes are presented in Table E.1 to Table E.5, Annex E.

3.3.2.2 Design of Experiments—Multiple Parameter Variation

To identify interactions between different parameters of the concrete composition, the software Minitab (19.2020.1, Minitab LLC, State College, PA, USA) was used to develop a statistical design of experiments. Based on the basic concrete mix design (Table 3.3), the cement type of the parameters, the w/c ratio, the binder content and the amount of GGBS were varied, and a matrix of 9 mixtures was investigated (Table 3.4). The fibre type was kept constant in these experiments to keep the number of mixtures as small as possible, and no large effects of the fibre type on the electrical resistivity were identified in the experiments with single parameter changes. An evenly distributed matrix of mixtures was important, so that each parameter at each of its three tested levels is presented three times within the complete evaluation. The mix designs of the additional concretes are presented in Table E.6 to Table E.9, Annex E.

Table 3.4 Statistical concrete matrix with combined variations

Concrete designation	Cement type	w/c ratio	Binder content in kg/m³	Amount of GGBS in %
32-55-270-35	CEM I 32.5 R	0.55	270	35
32-60-300-00 *	CEM I 32.5 R	0.60	300	0
32-65-330-65	CEM I 32.5 R	0.65	330	65
42-55-330-00	CEM I 42.5 R	0.55	330	0
42-60-270-65	CEM I 42.5 R	0.60	270	65
42-65-300-35	CEM I 42.5 R	0.65	300	35
52-55-300-65	CEM I 52.5 R	0.55	300	65
52-60-330-35	CEM I 52.5 R	0.60	330	35
52-65-270-00	CEM I 52.5 R	0.65	270	0

* Basic concrete mix design.

3.3.2.3 Investigations of Leaching Effects

In addition, the possible impact of leaching of the concrete during its storage was investigated. To identify this effect, one series consisting of nine specimens out of one batch of concrete was produced as described in Section 3.3.1.2. Samples produced from the basic concrete mix with fibre contents of 0 kg/m³, 40 kg/m³ and 80 kg/m³, three almost identical specimens of each fibre content, were tested. Directly after demoulding, the specimens were stored under varying

conditions. One specimen of each fibre content was stored in water as described above, while the other two specimens of each fibre content were exposed to alkaline solutions with higher pH to minimise leaching effects over time. Among these solutions was saturated calcium hydroxide solution, and another was synthetical pore solution with the composition presented in Table 3.5. The specimens were only taken out of their storage boxes for the measurements at concrete ages of 7 days, 14 days, 28 days, 56 days, 91 days and 185 days and afterwards stored in the same boxes again without a change in the storage medium with the aim of the harmonisation of the concrete and storage medium over time. The volume to surface ratio of all storage media was constantly 20 L/m³.

Table 3.5 Initial composition of synthetical pore solution

Component	Unit	Value
KOH		170
NaOH	mmol/L	17
$Ca(OH)_2$		23

3.3.3 Resistivity Measurements

Each specimen was taken out of the storage boxes at a concrete age of 7 days, and the electrical resistance between two opposite surfaces of the specimen was measured under wet surface conditions using an alternating current. The aim was to contact the whole surface due to the large ratio between the fibre length and dimensions of the specimen to inhibit the effects of single fibres or grains near the surfaces. To consider effects based on the inhomogeneity and anisotropy of the concrete, especially in the case of fibre addition, all three directions, two horizontal ones and the vertical direction, which is the pouring direction, were contacted consecutively using an LCR meter. Additionally, every direction was investigated with five different frequencies of alternating current, 100 Hz, 120 Hz, 1 kHz, 10 kHz and 100 kHz, with a voltage amplitude of 600 mV rms. The test setup is illustrated in Figure 3.2.

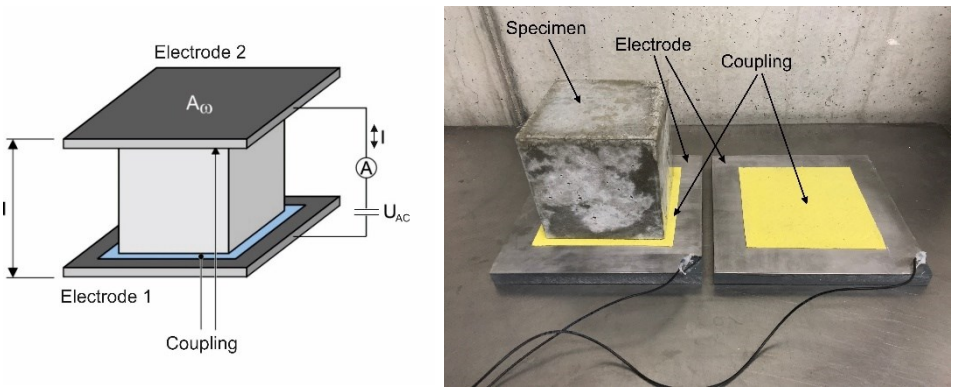

(a) **(b)**

Figure 3.2 Test setup for conductivity measurements, schematical setup (**a**) and photo of test setup with investigated specimen (**b**)

The whole test setup consisted of two stainless steel plates with edge lengths of 200 mm. Due to the uneven and porous surface of the concrete, a direct electrical connection of steel and concrete led to irreproducible results; therefore, a wet sponge cloth was used as a connector between both materials, and the humidity of the sponge was constantly checked to inhibit

drying effects. The steel plates were directly connected to the LCR meter via equally long cables. After placing the specimen between both electrodes, a defined reference weight was placed on top of the test setup to gain a constant and reproducible contact pressure.

Since the dimensions of the specimens slightly differed, the resistivity of the concrete for each direction was calculated by (eq. *3-1*).

$$\rho = R * k \qquad \text{(eq. 3-1)}$$

with:

ρ: *electrical resistivity in Ωm*
R: electrical resistance in Ω
k: geometry factor depending on dimensions of specimen in m (eq. 3-2)

$$k = A / l \qquad \text{(eq. 3-2)}$$

with:

A: effective contact area in m²
l: electrode gap in m

Due to the inhomogeneity and anisotropy of SFRC, it was necessary to carry out several measurements in three possible specimen directions. For this purpose, the resistivities of the three directions for each specimen were averaged, and the so called global electrical resistivity $\rho_{,g}$ was used to compare different specimens. Values for different directions were examined in detail in only a few instances. Even though the whole study was performed using a constant production method, effects based on the compaction, manufacturing of specimens and flowing behaviour of concrete and fibres would result in a considerable scatter of material characteristics, especially in fibre orientation and distribution, so the use of a global value independent of specimen orientation would ideally minimise this scatter. The calculated global electrical resistivity of the material represents the approximated electrical resistivity of an equivalent material with homogenous and isotropic behaviour in electrical conduction. All results of the calculations of the global electrical resistivity can be found in Table E.10 to Table E.52, Annex E.

3.4 Results

3.4.1 General Results of the Evaluation

In the first step, the influences of the frequency of the alternating current as well as the fibre content on the global electrical resistivity were analysed based on the results of basic concrete mixture. As seen in Figure 3.3 (a), an increasing frequency, as expected, led to a small decrease in the global electrical resistivity independent of the fibre content. Based on all 180 specimens, independent of concrete composition and fibre content, the main effect plot also shows the decrease in the electrical resistivity with a higher frequency, where a linear tendency is visible for a logarithmic increase in the frequency (Figure 3.3 (b)). In addition, it can be seen that there was an almost constant 95 % confidence interval for all frequencies. The main effect plot was calculated by Minitab by compiling the mean values of different groups of results to identify effects that are only caused by one parameter. In comparison to the influences of the concrete composition and the fibre addition, this tendency was scarce, so for this study, it could be neglected. Due to the independency of the alternating current and all other investigated parameters, which can be presumed based on the main plot by Minitab, for further

investigation, all the measurement results of the five frequencies were included in the evaluation, and the software Minitab was used to calculate the main effect plots to eliminate the effect of frequency and enlarge the database.

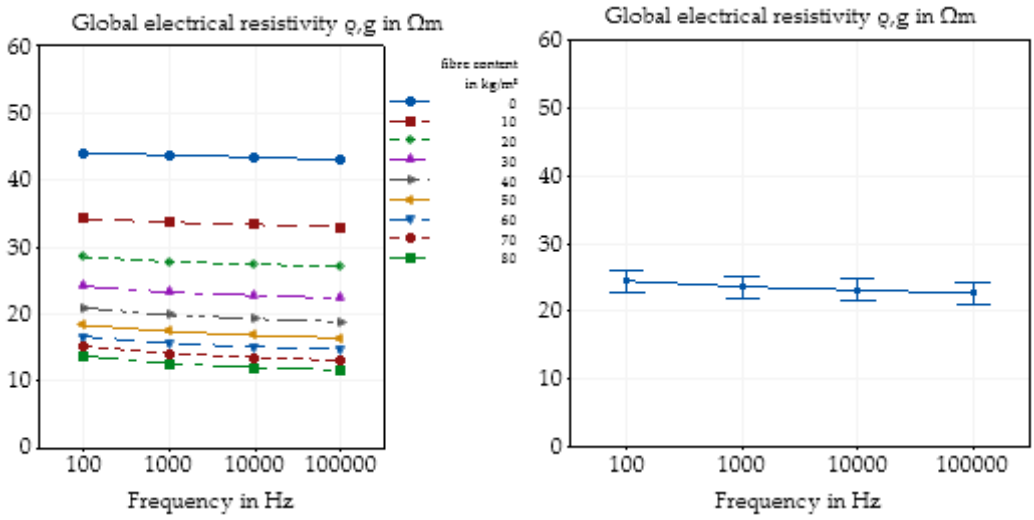

(a) **(b)**

Figure 3.3 Effect of different frequencies of alternating current on the global electrical resistivity of SFRC as function of the fibre content in the basic concrete mixture (**a**) and main effect plot with 95 % confidence interval of different frequencies of alternating current on the global electrical resistivity of SFRC calculated by Minitab based on all experimental data (**b**)

Additionally, as shown in Figure 3.4 (a), where the basic concrete mixture and the mixtures with the maximum and minimum electrical resistivity, respectively, are presented, the content of fibres in SFRC had a huge effect on the electrical resistivity. A higher fibre content, for this mixture, led to a lower resistivity. The same behaviour was visible for the main effect plot, including all specimens with different concrete mixtures and the 95 % confidence interval (Figure 3.4 (b)), which almost exactly presented the basic concrete mixture, indicating that the parameter variations led to both increasing and decreasing global electrical resistivities. With increasing fibre content, the difference in the electrical resistivity of varying concrete mixtures reduced in size. While the absolute difference of the maximum and minimum electrical resistivity for the plain concrete was 43.2 Ωm, that for a fibre content of 80 kg/m³ with 10.7 Ωm was significantly lower; however, the confidence interval for the mean values remained almost constant. Relative to the mean values, the maximum and minimum spread was 99 % for the plain concrete and 71 % for the SFRC with 80 kg/m³ of fibres.

In contrast to the frequency of alternating current, the influence of different fibre dosages was significantly higher, and a non-linear correlation between fibre content and global electrical resistivity was evident. As interactions between the fibre content and other parameters of the concrete composition were not visible and also not expected to take place, Minitab was used to calculate the main effect plots of the varied parameters to easily compare changes in concrete composition without the effects of fibres. Until an interaction between concrete composition and fibre content cannot be ruled out, especially due to the charge transport in the steel concrete interface, in the following chapters of this paper, the influence of each parameter is examined individually for each fibre content.

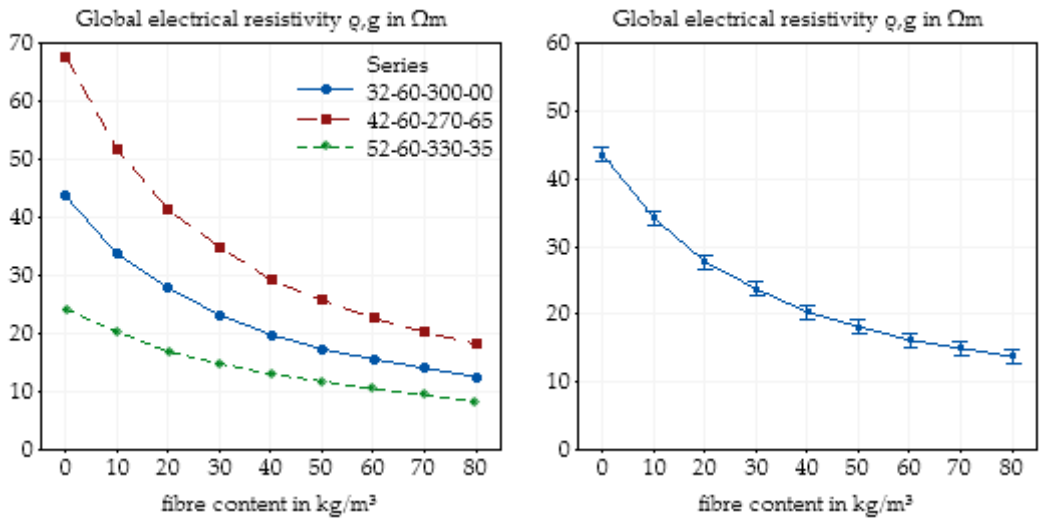

(a) **(b)**

Figure 3.4 Effect of the fibre content on the global electrical resistivity of SFRC in the basic concrete mixture (**a**) and main effect plot with 95 % confidence interval of the fibre content on the global electrical resistivity of SFRC calculated by Minitab based on all experimental data (**b**)

3.4.2 Effects of Single Parameter Variations in Concrete Composition

3.4.2.1 Changes in Water/Cement Ratio

The basic concrete mix design (Table 3.3) was modified with respect to its water/cement ratio. As shown in Figure 3.5 (a), for all fibre contents, there was a visible influence of the w/c ratio on the resistivity, and an increasing fibre content resulted in a significant reduction in the global electrical resistivity. While a w/c ratio of 0.55 led to the highest global electrical resistivity for all fibre contents, the higher w/c ratios of 0.60 and 0.65 did not show an equally continuous tendency. The curves for w/c ratios of 0.55 and 0.60 can be characterised through an almost parallel shift, but the curve for a w/c ratio of 0.65 showed a different behaviour and a smoother progression. It is apparent that at w/c ratios greater than 0.6 and at a fibre content higher than 30 kg/m³, a plateau was reached, at which an increase in the w/c ratio did not significantly impact the resistivity.

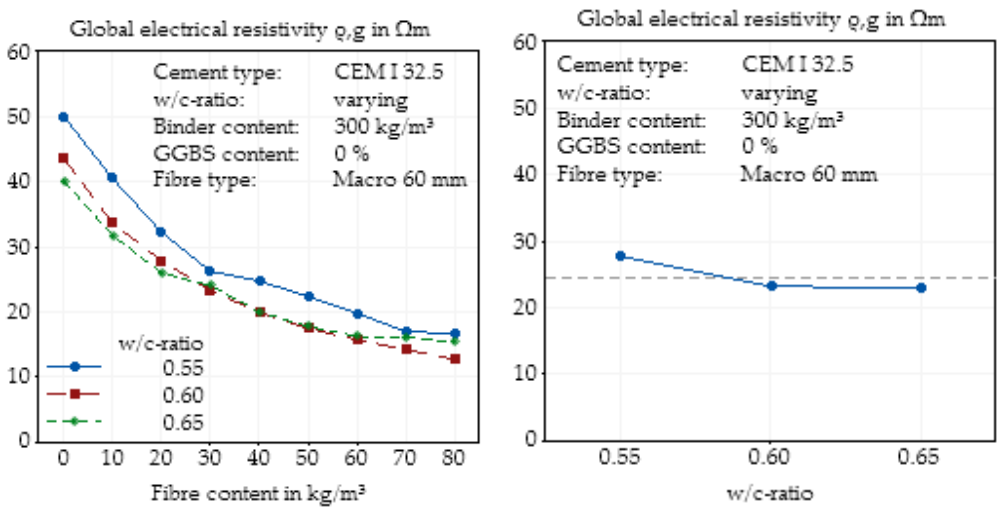

Figure 3.5 Effect of the water/cement ratio on the global electrical resistivity of SFRC as a function of fibre content (**a**) and main effect plot of the water/cement ratio on the global electrical resistivity of SFRC calculated by Minitab (**b**)

In summary, independent of fibre content, an increase in the w/c ratio leads to a decrease in resistivity or to an increase in conductivity, due to the higher water amount in concrete and the enlarged porosity (Figure 3.5 (b)). This effect already is described for plain concrete in several papers (see e.g., Elkey & Sellevold, 1995; van Beek & Stenfert Kroese, 2019). Nevertheless, there is no linear correlation between the w/c ratio and resistivity, especially when fibres are added. For the higher fibre contents, the discrepancy between the expectation and results of the measurement can be explained by the influence of fibres and the lower resistivities. While for low fibre contents, the concrete had a huge influence on the electrical resistivity, with increasing fibre content, the fibres progressively became the main conductive part of the material. Variations of the fibre distribution and orientation based on slightly varying flowabilities of the concrete can have a significant influence on the global electrical resistivity of the SFRC.

3.4.2.2 Changes in Binder Content

In addition to the water/cement ratio, the binder content, which in this case was synonymous to the cement content due to the lack of SCM in the basic concrete mix design, directly influenced the total amount of water and hydrated cement paste in the concrete mixture. Hence, the total porosity of the concrete varied, whereas the pore size distribution was only marginally impacted. Figure 3.6 (a) clearly shows the expected effect (see e.g., Elkey & Sellevold, 1995; Hughes et al., 1985) of a higher amount of water, which led to a decrease in electrical resistivity for almost every fibre content. The curves for all cement contents in Figure 3.6 (a) show almost the same behaviour with a decrease in electrical resistivity with increasing fibre content and a flattening of the curve for higher fibre contents. Only the concretes with a cement content of 270 kg/m³ and fibre contents of 10 kg/m³ to 30 kg/m³ seemed to deviate from the constant decreasing behaviour, but this can be explained by the scatter of the experiments.

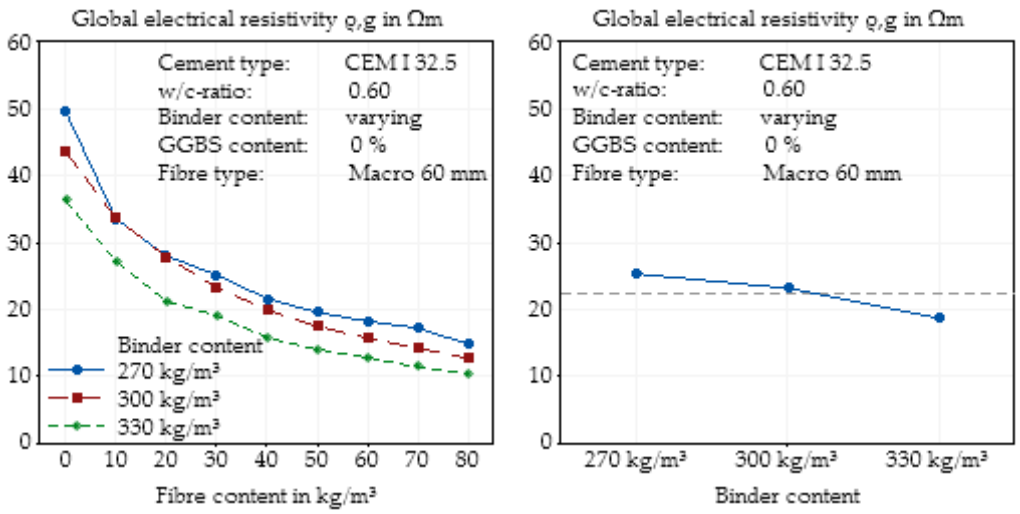

(a) **(b)**

Figure 3.6 Effect of the binder content on the global electrical resistivity of SFRC as a function of fibre content (**a**) and main effect plot of the binder content on the global electrical resistivity of SFRC calculated by Minitab (**b**)

In Figure 3.6 (b), the total effect of the variation of the cement content independent of fibre content is presented. For the investigated cement contents, an almost linear correlation between cement content and electrical resistivity can be observed. The constant w/c ratio in this series of experiments caused a change in the total amount of cement stone with presumably no changes in the pore structure. Based on the isolating properties of the aggregates, this is paired with an increase in the conductivity of the whole material.

3.4.2.3 Changes in Cement Type

The cement type, in this case, the strength class, synonymous with the specific surface of the cement, was varied to identify the effects of a finer pore structure of cement on higher strength classes. Comparing the results of CEM I 32.5 R and CEM I 42.5 R, this expected behaviour could be observed, but the finest cement (CEM I 52.5 R) does not fit into those expectations (Figure 3.7 (a)). As described in Section 3.3.1.2, the specific surfaces of the three used cements were determined, showing near linearity, where CEM I 32.5 R showed the lowest surface and CEM I 52.5 R the highest surface, and the specific surface of CEM I 42.5 R was approximately the mean value of both. When the curves of the global electrical resistivities of the three concrete mixtures, it is apparent that especially for small fibre contents, the cement with the highest surface showed the lowest electrical resistivity. For higher fibre contents, contrary expectations, the curves of the cement intersected and the resistivity of CEM I 52.5 R exceeded that of CEM I 32.5 R, but they were still lower than those of CEM I 42.5 R. These effects could not be explained and will be addressed in a future analysis.

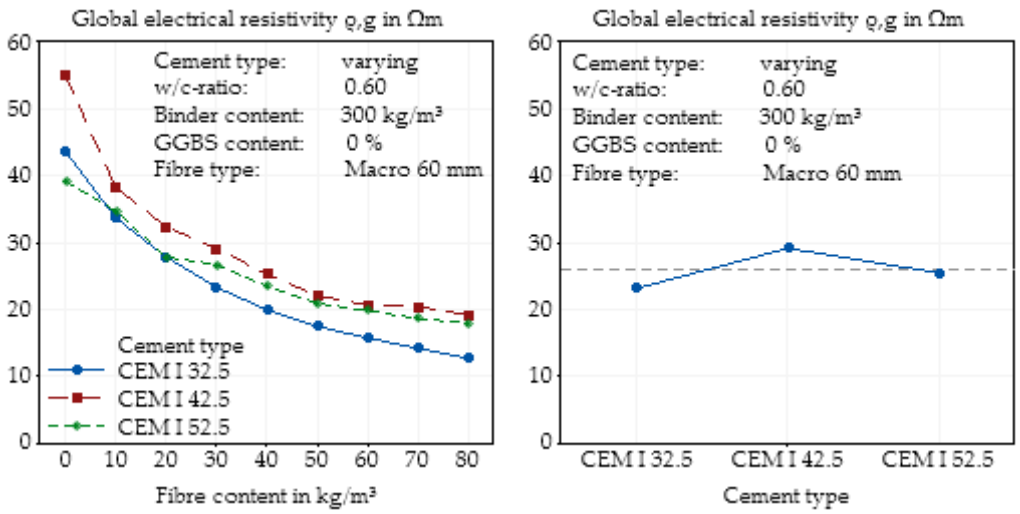

Figure 3.7 Effect of the cement type on the global electrical resistivity of SFRC as a function of fibre content (**a**) and main effect plot of the cement type on the global electrical resistivity of SFRC calculated by Minitab (**b**)

In Figure 3.7 (b), the effect of the cement type on the electrical resistivity is presented independent of the fibre content. As already described, the expected tendency of a higher resistivity with a higher fineness of cement is only visible for the two lower strength cements, and the results of the CEM I 52.5 R are much lower than expected. A plausible explanation could be the slightly different compositions within the cement clinker, although all cements were produced in the same production plant.

3.4.2.4 Addition of Ground Granulated Blast-Furnace Slag (GGBS)

In addition to the different cement strength classes, GGBS was used as a concrete component due to its well-known ability to significantly alter the pore structure of the concrete. To identify the effects of GGBS without any interactions with different cement clinkers, the same base cement (CEM I 32.5 R) was blended with GGBS at a constant water/binder ratio. The contents of GGBS were chosen considering the limits for additives for slag cements.

The use of a GGBS content of 35 % of the total binder content did not result in any significant changes in the electrical resistivity (Figure 3.8 (a)). For small fibre dosages, the OPC concrete had a slightly higher resistivity, while the difference decreased with increasing fibre content. In contrast, using a GGBS content of 65 % led to a significant increase in the electrical resistivity, where the difference again decreased for higher fibre contents.

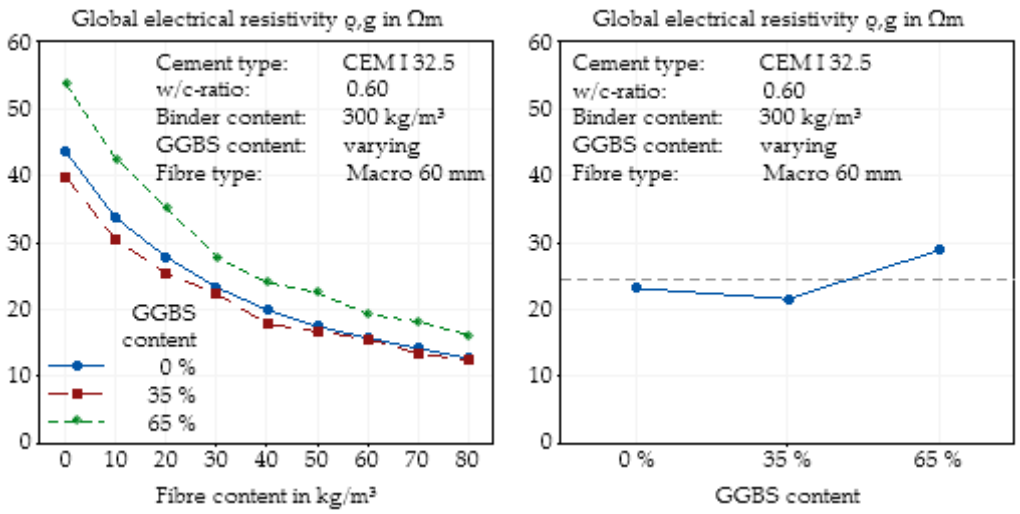

Figure 3.8 Effect of the addition of GGBS on the global electrical resistivity of SFRC as a function of fibre content (**a**) and main effect plot of the addition of GGBS on the global electrical resistivity of SFRC calculated by Minitab (**b**)

The summarising main effect plot (Figure 3.8 (b)) shows that a GGBS content of 35 % led to almost no changes in the conductivity of the concrete independent of the fibre content. It can be concluded that after 28 days of hydration, there were only small effects on the pore structure due to the addition of 35 % of GGBS, and the conductivity of the pore solution was only marginally influenced by the resulting changes in the chemical composition of the pore solution. The addition of a high content of GGBS showed almost the same effect as using a finer cement. The resulting finer pore structure, which was expected by the addition of GGBS (see e.g., Chen & Brouwers, 2006; Liu et al., 2014) and thus a reduced transmissibility of the pore solution, which functions as an electrical conductor, was caused by a higher resistivity than the reference sample. Earlier investigations (see e.g., Elkey & Sellevold, 1995; Polder & Ketelaars, 1991) have already shown that, for plain concrete, the addition of GGBS leads to an increase in electrical resistivity.

3.4.2.5 Effects of Multiple Parameter Variations

A statistical design of experiments was used to detect possible interactions among different parameters to check the possibility of the superposition of the single effects of different parameters on the global electrical resistivity. Comparing the results of the single parameter variation to the results of the multiple parameter variation, it is clear that there were differences in the main effects of the analysis of Minitab (Figure 3.9). All four parameters do not show any constant behaviour—neither a continuous increase nor a continuous decrease in the electrical resistivity.

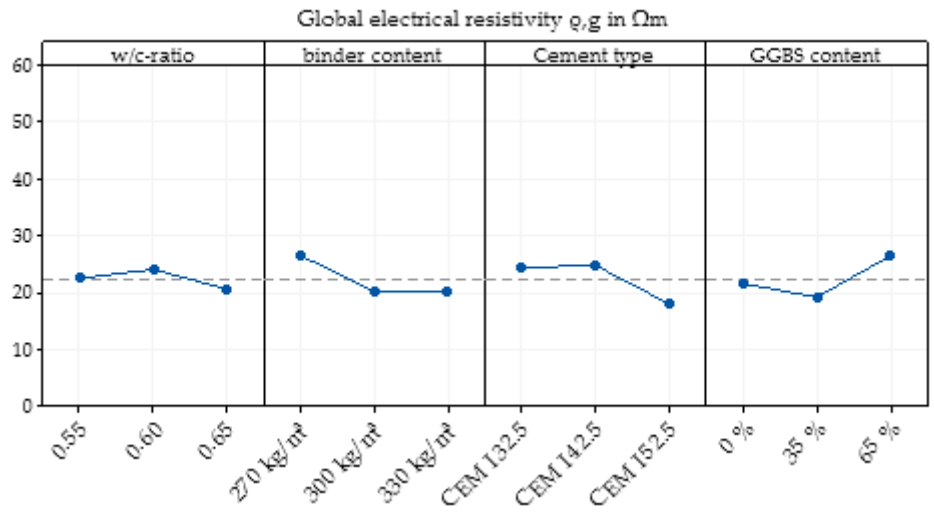

Figure 3.9 Main effect plot of the concrete composition on the global electrical resistivity of SFRC calculated by Minitab based on the mixtures of the multiple parameter variation

The results of the first three parameters, w/c ratio, binder content and cement type, of the multiple parameter variation differed from that of the single parameter variations, which shows that a superposition of these parameters is not possible in every case. Only the results of the addition of GGBS content are slightly similar to those of the single parameter variation.

In sum, it is clear that the results of single parameter variation and multiple variation completely differ. This result can be confirmed by observing the interaction plot of the multiple parameter changes (Figure E.**1**, Annex E). There, all possible interactions between changes in multiple parameters with an interaction level of 2 are presented, which means that interactions among the three parameters were not observed. An independency of two parameters would be presented through three curves in one sector that are only shifted in parallel. As can be seen, there is no such sector in the whole plot. Often, only one point did not reflect this behaviour, as with an interaction of cement type and GGBS content, but sometimes, totally different behaviours of the curves were noticeable, as with a combined observation of the w/c ratio and GGBS content (lowest left sector), where, for a GGBS content of 0 %, there was almost no influence of the w/c ratio on the resistivity; for a GGBS content of 35 %, a decrease, followed by a slight increase, with an increase in the w/c ratio was visible; and for a GGBS content of 65 %, the opposite behaviour was observed.

One problem of the statistical design of experiments was the low number of tested concretes, since a full matrix of 81 possible mixtures was investigated and approximated by the analysis of only 9 mixtures. Through the partially low influences of single parameters and the presented interactions, a more detailed analysis of interaction effects was not possible.

3.4.3 Effects of Variation of Steel Fibre Type

3.4.3.1 Effects of Fibre Type on Global Electrical Resistivity

The last parameter that was analysed via single parameter variation was the fibre type. Two macroscopic fibres with fibre lengths of 60 mm and 35 mm, respectively, and one microfibre with a fibre length of 8 mm were used. The results of the variation show that there was almost no influence on the electrical resistivity for all three types of fibres. While all three plain concrete mixtures are almost identical, which indicates comparable basic mixtures, with an increasing fibre content, only the addition of the smaller macrofibre (35 mm length) led to a slightly higher

electrical resistivity (Figure 3.10 (a)). The longest and shortest fibre showed almost identical results. Hence, the main effect plot (Figure 3.10 (b)) shows that all three types of fibres behaved similarly for this concrete mixture.

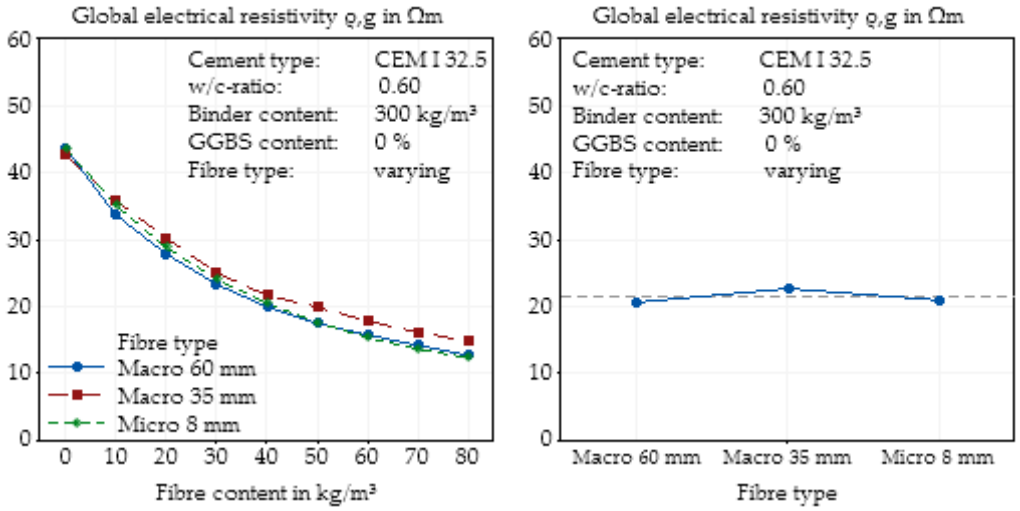

(a) **(b)**

Figure 3.10 Effect of the steel fibre type (geometry) on the global electrical resistivity of SFRC as a function of fibre content (**a**) and main effect plot of the steel fibre type (geometry) on the global electrical resistivity of SFRC calculated by Minitab (**b**)

3.4.3.2 Effects of Fibre Type on Electrical Resistivity in Horizontal Direction

While there was almost no visible effect on the global electrical resistivity of the concretes with different types of fibres, possible variations in the distribution of different specimen directions, depending on the fibre type and manufacturing process, were identified, which was performed by the use of a vibrating table. Figure 3.11 shows the effects of different fibres on the electrical resistivity measured in the two horizontal directions of the specimens. The horizontal directions are those which are orthogonal to the direction of the vibrating table. Analogous to the last chapter, almost no influence was visible for all fibre contents. The longest fibre again led to the smallest resistivities, but there were no significant effects measurable.

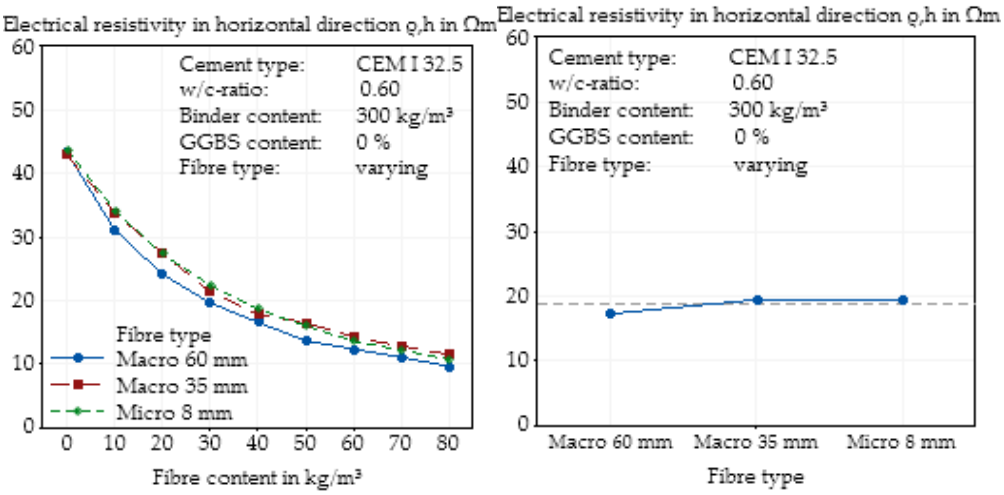

(a) **(b)**

Figure 3.11 Effect of the steel fibre type (geometry) on the electrical resistivity in horizontal direction of SFRC as a function of fibre content (**a**) and main effect plot of the steel fibre type (geometry) on the electrical resistivity in horizontal direction of SFRC calculated by Minitab (**b**)

Comparing the global electrical resistivity (Figure 3.10 (a)) and that in the horizontal direction (Figure 3.11 (a)), it is noteworthy that the electrical resistivity of the SFRC in the horizontal direction is slightly smaller than the global resistivity, and so the slope of the curves in Figure 3.10 (a) is steeper.

3.4.3.3 Effects of Fibre Type on Electrical Resistivity in Vertical Direction

In contrast to the electrical resistivity in the horizontal, the vertical electrical resistivity was significantly higher than the global electrical resistivity, and the spread of the curves of the different fibres was wider than seen for global electrical resistivity or in the horizontal direction (Figure 3.12 (a)). This phenomenon was expected based on the manufacturing process, where the concrete was filled into the formworks in two layers, and the compaction was performed by a vibrating table in the vertical direction, which led to a more horizontal orientation of the fibres and thus to a higher conductivity in the horizontal direction. For higher fibre contents, the electrical resistivity in the vertical direction of the concrete with microfibres was lower than that of the macrofibres.

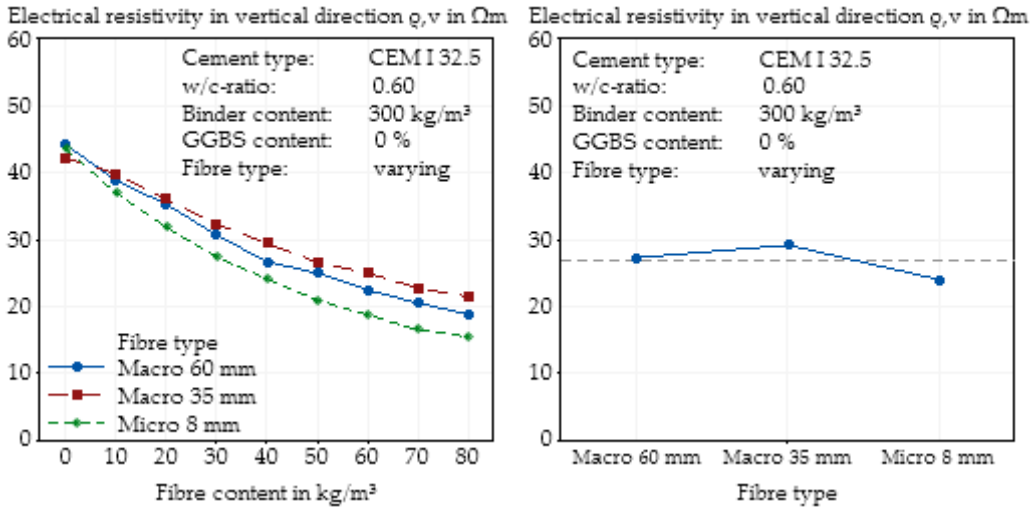

(a) **(b)**

Figure 3.12 Effect of the steel fibre type (geometry) on the electrical resistivity in vertical direction of SFRC as a function of fibre content (**a**) and main effect plot of the steel fibre type (geometry) on the electrical resistivity in vertical direction of SFRC calculated by Minitab (**b**)

Independent of fibre content, a difference between the electrical resistivity of the concretes with the macrofibre with a length of 60 mm and the microfibre in the vertical direction (Figure 3.12 (b)) was clear, while the global electrical resistivity was almost equal. This fact suggests a preferred orientation of the microfibres in the vertical direction, although the compaction was performed vertically. For the microfibre, the difference of the resistivity between the horizontal and the vertical electrical resistivity was rather small, at lower than 5 Ωm, while there was a significant difference for the macrofibres, at higher than 10 Ωm.

3.4.4 Effects of Concrete Age and Storage Medium

In addition to the investigated influencing factors, concrete composition and fibre content, the age of the concrete and the storage conditions can influence the electrical resistivity of the concrete. To show the effects of these factors, specimens from the same mixing batch were used. The influence of concrete age, independent of the storage medium, on the electrical resistivity is presented in Figure 3.13. As can be seen, for all fibre contents, a higher concrete age resulted in a higher resistivity, which can be explained by the forming of a pore structure and closing of conductive pore channels. It is clear that for plain concretes, the age of the concrete has a greater impact on the resistivity than SFRC, since fibres take part in the conduction process, and thus, the influence of the concrete decreases.

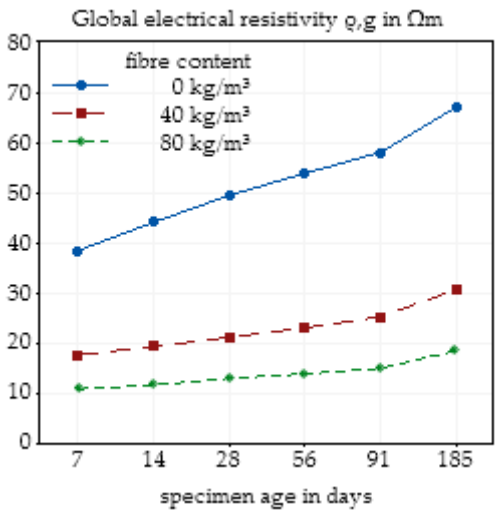

Figure 3.13 Effect of the concrete age on the global electrical resistivity of SFRC depending on the fibre content based on nine specimens

An analysis of the effect of different storage media on the electrical resistivity is presented in Figure 3.14. From H_2O over $Ca(OH)_2$ to synthetic pore solution, the electrical resistivity decreased, which is in agreement with the increasing initial conductivity of the used storage media.

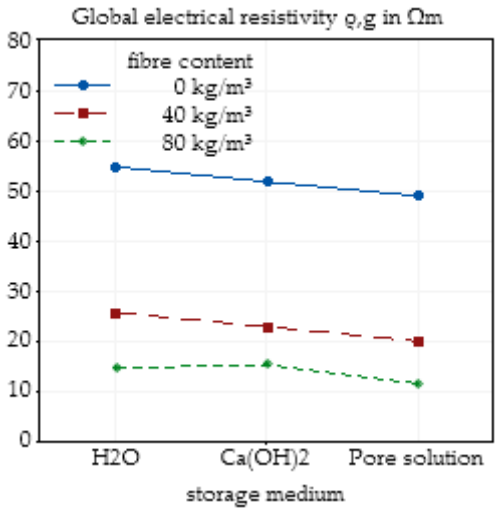

Figure 3.14 Effect of the storage conditions on the global electrical resistivity of SFRC depending on the fibre content based on nine specimens

The effect of the age of the concrete and the storage conditions independent of fibre content are presented in Figure 3.15. As already described, a higher concrete age leads to an increase in electrical resistivity, while storage in a higher alkaline solution reduces resistivity.

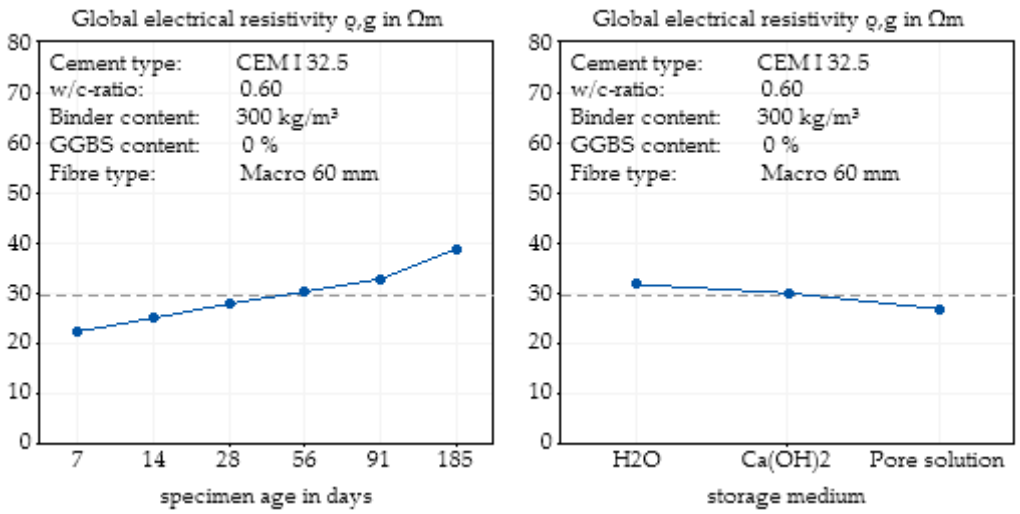

(a) **(b)**

Figure 3.15 Main effect plot of the concrete age on the global electrical resistivity of SFRC calculated by Minitab based on nine specimens (**a**) and main effect plot of the storage conditions on the global electrical resistivity of SFRC calculated by Minitab based on nine specimens (**b**)

3.5 Discussion

The aim of this study was to identify the relevance of the influencing parameters on the electrical resistivity of SFRC. Hence, variations of the concrete composition as well as changes in storage conditions and concrete age were analysed. To enable the possibility of using electrical resistivity measurements for the detection of the fibre content of SFRC, the fibre content is the most influencing parameter on the electrical resistivity. As presented in Section 3.4.1, the electrical resistivity, measured with a two-electrode setup, as expected (see e.g., Hedjazi & Castillo, 2020), was significantly influenced by changes in the fibre content of steel fibre-reinforced concrete. The average results of all the measurements showed that the addition of 80 kg/m³ of fibres resulted in a reduction in the electrical resistivity from approximately 43.5 Ωm to 13.8 Ωm for the mean values, which is equivalent to a reduction of approximately 70 % and has the main influence on the electrical resistivity, and no interactions between the fibre content and other varied parameters on the electrical resistivity could be observed. The variation of the concrete composition also led to effects on the electrical resistivity, but compared to the fibre content, the effect is much smaller, which can be seen in Table 3.6. The percentage influence of all parameters was calculated as the ratio of the minimum to maximum electrical resistivity of the main effect plots (Figure 3.3 (b) and Figure 3.4 (b), Figure E.2 and Figure E.3, Annex E). Since a superposition of the single effects of the plain concrete mix design was not applicable (Section 3.4.2.5), the influence of the fibre content exceeded that of the concrete mixture by at least a factor of 2.5 and of the fibre type by a factor of 6.

Table 3.6 Effect of the single parameters on the electrical resistivity of SFRC

Parameter	Minimum electrical resistivity in Ωm	Maximum electrical resistivity in Ωm	Percentage influence of the parameter in %
Frequency	22.7	24.5	7.3
Fibre content	13.8	43.5	68.3
w/c ratio	21.2	24.5	13.5
Binder content	20.0	26.2	23.7
Cement type	19.9	25.9	23.2
GGBS content	19.8	27.0	26.7
Fibre type	20.6	22.7	11.9

As steel fibres are metallic conductors, their conductivity exceeds the ionic conductivity of concrete pore solution, even if the concrete is fully saturated, and so the huge impact of the amount of steel fibres that was identified can be explained. In addition, a high amount of fibres leads to a higher permeability of the concrete (see e.g., Lehner et al., 2020). For a lower saturation of the concrete, the difference between the conductivity of fibres and concretes may be enlarged significantly, but the measurement of the electrical resistivity will be much more complicated due to coupling effects on the electrodes. Therefore, the large difference in the conductivity allows the use of electrical resistivity measurements to characterise the fibre content of a well-known concrete composition. Since there are additional influencing factors on electrical resistivity, which result from the concrete composition and the age of the concrete, it is necessary to determine the electrical resistivity of the concrete. For this purpose, these parameters were analysed to find possible interactions with the fibres regarding resistivity and to gain a database for the future use of a test setup for the determination of the fibre content of SFRC.

The use of different fibre types, two macrofibres with different lengths of 60 mm and 35 mm and one microfibre with a length of only 8 mm, which was coated with brass, showed almost no effects on the global electrical resistivity of the concretes (Section 3.4.3.1). This indicates that the fibre content of SFRC can be detected almost independently from the fibre that is used. This fact can be explained by the huge difference between the conductivity of the fibre material and the pore solution of the concrete. Even differences in fibre material only led to nonrecognizable effects on conductivity compared to the high electrical resistivity of the plain concrete. Effects of the fibre length were only expected for small fibre contents in several studies (see e.g., Banthia et al., 1992; Chen et al., 2004; Lataste et al., 2008) due to the possible phenomenon of direct connections of two or more fibres. However, as shown in our experiments, even for a fibre content of 10 kg/m³, which is uncommon in practice, no such influences could be detected. In summary, it can be concluded that the electrical conductivity of SFRC is mainly influenced by the amount of fibres, respectively, steel and not by the number of fibres, so differentiation between a continuous conductive path via one fibre or a discontinuous conductive path via a plurality of fibres and concrete with transition zones between both materials is not possible.

The only effects of different fibres that were observed resulted from an expected slightly varying distribution and orientation of the microfibres through the mixing and compacting processes. Due to the limited specimen dimensions, long fibres can freely align in the formwork but are extremely influenced by the production procedure. Since the concrete formworks were

filled in accordance with European standards, two layers of concrete were filled in and long fibres tended to align more horizontally. In addition, the compaction process via the vibrating table led to a vertical compaction force and thus also supported a horizontal orientation of the fibres. On the contrary, microfibres are sufficiently small to align in the concrete almost freely and are mostly not influenced by aggregates, manufacturing processes in layers or vertical compaction. However, a difference between the macrofibres could not be observed. Therefore, it can be concluded that there is a critical fibre length and a number of fibres per kg, which leads to effects on the fibre orientation, and when this critical value is not reached, no influences will be visible.

The age of concrete, in the investigated range of 7 days to 185 days, led to changes in the electrical resistivity between 40 Ωm and 70 Ωm for plain concrete, and 10 Ωm and 20 Ωm for SFRC, but again, the effects of fibre addition dominated the influence of concrete age. These results confirm the observations of Hedjazi & Castillo, 2020, where effects of concrete age, fibre addition and w/c ratio were also investigated. In the first days and months of concrete life, the reaction process caused significant changes in the degree of hydration and thus in the pore structure. Based on the binder material, the greatest part of the hydration was completed after 28 days to 90 days. Hence, the effect of the concrete age on the electrical resistivity decreases with increasing age, which is synonymous to an increasing degree of hydration.

Even though the initial conductivity of the pore solution had an impact on the electrical resistivity of the concrete, for SFRC, the storage medium only had a minor influence on the electrical resistivity. A higher initial alkalinity slightly reduced the electrical resistivity of the concrete. For future analysis, this implies the necessity to use constant storage conditions, namely, a certain conditioning of the specimens before the measurement of the electrical resistivity should be performed, but unknown conditions of concrete in structural elements are not an exclusion criterion for this test method.

As expected, a variation of the concrete also influenced the electrical resistivity, mostly due to changes in the pore structure of the concrete. The observed parameters, w/c ratio, binder content, cement type and GGBS content, all caused changes in the electrical resistivity.

As stated in several studies (see e.g., Andrade, 2005; Azarsa & Gupta, 2017; Bürchler, 1996; Cosoli et al., 2020; Elkey & Sellevold, 1995; Hedjazi & Castillo, 2020; Hughes et al., 1985; Layssi et al., 2015; Monfore, 1968; van Beek & Stenfert Kroese, 2019), the increase in porosity, which can be a result of a higher w/c ratio or due to an increased binder content, generally led to a reduced electrical resistivity. However, in contrast to Azarsa & Gupta, 2017; Cosoli et al., 2020; Elkey & Sellevold, 1995; Hughes et al., 1985; Monfore, 1968; van Beek & Stenfert Kroese, 2019, both parameters in this study showed interaction effects.

The same effect of reduced electrical resistivity was detected with the decreasing content of GGBS. Generally, GGBS has a finer pore structure than the concrete, and so the conductivity is reduced by its addition (see e.g., Chen & Brouwers, 2006; Cosoli et al., 2020; Gastaldini et al., 2009; Hauck, 1993; Hope & Ip, 1987; Liu & Presuel-Moreno, 2014; Liu et al., 2014; Lübeck et al., 2012; Mazloom et al., 2017; Montemor et al., 2000; Naik et al., 2010; Polder & Ketelaars, 1991; Topçu et al., 2012; Tumidajski, 2005). In this study, no effect on the electrical resistivity was observed by the replacement of only small amounts of cement by GGBS, but with higher contents of GGBS, 65 % of the total binder content, a significant change in electrical resistivity was measured. Due to the young concrete age of only 7 days, it can be assumed that the GGBS, which is a latent hydraulic binder material, only had a minor impact on the initial

hydration process and hence on the resistivity of the concrete especially at replacements of 35 %. Nevertheless, a higher content of GGBS apparently caused a finer pore structure, visible by the increased electrical resistivity.

For different cement types, in this case, the variation of the grinding fineness for cements with almost identical clinker composition, it was assumed that the finest material leads to the finest pore structure and thus to the lowest conductivity. Comparing the two cements with lower strength classes, the observations fit our expectations, while the highest cement fineness resulted in a decrease in electrical resistivity.

In addition to the single parameter changes, multiple simultaneous changes in the concrete composition were also investigated, and based on the investigated number of samples, the conclusion must be drawn that interaction effects do not enable the superposition of the effects of single parameter changes. Figure E.**1**, Annex, shows the interaction plot of all the varied parameters. While a parallel shift of the single curves of each parameter combination would represent the independence of these parameters, no group of curves showing this behaviour is visible. On the contrary, all parameter combinations show intersections between the single curves.

Since the most influencing factor of the conductivity of the concrete, in the literature as well as in several experiments (see e.g., Andrade, 2005; Bürchler, 1996; Layssi et al., 2015), was determined to be the porosity of the concrete, with the exception of the saturation of the pores, which is stated to be preferably high, simultaneous changes in parameters must be considered for the measurement of electrical resistivity. Thus, it is not possible to generate a database of concretes and interpolate, respectively, extrapolate the electrical resistivity of nonincluded compositions in a trivial manner; however, it is necessary to identify the composition of the concrete and, ideally, the electrical resistivity of the plain concrete if the fibre content is determined by the use of electrical resistivity measurements.

3.6 Conclusions

This study showed that the determination of the electrical resistivity of SFRC is a suitable test method for the monitoring of fibre content, e.g., in precast factories or for new construction buildings where the electrical resistivity of the plain concrete composition can be characterised. The large difference between the conductivity of steel as a metallic conductor and concrete as an ionic conductor led to significant influences of the fibre content on the electrical resistivity, which resulted in a 70 % lower electrical resistivity of SFRC, 80 kg/m³, in comparison to plain concrete. Nevertheless, since there are also influences from the concrete composition, such as on the w/c ratio and binder content, the application field of this test method requires previous calibration on concrete mix designs without the addition of fibres. Otherwise, the effects of the concrete composition, which can influence the electrical resistivity by approximately 15 % to 25 %, can induce significant errors in the analysis of the fibre content. Investigations of existing structures in the case of repair or maintenance work can only lead to sufficient approximations for the fibre content if either the composition or electrical resistivity of the plain concrete are well known, e.g., with the help of an extensive database or the characterisation of plain concrete without fibres. Both possible methods of extending the test setup to enable its use for the characterisation of existing structures and additionally in the evaluation of fibre orientation are the subject our future studies.

4 Advanced Investigations on Concrete Cubes

This section was published as scientific paper under the title “Electrical resistivity measurements to determine the steel fiber content of concrete” in the journal Structural Concrete in 2022 (Cleven et al., 2022c).

4.1 Abstract

Although steel fiber reinforced concrete is becoming increasingly popular in the construction industry, its application is currently limited to certain areas. One reason is the lack of an economical non-destructive testing method to determine the content, distribution, and orientation of steel fibers in fresh and hardened concrete. However, these parameters are decisive for the assessment of the static performance of a building component. In this article a new test method is proposed, which is based on the electrical conductivity of concrete.

Using a two-electrode experimental set-up, measurements of the electrical conductivity were done on hardened concrete cubes with defined fiber content and a correlation between electrical conductivity and fiber content could be identified. Within the scope of extensive test series, the fiber content and the age of specimens were varied, and several identical series were produced and observed to ensure statistically verified results.

At this stage of research the test method based on electrical conductivity measurement provides reliable results on the fiber content of pre-conditioned concrete cubes. Based on the results a new model was developed to quantify the fiber content of the examined cubes. This model is based on the estimation of the relative conductivity, the so-called increase of conductivity. Undesired influences caused by ageing, respectively hydration in the young concrete age were eliminated, by relating the conductivity of fiber reinforced concrete to an unreinforced concrete. Further investigations with focus on the influence of concrete composition and other specimen sizes are going to be conducted as next steps for the development of an in-situ test setup for the diagnosis of concrete structures.

4.2 Introduction

Steel fiber reinforced concrete (SFRC) is a commonly used material for civil construction. It consists of plain concrete (PC) and macroscopic steel fibers, which are mostly produced out of wires (see e.g., Di Prisco et al., 2009; Ding et al., 2019; Ferdosian & Camões, 2021; Kachouh et al., 2019; Lehner et al., 2020; Shan & Zhang, 2014). SFRC combines positive features from both of its components and compensates their disadvantages. PC as an unreinforced material is nearly freely shapeable and can resist high compressive loads, but nearly no tensile stresses, whereas drawn steel wires are characterized as reinforcements with an extremely high tensile strength.

The combination of the materials leads to an improvement of tensile strength, ductility, and impact strength (see e.g., Hedjazi & Castillo, 2020; Kobaka et al., 2019; Luo et al., 2020; Song & Hwang, 2014; Zhang et al., 2019). As alternative material for conventional steel reinforced concrete in some cases, constructions can be planned and realized with SFRC without the time-consuming process of reinforcing. Because of limitations of the tensile strength in ultimate limit stage in comparison to steel reinforced concrete, the main application of SFRC can be found in constructions with lower static requirements, which is why SFRC is often used for industrial floorings, residential construction. Also, underground construction in the form of precast tunnel segments, so called tubbings, which have the highest static requirements in building condition, can be an interesting application for SFRC (see e.g., Brandt, 2008; Facconi et al., 2021; Li et al., 2019).

The mechanical parameters of SFRC are strongly affected by the content of fibers in the concrete, their distribution and orientation. All three parameters show a considerable influence on the load bearing capacity after initial cracking of the concrete (see e.g., Barnett et al., 2010; Gettu et al., 2005; Li et al., 2018; Martinelli et al., 2021a; Martinelli et al., 2021b). In general, the flexural strength of SFRC lies in between the ones of PC and conventional steel reinforced concrete, but with high amounts of steel fibers a ductile and strengthening behavior after first crack building in concrete can be observed. Lower dosages of fibers lead to a strain softening behavior, but nevertheless a significant increase of its residual strength in comparison to PC and a uniform and fine crack distribution (see e.g., Hedjazi & Castillo, 2020; Kobaka et al., 2019; Luo et al., 2020; Song & Hwang, 2014; Zhang et al., 2019).

One challenge in the use of SFRC is the uneven and often unknown distribution and orientation of the fibers in concrete elements. While the global fiber content can be controlled by a precise dosing process, the local parameters can deviate from the global ones. Based on this problem, relatively large deviations of up to 20 % of test results for mechanical properties can occur. Therefore, the safety factors for the static calculations must be high to ensure a secure way of construction (see e.g., Cugat et al., 2020; Herrmann et al., 2019; Molins et al., 2009; Tarawneh et al., 2021). Also, the orientation of fibers has a big effect on the strength of the compound material. The maximum load transmission between two crack edges can be reached by fibers that are oriented parallel to the applied stress. In this position the angle between the fiber and the crack is 90 °. A decrease of this angle leads to a significant decrease of the transmittable tensile strength (see e.g., Cao & Yu, 2018; Park et al., 2021; Zhou & Uchida, 2017). For these reasons, the knowledge of the local fiber content and their orientation is of great importance for test specimens and for construction elements. Various test setups have been developed and applied in scientific studies. So far, no accurate and easy to apply setup was found, which can be used for in situ monitoring or at the construction site.

The highest detailed and specific results on fiber content, distribution and orientation in concrete specimens can be obtained by computed tomographic analysis (see e.g., Balázs et al., 2017; Nezhentseva et al., 2013; Park et al., 2021; Ponikiewski & Katzer, 2016; Rajeshwari et al., 2020; Schnell et al., 2009; Suuronen et al., 2013). With high effort and expensive equipment, a 3-dimensional visualization of the specimen is possible, where the fibers and concrete can be distinguished by their different densities. The biggest problems of this test method, however, are the excessive costs for the equipment and the relatively small specimens that can be analyzed.

An easier setup can be used to generate 2-dimensional sectional images of SFRC, the so-called photo-optical method. Based on a large number of sectional images an acceptable evaluation of the fiber amount and orientation in different areas of concrete elements is possible (see e.g., Lee et al., 2015; Zak et al., 2001). Even so the equipment for this method is much cheaper it is a very time-consuming work because many sectional images out of different sections of the specimens and of course in different orientations are needed to get a sufficient overview of a structural element. Other methods based on inductivity (see e.g., Al-Mattarneh, 2014; Faifer et al., 2010a; Faifer et al., 2010b; Faifer, 2011; Ferrara et al., 2012; Hobst & Bílek, 2016; Juan-García et al., 2016; Lei et al., 2019; Li et al., 2020; Torrents et al., 2012; Wichmann et al., 2011) or permittivity (see e.g., Akgol et al., 2019; Franchois et al., 2004; Jamil et al., 2013; Karlovšek et al., 2012; Mehdipour et al., 2017; Roqueta et al., 2011; van Damme et al., 2004; van Damme et al., 2005) are also used in scientific research but cannot be realized yet in the process of construction of huge elements or even buildings. An example

for a test setup using permittivity measurements of SFRC is given in van Damme et al., 2004, where an open-ended coaxial probe is applied to the surface of concrete slabs. Although the laboratory results show that the determination of the fiber volume fraction is possible, using this method, a high effort of equipment and time, especially for applying complex models with different simplifying assumptions, is necessary.

For that reason, first results of an experimental program using electrical resistivity measurements on SFRC to set up a model for fiber content, distribution, and orientation of distinct types of specimens are presented in this paper. Electrical resistivity measurements are currently used for the monitoring of the corrosion behavior of steel rebars in concrete elements using multiringelectrodes (see e.g., Raupach et al., 2006; Raupach et al., 2013; Reichling, 2014; Reichling & Raupach, 2012; Reichling et al., 2015). By extending this idea, the objective of this study is to develop a test setup that can be adapted on nearly all types of concrete elements and can be used for in situ measurements on SFRC buildings (see e.g., Molodtsov & Molodtsova, 2018; Ozyurt et al., 2006b; Ruan & Poursaee, 2019; Uygunoglu et al., 2018). In a first step, separately cast cubic specimens with a defined concrete composition are investigated to get a basic approach and correlation between the electrical resistivity of SFRC and its fiber content. Further investigations are ongoing to extend the setup to cylindrical specimens, like drilling cores, and with help of finite element modeling to structural elements or whole concrete structures. Even if this further development will be much more complicated and time consuming, the presented study shall be the first step of the development.

4.3 Experimental Program

4.3.1 Materials

To investigate the influence of fiber content, distribution, and orientation in concrete specimens on the electrical resistivity, respectively, electrical conductivity, of the SFRC, specimens of one type of concrete mixture with varying fiber content have been produced. To eliminate possible influences of supplementary cementitious materials, ordinary Portland cement was used as binder. The water/cement-ratio was set to 0.45. For the aggregates, a quarzitic material with a fine grain size distribution of C16 according to DIN 1045-2, 2008 was used. The maximum grain size of 16 mm was chosen to ensure a nearly free distribution of the fibers without a considerable influence of the biggest grains. The cement content was set to 470 kg/m³ to attain a high workability and low porosity of the concrete mixture without the use of superplasticizer. The mix design of the resulting concrete is presented in Table 4.1.

Table 4.1 Concrete mix design

Parameter		Unit	Content
CEM I 52.5 R			470.0
water			211.5
aggregates	Milisil W3	kg/m³	218.3
	0.1 – 0.5 mm		326.9
	0.5 – 1.0 mm		238.4
	1.0 – 2.0 mm		210.0
	2.0 – 4.0 mm		186.8
	4.0 – 8.0 mm		234.9
	8.0 – 16.0 mm		193.8
	total		1609.1
water/cement-ratio		-	0.45

The production of the concrete was done in the following way. First the cement and the aggregates were homogenized in a compulsory mixer with a nominal volume of 160 L. After 30 s the water was added, and the concrete was mixed for at least 2 min. Then the PC was visually inspected, and the walls of the mixer were scratched from adhering components and an additional mixing phase of 1 min was performed. Afterward the target consistency of the PC was examined via flow table test in accordance with EN 12350-5, 2019 and the air content and fresh concrete density were determined in accordance with EN 12350-6, 2019 respectively EN 12350-7, 2019. Each concrete production was performed with a material volume of 70 L. Following the fresh concrete testing, samples of 4 L each were extracted of the mixer and placed in a bucket mixer. Also, a defined fiber content of 10–120 kg/m³, appropriate to 0.1 %–1.5 % by volume, was added in the mixer and mixed for about 1 min before the concrete was filled into cubical steel formworks with dimensions of 150 mm³. Before the casting of the formworks, the SFRC was visually inspected to ensure that no negative effects of the fiber addition, like agglomerations of fibers or an insufficiently high porosity, took place. Although the maximum fiber content of 120 kg/m³ was very high, no defects in the concrete structure could be identified. Additionally, one PC specimen without fibers was produced. The used fibers were hooked steel fibers with a length of 60 mm, a diameter of 1 mm and a tensile strength of about 1500 N/mm². This procedure was performed six times, so there are six identical series of specimens with different fiber contents from 0 to 120 kg/m³, what gives in total 72 specimens.

4.3.2 Test Setup

All specimens were stored in the formworks, covered with foil, for 1 day. After demolding, the upper surfaces of the specimen were ground down to ensure a flat surface for a good electric connection. Then the specimens were stored in separate storage boxes under water at a temperature of 20 °C till testing. Because of the small dimensions of the specimens in relation to the fiber length an electric connection over the entire sample surface areas was chosen to reduce effects of single fibers or grains near the surfaces. To compare different geometries of the specimen, the specific resistance respectively conductivity values can be calculated by using absolute values and a geometrical factor k. The specific values are necessary to compare different specimens and represent independent material properties. In the case of a

full connection of two parallel surfaces of a specimen the shape of the electric fields can be described as shown in Figure 4.1. The factor k for this configuration of electrodes can be calculated by the percolated area A and the distance of the electrodes l by following (eq. *4-1*).

$$k = A \,/\, l \qquad \text{(eq. 4-1)}$$

where, k is the geometry factor depending on dimensions of specimens in m; A is the effective contact area in m²; l is the electrode gap in m.

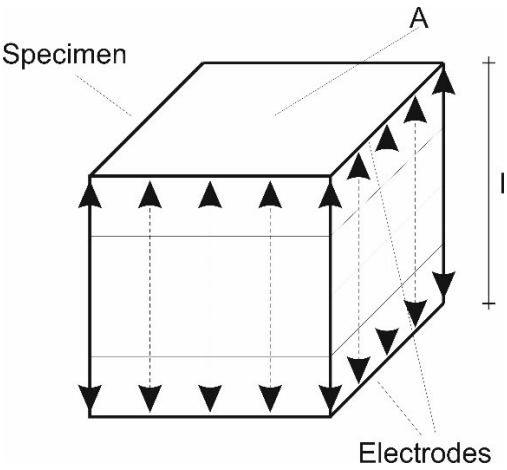

Figure 4.1 Shape of the electric field of two parallel electrodes

The resulting test setup consists of two electrodes made of stainless steel with an edge length of 200 mm to inhibit corrosive effects on the surfaces, which are connected to a resistivity analyzer with identical cables. Since the connection to the concrete surface solely by the steel electrode was not possible in a reproducible way, a wetted sponge cloth was used to allow a connection over the entire surface. The moisture of the sponge clothes was constantly checked and adjusted with fresh water, tempered to 20 °C. The full test setup can be seen as schema in Figure 4.2 (a), and a picture of the setup is presented in Figure 4.2 (b).

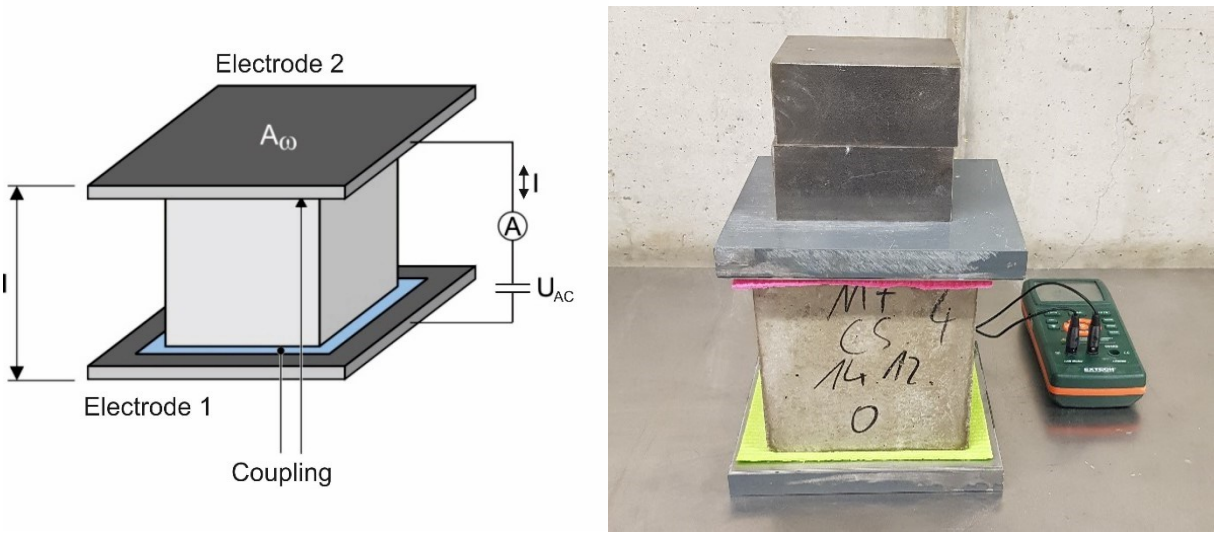

Figure 4.2 Scheme of the test setup (a) and photo of the test setup (b) for conductivity measurements

Every specimen was evaluated in all three directions to receive results of the global fiber content and values for different orientations of the specimens. Before the measurement was performed, a single specimen was taken out of its storage box and the surface water was removed by using paper towels. Then the specimen was placed on the first electrode and the second one was placed on top. To obtain a constant und reproducible contact pressure a defined reference weight was placed on top of the test setup.

As resistivity analyzers two different devices were used, depending on the investigated parameters. The first on was a so called LCR meter, type Extech Instruments LCR200, and the second one was a potentiostat, type Gamry Instruments 1010E. The parameters of both devices can be found in Table 4.2.

Table 4.2 Parameters of the resistivity analyzers

Parameter	LCR meter	Potentiostat
Type designation	Extech Instruments LCR200	Gamry Instruments 1010E
AC amplitude	600 mV rms	17.8 µV to 2.33 V
Frequency	100 Hz, 120 Hz, 1 kHz, 10 kHz, 100 kHz	10 µHz to 2 MHz
Measuring range of impedance	0,000 Ω to 200,0 MΩ	-
Accuracy	± 0,5 %	± 0,5 %

By use of the LCR meter an alternating current (AC) with a voltage amplitude of about 600 mV rms was induced at a fixed frequency. For the measurements in this study all possible frequencies were used. The LCR meter then reports the electrical resistance as resulting parameter. After the measurement of all frequencies in one direction of the cube, it was turned around until all three possible directions were analyzed.

By use of a digital potentiostat different amplitudes of AC as well as different frequencies were assessed. In one continuous test series the amplitude of the AC was changed in the range of 10–200 mV while the frequencies varied between 1 Hz and 100 kHz on one SFRC specimen (see Section 4.4.3). Due to the continuous monitoring only one direction of the specimen was evaluated. Another series of tests was performed at a constant amplitude and only varying frequency over a period of about 17 h to identify effects of drying of the coupling and the specimens on both PC and SFRC (see Section 4.4.2).

4.4 Results and Discussion

4.4.1 Correlation between Electrical Resistivity and Fiber Content

All results confirm a considerable influence of the fiber content onto the measured electrical resistivity respectively conductivity of the investigated SFRC specimens. The results presented in Figure 4.3 include all six series of each 13 specimens, investigated by use of the device Extech Instruments LCR200. The electrical resistivity combines both the conductivity of the steel fibers and of the concrete. A deviation in results could be seen which is based on the inhomogeneity and anisotropy of the material. The maximum coefficient of variation of 9.65 % was found for a fiber content of 90 kg/m³. A relation between fiber content and deviation could not be identified. Usually, conductivity is a homogenous parameter for isotropic materials, but

in case of SFRC the calculation of a global value of the specific material's resistance as mean value of all three cube directions was necessary. The global conductivity was calculated analogously. The presented values were measured at a frequency of 10 kHz for a concrete age of 7 days.

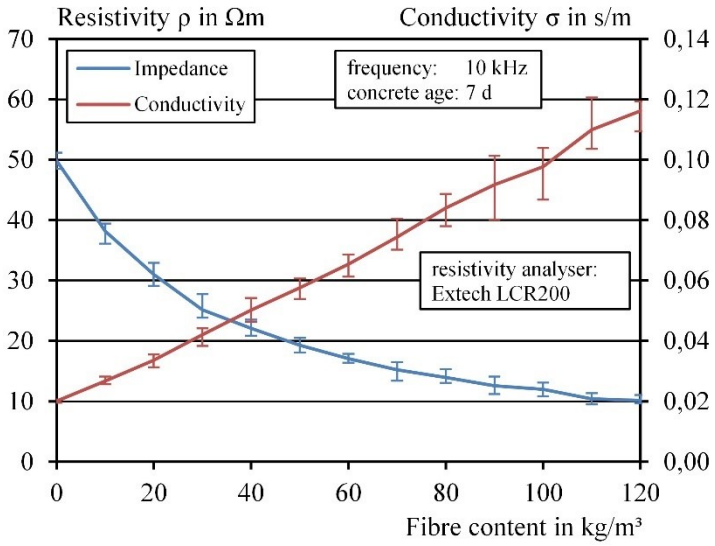

Figure 4.3 Correlation between electrical resistivity, respectively, conductivity and fiber content, resistivity analyzer: Extech Instruments LCR200

It is obvious that the addition of fibers to the concrete led to a higher conductivity or lower electrical resistivity. Especially low fiber dosages showed a high impact on the measured electrical resistivity, whereas at higher fiber dosages the differences were less clear. An addition of 30 kg/m³ of fiber to the unreinforced concrete resulted in a bisection of the electrical resistivity from about 50 to 25 Ωm. When another 30 kg/m³ of fibers were added the loss of electrical resistivity was only about 30 %, so there is no linear correlation between fiber content and electrical resistivity. In contrast it could be seen that the conductivity nearly correlates to the fiber content in a linear way.

4.4.2 Influence of Frequency and Measuring Time

To evaluate the influence of the frequency and the measuring period in detail the test setup was changed for two additional measurements. For this test series the potentiostat (Gamry Instruments 1010E) was used to get results of different frequencies over a prolonged period of time. The specimen without fibers was analyzed at a concrete age of 14 days, in only one direction because the potentiostat was able to log results continuously over a period of about 17 h whereat the frequency was varied from 1 Hz to 100 kHz. The influence of the measuring time on the electrical resistivity is presented in Figure 4.4.

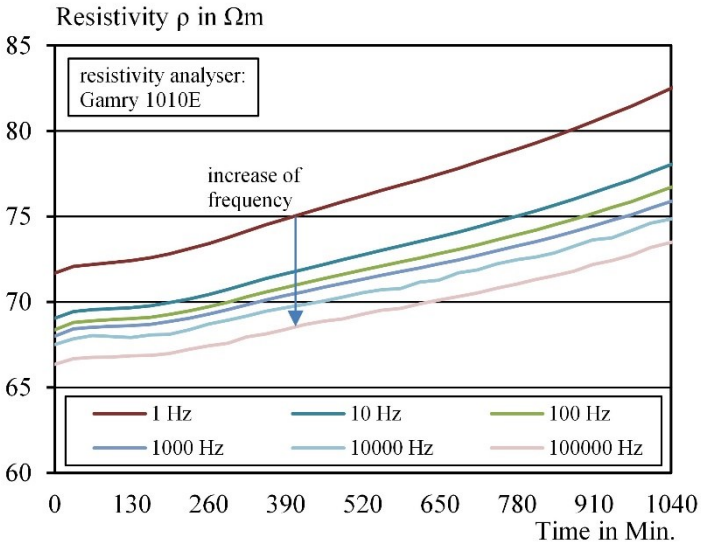

Figure 4.4 Effect of varying measuring time on the electrical resistivity of PC, resistivity analyzer: Gamry Instruments 1010E

Because of the higher concrete age of 14 days, the electrical resistivity in general was higher than for the same specimen at a concrete age of 7 days (cf. Figure 4.3). This phenomenon will be investigated in detail in Section 4.4.4. It can be determined that in the first 30 min there was an increase in electrical resistivity, followed by a small plateau and another nearly linear increase until

the end of the observations. This behavior occurred independently from frequency of AC, whereat an increase of the electrical resistivity could be observed with increasing frequency. The time-depending effects can be explained by the drying process of the sponge cloths and the concrete and the resulting loss of saturation of the pore structure, which is the conductive part of both the concrete and the sponge cloths. The dehydration process starts at the surface of the concrete, but a small reservoir of water can possibly be found in the sponge cloth that serves for the connection of the electrodes.

During the first minutes the loss of moisture of those couplings is high because of the open pore system of the surface dry concrete specimen. After a first water exchange process the moisture of the coupling and the concrete will be balanced and the water exchange will nearly stop. But after a time both materials will start to interact with the surrounding air, which has a lower moisture content and so a dehydration process of the whole measuring system will start. For the measuring process the conclusion can be drawn that the time of contact of specimen and coupling should be minimized, and the sponge cloths must be kept in a nearly constant condition of moisture.

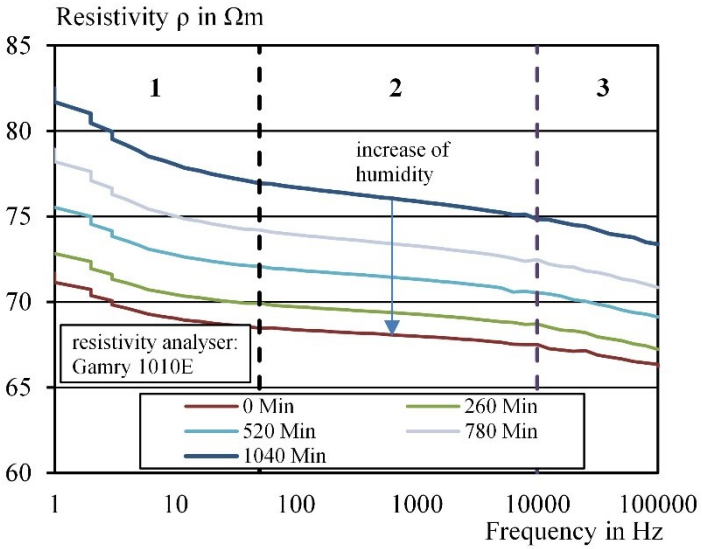

Figure 4.5 Effect of varying frequency on the electrical resistivity of concrete, resistivity analyzer: Gamry Instruments 1010E

In Figure 4.5 a predictable loss of electrical resistivity with increasing frequency could be observed, which was nearly independent from the moisture of the coupling, what is clearly visible through the parallelism of the single curves for different measuring times. In general, the fact that an increase of humidity leads to a decrease of the electrical resistivity, which is described above as well as in earlier studies of the authors (see Cleven et al., 2021), also can be identified in this figure. The single curves can be divided by dashed lines into three parts, based on different sectors of frequency. In the first sector, between frequencies of 1 Hz to about 50 Hz, a disproportional decrease of the electrical resistivity was visible. An explanation of this behavior can be found in polarization effects which can appear on both electrodes at low frequencies and are the reason to use AC instead of direct current (DC) in this study. At higher frequencies in sector two there was a linear decrease of the electrical resistivity, followed by another disproportional descending above a frequency of 10 kHz in sector three, that can be explained by inductive effects in cables or connections of the measuring system. For the following measurements based on these results it was decided to investigate the electrical resistivity in the range of 100 Hz to 100 kHz to avoid polarization effects that possibly modify the concrete surfaces or couplings of the system.

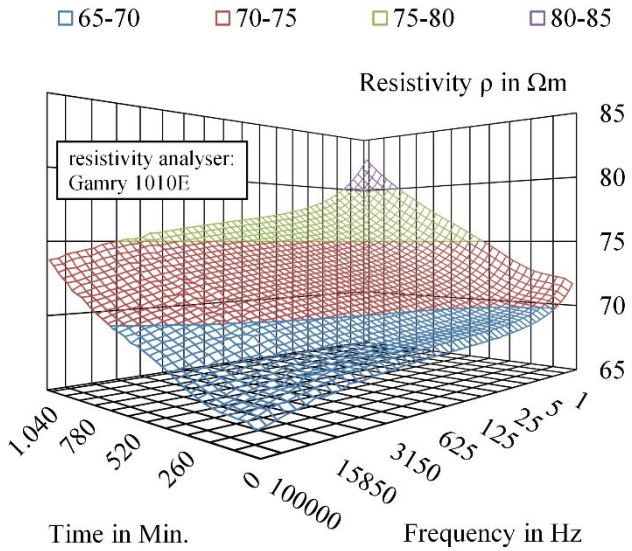

Figure 4.6 Effect of varying frequency and measuring time on the electrical resistivity of PC, resistivity analyzer: Gamry Instruments 1010E

As can be seen in Figure 4.6, which shows the complete set of data of the investigations of measuring time and frequency, both parameters show a huge effect on the electrical resistivity, while there is no influence of the parameters among each other.

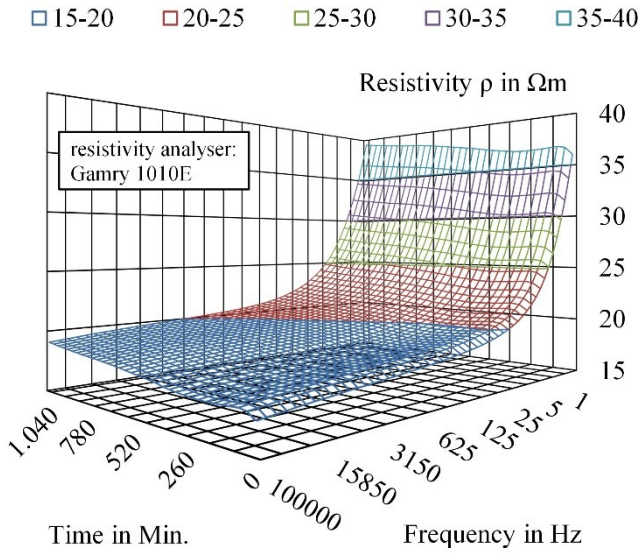

Figure 4.7 Effect of varying frequency and measuring time on the electrical resistivity of SFRC with a fiber dosage of 80 kg/m³, resistivity analyzer: Gamry Instruments 1010E

The same results could be identified on a SFRC specimen with 80 kg/m³ of fibers (Figure 4.7). This specimen was tested at a concrete age of 14 days in one horizontal direction so that the fibers were supposed to show a huge effect because it can be assumed that most of the fibers will be oriented in horizontal direction when the specimens are produced in layers and compacted on a vibration table. As can be seen the influence of the frequency on the electrical resistivity was significantly higher for SFRC than for unreinforced concrete for frequencies below 10 Hz. This is probably based on the polarization effects on every connection point of fiber and concrete which takes part in the electrical connection. Because of the high effect of the frequency the measuring time or dehydration status of the specimen becomes

subordinated. A comparison of both figures leads to the conclusion, that a higher frequency is better for the differentiation of the fiber content because at low frequencies a fiber content of 80 kg/m³ resulted in a doubling of the electrical resistivity whereas at high frequencies it led to a nearly four times higher electrical resistivity so the selectivity of the results will be higher.

4.4.3 Influence of Amplitude

Another parameter to be investigated was the amplitude of the AC. With help of the potentiostat (Gamry Instruments 1010E), different amplitudes in the range of 10–200 mV could be realized in combination with frequencies in the same range than in Section 4.4.2. The investigation was done to see if any effects, like corrosion or polarization, occur if the amplitude is set too high. To see beneficial effects over a big spread of electrical resistivities, the SFRC specimen containing 80 kg/m³ of fibers from Section 4.4.2 was also used in this investigation. This specimen was also evaluated with the LCR meter with a fixed amplitude of 600 mV to see if the LCR meter gives comparable results to the potentiostat. The results in Figure 4.8 showed no significant effects of the amplitude on the measured electrical resistivity while the influence of the frequency was clearly visible like described in Section 4.4.2. For the measurements with the potentiostat, frequencies between 1 Hz and 100 kHz were investigated and for the LCR meter only the five frequencies 100 Hz, 120 Hz, 1 kHz, 10 kHz, and 100 kHz were possible. This means that the highest impact of the frequencies on the electrical resistivity was not visible in the results produced with the LCR meter. Because nearly no differences in the measured resistivity for different amplitudes was visible, it can be concluded that in the tested range of amplitudes no damage based on the AC were induced to the concrete. Therefore, the highest amplitude can be used for the further investigations, what will result in the best resolution of the results, because higher voltages will be induced and so the resistivity of the concrete can be calculated with a higher accuracy. This shows that the LCR meter is an appropriate measurement system with the given amplitude of 600 mV.

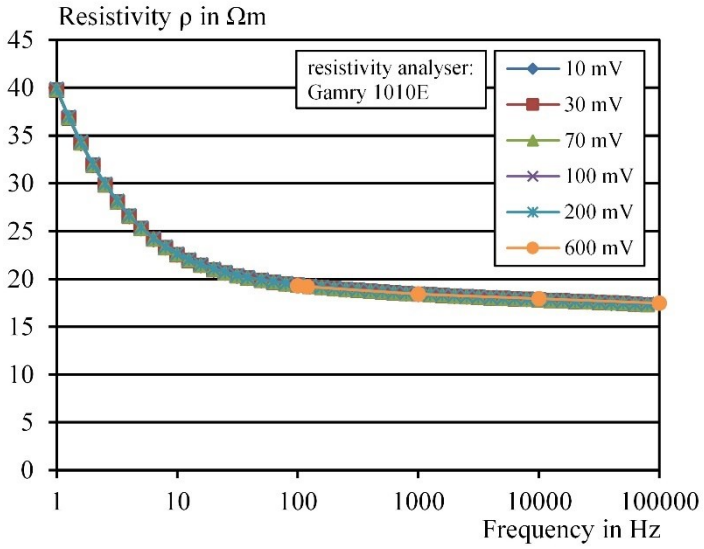

Figure 4.8 Effect of varying amplitudes on the electrical resistivity of SFRC, resistivity analyzer: Gamry Instruments 1010E

4.4.4 Influence of Specimen Age

The last investigated parameter in this research was the age of the specimen and so the hydration progress and the resulting pore structure. This effect was analyzed over a period of

56 days, on specimens with fiber contents from 0 to 120 kg/m³ with the Extech Instruments LCR200 at all five possible frequencies. Like described in Section 4.4.1, a significant loss of the electrical resistivity was visible with increasing fiber content. This can also be seen in Figure 4.9 for a frequency of 10 kHz. Also, the hydration changed the electrical resistivity of the PC, respectively of SFRC. With increasing specimen age and therefore increasing hydration process and building of pore structure, an increase of the electrical resistivity is accompanied. The effect from an age of 7–28 days thereby was bigger than the increase from 28 to 56 days. Because of the used binder, OPC, it is obvious that the greatest part of the hydration will be completed at the age of 28 days, so that most of water will be bound to the cement clinker and the pore structure will be almost finalized. After 28 days the changes in the pore structure will be smaller than in the first days, so the resulting increase in electrical resistivity is also smaller.

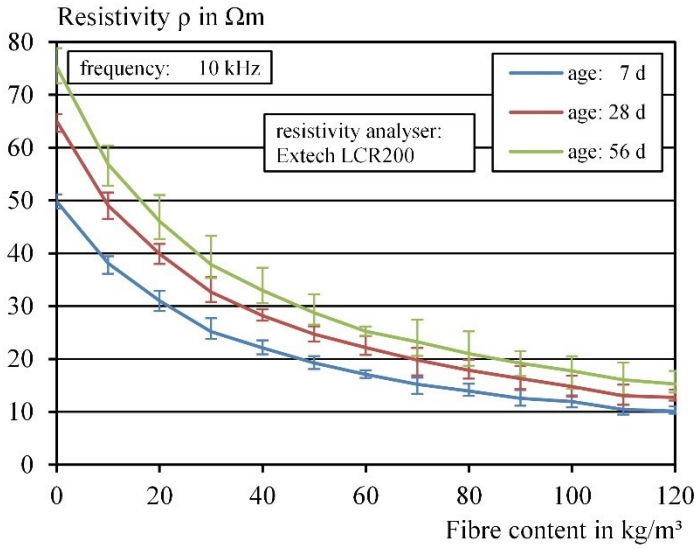

Figure 4.9 Effect of specimen age/storage duration on the electrical resistivity, resistivity analyzer: Extech Instruments LCR200

The changes of the microstructure based on the hydration process showed a higher effect on concrete with lower fiber dosages, what means that effects on connectivity between fibers and concrete did not take place. With increasing concrete age, the influence of fibers in the concrete on the measured electrical resistivity increased what would be a good tendency for the analysis of structural buildings in case of maintenance and repair. But it should be noted that the age of the concrete must be considered to predict the fiber content of an analyzed concrete based on its electrical resistivity.

4.4.5 Statistical Verification

At the end of investigations the variance of the electrical resistivity of different concrete specimens within the same composition and identical curing conditions was proved by a statistical analysis of all six series of identical concretes with identical curing conditions. A graphical presentation of the coefficients of variation of the electrical resistivities of the specimens with an age of 7 days can be seen in Figure 4.10. It is evident that the PC without fibers only showed a small spread in the electrical resistivity while the fiber reinforced specimens had slightly bigger COV's. No correlation between fiber content and spread was identified. Therefore, the addition of fibers generally led to an increased COV with respect to

the measurement of the electrical resistivity. The main reason seems to be the random distribution and orientation of fibers in the specimen. Also, no significance between the frequency and the spread could be seen in the results of the 7 days old concrete.

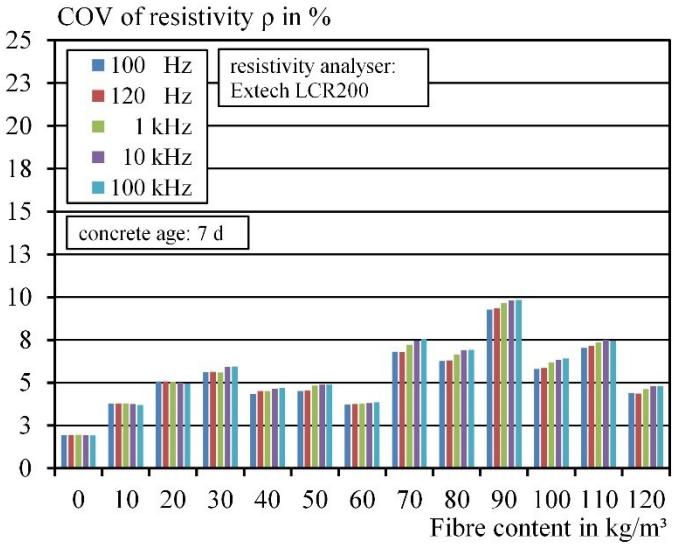

Figure 4.10 COV of the electrical resistivity in measurements at specimen age of 7 days, resistivity analyzer: Extech Instruments LCR200

In contrast to those results the variance of measurements of the electrical resistivity for the older specimens with an age of 56 days was significantly higher (Figure 4.11). Even the PC shows a higher COV, for the SFRC specimens, except for a fiber content of 60 kg/m³, a much higher spread of the electrical resistivity occurred. In this specimen age an effect of the frequency was also clearly visible. For the frequencies below 10 kHz it seems that with an increasing fiber content the COV of the electrical resistivity likewise increased. With a fiber content of 80 kg/m³, it seems to be a limit with a COV of about 18 % and a further increase of fibers did not lead to a higher spread if the results of a fiber content of 110 kg/m³ were assessed as outliers.

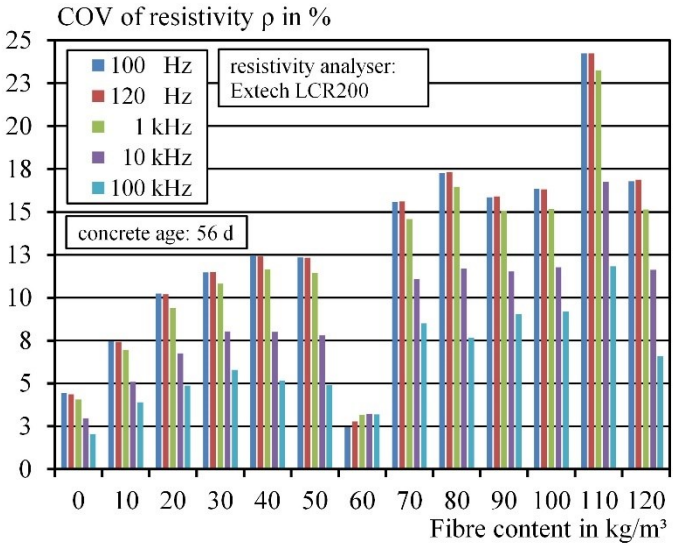

Figure 4.11 COV of the electrical resistivity in measurements at specimen age of 56 days, resistivity analyzer: Extech Instruments LCR200

The positive aspect of these results is that for higher frequencies the spread is significantly smaller and only slightly above the results of the very young concrete. So, the effects of hydration of the concrete within this testing conditions showed the lowest significance. For the development of a model that predicts the fiber content based on measurements of the electrical resistivity, high frequencies should be used to reach statistically valuable results.

4.5 Development of a Prediction Method

4.5.1 Basic Approach

Because of the influence of the specimen age (Section 4.4.4), the electrical resistivity itself as a direct parameter for the prediction of the fiber content of concrete is not suitable. The conductivity of the concrete is too much influenced by the hydration process and by the humidity of the concrete. Therefore, a parameter must be found that compensates for such effects. Based on physical fundamentals, equivalent circuits were analyzed but because of the inhomogeneity and anisotropy, simple models like parallel connection or series connection were not applicable. For this reason, the increase of conductivity of SFRC relative to the PC λ was calculated for each fiber content by the following (eq. *4-2*).

$$\lambda = \sigma_{SFRC} \,/\, \sigma_{PC} \qquad \text{(eq. 4-2)}$$

where, λ is the increase of conductivity in %; σ_{SFRC} is the conductivity of SFRC in s/m; σ_{PC} is the conductivity of PC in s/m. For developing a prediction method, only the measurements are used, that were performed with use of the Extech Instruments LCR200. The correlation between fiber content and increase of conductivity is presented in Figure 4.12. A nearly linear correlation between fiber content and increase of conductivity could be observed, where the spread increased with increasing fiber content. This means a relative failure of the correlation of about ± 10 % could be identified while the mean values showed a coefficient of determination of 0.9984. For the adaption of the test setup as in situ test method for concrete structures the determination of the conductivity of the PC will be difficult. Investigations of very small volumes of SFRC are going to be performed to check if it is possible to estimate the conductivity of PC without steel fibers if the volume of the specimen or the percolated volume is small enough.

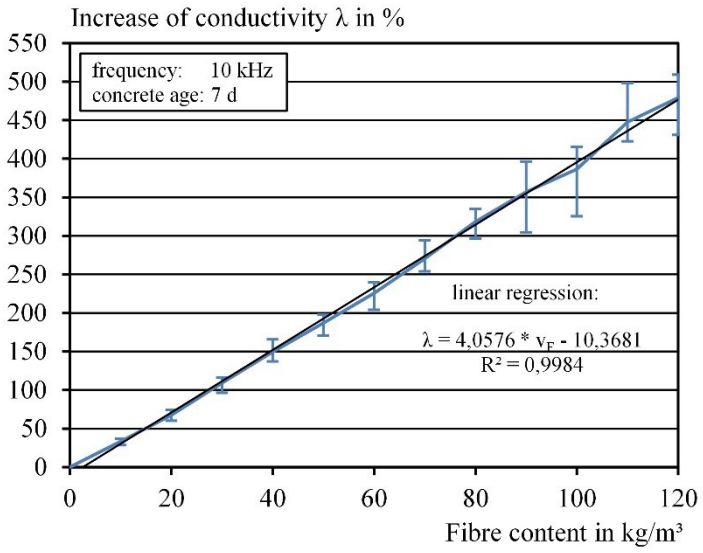

Figure 4.12 Correlation between fiber content and increase of conductivity

For the prediction of the fiber content the axes of the diagram have been swapped in Figure 4.13 so the fiber content c_F becomes the result of the calculated increase of conductivity λ. With this diagram and the equation the fiber content of a specimen can be predicted based on the measured electrical resistivity by the following (eq. *4-3*).

$$c_F = 0.25 * \lambda + 2.65 \qquad \text{(eq. 4-3)}$$

where, c_F is the fiber content in kg/m³; λ is the increase of conductivity in %.

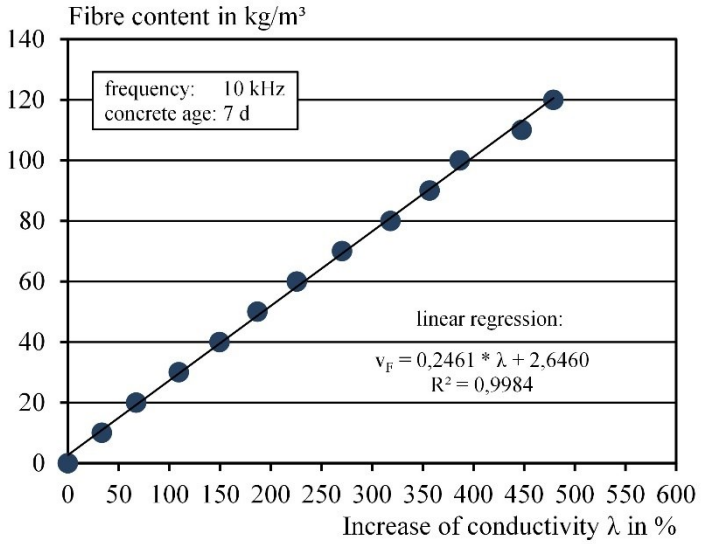

Figure 4.13 Prediction method of fiber content based on increase of conductivity

As can be seen in (eq. *4-3*) a higher fiber content goes along with a high increase of conductivity and a linear correlation can be used to display this behavior. One inaccuracy in the function can be found in the axial intercept that deviates from the origin of the coordinate system. Based on theoretical considerations a fiber content of 0 kg/m³ that represents the PC must lead to an increase of conductivity of 0 % but as a result of a limited data base the empirical analysis led to the best agreement of the function and the data with this inaccuracy.

4.5.2 Extension to Different Concrete Ages

In the last step the prediction method has been validated with all gained raw data. For this purpose, all single values of the six test series in the three different concrete ages were compared with the basic model from Section 4.5.1. Also, the mean values of the six series were included in Figure 4.14. It is evident that the parameter λ gave the possibility to approximate the fiber content of the concrete almost independent to the concrete age from 7 to 56 days. The mean values for all ages showed a good agreement with the regression, while the single values partially differed from it.

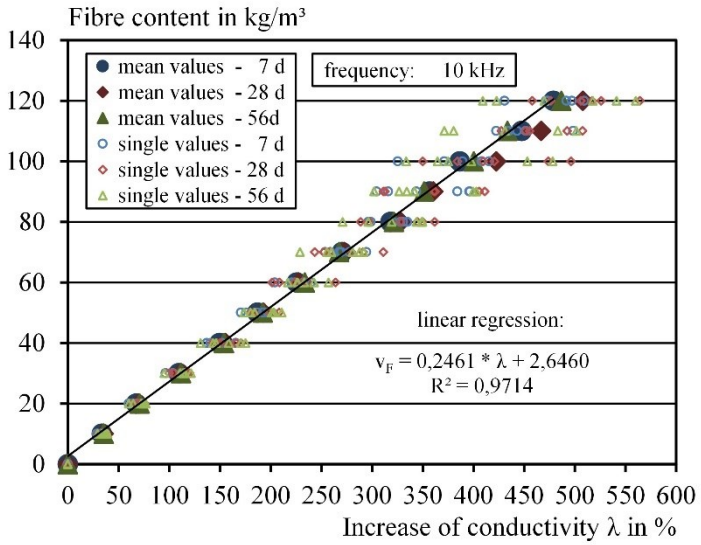

Figure 4.14 Extension of the prediction method to different concrete ages

With increasing fiber content, the scatter between the model and the single values also increased, what can be interpreted as a relative scatter in material parameters. An absolute error was not visible because for low fiber dosages neither the single values itself showed nearly any deviation nor a difference from the model curve. For the possibility of an approximation of the fiber content via the electrical conductivity this tendency means that an adequate number of specimens must be taken and tested to gain sufficient raw data. Otherwise, large safety factors must be considered to not overestimate the fiber content. With a series of six specimens for example it is possible to estimate the fiber content with an accuracy of ± 8 %. For fiber contents in the practical range of above 20 kg/m³ an accuracy of ± 3 % could be observed. In contrast to the mean values by use of the single values the largest discrepancies in the estimated fiber content to the real one were ± 17 %.

Looking onto the mean values for the higher concrete ages it can be noticed that the model seemed to be imperfect, since the mean results for high fiber contents from over 100 kg/m³ did not show a linear trend but the curve bottomed out. With a higher amount of data and even older specimens the model could be optimized to reach a more sufficient estimation. The second problem was the divergence of the model curve from the point of origin. This point represented the PC and so the increase of conductivity using fibers was definitively 0 %. For low fiber contents because of this shift of the curve an additional inaccuracy was intrinsic so that a sufficient estimation of contents of about 10 kg/m³ was not possible. On the other hand, it is questionable if such low fiber contents are used in practice and a need to determine the parameters of the SFRC in detail exists.

4.6 Conclusions

The fiber content is an important parameter which has an immense effect on the mechanical performance of SFRC. Because of the lack of determination methods for the fiber content in hardened concrete, relatively high safety factors must be used in static analysis. Based on the electrical conductivity, a new method was presented to estimate the fiber content of a known concrete mixture with ordinary steel fibers.

To set up this model investigations on concrete specimens with fiber contents from 0 to 120 kg/m³ were performed and a statistical evaluation was done by the comparison of six

series of specimens. The results show an influence of different parameters on the electrical conductivity respectively resistivity. While the amplitude of AC nearly has no effect on the electrical resistivity of SFRC, the frequency must be taken into consideration. Low frequencies especially for SFRC result in a significantly higher electrical resistivity based on polarization effects than frequencies above about 10 kHz, where a nearly constant electrical resistivity can be measured. For PC, the effect of frequency is much smaller, so this parameter could be a good research topic for further studies. The measuring period, synonymous to the dehydration of the specimens, which were stored under water, shows only a small effect, when it is smaller than a few hours and the biggest effect can be seen on PC. On the contrary an increase of the age of specimen from 7 to 56 days leads to a significant increase of the electrical resistivity because of the change of its pore structure. However, the biggest effect on conductivity results in the addition of fibers which lead to an additional conductive part in the material and therefore increase the conductivity.

By the calculation of the increase of conductivity λ the effects of the aging could be compensated and a linear correlation between fiber content and λ was identified. Based on this correlative model it was validated which accuracy of estimation for the fiber content is possible by measuring the electrical conductivity. It was observed that an amount of six specimens leads to an efficient estimation of the fiber content with deviations of about ± 6 %, which could help to minimize safety factors for static analysis.

In comparison to different research directions, like the use of microwave analysis of SFRC (see e.g., Franchois et al., 2004; van Damme et al., 2004) the presented method is still limited to concrete specimens and not yet ready for in situ analysis of concrete structures. Nevertheless, the very fast measuring process, the low modeling effort and the observed independence of the results from the concrete hydration, are advantageous compared with permittivity measurements, where a constant behavior is expected only for fully hydrated concrete.

However, it shall be observed in further investigations if the identified model of this study can be optimized by an increased data base and if the effect of different concrete mixtures can be as easily compensated as the different concrete ages. Also, a method shall be identified that allows an estimation of the conductivity of the PC so the test method can be used on concretes in practice when no PC is available. Additionally, in further test series of the authors, the test setup has been modified for tests of cylindrical specimens like drilling cores that can be extracted out of existing structures (see Cleven et al., 2022a; Cleven et al., 2022b). With help of a finite element modeling of the electrical current flow an extension of the test setup is supposable that can be applied directly on structural elements, since it has already been shown for drilling cores. By adopting the finite element model to more difficult geometries, in a first step to precast elements, the possibility of in situ testing of structures shall be analyzed and possible limitations of the test setup shall be identified and removed. One major challenge concerning further development of the presented technique is the need to consider the saturation state, respectively the moisture content, of the concrete to be tested, which varies according to age and geometry of the investigated concrete structures. To address this challenge, preconditioning tests on laboratory concrete samples may be used to derive calibration curves, which enable a subsequent correction of the moisture effect.

5 Investigations on Concrete Cylinders

This section was published as scientific paper under the title “A New Method to Determine the Steel Fibre Content of Existing Structures — Test Setup and Numerical Simulation” in the journal Applied Sciences in 2022 (Cleven et al., 2022a).

5.1 Abstract

The diagnostics of constructions built with steel fibre reinforced concrete are extremely difficult to conduct because, typically, no information on the actual amount and orientation of the fibres is available. Therefore, it is of great interest to engineers to have the possibility to determine the steel fibre content and, at best, also the orientation of the fibres in existing structures. For this purpose, an easy-to-use test setup was developed and tested, in the course of laboratory investigations. This method can be used for cylinders, for example drilling cores, that can later be taken of existing structures, to determine both the fibre content and orientation. Based on these results, a model for cylindrical specimens was derived, which can be used for varying concrete compositions with steel fibre contents of up to 80 kg/m³. In the case of missing information concerning the concrete composition, it allows an initial estimation for the fibre content. In case additional information about the concrete composition is available, a much higher accuracy of the projected steel fibre content and therefore, an assessment of the building’s condition is possible.

5.2 Introduction

Short fibres, especially steel fibres, can be used for the reinforcement of concrete to increase ductility, toughness, resistance to cracking and tensile strength (see, e.g., Gouri et al., 2010; Kobaka et al., 2019; Luo et al., 2020; Rossi & Wolf, 2019; Woo et al., 2005; Zhang et al., 2019). As a consequence, it is possible to reduce or even avoid the use of traditional reinforcements. The mechanical properties of steel fibre reinforced concretes (SFRCs) are highly dependent on the fibre content and the fibre distribution and orientation inside the concrete elements (see, e.g., Gettu et al., 2005; Gouri et al., 2010; Martinelli et al., 2021b). Areas with a very low number of fibres or fibres that are not oriented in the direction of the tensile tension lead to a higher risk of cracking and can cause the failure of the whole structure (see, e.g., Barnett et al., 2010; Zak et al., 2001). For this purpose, during the casting of SFRC, significant quality control measures, e.g., the regular testing of the amount of steel fibres by wash out procedures, need to be applied. Assuming an optimum concrete composition, SFRC typically possesses a longer service life and thus, a lesser need for maintenance. This makes it an interesting material for the repair of reinforced concrete structures (see, e.g., Plizzari, 2018; Rossi & Wolf, 2019). Nevertheless, in the case of SFRC application, the real fibre content and, especially, the fibre distribution are not well known and so, the use of significant safety factors is necessary during the design stage (see, e.g., Cugat et al., 2020; Herrmann et al., 2019; Molins et al., 2009; Tarawneh et al., 2021).

These problems show the need for a test setup that is easy to apply, ideally non-destructive and can be used for rehabilitation processes to determine the fibre parameters, for example (see, e.g., Komárková, 2016; Li et al., 2020; Li et al., 2021; Woo et al., 2007). Possible methods that were used in different studies are based on computed tomography (CT), microscopic analysis of sectional images or inductivity measurements (see, e.g., Al-Mattarneh, 2014; Balázs et al., 2017; Ferrara et al., 2012; Lee et al., 2015; Li et al., 2020; Li et al., 2021; Park et al., 2021; Ponikiewski & Katzer, 2016; Torrents et al., 2012; Zak et al., 2001). The main

problems with CT analysis are its high cost and the limited size of specimens. Furthermore, it is not possible to use this technique in situ on construction sites. The same arguments can be found for cross sectional image analysis, whereas this technique is even less accurate than CT-scanning. Inductive techniques are easier to use but are also limited to small specimen sizes.

A technique that is already used for structural concrete monitoring to identify and locate steel rebars is the electric resistivity measurement (see, e.g., Ozyurt et al., 2006b; Raupach et al., 2013; Reichling, 2014; Reichling & Raupach, 2012; Reichling et al., 2015; Ruan & Poursaee, 2019). Based on an easy-to-use test setup, which was already tested in past studies conducted by the authors (Cleven et al., 2021), a new application test based on the analysis of cylindrical specimens is proposed in this research paper. In the first part of the study, the test setup is adjusted and a numerical model is generated to simulate the flow of the alternating current, which enables the comparison and calculation of the resistivity of the different specimen directions that are possible. With help of the proposed setup, cylindrical specimens with fibre contents of up to 80 kg/m³ are analysed and correlations between the electrical resistivity and the fibre content and fibre orientation are developed to enable the use of drilling core samples in the second part (Cleven et al., 2022b).

5.3 Materials and Methods

5.3.1 Concrete Mix Design

The concrete used in all experiments was the same mixture, which was also used in Cleven et al., 2021. It was designed for a good workability, even at high fibre contents, and adherence to the regulations of EN 206, 2017. To investigate both plain concrete (PC) and steel fibre reinforced concrete (SFRC), the basic concrete mix design, shown in Table 5.1, was used for all mixes. Fibre dosages of 40 kg/m³ and 80 kg/m³ were used, respectively. The macro steel fibre was produced from steel wire with hooked ends and had a length of 60 mm and a diameter of 1 mm, which equals an aspect ratio of 60.

Table 5.1 Concrete mix design of the basic concrete

Parameter	Unit	Content
CEM I 32.5 R		300.0
Water	kg/m³	180.0
Aggregates		1849.5
Water/cement ratio		0.60
Grain size distribution	-	A/B16
Steel fibre type		Macrofibre 60 mm
Steel fibre content	kg/m³	0, 40, 80

The concrete was mixed in a compulsory mixer with a nominal volume of 160 L. First, the cement and the aggregates were homogenized for 30 s before the water was added in the ongoing mix process. After a first mixing phase of two minutes, a visual inspection of the concrete was carried out and adhering components on the mixer wall were removed. Afterwards, the concrete was re-mixed for one minute before the consistency was tested via a flow table test. Additionally, the fresh concrete density and the air content were determined in accordance with EN 12350-5, 2019, EN 12350-6, 2019 and EN 12350-7, 2019. For the SFRC,

the fibres were added subsequently and followed by another mixing period of at least one minute.

After the final mixing, six cylinders with included electrodes (see Section 5.3.2) were produced and compacted on a vibrating table. The specimens were covered with foil to avoid the dehydration of the surface. The specimens were left in the formwork and were stored in a climate of 20 °C and 65 % relative humidity, since water storage was suspected to damage the electrical contacts of the electrodes. For each combination of fibre content and electrode array, one specimen was produced and tested. The small number of samples was chosen in order to gain the initial results of the new test setup and to investigate the general suitability of the newly developed method for the detection of fibre content and orientation. Therefore, a statistical analysis of the results was not possible and is planned to be performed in further investigations with a larger number of samples.

5.3.2 Experimental Setup

The basic setup from Cleven et al., 2021, consisting of two stainless steel electrodes with dimensions of 200 × 200 mm² connected to an LCR meter, was adjusted to enable the measurement of cylindrical specimens. The LCR meter used for impedance measurements was an Extech Instruments LCR200 with a voltage amplitude of 600 mV rms and variable frequencies of the alternating current of 100 Hz, 120 Hz, 1 kHz, 10 kHz and 100 kHz.

For the investigation of the cylindrical specimens, an advanced test setup was developed based on the existing equipment. Therefore, as the first step, a breadboard (see Figure 5.1) was configured, including the LCR meter, which was directly connected to the different electrodes. With this approach, it was possible to analyse the electrical resistivity, which was calculated from the electrical resistance and the dimensions of the specimens in different directions inside the specimens.

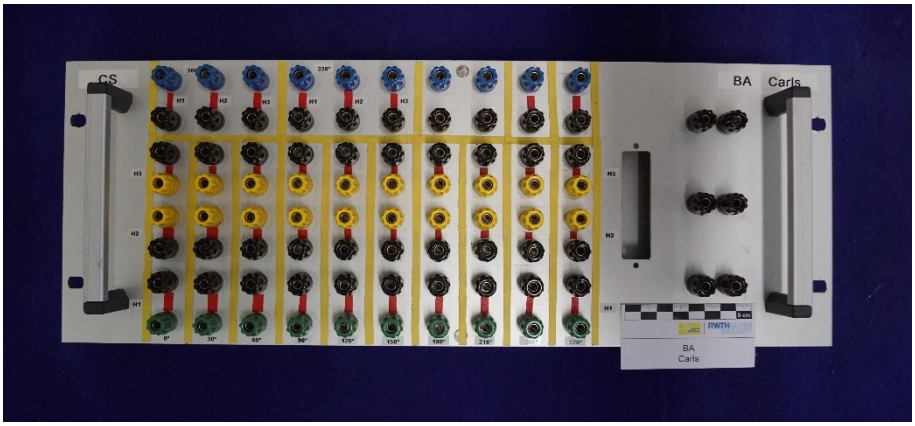

Figure 5.1 Breadboard for the connection of the LCR meter and different electrodes

The setup was validated using cylindrical specimens with a height of 200 mm and a diameter of 100 mm with built-in metal oxide coated titanium (MMO) electrodes. Those electrodes were included in PVC formworks with a resulting connection area of 40 x 10 mm² each and could be connected via a notch to the breadboard from the outside. This setting was chosen in order to ensure a good connectivity between the electrodes and concrete and eliminate the effects of contact pressure. In total, six specimens with electrodes at three different heights with vertical distances of 20 mm each were prepared. Three of the specimens consisted of twelve electrodes with angular distances of 90 ° and the other three six electrodes with angular

distances of 180 °. The resulting formwork, consisting of twelve electrodes, and the electrodes themselves are presented in Figure 5.2.

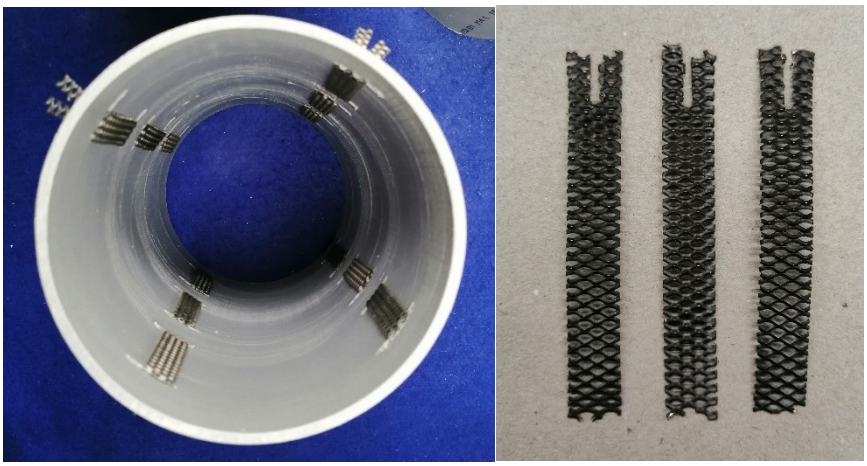

(a) **(b)**

Figure 5.2 PVC formwork with 12 MMO grid electrodes at three height levels with angular distances of 90 ° (**a**) and MMO grid electrodes with notches for the clamp (**b**)

5.3.3 Modelling of Current Flow

For the comparison of the resulting values of the measurements with the LCR meter, the electrical resistance must be converted to electrical resistivity considering geometry factors, which depend on the current flow. While the electrical resistivity, measured in Ωm, is a material-specific parameter and is free of any geometrical influences, the electrical resistance, measured in Ω, is a measurable value based on a specific configuration of the test setup and the specimen geometry. For trivial electrode configurations, such as two parallel plates, which have been used for the cubic specimens in earlier studies (Cleven et al., 2021), this geometry factor is easy to calculate, but a simulation of the electrical current flow is necessary for more complex configurations. For this purpose, the software Comsol Multiphysics (version 5.3a, build version 229) was used and a grid model of the cylindrical specimens was generated.

The model consists of a cylinder with a diameter of 100 mm and a height of 200 mm and represents the concrete specimen. On the surface, there are 12 electrodes at three height levels, 4 on each level, in circular distances of 90 ° and with a thickness of 1 mm. Each electrode has an area of 40 x 10 mm² and is simulated as a segment of a circle to enable optimal connection to the cylinder. In this way, the model can be used for various electrode configurations. The FEM model of the test setup is presented in Figure 5.3 (a) and the resulting grid model for a 12-electrode configuration can be seen in Figure 5.3 (b). The model presented was set up using the following assumption: the concrete and steel domain are considered to show homogeneous and isotropic behaviour and the sponge cloths as well as the polarization behaviour of the steel electrodes can be neglected. The latter is considered to be a valid assumption for the alternating current (AC) measurements using the parameters stated above.

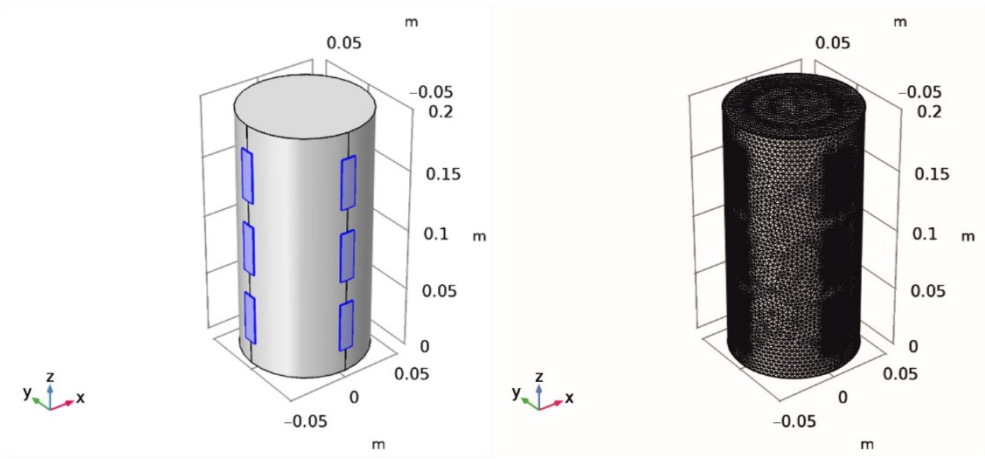

(a) **(b)**

Figure 5.3 FEM model for cylindrical specimens consisting of a concrete cylinder (grey) and twelve electrodes (40 x 10 mm²) at three height levels and with angular distances of 90 °C (blue) (**a**) and grid model to simulate current flow with an extremely fine grid (**b**)

With this model, the geometry factors (k) of all applied electrode configurations were determined assuming a specific material resistance for the concrete of 100 Ωm and an electric potential of 0 V for one electrode or set of parallel connected electrodes and 600 mV for the second electrode or set of parallel connected electrodes. Those values were chosen for the simulations as near realistic values for the test setup and materials (see Section 5.3.2). The simulations resulted in a calculated current by Comsol, which enabled the estimation of the geometry factor using (eq. *5-1*). The calculated k factors are mentioned in respective areas for each section of the results.

$$k = \frac{I * \rho}{U} \qquad \text{(eq. 5-1)}$$

with:

k: the geometry factor in m
I: the electric current in A
ρ: the electrical resistivity (set to 100 Ωm)
U: the electric potential (set to 1 V)

Since the connection of the MMO grids, embedded in the concrete, illustrate a near optimal connection of electrodes and concrete, the electrical conductivity of the electrodes was set to that of titanium, for MMO, of 2.5 x 10^6 S/m. The visualisation in Figure 5.4 (a) shows that unconnected electrodes (at the middle height level) have an impact on the iso-surfaces of the current, which represent locations with identical electric potential, in the case of a good electrical connection between the concrete and the electrodes. The current flow can be supposed to be orthogonal to those iso-surfaces. For the setup with a lower number of embedded electrodes with angular distances of 180 °, Figure 5.4 (b) shows that the iso-surfaces are more parallel in the parts of the specimen where no electrodes are embedded, but less uniformly distributed over the whole specimen. Additionally, for a horizontal current flow, the setup with electrodes with angular distances of 180 °, only one direction (y) is measurable, while for the setup with a higher number of electrodes, both directions (x and y)

can be analysed. In the later experiments, therefore, it is assumed that both horizontal directions have almost the same electrical resistivity and thus, the relative conductivity of different directions, representing the relative orientation of the fibres (orientation factor), can be calculated.

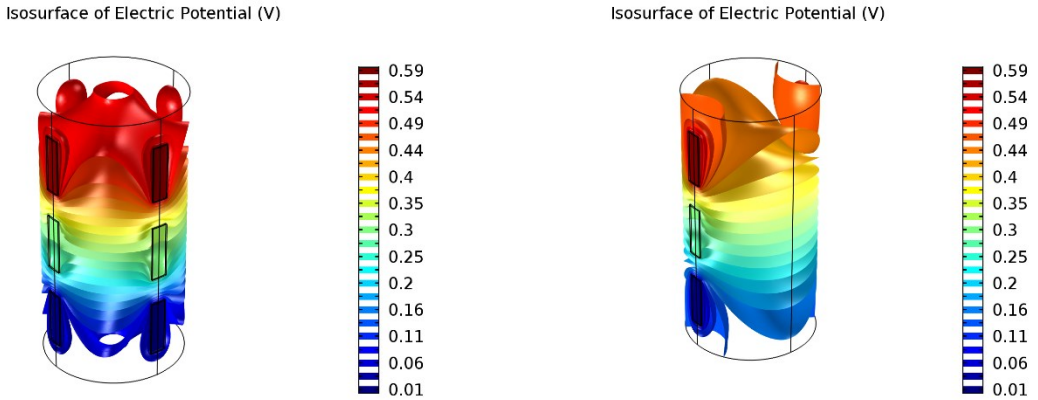

(a) **(b)**

Figure 5.4 Resulting iso-surfaces, calculated by Comsol, for angular distances of the electrodes of 90 ° (**a**) 180 ° (**b**)

5.3.4 Evaluation of the Results

After the calculation of the electrical resistivity of each electrode configuration was carried out, the fibre content and the fibre orientation inside the concrete were analysed using the equation of Woo et al., 2005 (eq. *5-2*):

$$\frac{\sigma}{\sigma_m} = 1 + [\sigma]_\Delta * \Phi \qquad \text{(eq. 5-2)}$$

with:

- σ: the electrical conductivity of the SFRC in Ωm
- σ_m: the electrical conductivity of the PC in Ωm
- Φ: the fibre volume fraction
- [σ]: the intrinsic conductivity (eq. 5-3)
- Δ: the ratio of conductivity of fibres and PC

For steel fibres, the ratio of conductivity of the fibres and plain concrete Δ tends to infinity, so the intrinsic conductivity can be calculated as follows Woo et al., 2005:

$$[\sigma]_\infty = \frac{1}{3}\left(\frac{2 * (AR)^2}{3 * ln[4(AR)] - 7} + 4\right) \qquad \text{(eq. 5-3)}$$

with:

- AR: the aspect ratio of the fibres

For the given aspect ratio of 60, an intrinsic conductivity of 255.5 can be calculated. By converting (eq. *5-2*), the fibre content can be directly determined from the results of the measurements. Therefore, for all types of specimens, a global value of electrical resistivity

respectively conductivity has to be determined. For the cylindrical specimens, several combinations were tested to find the optimum result.

When (eq. *5-2*) is used with the single direction test results of only one electrode configuration, it can be used to estimate the fibre orientation of this direction in context to the whole specimen by building the ratio to the sum of the other directions or three times the global fibre content.

5.4 Results and Discussion

5.4.1 Validation of the Test Setup

5.4.1.1 Impact of the Frequency of the Alternating Current

In the first series of six specimens, one of each fibre content and electrode array, with fibre contents of 0, 40 and 80 kg/m³, the test setup was assessed in combination with the FEM model, where the electrical conductivity of the electrodes was set to that of titanium (2.5×10^6 S/m). The corresponding geometry factors are given in Table E.53 and Table E.54, Annex E. The specimens were left covered with foil in the formworks and were tested at 9 days and 38 days of age. The different test dates were chosen to see whether changes in the pore structure of the concrete, based on hydration, show significant influences on the results of the electrical resistivity measurements. The age of 9 days represents a very early stage of the concrete, where the hydration process has not yet been finished but an initial investigation of concrete structures would be possible because partial demoulding could be performed, depending on the structure itself. The age of 38 days was chosen because it was assumed that the hydration process would be almost complete and the drying process of the concrete should not have taken place, so a comparison of the results of both ages will provide information about the influence of the hydration process and will not be affected by the different saturation of the specimens. For each specimen, the electrical resistivity in the horizontal and vertical direction was determined with several electrode configurations and the five possible frequencies of the alternating current (100 Hz, 120 Hz, 1 kHz, 10 kHz, 100 kHz). As presented in several previous studies (see, e.g., Cleven et al., 2021; Woo et al., 2005), the frequency of the alternating current influenced the electrical resistivity, where a higher frequency led to slightly lower resistivity values. While for the PC there was almost no influence and a change in frequency from 100 Hz to 100 kHz only resulted in a decrease in the resistivity of about 2 %, for SFRC, depending on the fibre content, a decrease of 10 to 20 % was observed (see Figure 5.5).

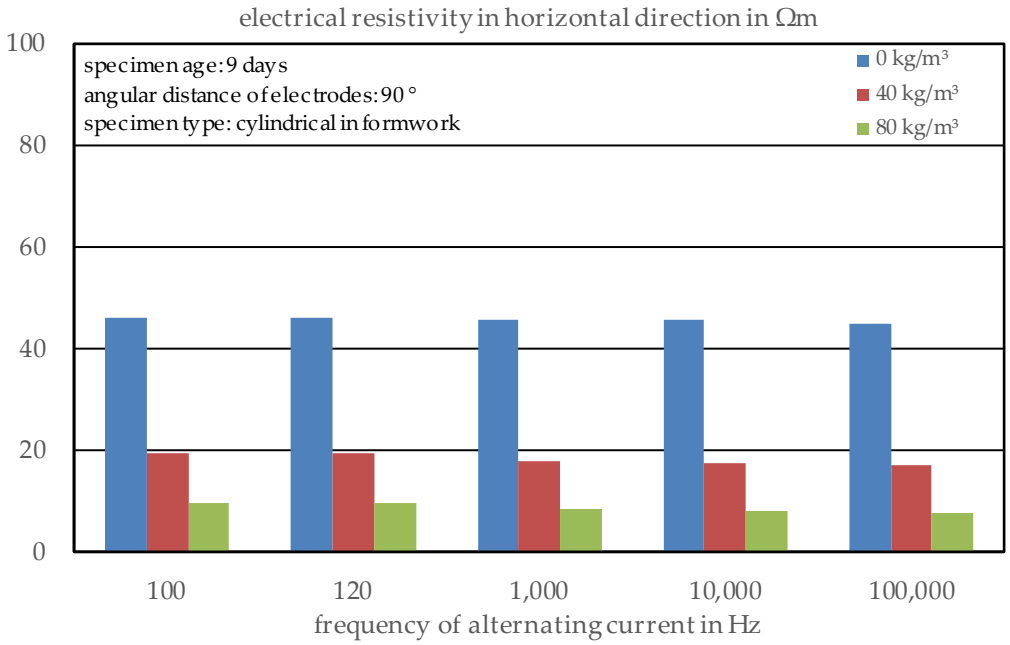

Figure 5.5 Electrical resistivity in the horizontal direction depending on the frequency and fibre content at a specimen age of 9 days and an electrode array with angular distances of 90 °

To identify effects based on the specimen's direction, the age of the specimen and the number of electrodes inside the specimen, the calculated resistivity of the concrete, based on a measurement with an alternating current frequency of 1 kHz, was used throughout the study. With this approach, we were able to exclude polarisation and induction effects. Afterwards, the results of all frequencies were evaluated according to Section 5.3.4 to estimate the fibre content and the orientation of fibres inside the specimen.

5.4.1.2 Electrode Array with Angular Distances of 180 °

The results of the three specimens with an electrode array of only six electrodes with angular distances of 180 ° show that a higher fibre content results in a lower electrical resistivity of the composite material (see Figure 5.6), which is in line with several studies (see, e.g., Chen et al., 2004; Hedjazi & Castillo, 2020; Lataste et al., 2008; Reichling, 2014). This behaviour is the same for every direction that was analysed within this study. In the horizontal direction, the maximum area that was possible to analyse was investigated using a parallel connection of the electrodes at all three height levels on each side of the specimen (blue column). Compared to the measurements of single electrodes in the horizontal direction (red column) which means that the electrical resistance between both electrodes at height level one, level two and level three was measured, there is almost no difference in the electrical resistivity of the plain concrete, while for the fibre reinforced concretes, higher differences were observed. This can be explained by the inhomogeneity of the concrete and fibres and the anisotropy of the fibres, which are of a higher consequence if a smaller volume of materials is analysed.

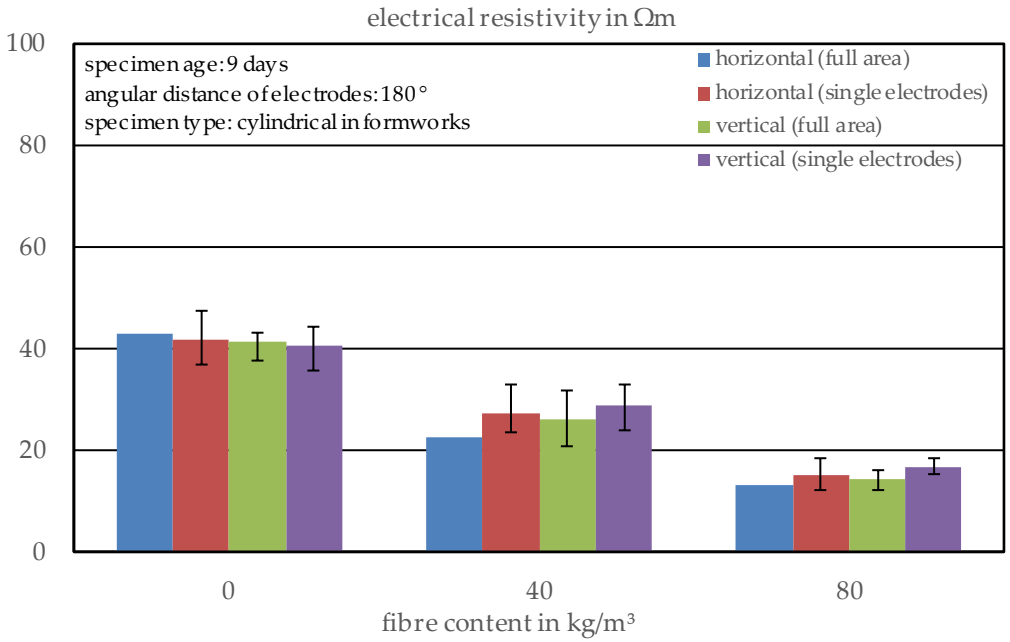

Figure 5.6 Electrical resistivity in different directions depending on fibre content at a specimen age of 9 days and an electrode array with angular distances of 180 °

For the electrical resistivity in the vertical direction, the same behaviour is detected, with higher electrical resistivities of the single electrode measurements (violet column) compared to the full area measurements (green column). Here, the full area measurements were performed using a parallel connection of each of the two electrodes at a height level and the current flow to the electrodes on another height level, while the single electrode measurements were based on a vertical current flow from one electrode to the other on the same side of the specimen at another height level. The slightly higher resistivity in the vertical direction, which can be seen for the fibre reinforced concretes, is probably caused by the compaction of the concrete on the vibrating table, which leads to the preferred orientation of the fibres in the horizontal direction and thus, an increased conduction ability in the horizontal direction.

When comparing the results of the same specimens at the age of 38 days (see Figure 5.7), it can be observed that the higher age of the concrete leads to a higher electrical resistivity, which is based on the development of the pore structure that gets finer through a higher degree of hydration. This effect is already described in several studies (see, e.g., Daniel et al., 2001; Gjørv et al., 1977; Liu & Presuel-Moreno, 2014; Spragg et al., 2017). In addition, as a result of the storage conditions, the drying process of the concrete itself takes place, which results in a lower pore saturation and thus, also increases the electrical resistivity of the concrete (see, e.g., Andrade, 2005; Bürchler, 1996; Reichling et al., 2015). Since the aging effect seems to be almost constant for all fibre contents with an increase in resistivity of about 50 %, it can be stated that the age or condition of the concrete must be identified to enable a prediction of the fibre content, while the fibre orientation, vertical and horizontal, can be estimated independent of the concrete.

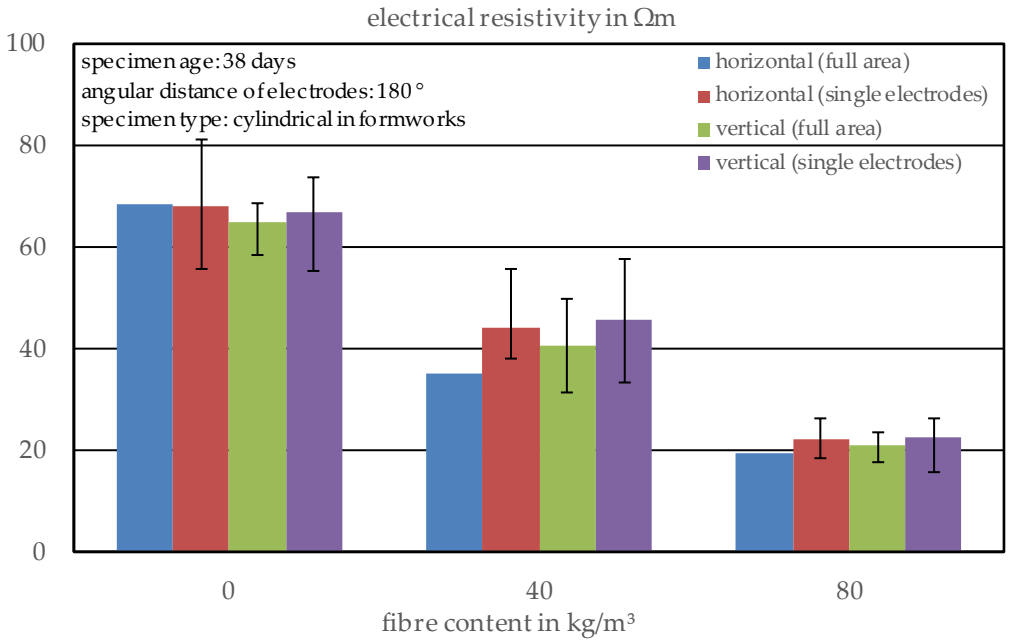

Figure 5.7 Electrical resistivity in different directions depending on fibre content at a specimen age of 38 days and an electrode array with angular distances of 180 °

5.4.1.3 Electrode Array with Angular Distances of 90 °

The second series of three specimens was produced with four electrodes at each height level, corresponding to angular distances of 90 ° and so, more electrode arrays for the measurement were possible (see Figure 5.8 and Figure E.4, Annex E). According to the investigations described above, the electrical resistivities in the horizontal and vertical direction were determined too. For the plain concrete, it is again visible that the electrical resistivity in both directions is almost identical, while for the fibre reinforced concrete, especially with a fibre content of 40 kg/m³, the resistivity in the vertical direction is higher than that in the horizontal direction. For the specimens with a higher fibre content, this phenomenon is not visible at the age of 9 days, while at a specimen age of 38 days, the maximum values of the resistivity in the vertical direction are at least higher than those in the horizontal direction. Nevertheless, based on the higher fibre content, a more three-dimensional fibre distribution and orientation can occur and so, the differences in the horizontal and vertical directions will be exalted at medium fibre contents, such as 40 kg/m³.

Again, a higher concrete age leads to a higher variation that is caused by differences in the hydration and drying of the different parts of the specimens, where the outer surface shows the fastest drying process and the core of the sample has the highest saturation over time (see Figure E.4, Annex E).

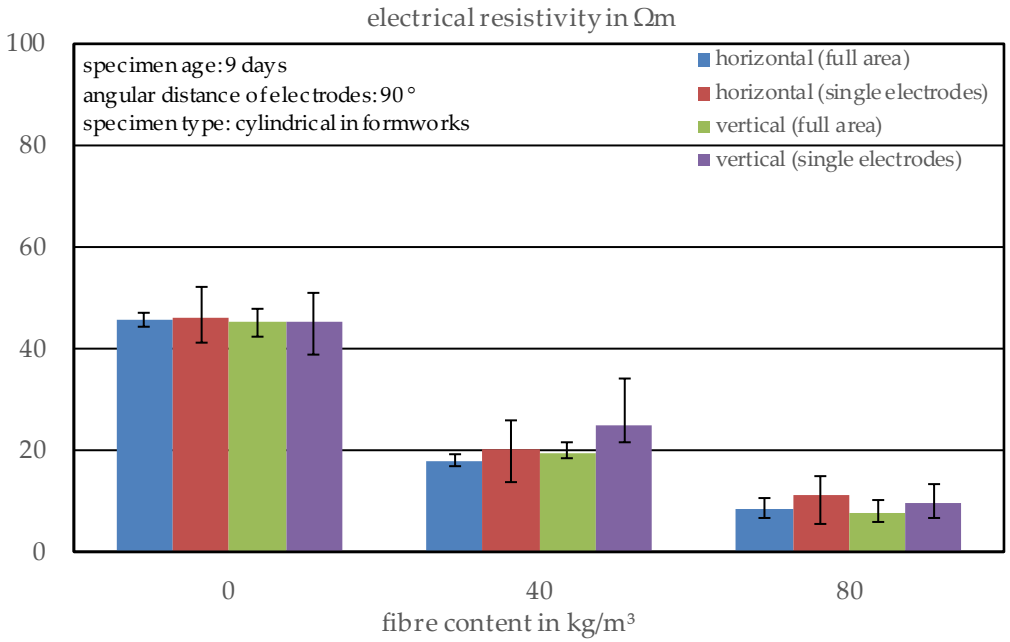

Figure 5.8 Electrical resistivity in different directions depending on fibre content at a specimen age of 9 days and an electrode array with angular distances of 90 °

5.4.1.4 Evaluation of the Electrode Arrays

When comparing both electrode arrays, it can be noticed that for the plain concrete, the calculated resistivity of the array with angular distances of 90 ° was slightly higher, while for the fibre reinforced concretes, lower values were determined. Since the setup with more electrodes was able to describe the concrete in more detail and thus, different measuring directions were able to be analysed, the variations of the single electrode measurements, especially, but also of the full area measurements were higher than for the setup with a lower number of electrodes (see Figure E.5 to Figure E.8, Annex E). The differences in the total results could be based on the variations of the single specimens but could also imply that the FEM model is not perfectly befitting of the test setup. A comparison of the single results of the measurements of both series was carried out to evaluate whether the differences between both test series could be a result of the FEM model. In evaluations up to now, it was assumed that all electrodes have a very good connection to the concrete and thus, no initial resistance occurs, but only the resistivity of the composite material has an influence on the measured electrical resistance.

To decide whether there is a general problem with the FEM model, the comparison of two different specimens can indeed offer a hint but cannot be seen as an absolute validation. So, the fact that, for the 90 ° electrode array, all values for the fibre reinforced concrete specimens were lower than for the other electrode array is no proof that the FEM model is not suitable just because the opposite behaviour is identified in the plain concrete.

As both electrode arrays consisted of three height levels of electrodes, the easiest way to identify the possible weaknesses of the model is to analyse the resistivity in the vertical direction. Here, three possibilities of the current flow are feasible: from height level one to height level two; from height level two to height level three; and from height level one to height level three. In this way, the percolated volume of the measurement from height level one to

height level three should contain both volumes of the other measurements and thus, the resistivity will be approximately the mean value of the resistivities of both other combinations.

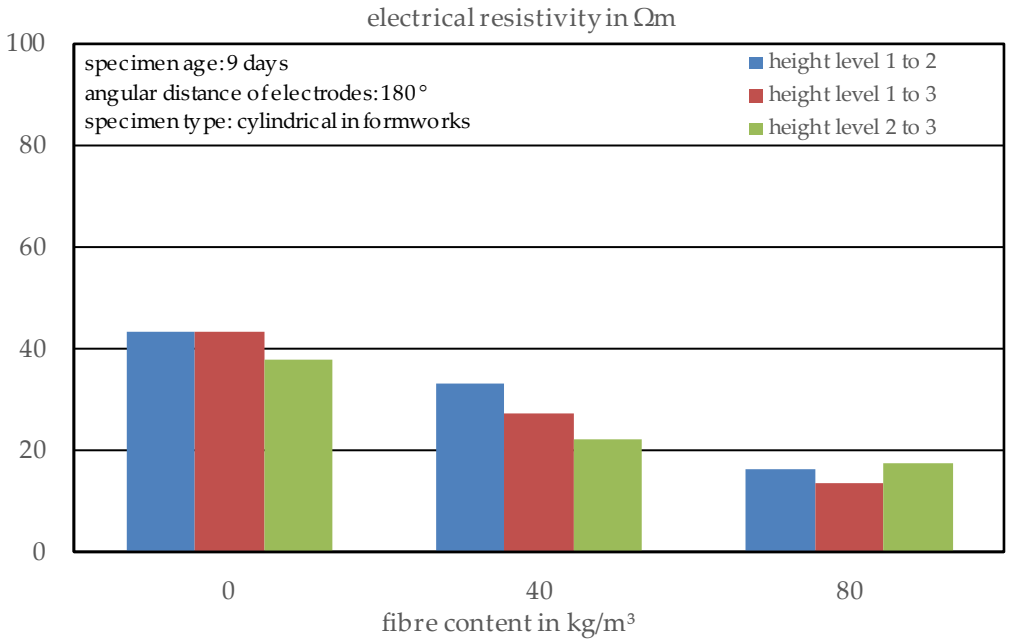

Figure 5.9 Electrical resistivity in the vertical direction with different combinations of electrodes depending on fibre content at a specimen age of 9 days and an electrode array with angular distances of 180 °

For the specimens with angular distances of the electrodes of 180 °, the expected behaviour was almost identified for the PC and perfectly identified for the SFRC with a steel fibre content of 40 kg/m³ (see Figure 5.9). In addition, the electrical resistivity from height level one to height level two, which represents the lower part of the specimen, was higher than the other values. This can be explained by an increased fraction of large aggregates and a lower porosity, based on the rise of water in the wet condition of the specimen as part of a small segregation process, even if the mixture was very stable. Only the specimen with a high fibre content the resistivity that was measured from the lowest to the highest height level of electrodes did not fit the expectations, but based on the high fibre content, it can be presumed that vertically orientated fibres in the middle area of the specimen could have a huge impact on the resistivity and thus, explain this result. Another explanation could be an increased number of short circuits as a result of the contact between a vertically oriented fibre and an electrode at height level two. The specimens with the second electrode array, with angular distances of 90 °, showed the same tendency, where the expected behaviour could not be detected for the highest fibre content only (see Figure 5.10). In combination with the fact that the total resistivity for PC was smaller for the specimens tested with electrodes with angular distances of 180 °, while for the SFRC the opposite behaviour was observed, and the changes in the electrical conductivity of the electrodes in the model did not lead to significant changes in the results, the conclusion was drawn that the small number of specimens was the reason for the partially unexpected results and thus, the model is probably applicable for a larger test series of drilling cores.

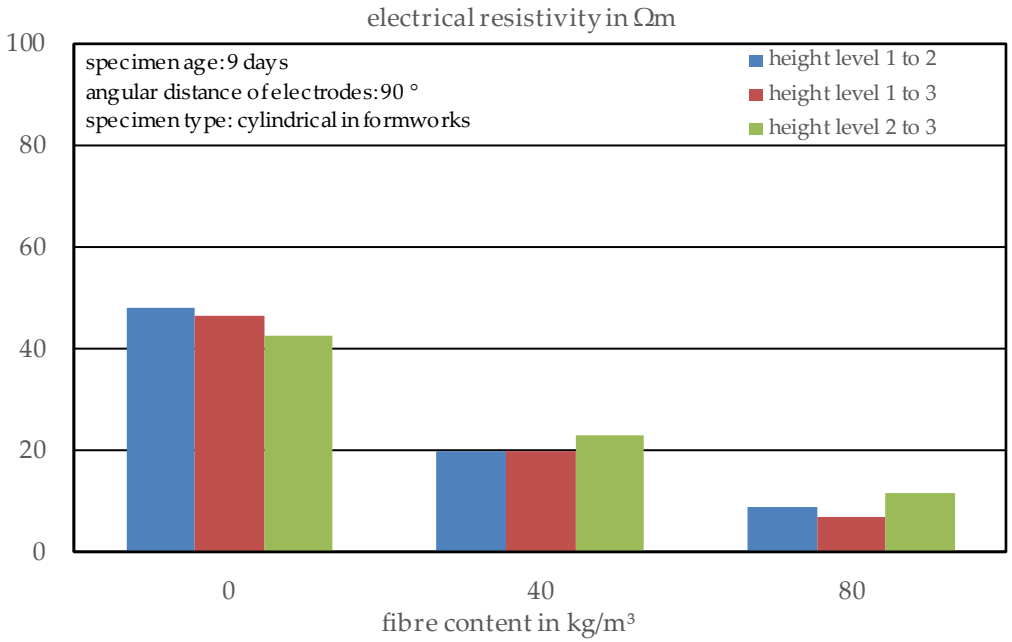

Figure 5.10 Electrical resistivity in the vertical direction with different combinations of electrodes depending on fibre content at a specimen age of 9 days and an electrode array with angular distances of 90 °

5.4.2 Estimation of the Fibre Content

Nevertheless, based on the results of the validation series, the fibre contents of the single specimens and the fibre orientations inside the specimens were calculated using (eq. *5-2*) (see Section 5.3.4). For this purpose, each series of three specimens, the first with six electrodes with angular distances of 180 ° and the second with twelve electrodes with angular distances of 90 °, was analysed separately. For the specimens with only six electrodes, only one horizontal direction of the specimens was tested, so it was assumed that the other direction was almost identical and that the global value of the resistance was calculated as the mean value of the vertical resistivity and two times the horizontal resistivity. For the specimens with twelve electrodes, both horizontal directions were used for the calculation of the global value. Due to the influence of the embedded electrodes at height level two on the vertical current flow, the vertical resistivity was calculated as the mean value of the vertical arrays from level one to level two, level one to level three and level two to level three to prevent any direct connections between the fibres and the electrodes and thus, a short circuit. Each plain concrete specimen was used as the reference for the conductivity of the matrix for the corresponding SFRC specimens.

As can be seen in Figure 5.11, the calculated fibre contents for both electrode arrays were not satisfactory. Only in two cases was a good estimation possible. The first case was an electrode array with angular distances of 180 ° for a fibre content of 40 kg/m³ and low frequencies of the alternating current. The second case was an electrode array with angular distances of 90 ° for a fibre content of 80 kg/m³ and high frequencies of the alternating current. In all other cases, the calculated results did not correspond to the produced concrete. It is obvious that the fibre content is underestimated by the array with more electrodes, while the concrete with 80 kg/m³ is strongly overestimated by the array with angular distances of 180 °. Independent of fibre content and electrode array, the frequency of the alternating current showed an effect on the calculated results, where a higher frequency resulted in a higher fibre content. This is because

without knowing the phase angle of the impedance, which cannot be detected with this test setup, it is not possible to determine the real part of the impedance and thus, based on those results, it is not possible to evaluate the possibility of determining the fibre content via the electrical conductivity. For a higher specimen age, the tendency is almost the same, while all calculated fibre contents are increased by 5 to 15 % (see Figure E.9, Annex E), the electrode array with angular distances of 90 ° provides a large discrepancy between the results and expectations and the results become better fitting for the other electrode array.

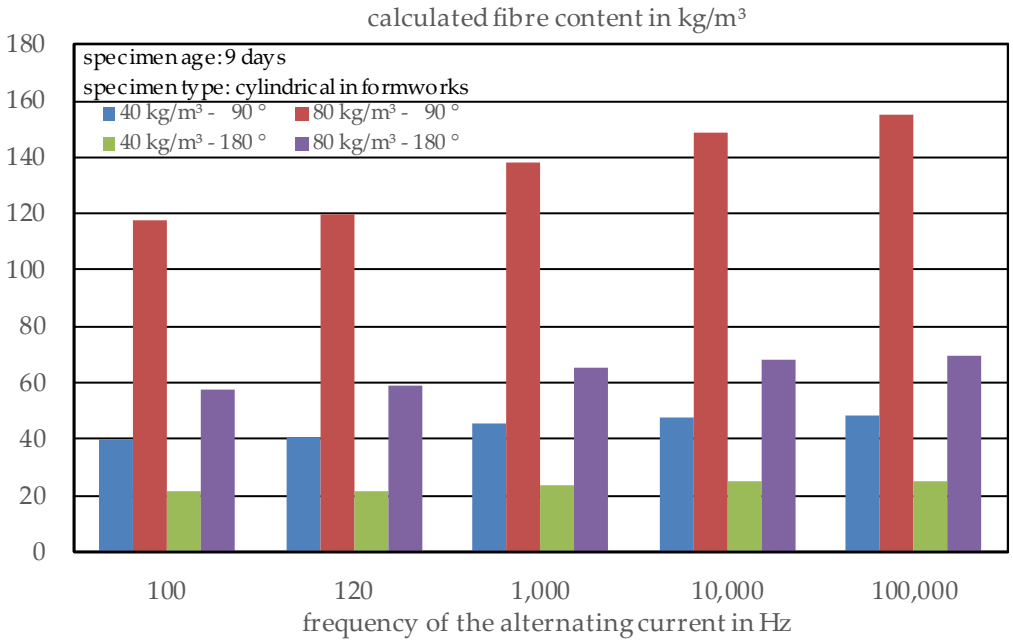

Figure 5.11 Calculated fibre content of the concrete specimens with different electrode arrays depending on fibre content and frequency of the alternating current at a specimen age of 9 days

5.4.3 Estimation of the Fibre Orientation

According to the procedure described in Section 5.3.4, the fibre orientation inside the specimen was calculated. For the electrode array with angular distances of 90 °, the orientation in two orthogonal horizontal directions and the vertical direction was possible, while for the setup with angular distances of 180 °, it was only possible to measure one horizontal direction and it was assumed that the other horizontal direction would show the same value.

It was presumed that SFRC compacted by a vibrating table would show a higher number of fibres oriented in the horizontal direction than the vertical and, as Figure 5.12 shows, the calculations absolutely support this expectation for an alternating current frequency of 1 kHz, except for the specimen with 80 kg/m³ of fibres and an electrode array with angular distances of 90 °. Changes in the frequency did not lead to any important changes in the results. For most of the specimens, at a specimen age of 9 days, the calculation orientation factor in the horizontal direction was lower than that in the vertical direction. For the specimens with an electrode array of electrodes with angular distances of 90 ° it was observed that one horizontal direction always provided the highest calculated orientation and the other horizontal direction provided the lowest, while the vertical direction had an orientation factor of about 30–35 %. For the specimens with angular distances of 180 °, high orientation factors for the horizontal direction of more than 35 % were calculated. This could confirm the expectations but could

also be a random result, because only one horizontal direction was investigated and, as the results of the investigations with more electrodes show, one horizontal direction could have very high orientation factors.

Comparing the results of the same specimens investigated at a concrete age of only 38 days, there were only small differences (see Figure E.10, Annex E). It was concluded that the ongoing hydration process and thus, the pore structure in different parts of the specimen, would differ slightly based on small variations in the local water and cement content and so, lead to small variations in the calculated orientations for different concrete ages. While for the calculation of the fibre content, there was almost no influence of aging since the whole specimen was considered in its entirety for the calculation of the fibre content.

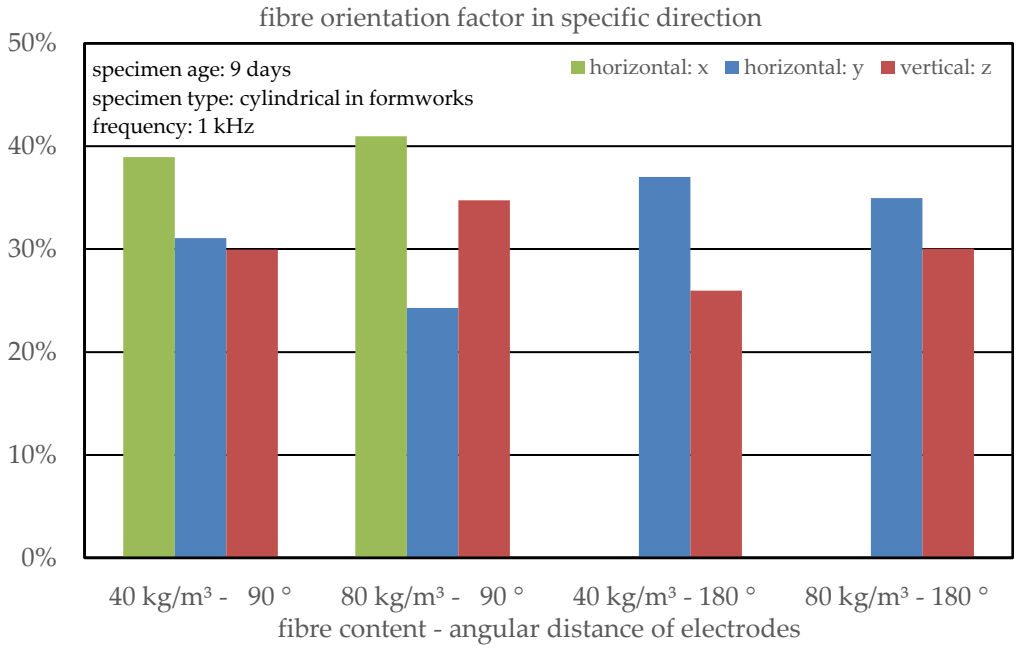

Figure 5.12 Calculated fibre orientation of the concrete specimens with different electrode arrays depending on fibre content at a specimen age of 9 days

5.5 Conclusions

In summary, the test setup, consisting of a breadboard and a LCR meter, can be used for the analysis of both plain concrete and fibre reinforced concrete, and the FEM model provides the possibility to calculate the resistivity of the material and thus, to compare the different directions of the specimens. The evaluation of the specimens, included in formworks with electrodes, showed that the FEM model fits the real current flow inside the whole test setup, although the small number of specimens did not allow for a detailed analysis. While the age of the specimen, as well as the frequency of the alternating current, showed an impact on the calculated fibre content, neither parameter have any effect on the fibre orientation. The results show that with the increasing age of the concrete, the electrical resistivity also increases. For plain concrete, it increases from about 40 Ωm to 70 Ωm from 9 days to 38 days, but the proportion between steel fibre reinforced concrete and plain concrete is not affected because the electrical resistivity of the steel fibre reinforced concrete shows a proportionally smaller increase for a fibre content of 80 kg/m³, based on the conductivity of the fibres.

Since the setup with angular distances of 90 ° allowed the analysis of specimens in at least three directions without the repeated mounting and demounting of the specimen, it was decided to use this number of electrodes and check which electrical resistivity of the electrodes showed the best results in the FEM model for further tests with drilling core samples. The electrical parameters of the electrodes should be varied between the electrical resistivity of steel, to represent a good connection between the electrode and concrete, and the electrical resistivity of concrete, so a low connection could be analysed. With help of the developed test setup and the FEM model, a comparison between cubic specimens and drilling cores is part of current investigations being conducted by the authors (Cleven et al., 2022b) to validate the suitability of the setup for in situ analyses of existing structures.

6 Investigations on Concrete Drilling Cores

This section was published as scientific paper under the title “A New Method to Determine the Steel Fibre Content of Existing Structures—Evaluation and Validation” in the journal Applied Sciences in 2022 (Cleven et al., 2022b).

6.1 Abstract

The in-situ measurement of the content and orientation of steel fibres in concrete structures is of great importance for the assessment of their specific mechanical properties, especially in the case of repair. For existing structures, the actual fibre content as well as the orientation of the fibres, which is based on many factors such as casting or compacting direction, is typically unknown. For structural maintenance or rehabilitation, those factors have to be determined in order to apply meaningful structural design calculations and plan necessary strengthening methods. For this reason, a new method based on the analysis of drilling cores of concrete structures has been established. The newly developed non-destructive test setup used in this research consists of a framework for cylindrical specimens in combination with an LCR meter to determine the electrical resistance of the fibre reinforced concrete. In combination with a suitable FEM model, concretes with fibre contents up 80 kg/m³ were analysed to derive a first model to assess the actual fibre content of steel fibre reinforced concretes. After a calibration of the literature’s equation by use of an adjusted aspect ratio for the analysis of drilling cores, the estimation of the fibre content is possible with high accuracy for the tested material combination. The results show that the newly developed test method is suitable for the rapid and non-destructive structural diagnosis of the fibre content of steel fibre reinforced concrete based on drilling cores using electrical resistivity measurements.

6.2 Introduction

Based on a recently developed easy-to-use test setup (Cleven et al., 2021), a new application to assess the steel fibre content of existing structures based on the electrical resistivity analysis of drilling cores is described in this two-part study. Therefore, in the first part (see Cleven et al., 2022a), the test setup was adapted. A new numerical model was also generated to simulate the flow of the alternating current, which enables the calculation of the electrical resistivity in different specimen directions. An in-depth literature review on the methods concerning the determination of the steel fibre content is presented in (Cleven et al., 2021; Cleven et al., 2022a).

Both parameters, fibre content and fibre orientation, are tremendously important for influencing the mechanical parameters of steel fibre reinforced concrete (SFRC) (see e.g., Gettu et al., 2005; Gouri et al., 2010; Martinelli et al., 2021b; Molins et al., 2009). In general, a higher fibre content and fibres, oriented in direction of the tensile forces, lead to very ductile material behaviour and an increase in the tensile strength of the composite material (see e.g., Barnett et al., 2010; Gouri et al., 2010; Kobaka et al., 2019; Luo et al., 2020; Rossi & Wolf, 2019; Woo et al., 2005; Zak et al., 2001; Zhang et al., 2019). In the case of new structures, the global fibre content can easily be determined and monitored during the mixing process by the mass of the fibres that are added to the concrete or alternatively by washing the fibres out of a fresh concrete sample. After the casting process, the determination of the fibre content and the detection of areas with locally lower fibre contents or an unfavourable fibre orientation is no longer possible via an easy method. Hence high safety factors are required for the structural design of SFRC (see e.g., Cugat et al., 2020; Herrmann et al., 2019; Molins et al., 2009;

Tarawneh et al., 2021). Additionally, the repair and restoration of SFRC buildings only can only be planned and realised in a safe way when the fibre content of the existing structure is known (see e.g., Plizzari, 2018; Rossi & Wolf, 2019). In case it is not possible to determine the actual fibre content of concrete structures, a repair process is only possible with very pessimistic assumptions for the flexural strength of the SFRC elements. Based on this, an economical method of construction is not possible, and additionally, areas with a very low percentage of reinforcement cannot be detected and could lead to a local collapse of the whole structure. Electrical resistivity measurements are one possible non-destructive test method for this analysis. This approach is beneficial since it is easier to apply and less costly compared to other methods such as CT-scanning, cross-sectional analysis via microscope or inductive techniques (see e.g., Al-Mattarneh, 2014; Balázs et al., 2017; Ferrara et al., 2012; Komárková, 2016; Lataste et al., 2008; Lee et al., 2015; Li et al., 2020; Li et al., 2021; Park et al., 2021; Ponikiewski & Katzer, 2016; Torrents et al., 2012; Woo et al., 2007; Zak et al., 2001). With the help of an optimised experimental setup, this study focuses on the validation of electrical resistivity as a novel approach to assess the fibre content and orientation of drilling cores extracted from concrete plates with fibre contents up to 80 kg/m³. Correlations between the electrical resistivity and the fibre content and fibre orientation are derived, which enable a later non-destructive use of adjusted electrode configurations on structural elements and buildings.

6.3 Materials and Methods

6.3.1 Concrete Mix Design

The concrete mix design was already used in earlier studies of the authors such as Cleven et al., 2021. The design focussed on sufficient workability for plain concrete (PC) and fibre contents up to 80 kg/m³ in steel fibre reinforced concretes (SFRC). The concrete mix design presented in Table 6.1 enables the analysis of both PC and SFRC without the addition of a superplasticizer. For the SFRC hooked end, macro steel fibres with a length of 60 mm and a diameter of 1 mm were added to the plain concrete after mixing. The fibres thus had an aspect ratio of 60 and were produced out of steel wire.

Table 6.1 Concrete mix design of the basic concrete

Parameter	Unit	Content
CEM I 32.5 R	kg/m³	300.0
Water		180.0
Sand 0–4 mm		845.5
Gravel 4–16 mm		1004.0
Water/cement ratio	-	0.60
Grain size distribution		A/B16
Steel fibre type	kg/m³	Macrofibre 60 mm
Steel fibre content		0, 40, 80

The mixing process was performed according to the following scheme: First, the solid components, cement and aggregates, were mixed in a compulsory mixer with a nominal volume of 170 l for 30 s to obtain a homogenous mixture. In the next step, the water was added to the solids while the mixing process was still ongoing, followed by a mixing phase of two minutes. After a visual inspection of the concrete, adhering components were removed from

the mixer walls, followed by a final mixing process of one minute. On the final PC mixture, fresh concrete tests, such as the flow table test as well as the density and the air content in accordance with EN 12350-5, 2019, EN 12350-6, 2019, and EN 12350-7, 2019, were assessed. In the case of the SFRC with fibre contents of 40 kg/m³ and 80 kg/m³, the fibres were added after the fresh concrete tests, and the concrete was mixed for another minute.

In total, three concrete batches were produced. Out of each concrete batch three cubic specimens with an edge length of 150 mm as well as one plate with dimensions of 500 × 500 × 212 mm³ were cast, each in two layers with subsequent compaction on a vibrating table. A height of 212 mm was chosen to enable grinding of both the bottom and surface of the later extracted drilling cores and gain specimens of a height of 200 mm. The specimens were covered with foil to inhibit dehydration of the surface. After 24 h, the specimens in steel formworks (cubes) were demoulded. Moreover, the upper surface was ground to ensure a flat surface with a good connection to the electrodes and afterwards stored underwater. The plates were left in the formwork to simulate a hardening of structural elements such as floor plates or walls and were stored at a climate of 20 °C and 65 % relative humidity. After 14 days, nine drilling cores with diameters of 100 mm were extracted out of each concrete plate. Thereby two different edge distances were used. The first six specimens were drilled with edge distances to the formworks of 60 mm, appropriate to the length of the fibres, while the last three cores were drilled with edge distances of 30 mm, appropriate to half of the fibre length. A schematic figure of the arrangement of the drilling cores is presented in Figure 6.1. After drilling, the lower and upper surfaces of the cores were ground analogue to the cubic specimens and the specimens were stored underwater.

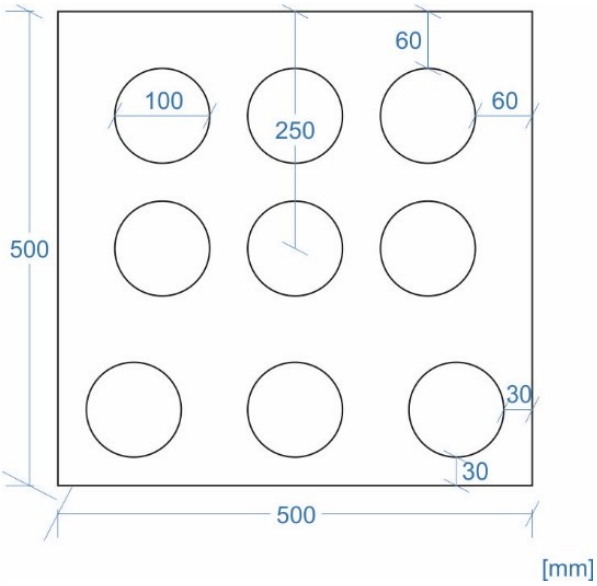

Figure 6.1 Schematic figure of the arrangement of the drilling cores in the concrete plates

6.3.2 Experimental Setup

6.3.2.1 Basic Setup

The basic setup of the measurements is described in Cleven et al., 2021 and consists of two stainless steel electrodes with dimensions of 200 × 200 mm², which are connected to an LCR meter. The LCR meter used for the impedance measurements was Extech Instruments LCR200 with a voltage amplitude of 600 mV rms and variable frequencies of the alternating current of 100 Hz, 120 Hz, 1 kHz, 10 kHz, and 100 kHz. The setup is presented in Figure 6.2.

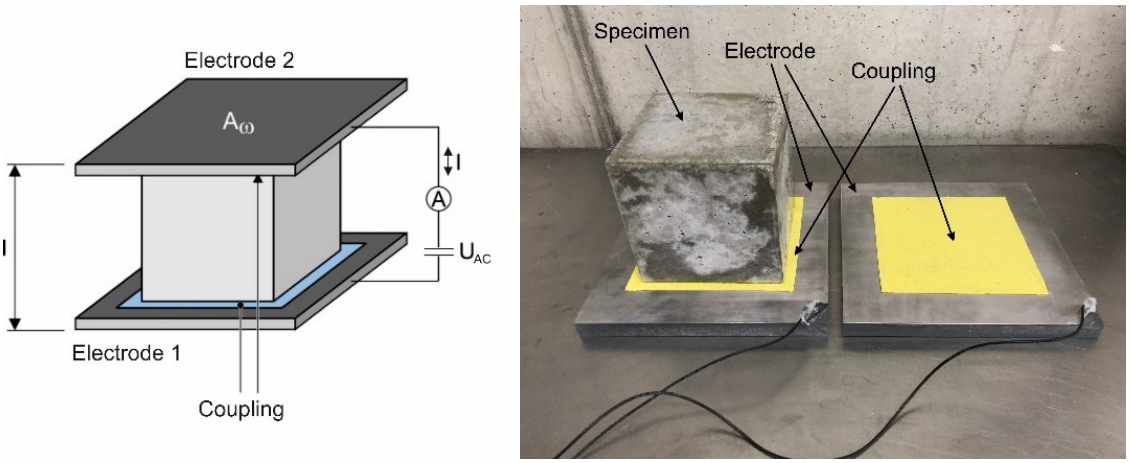

(a) **(b)**

Figure 6.2 Test setup for conductivity measurements, schematical setup (**a**) and photo of a test setup with the investigated specimen (**b**) by Cleven et al., 2021

6.3.2.2 Advanced Test Setup for Cylindrical Specimens

For the investigation of drilling cores, an advanced test setup was developed and tested in Cleven et al., 2022a based on the existing equipment and the extended setup. The LCR meter was connected to a breadboard (see Cleven et al., 2022a), which could be used for various electrode configurations with several numbers of electrodes.

After extensive tests of the setup for cylindrical concrete specimens in combination with the breadboard (see Cleven et al., 2022a), a cylindrical frame for the analysis of drilling cores was developed (see Figure 6.3 (a)). The frame was applicable for concrete specimens with different dimensions, such as a diameter of 100 mm or less. The setup consists of stainless steel electrodes with dimensions of 40 × 10 mm² in three heights, which are arranged in angular distances of 90 °. Those electrodes were covered with sponge cloths and isolated with insulating tape to inhibit a short circuit (see Figure 6.3 (b)). The electrodes were fixed with screws to a circular frame, so they could be adjusted to the specimen's dimensions, and a reproducible contact pressure could be ensured. The whole setup can be connected to the breadboard, so measurements of various combinations of the twelve electrodes are possible.

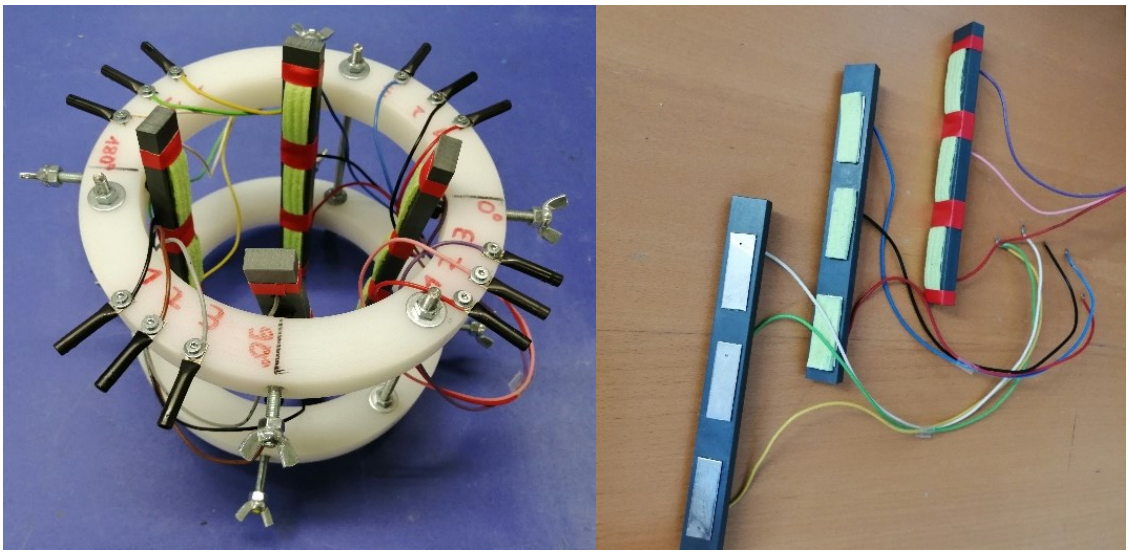

(a) **(b)**

Figure 6.3 Cylindrical frame with 12 stainless steel electrodes on three height levels with angular distances of 90 ° (**a**) and electrodes with covering and isolation (**b**)

6.3.3 Modelling of the Current Flow

To analyse different electrode configurations and different specimens, the LCR measurements, which give the electrical resistance, as a result, have to be further converted into electrical resistivities, which are independent of geometry. As for trivial electrode configurations (two parallel plates of basic setup, see Section 6.3.2.1) the geometry factors for the conversion of resistance into resistivity can be easily calculated; for the advanced test setup with a more complex structure, FEM modelling of the test setup and the current flow is needed. The software Comsol Multiphysics (version 5.3a, build version 229) enables the generation of a network model and thus the simulation of the current flow between several electrodes in various configurations.

For the analysis of the specimens in this study, the model of Cleven et al., 2022a was used, but because effects of surface pressure of the electrodes and electrical conductivity of the sponge cloths contacts cannot directly be considered, different electrical material parameters for the electrodes have been analysed to find the optimum accordance of the model and the real experiment. The drilling core inside the model was represented by a cylinder with a diameter of 100 mm and a height of 200 mm. The electrical resistance was set to 100 Ωm, which fits the experimental data. Similar to the cylindrical frame of the test setup, also in the model, twelve electrodes were added as stainless steel elements with an area of 40 x 10 mm² and a thickness of 1 mm. The electrodes were placed on three height levels with 20 mm in between each level and angular distances of 90 ° as segments of a circle. This way, a good connection of the specimen's surface and the electrode was guaranteed. The grid size of the single elements in the simulation was set to extremely fine because a high accuracy was needed for the simulation of the current flow. For the modelling, the following assumptions have been made: The behaviour of all materials, such as concrete and steel, is presumed as homogeneous and isotropic. Polarization effects on the electrodes have been disregarded because of the use of alternating current. The simplification of homogeneity of the materials, especially the concrete, was conducted to keep the numerical model as easy as possible to reduce computing time and not predictable results based on a presumed inhomogeneity which

is not well known. It was decided that the inaccuracy of the model based on this simplification is better to accept than the assumption of any parameters to describe an inhomogeneity of the concrete, especially in the context of unknown fibre distribution and orientation that lead to another inhomogeneity and will not be constant for different specimens with varying fibre content.

This FEM model makes it possible to simulate the current flow and the resulting electric current of several configurations and thus calculate the geometry factors of those electrode configurations. For the simulations, the electric potential of the contacted electrodes was set to 0 V respectively 600 mV. Thus, the current flow between a pair of electrodes or a group of electrodes was simulated. The chosen values of 0 V and 600 V at this juncture represented the real experimental setup with the LCR meter, which uses a voltage amplitude of 600 mV rms. The simulations were carried out with two different electrical parameters for the electrodes. First, the electrical conductivity of the electrodes was set to the one of stainless steel with 1.4 x 10^6 S/m to represent a perfect connection between concrete and electrodes. In this case, the not contacted electrodes show conduction effects and thus have a great influence on the current flow. The second set of simulations has been carried out with an electrical resistivity of 100 Ωm of the electrodes (corresponding to the resistivity of the concrete), which was meant to represent a bad connection of the electrodes and thus nearly neglects the influence of uncontacted electrodes. By use of (eq. *6-1*) then the k-factors can be calculated for each electrode configuration and assumption of the electrode's electrical behaviour.

$$k = \frac{I * \rho}{U} \qquad \text{(eq. 6-1)}$$

with:

- k: geometry factor in m
- I: electric current in A
- ρ: electrical resistivity (set to 100 Ωm)
- U: electric potential (set to 1 V)

The visualisation in Figure 6.4 (a) shows that not connected electrodes (in the middle height level) have an impact on the isosurfaces of the current, which represent locations with identical electric potential in case of a good electrical connection of the concrete and the electrodes. The current flow can be supposed to be orthogonal to those isosurfaces. In the case of a low conductivity between concrete and electrodes (Figure 6.4 (b)), there is no influence of the current flow by unconnected electrodes, which is visible through the constant isosurfaces around the mid-level electrodes. Since those results illustrate the marginal principles, both are used for the subsequent discussions.

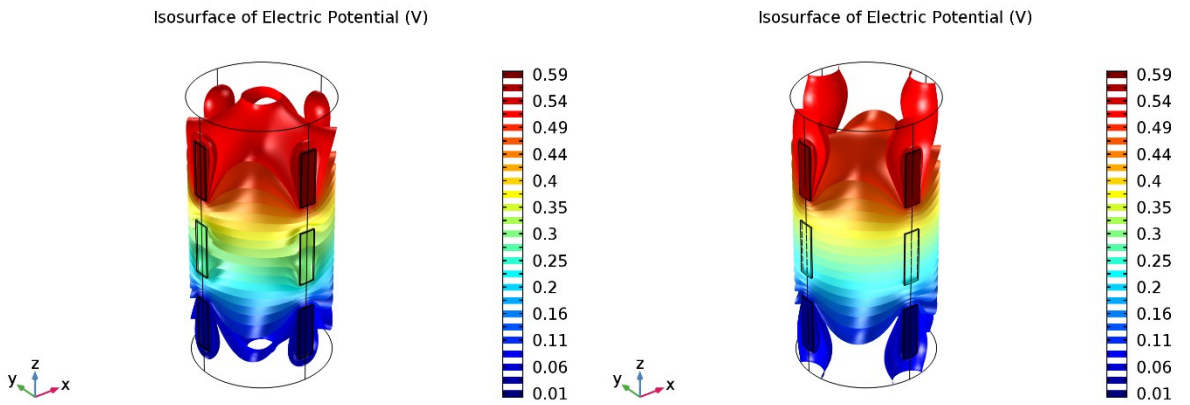

(a) **(b)**

Figure 6.4 Resulting isosurfaces, calculated by Comsol with different simulated electrical conductivity/resistivity of the electrodes. (**a**) electrical conductivity of electrodes: 1.4 x 10^6 S/m; (**b**) electrical resistivity of electrodes: 100 Ωm

6.3.4 Evaluation of the Results

The fibre content of the specimens, as already presented in Cleven et al., 2022a, was calculated from the electrical resistivity of the SFRC specimens in relation to one of the PC specimens by the equation of Woo et al., 2005 (eq. *6-2*).

$$\frac{\sigma}{\sigma_m} = 1 + [\sigma]_\Delta * \Phi \qquad \text{(eq. 6-2)}$$

with:

σ: electrical conductivity of the SFRC in Ωm
σ_m: electrical conductivity of the PC in Ωm
Φ: fibre volume fraction
[σ]: intrinsic conductivity (eq. 6-3)
Δ: ratio of conductivity of fibres and PC

The intrinsic conductivity in (eq. *6-2*) was calculated in dependence of the aspect ratio of the fibre by an empiric equation in accordance with Woo et al., 2005:

$$[\sigma]_\infty = \frac{1}{3}\left(\frac{2 * (AR)^2}{3 * ln[4(AR)] - 7} + 4\right) \qquad \text{(eq. 6-3)}$$

with:

AR: aspect ratio of the fibres

The aspect ratio of the fibres in this study was 60, and thus the intrinsic conductivity of 255.5 resulted. With this factor, the fibre volume fraction of each concrete specimen could be calculated by (eq. *6-2*). As several directions of the specimens were analysed, a global conductivity value had to be determined for each kind of specimen. For the cubic specimens, it was calculated as a mean value of the three pairs of parallel surfaces, while for cylindrical specimens, several configurations have been checked to find an optimum according to the real behaviour of the material.

The use of (eq. *6-2*) in different directions, such as only one pair of parallel surfaces of the cubic specimens, in relation to two orthogonal directions, enables the calculation of orientation factors for the single directions. It is summarized that the three orientation factors of one concrete specimen give 100 %; therefore, each of the factors is between 0 and 100 %.

6.4 Results and Discussion

6.4.1 Tests on Concrete Cubes as Additional Specimens

6.4.1.1 General Evaluation of the Cubic Specimens

In addition to the production of the concrete plates, where the drilling cores were extracted, three cubic specimens with edge lengths of 150 mm were produced out of each concrete batch to analyse the electrical behaviour of the concrete in the early age and the changes with ongoing aging. For this purpose, the cubes were analysed via the basic test setup (Section 6.3.2.1) in concrete ages of 7, 28, and 135 days. The electrical resistivity was calculated, and the fibre content and fibre orientation were estimated according to Section 6.4.2. Since the specimens were stored underwater for the duration, a good conductivity of the concrete was reached, and thus no negative effects of the coupling of the electrodes to the concrete surface were observed. Figure 6.5 shows the results of the measurements. As already explained, the resistivity of the PC, as well as of the SFRC, increases with increasing concrete age and a higher fibre content results in a significantly lower resistivity due to the conductivity of the fibres inside the concrete matrix (see e.g., Cleven et al., 2021; Lataste et al., 2008; Reichling & Raupach, 2012).

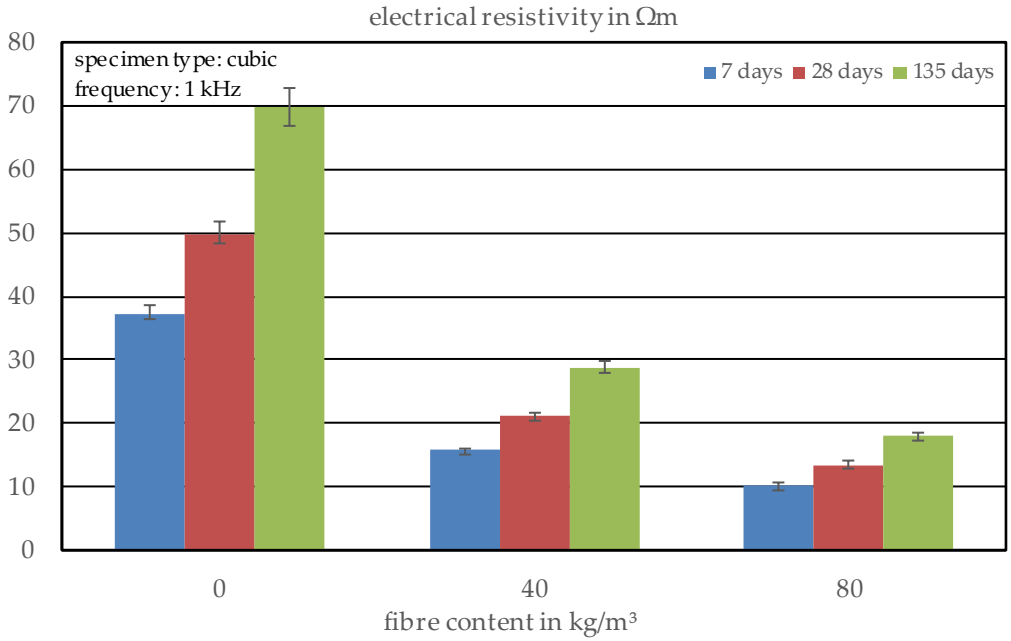

Figure 6.5 Electrical resistivity of the concrete cubes in different ages

6.4.1.2 Estimation of the Fibre Content and Orientation

Based on these results, it was possible to calculate both the fibre content and the fibre orientation inside of each specimen, whereby it must be said that the electrical resistivity of the PC was averaged to have an ascertained reference value for the calculations. The calculated fibre content of the series of specimens is shown in Figure 6.6.

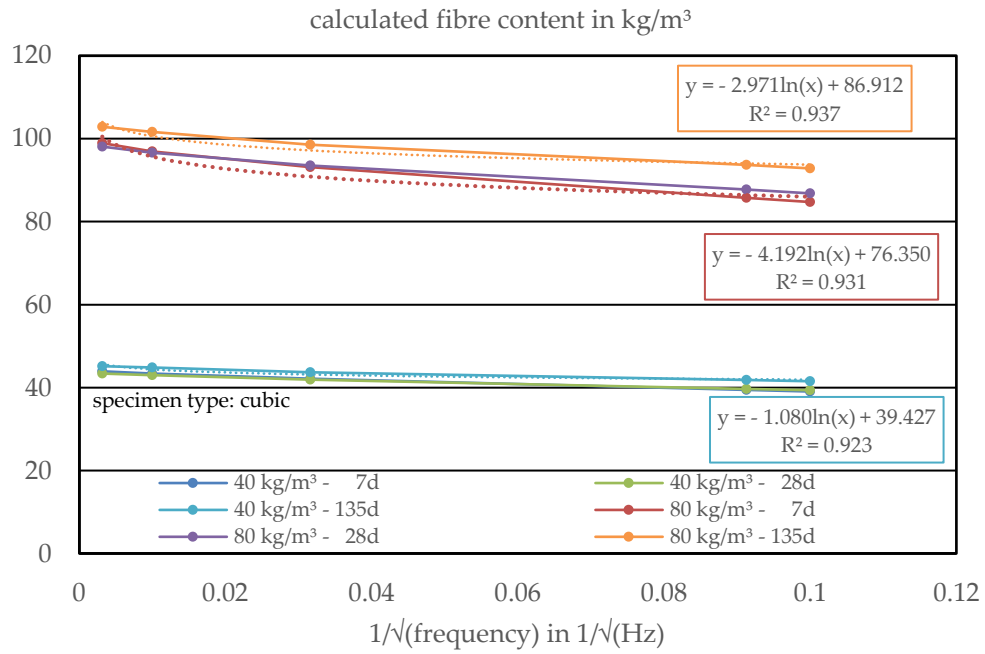

Figure 6.6 Calculated fibre content of the cubic specimens at varying frequencies of the alternating current depending on the age of the concrete and the actual fibre content of the samples (dotted lines represent the fitted trend lines according to the equations given in the corresponding graph)

One can see that a higher concrete age results in a slightly higher value for the fibre content, as well as a higher frequency of the alternating current. These effects can be explained by the higher differences of conductivity of the concrete and the fibres in higher age, based on the hydration process and thus the refinement of the pore structure as well as changes in the pore chemistry. The differences in the results for varying frequencies are a result of the missing information for the phase angle of the current, which makes the calculation of the real part of the impedance impossible (see e.g., Cleven et al., 2021; Woo et al., 2005). Nevertheless, it is clear to see that the graph of the fibre content versus the inverse of the square root of the frequency can be described by a logarithmic function a * ln(x) + b, where the constant b can be used as an indicator for the fibre content of the material, where a higher concrete age gives a better coefficient of determination as well as a better fit of the calculated fibre content to the expectations based on the composition of the concrete. Therefore, an extrapolation of the graph infinity, which would mean a frequency of 0 Hz or direct current (DC), would lead to the corresponding fibre content of 39.427 kg/m³ and 86.912 kg/m³, respectively, for a concrete age of 135 days. For a concrete age of 28 days and a fibre content of 80 kg/m³, the calculated fibre content would be 76.350 kg/m³ and significantly lower than after 135 days. For the analysis of existing structures, a positive effect can be seen because the concrete is much older, and the hydration process has been completed. Looking at the results of the single specimens for the fibre content of 80 kg/m³ shows that specimen 1 must contain a much higher amount of fibres than the other two, and thus leads to an overestimation of the fibre content (see Figure 6.7). For the other two specimens, the calculated fibre content fits almost perfectly to the fibre content that was mixed in the PC. Even if the extrapolation of the curve to the infinite represents the use of DC, a test setup using DC cannot be recommended because of polarisation effects on the electrodes and thus time-depending results for the measurements.

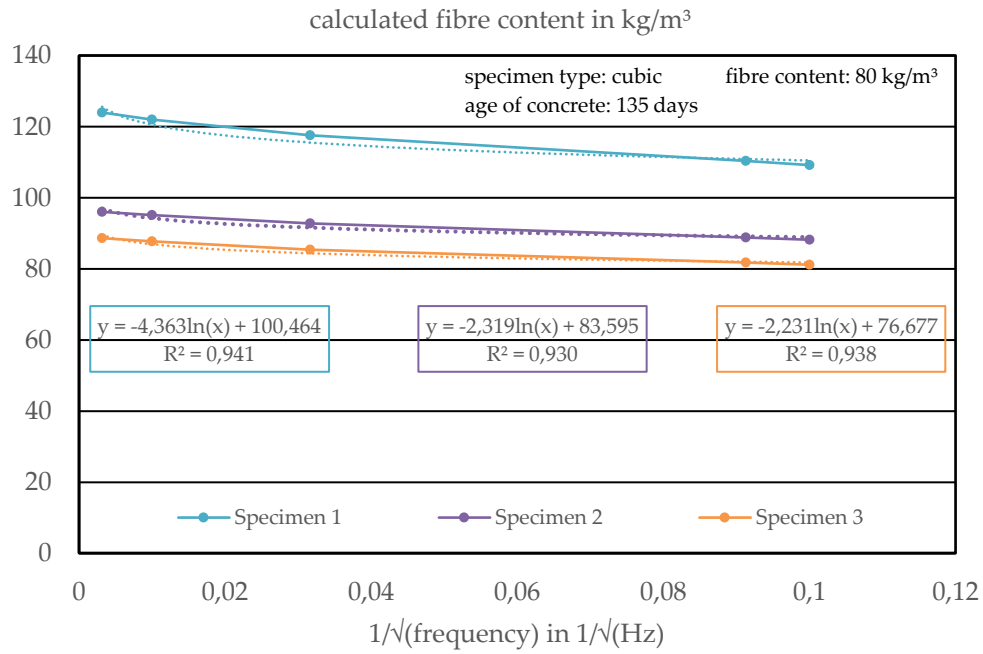

Figure 6.7 Calculated fibre content of the cubic specimens at varying frequencies of the alternating current of the samples with a fibre content of 80 kg/m³ (dotted lines represent the fitted trend lines according to the equations given in the corresponding graph)

While the frequency of the alternating current, as well as the age of the specimens, showed an influence of the calculated fibre content, for the fibre orientation, both parameters seem to be independent, as it was already occupied in the earlier tests (see Cleven et al., 2022a). Both the age of the specimen and the frequency of the alternating current led to results for the fibre orientation inside the concrete cubes with no significant variations. For a fibre content of 40 kg/m³, much more fibres are oriented in the horizontal directions with a proportional distribution of approximately 42 % in each of the horizontal directions (see Figure 6.8). Since the concrete was compacted by a vibration table in a vertical direction, this result was expected. In addition, it can be analysed that there is a higher scatter in the horizontal directions than in the vertical one with fibre orientation coefficients of 35 % to 50 %.

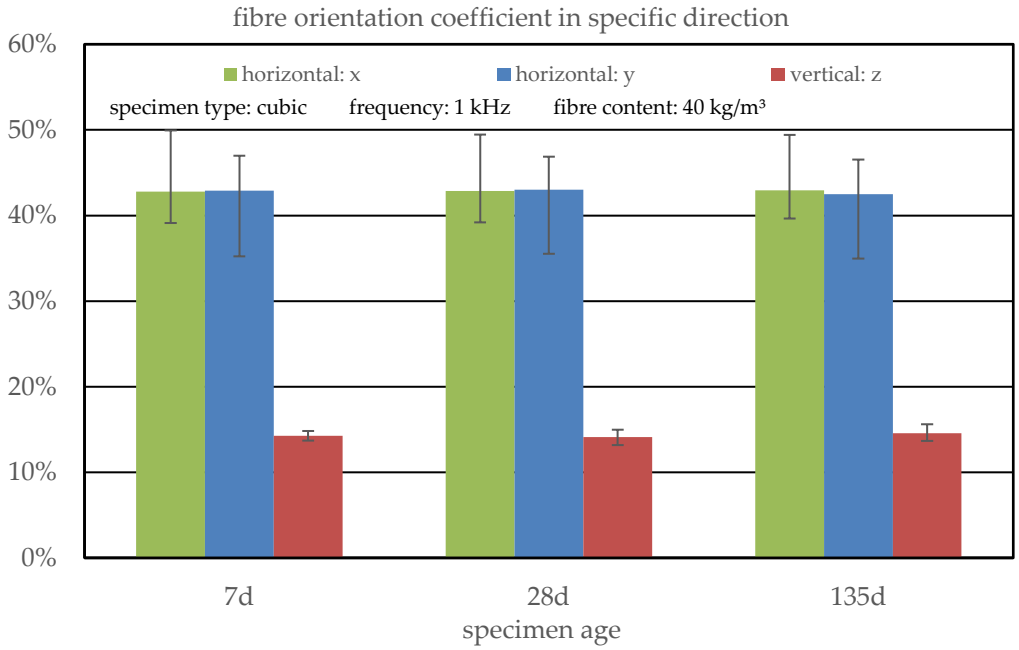

Figure 6.8 Calculated fibre orientation of the cubic specimens with a fibre content of 40 kg/m³, based on the electrical resistivity measurements on specimens with different concrete ages at a frequency of the alternating current of 1 kHz

In contrast to this, the concrete with a higher fibre content of 80 kg/m³ shows lower variations even in the horizontal direction, which is based on the higher fibre content where fibres are expected to be oriented more uniformly (see Figure 6.9). This hypothesis can be verified by comparing to the vertically oriented fibres in both concretes, where in the SFRC, with a higher fibre content, more fibres are oriented in a vertical direction. Overall, a more 3-dimensional orientation of the fibres is detected. One explanation can be the size of the specimens. Due to the ratio of fibre length to smallest specimen dimension, in smaller specimens, a free distribution and orientation of the fibres with ongoing compaction process can be hindered by the formwork, and edge effects are the main influencing parameter for small specimens. In contrast to this, inside the cubes, there seems to be a volume in the middle, where the fibres are able to freely orientate themselves and only interact with the large grains, but no interaction with the edges of the formwork occurs.

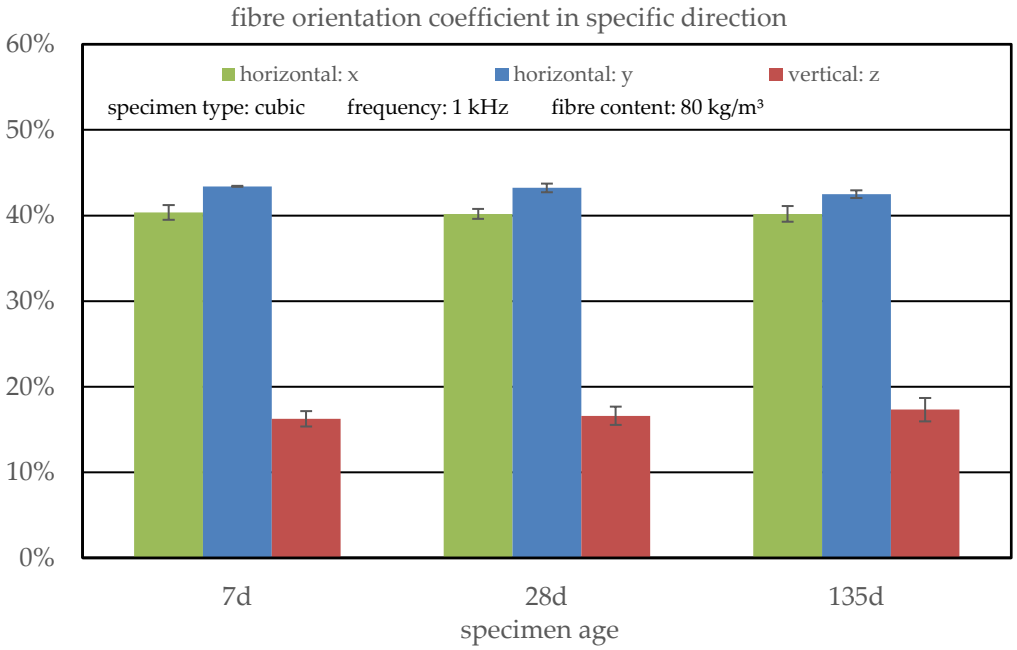

Figure 6.9 Calculated fibre orientation of the cubic specimens with a fibre content of 80 kg/m³, based on the electrical resistivity measurements on specimens with different concrete ages at a frequency of the alternating current of 1 kHz

6.4.2 Testing of Drilling Core Samples

6.4.2.1 Effect of the k-Value Based on the FEM Model

The first important step was to identify which parameters of the FEM model result in the most realistic and accurate geometry factors. On the one hand, simulating the electrodes with the electrical conductivity of stainless steel represents a good connection between concrete and electrode with no isolation. On the other hand, using the electrical resistivity of concrete represents an isolating effect by the wet sponge cloths that are soaked with pore solution and thus will have nearly the same resistivity as the concrete itself. Both possibilities have been tested, and the electrical resistivity of the PC was analysed with the help of both k-factors, given in Table E.55 and Table E.56, Annex E. As a measurement from the bottom of the cylinder to its top was performed with the electrical conduction of the whole upper and lower surface, where the k-factor can be calculated by the surface area and the specimen length, the real values of the electrical resistivity of the concrete are well known.

Figure 6.10 shows the comparison of the vertical resistivity, calculated with the easily calculated k-factor, and the vertical and horizontal resistivities of the drilling cores, calculated of the results of the FEM analysis, with the electrodes, simulated with the electric parameters of stainless steel. It is clear to see that the electrical resistivity of the nine drilling cores in a vertical direction, measured with the basic test setup, is approximately 68 Ωm with a very low deviation. The Comsol model with the electrodes' electrical conductivity set to the one of stainless steel with 1.4 x 10^6 S/m results in calculated resistivities that are significantly higher, and additionally have a higher scatter, based on a large number of test directions and the fact that only a part of the inhomogeneous specimen is analysed. Due to the good conductivity of the electrodes in the model, in this case, the geometry factors that are calculated are too high and do not represent the realistic behaviour of the test setup and the specimen. In particular, the vertical resistivity and the horizontal one with single electrodes show the largest deviations,

which can be explained by the higher number of possible measurement directions and the lower specimen volume that is observed each time.

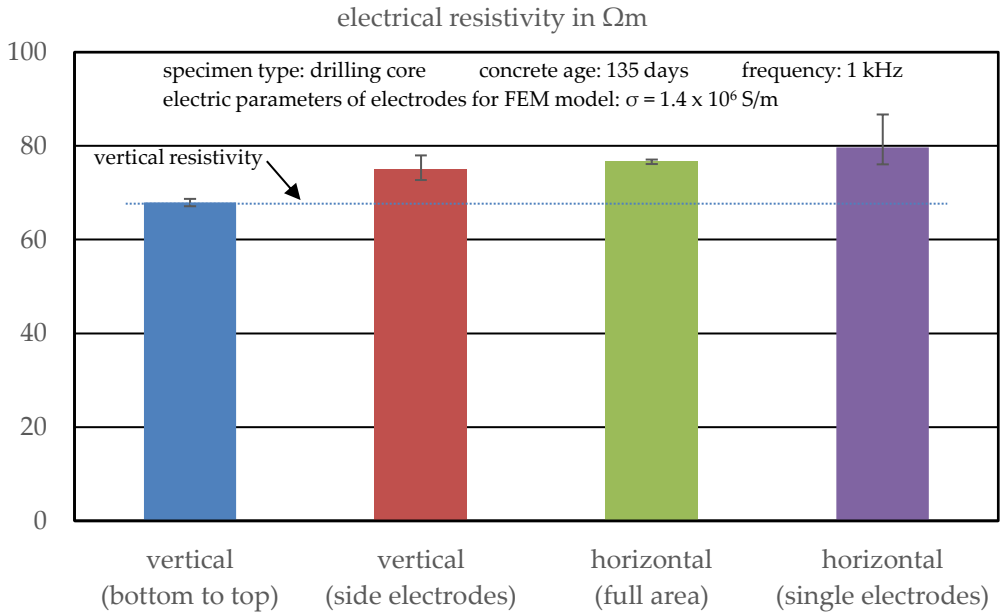

Figure 6.10 Calculated electrical resistivity of PC drilling cores in different electrode configurations, simulated with the conductivity of steel

In contrast to this, setting the electrical resistivity of the electrodes in the FEM model to the one of concrete with 100 Ωm gives perfectly fitting results of the PC specimens in comparison to the real values of the measurement from bottom to the top of the specimen (see Figure 6.11). The scatter of the results is comparable to the results with the other k-factors, which means that the variation is based on the measurement results and not on the FEM modelling. Based on those results, it seems that there is only a marginal influence of the electrodes that are connected to the surface of the specimen but not electrically conducted for single measurements. Thus, the lower k-factors of the model, where the electrodes were simulated as concrete, are used for the further examination of the results. This observed behaviour of the results with the newly developed test method shows the opportunity to directly measure the electrical resistance of drilling cores instead of preparing expensive specimens by high effort to determine the fibre content. Here, the full area measurement in a horizontal direction and the vertical resistance, measured by the side electrodes, have sufficient accuracy and can later be used to build an estimation model.

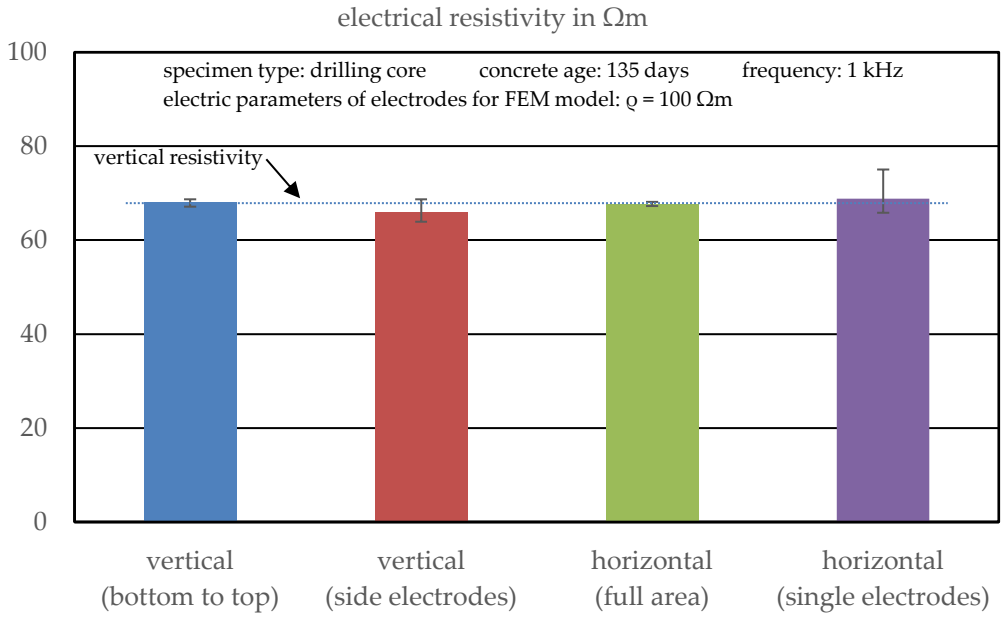

Figure 6.11 Calculated electrical resistivity of PC drilling cores in different electrode configurations, simulated with the resistivity of concrete

6.4.2.2 Statistical Analysis of the Test Results

After optimising the FEM model, the electrical resistivity of the concrete specimens in different directions, as well as the variation for different specimens, were analysed.

As already seen for the cubic specimens, an increase of the fibre content results in a lower electrical resistivity (see Figure 6.12). In contrast to the prior results, the difference between the results of different fibre contents and the PC is much lower for the drilling cores. As one can see, a fibre dosage of 40 kg/m³ only decreases the electrical resistivity by about 20 Ωm, while another 40 kg/m³ lead to a decrease by about 10 Ωm. For the cubic specimens cast together with the plates, where the drilling cores were extracted, the electrical resistivity was determined to 29 Ωm for a fibre content of 40 kg/m³ respectively 18 Ωm for fibre content of 80 kg/m³. This fact is expected to lead to a lower accuracy of discrimination of different concretes based on resistivity measurements. Since the electrical resistivity of the PC is exactly in the same range for the drilling cores as for the cubic specimens, and the results of the basic test setup fit those of the vertical advanced setup, both factors, the test setup as well as the k-values by the Comsol model, can be eliminated as reasons for the unexpected high resistivity values. A possible reason could be the unknown fibre distribution inside the plates and so local deviations in the fibre content, which would lead to higher resistivities based on lower fibre contents for some specimens. On the other hand, in this case, there should also be some specimens with very high fibre contents and thus very low electrical resistivity what is not the case here. The second possible explanation of the high results could be the size of the specimens compared to the fibre length and thus the high probability of truncated fibres by the drilling process, while for the earlier tests, only complete fibres were present. Another thing that can be seen in the results is a differing fibre orientation, compared to the cubic specimens, that can be estimated by the similarity of the resistivity in a horizontal and vertical direction for the SFRC drilling cores.

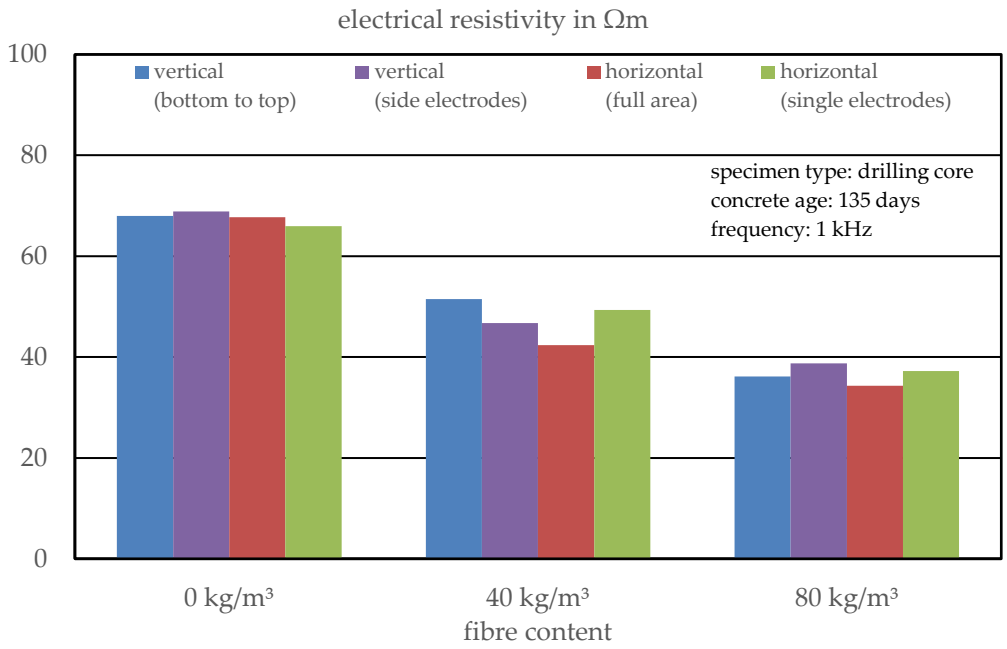

Figure 6.12 Calculated electrical resistivity of drilling cores depending on the fibre content

Regarding the variations of the different specimens, it was expected that the variations for PC would be the lowest because, for SFRC, the inhomogeneity and anisotropy of both concrete and fibres can be superpositioned and thus result in a higher variation. As presented in Figure 6.13, the expected behaviour can be observed, especially for a fibre content of 40 kg/m³, which shows the highest variations with up to 16 %, while the PC samples only show COVs of less than 8 %. For specimens with a higher fibre content of 80 kg/m³, the inhomogeneity of the fibres is tendentially lower than for lower fibre content, and thus the COV is also lower, but still not on the level of PC.

Comparing the variations in different directions of the specimens, it can be concluded that the variation in the vertical direction is slightly higher than for the horizontal direction. An explanation could be the possible segregation processes through the compaction even for robust concrete compositions, which result in small differences of the local water–cement ratio in different heights of the specimens as well as in a higher number of large aggregates in the lower zone of the specimen. In the horizontal direction for full area measurements and single electrode measurements, no significant differences regarding the variations can be detected, but it has to be considered that for the single electrode configuration, the number of measurements is three times higher than for the full area configuration because of the different height levels of the test setup. In summary, the results show that, especially for low fibre contents, but also for higher ones, several samples have to be analysed to gain robust results that allow the calculation of the fibre content and orientation of a concrete element, while for single specimens a comparably high inaccuracy can be expected.

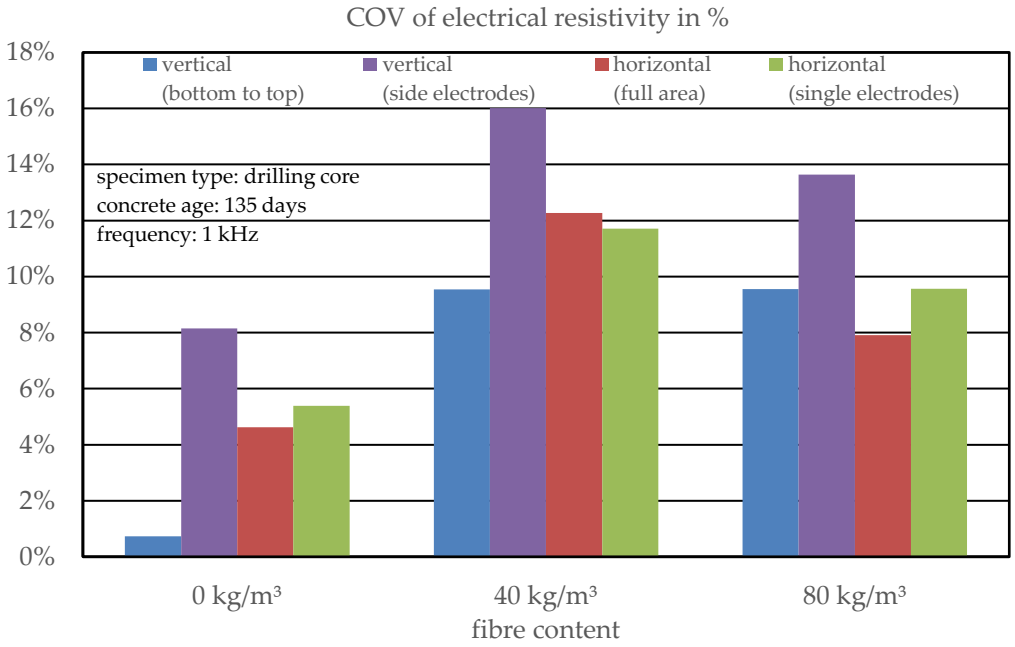

Figure 6.13 Coefficient of variation of the calculated electrical resistivity of drilling cores depending on the fibre content

6.4.2.3 Estimation of the Fibre Content

Based on the electrical resistivity, the fibre content of the concrete specimens was calculated with (eq. *6-2*). While for the cubic specimens (Section 6.4.1.2) for a frequency of the alternating current of 1 kHz, the fibre content was tendentially overestimated. For the drilling cores, a massive underestimation can be observed (Figure 6.14). For the specimens drilled of a plate with a fibre content of 40 kg/m³, a fibre content of 20.4 kg/m³ was calculated, which corresponds to 51 % of the actual mixed in fibres. Furthermore, for the specimens, with a mixed fibre content of 80 kg/m³, the difference between the result and expectation is even higher with a calculated fibre content of 28.1 kg/m³, representing 35 % of the expected content.

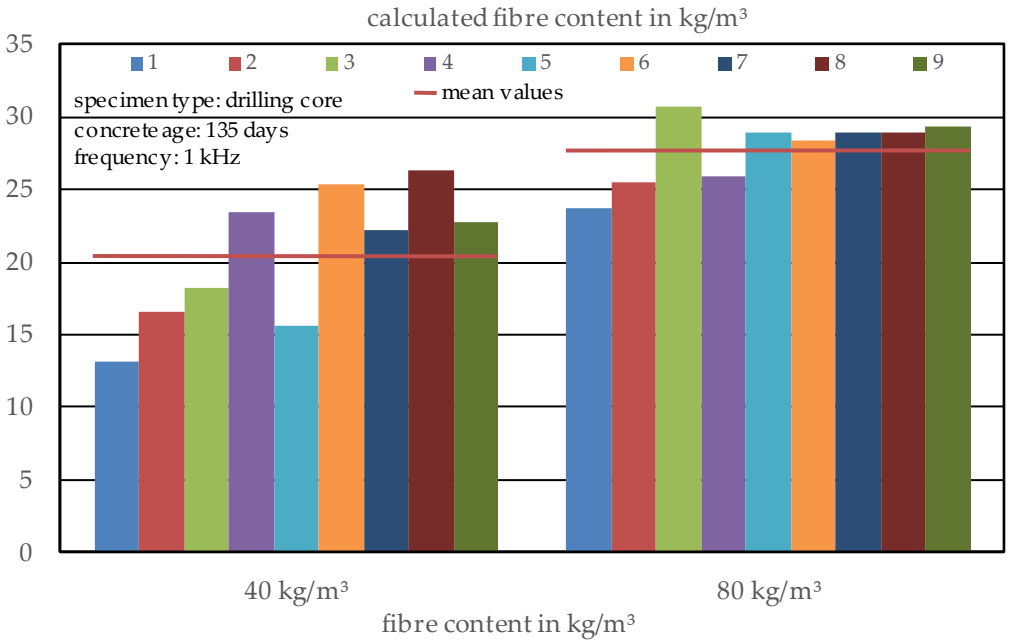

Figure 6.14 Calculated fibre content of the drilling cores as a function of the actually added fibre content

Both values are much too low, which is a result of the too high electrical resistivities of the specimens that were already described in Section 6.4.2.2 and could not be explained. In comparison to the results of earlier studies of the authors (see Cleven et al., 2022a) on casted cylindrical specimens, where the fibre content has been overestimated by trend, it seems that the open fibre ends and the cutting process of single fibres through the drilling process is the reason for this behaviour. The presumably best explanation could be the number of truncated fibres that lead to changes in the effective aspect ratio, which is used for the calculations. Truncated fibres thus could be calculated with a different aspect ratio, and so the estimation of the fibre content would be possible again. In this case, for the specimens with a fibre content of 40 kg/m³, a resulting aspect ratio of 39.9 can be calculated by use of (eq. *6-3*), when it is assumed that the fibre content inside the specimens is really 40 kg/m³. Concerning the fibre diameter of 1 mm, this can be interpreted as an average fibre length of 39.9 mm, which means a huge number of the fibres were cut by the drilling process. For the specimens with a fibre content of 80 kg/m³, the resulting fibre length to have a correct estimation of the fibre content is even smaller, with approximately 31.4 mm. Therefore, it can be concluded that the fibre length used for (eq. *6-3*) has to be adjusted and is a function of the fibre content itself with a decrease of the value by increasing fibre content or decreasing specimen size. As an asymptotic behaviour of this correlation can be assumed, an exponential curve was used to adjust (eq. *6-3*) based on the fibre content and the smallest dimension of the specimen. In this case, a factor could be derived from the results of the measurements that can be calculated by (eq. *6-4*) and has to be used to calculate the adjusted aspect ratio for (eq. *6-3*).

$$AR_{ad} = AR * \left(\left(1 - \frac{l_f}{d_{min}} \right) + \left(\frac{l_f}{d_{min}} \right) * V_f^{-\Phi * (d_{min} - l_f)} \right) \qquad \text{(eq. 6-4)}$$

with:

AR_{ad}: adjusted aspect ratio of the fibres
l_f: fibre length in mm

d_{min}: smallest specimen dimension in mm
V_f: fibre volume, calculated by l_f and d_{min} in mm³
Φ: expected fibre volume fraction

For the use of (eq. *6-4*), several parameters of the fibres, such as the fibre reinforced concrete, must be known or alternatively estimated. If there is no documentation of the fibre type and planned fibre content available, a small sample of concrete has to be crushed, and fibres have to be extracted to measure the actual fibre diameter and length. Additionally, the equation has to be used iteratively in combination with (eq. *6-3*) and adapted to determine the fibre content.

The calculation with the adjusted aspect ratio leads to significantly improved results for the fibre content (see Figure 6.15). For the lower fibre content of 40 kg/m³ large variations are visible with a minimum value of 25.1 kg/m³ and a maximum value of 50.5 kg/m³, which gives an accuracy of approximately ± 35 % for single measurements, but a very accurate value for a number of nine specimens. In contrast, for the higher fibre content of 80 kg/m³, the variations are smaller, with a minimum value of 67.8 kg/m³ and a maximum value of 88.0 kg/m³. This results in an accuracy of ± 15 % for single specimens.

Effects of the positions of the specimens inside the concrete plates, for example, specimen 5 in the middle and specimens 7 to 9 with low edge distances, can only marginally be detected, although the specimens 7 to 9 of both concretes show high values for the calculated fibre content, what could be a hint for fibre accumulations near the edges, which lead to a higher fibre content near the corners. However, the small number of samples and especially the inconsistent results for the other specimens makes it hard to decide if this observation is just a random phenomenon or if the position of the specimen really has an influence on the fibre content of the specimens.

One problem for future analysis is that either there must be an expected value for the fibre content to calculate the adjusted aspect ratio, or the specimen dimensions have to be chosen big enough to inhibit the problems with truncated fibres. Additionally, (eq. *6-4*) has to be reviewed with a large database of different SFRCs. After the revision of (eq. *6-4*) based on an enlarged database, the test setup in combination with the FEM model will give the opportunity to estimate the fibre content of concrete structures by extracting drilling core samples, which only causes small damage to the whole structure.

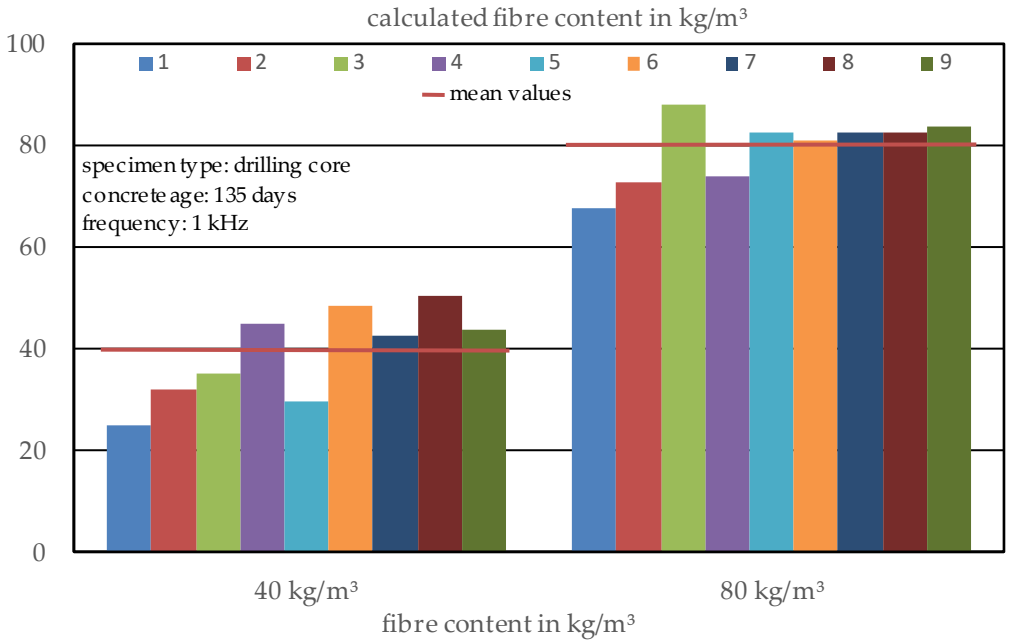

Figure 6.15 Calculated fibre content of the drilling cores depending on the fibre content by use of the adjusted fibre aspect ratio

6.4.2.4 Estimation of the Fibre Orientation

Although the determination of the fibre content seems to be problematic when no information about the concrete is available, the fibre orientation can be calculated without changes to any equations based on the electrical resistivity in different directions. As presented in Figure 6.16, for fibre content of 40 kg/m³, an unexpectedly high orientation factor in a vertical direction (mean value of 41 %) is observed, while for each specimen, the factor in a vertical direction is above 1/3, so most of the fibres are detected in a vertical direction. In comparison to the cubic specimens, this behaviour is contrary but could be based on the large dimensions of the concrete plate where the drilling cores have been extracted from. The large dimensions lead to a high volume of concrete and thus a lower effectivity of the compaction by the vibration table, which for smaller specimens is the most influencing parameter for the fibre orientation. In addition, one can see a high scatter in orientation that reaches from 34 % to 50 % for the vertical and 20 % to 38 % for the horizontal direction. One interesting fact can be identified by comparing Figure 6.15 and Figure 6.16. Where a fibre orientation in a vertical direction of more than 40 % is calculated, the calculated fibre content is significantly lower than the expected value of 40 kg/m³, which also is the mean value of all specimens. The same can be seen for specimen 8, which has the highest calculated fibre content and the lowest fibre orientation coefficient in a vertical direction. This correlation leads to the assumption that either the calculation of the global fibre content based on the three directions is slightly inaccurate, or the higher vertical orientation coefficient is a result of lacking horizontal fibres inside of single specimens. Again, a small influence of the specimen position inside the concrete plate could be assumed by looking at the results of specimens 7 to 9 with lower edge distances that show a higher horizontal orientation factor. Based on the compaction process, perhaps some fibres tend to orientate themselves on the walls of the formworks and thus are detected as horizontal fibres in the specimens near the formwork. Vertical fibres near the formwork are not detected because the distance between the drilling core and the formwork with half of the fibre length was chosen high enough not to be influenced by the walls.

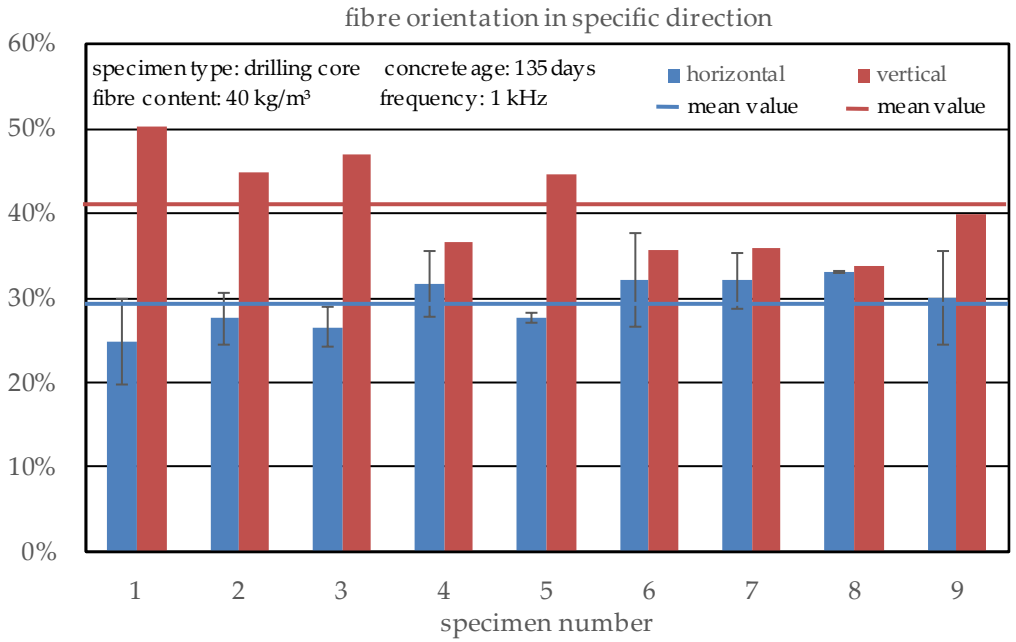

Figure 6.16 Calculated fibre orientation of the drilling cores with a fibre content of 40 kg/m³

For the specimens with a higher fibre content of 80 kg/m³, the expected orientation of more than 2/3 of the fibres in the horizontal direction is detected with maximum values up to 44 % and minimum values of about 28 % (Figure 6.17). In addition, the uniformity of the specimens is much higher, and only specimen number 5 shows a significantly lower vertical orientation coefficient. A correlation of the calculated fibre content and orientation factors was observed for the lower fibre content. In this case, it cannot be seen, probably based on the more uniform fibre distribution and orientation and thus the better acceptance of the calculated global values. Compared to the orientation of separately cast SFRC specimens, the difference in the fibre orientation is clearly visible which means that the orientation of fibres inside SFRC in contrast to the fibre content cannot be determined on such specimens and a direct analysis of structural elements is necessary. Here, no big influences of the specimen's position inside the concrete plate can be observed because of the relatively homogenous results in total. Only specimen number 5, which is in the centre of the plate, shows a significantly lower vertical fibre orientation factor, which can be explained by the flow process of the concrete through the compaction.

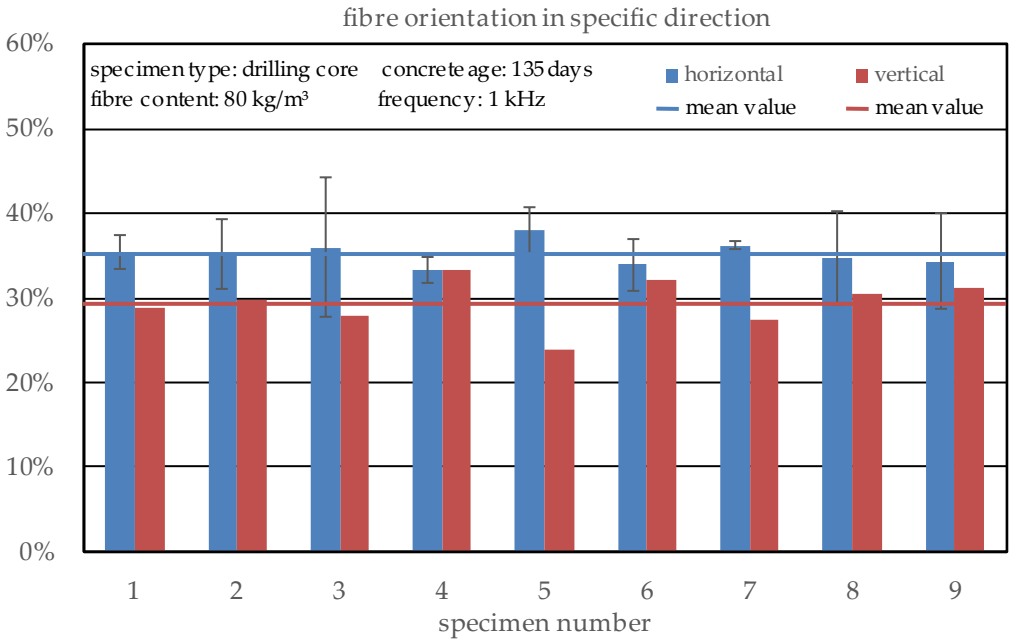

Figure 6.17 Calculated fibre orientation of the drilling cores with a fibre content of 80 kg/m³

6.5 Conclusions

This paper presents the results of the evaluation phase of a newly developed non-destructive test setup for the determination of the fibre content and orientation of steel fibres in concrete based on electrical resistivity measurements by the investigation of drilling cores. The basic test setup was already developed, and the FEM model was constructed in the first part of this research project (see Cleven et al., 2022a). This part of the study contains the validation process, which was performed on drilling core samples to enable statistical analysis and, of course, conclusions regarding the accuracy of the method. The main findings of this work can be summarised as follows:

- In contrast to AC-IS, the used method, based on electrical resistivity measurements, is much easier to use. However, similar models can be adapted to calculate both fibre content and orientation. One limitation in the application is the small amount of data that is used to calibrate the equations for the calculation of the fibre content for drilling cores which are needed to analyse structural elements or buildings.
- Based on the data gained in this study, a coefficient dependent on the expected value was found to calculate an adjusted fibre aspect ratio as a new coefficient for the literature's model for specimens with small dimensions where probably a huge number of fibres are truncated through the drilling process and thus the effective fibre length is much smaller than the original one.
- With this coefficient, the fibre content of drilling cores can be estimated in a satisfying way, and thus the basis for the analysis of the fibre content of existing structures in an easy way has been provided. Independent of such a factor, the orientation of the fibres inside a specimen can be calculated comparative from the electrical resistivity in different directions, which can be measured with the cylindrical test setup very easily and fast.

- The results show that the newly developed method is suitable for rapid and non-destructive structural diagnosis based on drilling cores using electrical resistivity measurements.
- In further studies, the authors will focus on the verification of the correlation between the fibre content and the coefficient for adjusting the aspect ratio, especially by a variety of specimen size and fibre lengths. Additionally, different concretes with deviant compositions will be analysed to see if those calculations are applicable in a universal way or if additional adjustments are needed in some cases. Finally, the test setup and the models will be adjusted for several geometries in case of precast elements or existing structural elements.

7 Conclusions and Outlook

7.1 Summary of the Optimum Test Setup

Until recently an easy-to-use non-destructive test setup for the determination of the fibre content and orientation of SFRC was missing, the thesis addresses the development of a setup based on electrical resistivity measurements. Other methods such as CT-scanning are not practical for in-field usage and methods based on crushing concrete specimens to manually count fibres are destructive, time consuming and need the extraction of drilling cores. Hence in this thesis, a simple and easy-to-use test setup for cubic and cylindrical specimens was developed, tested, and verified with different concretes to identify benefits and limitations of the applied test setup to enable the development of a general test method.

Because of the high differences of the electrical resistivities of plain concrete and steel a potential test method based on simple electrical resistivity measurements offers great potential to analyse the fibre content and orientation of SFRC. In the experimental investigations presented in this thesis several influencing factors on the electrical resistivity of SFRC have been systematically analysed. With a determined concrete composition, it is possible to determine the content of fibres as well as their global orientation inside specimens.

For cubic specimens the calculation is easily done, while for cylinders a more complex FEM simulation approach has to be applied to approximate the current flow and thus calculate geometry factors. A very important factor for the measurement is the humidity respectively saturation of the specimens since this significantly impacts the electrical resistivity measurements. Hence it is important to precondition or at least determine the saturation of the SFRC before the measurement takes place.

For optimum results the following additional parameters need to be obtained:

- The electrical connection between the electrodes and the concrete surface has to be replicable so that the resistance of the coupling can be neglected. This can be guaranteed via wet coupling material between steel electrodes and the concrete surface, form fit of the electrodes and a constant coupling pressure.
- The measurement system as well as the specimen size have to be chosen as function of the fibre type and geometry because too small specimen sizes or a too detailed measuring system will lead to misinterpretation and inaccuracy of the results.
- While the amplitude of the AC does not have a huge impact on the electrical resistivity measurements, the frequency is of high importance. Since with decreasing frequency the probability of polarisation effects gets highly increased, the amplitude should be in a range of 1 to 10 kHz. At higher frequencies artefacts based on cable dimensions may occur.
- Due to an ongoing pore refinement during cement hydration, an analysis of the SFRC should be best performed at concrete ages older than 28 days.
- The most accurate results can be generated if a plain reference concrete sample is available, or the composition is at least well-known, and the electrical resistivity of a similar concrete has been analysed before. A large database regarding electrical resistivity in context of different concrete compositions is currently missing and should be obtained in future research projects.
- The calculation of the fibre content and orientation is done by the equation of Woo et al., 2005, which is based on the ratio of the electrical resistivity of the SFRC and the

one of a plain reference concrete and in addition the aspect ratio of the fibres. This equation works fine for separately produced specimens but is limited through cutting surfaces of for example drilling cores. In such cases the aspect ratio needs to be adjusted in dependency of the specimen size and the fibre length.

7.2 Limitations of the Developed Test Method

The advantage of electrical resistivity tests is related to the fact that an occurring current will find the optimum path between two electrodes. Based on this, a spread of electrical field lines will occur, which can be simulated with help of FEM modelling. In first step geometrical assumptions have to be made, which can be easier computed to cubic specimens than for cylindrical specimens with different configurations of electrodes.

After the model is set up, the comparison of different specimen sizes and geometries regarding their electrical resistivity is possible. Thus, cubic, and cylindrical specimens as well as drilling cores were analysed. With a simple equation using the electrical resistivity as well as the aspect ratio of the fibres, the fibre content could be calculated. Thereby it was possible to generate reproducible results with sufficient accuracy. Ideally a series of at least three specimens should be tested. In addition to the number of specimens, the specimen size in relation to the fibre length has to be considered. For separately produced specimens it could be shown that a size of 2.5 times the fibre length is sufficient, whereas lower specimen dimensions resulted in inaccurate measurements. For drilling cores, the aspect ratio of the fibres has to be corrected because of the truncated fibres.

The calculation needs to be calibrated by the detection of the electrical resistivity of a plain reference concrete, which is used in the SFRC composition. This process limits the applicability of the developed test method to either newly produced concrete or structural analysis, where sample material of plain concrete is available for analysis. This sample material, for example, could be generated by drilling of small specimens, but this process has to be analysed in further research. Another possible method is the set-up of a database with several concrete compositions by use of an extensive material matrix, which ideally includes the most influencing parameters regarding electrical resistivity. For such a data base it is necessary to use a defined pre-conditioning of the concrete to generate a reproducible saturation and electrical conductivity of the pore solution like it was already done for the laboratory investigations in this thesis.

Since a further development of both the test setup and the calculation method has been performed in the process of this thesis, the optimized test setup has to be tested with different concrete compositions and the calculation method has to prove its accuracy and correctness.

All these steps in the meantime are currently performed in an additional ongoing research project at the IBAC in Aachen and will be presented in further scientific papers.

7.3 Summary of Additional Test Results

In addition to the experimental investigations supplementary test results were obtained (see Annex A to C), that show the influence of fibre content and orientation on the mechanical properties of SFRC. To validate the conclusions about the test setup, as presented in the scientific papers, further investigations using different test setups, like optoanalytical analysis and CT-scanning, are shown in Annex D. This helps to assess the accuracy of the electrical resistivity measurements.

The results of the investigations on single fibres proved the findings of the literature review (see section 2.2.3). The fibre orientation inside a concrete specimen has a big impact on the transmittable tensile force between fibres and concrete (see Annex A). The fibres with a larger angle between the fibre and the transmissible load are able to resist higher load levels due to a better utilisation of the friction between fibre and concrete matrix. Due to an additional plastic deformation during pull-out of the fibre, the probability of fibres to bridge occurring cracks during testing decreases with an increasing angle.

This can be seen in the analysis of the results of the wedge splitting test in Annex C, where the SFRC compositions are checked in different directions. Although the orientation of the fibres in relation to the tensile force is nearly parallel for two series of specimens and a much higher angle between tensile force and fibre orientation is proposed for the third series, the specimens with a parallel orientation show much better mechanical properties. This point is very interesting as the above-mentioned probability of a fibre to bridge the crack seems to be more relevant for the mechanical properties than the transmittable load of a single fibre.

In addition, the wedge splitting test shows that the fibre content as a parameter also influences the mechanical properties of SFRC, like already concluded from the literature review (see section 2.2.2). An increase of the fibre content from 40 kg/m³ to 80 kg/m³ enable a 60 % higher load transmission, especially for low specimen deflections, which are synonymous for a small crack opening. The increasing crack opening and thus the further pull-out of fibres leads to a decrease in the effect, but still 20 % to 40 % optimized mechanical properties are to be determined.

This phenomenon has also been observed during testing of the mechanical properties of SFRC in the 3-point bending test (see Annex B). Nearly the same relation between specimens with a fibre content of 40 kg/m³ and 80 kg/m³ was found as for the wedge splitting test. While for small crack openings the transmittable load can be increased by 60 % with a doubling of the fibre content, for larger crack openings only an increase of 30 % remains. Finally, the supplementary investigations have verified the findings of the literature review which show the significant influence of fibre content and fibre orientation on the mechanical properties of SFRC.

The comparison of different test setups, which in detail are electrical resistivity measurements, CT-scanning and optoanalytical analysis, showed the limitations of all three test methods (Annex D). The cross-sectional analysis and manual counting of fibres, as the easiest possible way of analysing was proven to be only accurate for a huge relation of cross-section of concrete to be analysed to fibre dimensions. For conventional macro SFRC thus, this test method is not applicable and additionally the investigation and preparation of specimens is very time consuming and above all a destructive test method.

CT-scanning can generate very detailed images of the fibres inside the specimen, but only if the specimen size is small enough for the X-ray source to be used and in best way also has a rotational symmetry. Otherwise, artificial inaccuracies occur that can’t be eliminated. Because of the limited specimen size, the same problem like for optoanalytical measurements takes part, as the specimen is not representative for the SFRC. In addition, expensive equipment and software is needed for the examination of CT-scanning. Except those facts, the method is highly detailed with a great accuracy. In relation to the electrical resistivity measurements only the lacking applicability is disadvantageous besides the fact that it can only be used on specimens and thus is a destructive method.

7.4 Conclusions

The objective of this thesis was the development of an easy-to-use test setup for the determination of the fibre content and orientation of SFRC. For this purpose, a test setup, based on electrical resistivity measurements was developed, tested, and further optimized. Therefore, an extensive test matrix was carried out with a variation of the test setup itself, the concrete composition, and the steel fibres. With help of this study, the main influencing factors of the electrical resistivity of SFRC as well as applicable test parameters could be determined. The setup consists of two-electrode measurements and uses alternating current to inhibit polarisation effects. This setup, with different electrode configurations is applicable for the measurement of cubic specimens as well as cylinders.

For the accurate calculation of the fibre content as well as the fibre orientation, it is necessary to determine the current flow inside the specimen because a comparison of different flow directions is needed to investigate the sample as a global geometric body. With help of a geometrical factor, based on the flow directions of the current, the electrical resistivity can be calculated and put into proportion to the one of a plain reference concrete, what enables the accurate estimation of the fibre content and orientation. The accuracy hereby is dependent on the representativeness of the sample or in the best case several samples and the possibility to analyse a plain concrete sample as well. In optimal cases a high accuracy of the estimation of the fibre content with deviations lower than 10 % is possible, what for practical use enables the application of much lower safety factors than today.

7.5 Outlook

In addition to the new measurement possibilities with help of the novel test setup, there are still open points for further research and development. The biggest open issue at the moment is the dependency of the accuracy of the estimation on the possibility of the analysis of a plain concrete sample. At the actual point of research there is no extensive database available, that contains the electrical resistivity of different concrete compositions considering the humidity conditions. In further research such a database should be developed and can then act as calibration method for the test method in total. Further use of the test setup as well as the professional implementation will lead to huge optimization step.

Additionally, it was shown that for separately produced lab or field specimens the calculation method of the fibre content results in accurate results. However, for extracted concrete samples like drilling cores the use of the aspect ratio reaches its limits. Further investigations have to focus on such samples as well as whole construction elements so the application on construction side can be addressed.

The last step of development should be done in cooperation with steel fibre producers and standardization committees, where the test method has to be standardized and the results are declared correct and authorised for the application in static calculations instead of using simple safety factors. For this purpose, an extensive test matrix of mechanical testing in combination with electrical resistivity tests has to be performed, after which a correlation between the mechanical properties and the fibre content, calculated with help of the novel test setup, can be drawn.

IX. References

Ackermann FP. Zum Tragverhalten von durchlaufenden stahlfaserbewehrten Stahlverbunddecken, Dissertation, Technische Universität Kaiserslautern. 2010 https://nbn-resolving.org/urn:nbn:de:hbz:386-kluedo-25485

Akgol O, Unal E, Bağmancı M, Karaaslan M, Sevim UK, Öztürk M, Bhadauria A. A nondestructive method for determining fiber content and fiber ratio in concretes using a metamaterial sensor based on a V-shaped resonator. J. Electron. Mater. 2019; 48(4):2469-81 https://doi.org/10.1007/s11664-019-06937-w

Al-Mattarneh HMA. Electromagnetic quality control of steel fiber concrete. Construct Build Mater. 2014; 73:350-356 https://doi.org/10.1016/j.conbuildmat.2014.09.101

Andrade C. Model for prediction of reinforced concrete service life based on electrical resistivity. IBRACON Mater. J. 2005; 1:1-5

Archie GE. The electrical resistivity log as an aid in determining some reservoir characteristics. Trans. Am. Inst. Min. Metall. Eng. J. 1942; 146:54-62

Azarsa P & Gupta R. Electrical resistivity of concrete for durability evaluation: A review. Adv. Mater. Sci. Eng. 2017; 8453095 https://doi.org/10.1155/2017/8453095

Balázs GL, Czoboly O, Lublóy E, Kapitány K, Barsi A. Observation of steel fibres in concrete with computed tomography. Construct Build Mater. 2017; 140:534-541 https://doi.org/10.1016/j.conbuildmat.2017.02.114

Banea PII. Study of electrical resistivity of mature concrete. Master thesis, Delft University of Technology. 2015 http://resolver.tudelft.nl/uuid:a927e4b3-5e8e-47f2-8273-090428108d83

Banthia N, Djeridane S, Pigeon M. Electrical resistivity of carbon and steel micro-fiber reinforced cements. Cem. Concr. Res. 1992; 22:804-814 https://doi.org/10.1016/0008-8846(92)90104-4

Barnett SJ, Lataste J, Parry T, Millard SG, Soutsos MN. Assessment of fibre orientation in ultra high performance fibre reinforced concrete and its effect on flexural strength. Mater. Struct. 2010; 43:1009-1023 https://doi.org/10.1617/s11527-009-9562-3

Barsoukov E & Macdonald JR. Impedance spectroscopy. Theory, experiment, and applications. John Wiley & Sons, Hoboken, New Jersey. 2005 https://doi.org/10.1002/0471716243

Berke NS, Dallaire MP, Hicks MC. Plastic, mechanical, corrosion, and chemical resistance properties of silica fume (microsilica) concretes. Proceedings, 4th Annual Conference on Fly Ash, Silica Fume, Slag and Natural Pozzolanes in Concrete, Istanbul. 1992; 2:1125-1149 https://doi.org/10.14359/1220

Berrocal CG, Hornbostel K, Geiker MR, Löfgren I, Lundgren K, Bekas DG. Electrical resistivity measurements in steel fibre reinforced cementitious materials. Cem. Concr. Compos. 2018; 89:216-229 https://doi.org/10.1016/j.cemconcomp.2018.03.015

Blanco A, Pujadas P, de la Fuente A, Cavalaro SHP, Aguado A. Assessment of the fibre orientation factor in SFRC slabs. Composites Part B: Engineering. 2015; 68:343-354 https://doi.org/10.1016/j.compositesb.2014.09.001

Bonzel J & Schmidt M. Verteilung und Orientierung von Stahlfasern im Beton und ihr Einfluß auf die Eigenschaften von Stahlfaserbeton. Betontechnische Berichte. 1984/85; 73-116

Brandt AM. Fibre reinforced cement-based (FRC) composites after over 40 years of development in building and civil engineering. Compos. Struct. 2008; 86:3-9 https://doi.org/10.1016/j.compstruct.2008.03.006

Breitenbücher R & Rahm H. Zerstörungsfreie Bestimmung des Stahlfasergehalts und der Stahlfaserorientierung im Frisch- und Festbeton. Beton, Verlag Bau + Technik GmbH, Erkrath. 2009; 99(3):88-93

Breitenbücher R. Herstellung und Eigenschaften von Stahlfaserbeton. Berichte aus dem Konstruktiven Ingenieurbau, Universität der Bundeswehr München. 2012; 12(4):137-144

Breitenbücher R. Spezielle Anforderungen an Beton im Tunnelbau. Beton-Kalender, Ernst & Sohn, Berlin. 2014; 1:391-422 https://doi.org/10.1002/9783433603352.ch10

Brux G. Fasern im Beton. Schweizer Baujournal. 2004; 2

Bürchler D. Der elektrische Widerstand von zementösen Werkstoffen. Dissertation, ETH Zürich. 1996 https://doi.org/10.3929/ethz-a-001687223

Cao YYY & Yu QL. Effect of inclination angle on hooked end steel fiber pullout behavior in ultra-high performance concrete. Compos Struct. 2018; 201:151-160 https://doi.org/10.1016/j.compstruct.2018.06.029

Chen B, Wu K, Yao W. Conductivity of carbon fiber reinforced cement-based composites. Cem. Concr. Compos. 2004; 26:291-297 https://doi.org/10.1016/S0958-9465(02)00138-5

Chen W & Brouwers HJH. The hydration of slag, part 2: Reaction models for blended cement. J. Mater. Sci. 2006; 42:444-464 https://doi.org/10.1007/s10853-006-0874-1

Clausert H, Hoffmann K, Mathis W, Wiesemann G, Beck HP. Elektrotechnik. Das Ingenieurwissen. Springer Vieweg, Berlin. 2014 https://doi.org/10.1007/978-3-662-44032-2_1

Cleven S, Raupach M, Gerguri V. Prüfmethoden zur Beurteilung der Leistungsfähigkeit von Stahlfaserbeton - Beurteilung der gängigen Verfahren und vergleichende Untersuchungen. Beton, Verlag Bau + Technik GmbH, Erkrath. 2018; 68(6):220-224

Cleven S, Raupach M, Matschei T. Electrical resistivity of steel fibre-reinforced concrete - influencing parameters. Materials. 2021; 14:3408 https://doi.org/10.3390/ma14123408

Cleven S, Raupach M, Matschei T. A new method to determine the steel fibre content of existing structures - test setup and numerical simulation. Appl. Sci. 2022; 12:561 https://doi.org/10.3390/app12020561

Cleven S, Raupach M, Matschei T. A new method to determine the steel fibre content of existing structures - evaluation and validation. Appl. Sci. 2022; 12:454 https://doi.org/10.3390/app12010454

Cleven, S, Raupach, M, Matschei, T. Electrical resistivity measurements to determine the steel fiber content of concrete. Structural Concrete. 2022; 23(3):1704-1717 https://doi.org/10.1002/suco.202100832

Cosoli G, Mobili A, Tittarelli F, Revel GM, Chiariotti P. Electrical resistivity and electrical impedance measurement in mortar and concrete elements: A systematic review. Appl. Sci. 2020; 10:9152 https://doi.org/10.3390/app10249152

Cugat V, Cavalaro SHP, Bairán JM, De La Fuente A. Safety format for the flexural design of tunnel fibre reinforced concrete precast segmental linings. Tunn. Undergr. Space Technol. 2020; 103:103500 https://doi.org/10.1016/j.tust.2020.103500

DAfStb Deutscher Ausschuss für Stahlbeton: Prüfung von Beton Empfehlungen und Hinweise als Ergänzung zu DIN 1048. 1991

DAfStb Deutscher Ausschuss für Stahlbeton. Heft 614 Erläuterungen zur DAfStb-Richtlinie "Stahlfaserbeton", Beuth, Berlin. 2015

Dahms J. Herstellung und Eigenschaften von Faserbeton, Beton, Verlag Bau + Technik GmbH, Erkrath. 1979; 29(4):139-143

Daniel JI, Gopalaratnam VS, Galinat MA, et al. Report on fiber reinforced concrete. Reported by ACI Committee 544; ACI544.1R-96; American Concrete Institute: Indianapolis, USA. 2001

de Brito J & Saikia N. Recycled aggregate in concrete: Use of industrial, construction and demolition waste. Springer, London. 2013 https://doi.org/10.1007/978-1-4471-4540-0

Di Prisco M, Plizzari G, Vandewalle L. Fibre reinforced concrete: New design perspectives. Mater. Struct. 2009; 42:1261-1281 https://doi.org/10.1617/s11527-009-9529-4

DIN 1045-2: Tragwerke aus Beton, Stahlbeton und Spannbeton—Teil 2: Beton—Festlegung, Eigenschaften, Herstellung und Konformität—Anwendungsregeln zu DIN EN 206-1; DIN 1045-2:2008-08; Beuth Publishing DIN: Berlin. 2008 https://doi.org/10.31030/1453177

DIN EN 196-1: Prüfverfahren für Zement - Teil 1: Bestimmung der Festigkeit; Deutsche Fassung EN 196-1:2016; DIN EN 196-1: 2016-11; Beuth Publishing DIN: Berlin. 2016 https://doi.org/10.31030/2482416

DIN EN 206: Beton—Festlegung, Eigenschaften, Herstellung und Konformität; Deutsche Fassung EN 206:2013+A1:2016; DIN EN 206:2017-01; Beuth Publishing DIN: Berlin. 2017 https://doi.org/10.31030/2584715

DIN EN 12350-5: Prüfung von Frischbeton - Teil 5: Ausbreitmaß; Deutsche Fassung EN 12350-5:2019; DIN EN 12350-5:2019-09; Beuth Publishing DIN: Berlin. 2019 https://doi.org/10.31030/3045714

DIN EN 12350-6: Prüfung von Frischbeton - Teil 6: Frischbetonrohdichte; Deutsche Fassung EN 12350-6:2019; DIN EN 12350-6:2019-09; Beuth Publishing DIN: Berlin. 2019 https://doi.org/10.31030/3045731

DIN EN 12350-7: Prüfung von Frischbeton - Teil 7: Luftgehalt—Druckverfahren; Deutsche Fassung EN 12350-7:2019; DIN EN 12350-7:2019-09; Beuth Publishing DIN: Berlin. 2019 https://doi.org/10.31030/3045732

DIN EN 14651: Prüfverfahren für Beton mit metallischen Fasern - Bestimmung der Biegezugfestigkeit (Proportionalitätsgrenze, residuelle Biegezugfestigkeit); Deutsche Fassung EN 14651:2005+A1:2007; Beuth Publishing DIN: Berlin. 2019 https://doi.org/10.31030/1386060

DIN EN 14721: Prüfverfahren für Beton mit metallischen Fasern - Bestimmung des Fasergehalts in Frisch- und Festbeton; Deutsche Fassung EN 14721:2005+A1:2007; Beuth Publishing DIN: Berlin. 2007 https://doi.org/10.31030/1386059

Ding X, Zhao M, Zhou S, Fu Y, Li C. Statistical analysis and preliminary study on the mix proportion design of self-compacting steel fiber reinforced concrete. Materials. 2019; 12:637 https://doi.org/10.3390/ma12040637

Dollase A. Mikrowellenverfahren zur Untersuchung des Erhärtungs- und Trocknungsverhaltens von zementgebundenen Baustoffen. Dissertation, Bergische Universität Wuppertal. 2019

Edgington J & Hannant DJ. Steel fibre reinforced concrete. The effect on fibre orientation of compaction by vibration. Matr. Struct. 1972; (5):41-44 https://doi.org/10.1007/BF02479076

Edwards LS. A modified pseudosection for resistivity and ip. Geophysics. 1977; 42(5):939-1087 https://doi.org/10.1190/1.1440762

Elkey W & Sellevold EJ. Electrical resistivity of concrete; Norwegian Road Research Laboratory: Oslo, Norway. 1995

Empelmann M, Teutsch M, Wichers M. Baukonstruktionen aus Faserbeton. Beton-Kalender, Ernst & Sohn, Berlin. 2011; 2:89-140

Facconi L, Minelli F, Ceresa P, Plizzari G. Steel fibers for replacing minimum reinforcement in beams under torsion. Mater. Struct. 2021; 54:34 https://doi.org/10.1617/s11527-021-01615-y

Faifer M, Ottoboni R, Toscani S, Ferrara L. Steel fiber reinforced concrete characterization based on a magnetic probe. Paper presented at the 2010 IEEE International Instrumentation and Measurement Technology Conference, I2MTC. 2010; 11501604 https://doi.org/10.1109/IMTC.2010.5488179

Faifer M, Ottoboni R, Toscani S. A compensated magnetic probe for steel fiber reinforced concrete monitoring. Proc IEEE Sens. 2010; 11831314 https://doi.org/10.1109/ICSENS.2010.5690066

Faifer M. Nondestructive testing of steel-fiber-reinforced concrete using a magnetic approach. IEEE Trans. Instrum. Meas. 2011; 60(5):1709-1717 https://doi.org/10.1109/TIM.2010.2090059

Ferdosian I & Camões A. Mechanical performance and post-cracking behavior of self-compacting steel-fiber reinforced eco-efficient ultra-high performance concrete. Cem. Concr. Compos. 2021; 121:104050 https://doi.org/10.1016/j.cemconcomp.2021.104050

Fehling E, Schmidt M, Walraven J, Leutbecher T, Fröhlich S. Ultra-high performance concrete UHPC. Ernst & Sohn, Berlin. 2014 https://doi.org/10.1002/9783433604076

Feliu S, Andrade C, Gonzalez JA, Alonso C. A new method for in-situ measurement of electrical resistivity of reinforced concrete. Mater. Struct. 1996; 29:362-365 https://doi.org/10.1007/BF02486344

Ferrara L, Faifer M, Toscani S. A magnetic method for non destructive monitoring of fiber dispersion and orientation in steel fiber reinforced cementitious composites - part 1: method calibration. Mater. Struct. 2012; 45:575-589 https://doi.org/10.1617/s11527-011-9793-y

Fischer R. Elektrotechnik. Für Maschinenbauer sowie Studierende technischer Fächer. Springer Vieweg, Wiesbaden. 2019; 16 https://doi.org/10.1007/978-3-658-25644-9

Franchois A, Taerwe L, Van Damme S. A microwave probe for the non-destructive determination of the steel fiber content in concrete slabs. 6th RILEM Symposium on Fibre-Reinforced Concretes (FRC) - BEFIB 2004, 20-22 September. 2004, Varenna, Italy

Frenkel J. Kinetic theory of liquids. Clarendon Press, Oxford. 1946

Frettlöhr B. Bemessung von Bauteilen aus ultrahochfestem Faserfeinkornbeton (UHFFB). Dissertation. Universität Stuttgart. 2011 https://doi.org/10.18419/opus-379

Funke K. Impedanzspektroskopie. Apparative Methoden in der Physikalischen Chemie. 2002

Gastaldini ALG, Isaia GC, Hoppe TF, Missau F, Saciloto AP. Influence of the use of rice husk ash on the electrical resistivity of concrete: A technical and economic feasibility study. Constr. Build. Mater. 2009; 23(11):3411-3419 https://doi.org/10.1016/j.conbuildmat.2009.06.039

Gettu R, Gardner DR, Saldívar H, Barragán BE. Study of the distribution and orientation of fibers in SFRC specimens. Mater. Struct. 2005; 38(1):31-37 https://doi.org/10.1007/BF02480572

Gjørv OE, Vennesland ØE, El-Busaidy AHS. Electrical resistivity of concrete in the oceans. Proc. Annu. Offshore Technol. Conf. 1977; 2:581-588 https://doi.org/10.4043/2803-MS

Gouri Mohan L, Nazeer M, Nizad A, Suresh S. Fibre reinforced concrete—A state-of-the-art review. Int. J. Earth Sci. Eng. 2010; 3:634-642

Gröger J, Nehls N, Silbereisen R, Tue NV. Einfluss der Einbau- und der Betontechnologie auf die Faserverteilung und -orientierung in Wänden aus Stahlfaserbeton. Beton- und Stahlbetonbau. 2011; 106(1):45-49 https://doi.org/10.1002/best.201000063

Grunert JP. Zum Tragverhalten von Spannbetonfertigteilbalken aus Stahlfaserbeton ohne Betonstahlbewehrung. Institut für Baustoffe, Massivbau und Brandschutz, IBMB der Technischen Universität Braunschweig - Materialprüfanstalt für das Bauwesen - MPA Braunschweig. Institut für Baustoffe, Massivbau und Brandschutz (IBMB), Braunschweig. 2006 https://doi.org/10.24355/dbbs.084-201707051249

Grünewald S &, Walraven JC. Case studies with self-compacting steel fibre reinforced concrete. Betonwerk und Fertigteiltechnik. 2004; 70(12):18-27

Hadl P, Gröger J, Tue NV. Experimentelle Untersuchungen zur Streuung im Zugtragverhalten von Stahlfaserbeton. Bautechnik. 2015; 92(6):385-393 https://doi.org/10.1002/bate.201500008

Hadl P & Tue N.V. Einfluss der Faserzugabe auf die Streuung im Zugtragverhalten von Stahlfaserbeton. Beton- und Stahlbetonbau. 2016; 111:310-318 https://doi.org/10.1002/best.201600002

Harriehausen T & Schwarzenau D. Moeller Grundlagen der Elektrotechnik. Springer Vieweg, Wiesbaden. 2020; 24 https://doi.org/10.1007/978-3-658-27840-3

Hauck K. The effect of curing temperature and silica fume on chloride migration and pore structure of high strength concrete. Ph.D. Thesis, Department of Civil and Engineering University, Trondheim. 1993

Hedjazi S & Castillo D. Effect of fibre types on the electrical properties of fibre reinforced concrete. Mater. Express. 2020; 10(5):733-739 https://doi.org/10.1166/mex.2020.1679

Heins TP. Entwicklung Impedanzspektroskopie-basierter Methoden zur mechanistischen Untersuchung der Bildung von Oberflächenfilmen auf Lithium-Ionen-Elektroden. Dissertation, Technische Universität Carolo-Wilhelmina zu Braunschweig. 2015 https://nbn-resolving.org/urn:nbn:de:gbv:084-16110209299

Henkensiefken R, Castro J, Bentz D, Nantung T, Weiss J. Water absorption in internally cured mortar made with water-filled lightweight aggregate. Cem. Concr. Res. 2009; 39(10):883-892 https://doi.org/10.1016/j.cemconres.2009.06.009

Herrmann H, Boris R, Goidyk O, Braunbrück A. Variation of bending strength of fiber reinforced concrete beams due to fiber distribution and orientation and analysis of microstructure. IOP Conf. Ser: Mater. Sci. Eng. 2019; 660(1):012059 https://doi.org/10.1088/1757-899X/660/1/012059

Hicks NJ. Fiber orientation in ultra-high-performance concrete (UHPC) shear connections in adjacent box beam bridges. Master's thesis, Ohio University. 2015 http://rave.ohiolink.edu/etdc/view?acc_num=ohiou1420459364

Hilsdorf HK, Brameshuber W, Kottas R. Abschlußbericht zum Forschungsvorhaben „Weiterentwicklung und Optimierung der Materialeigenschaften faserbewehrten Betons und Spritzbetons als Stabilisierungselemente der Felssicherung". Teil A und B. Karlsruher Institute of Technology. 1985

Hobst L & Bílek P. Nondestructive identification of material properties of fibre concrete: a stationary magnetic field. AIP Conf. Proc. 2016; 1738:380010 https://doi.org/10.1063/1.4952171

Hoffmann-Walbeck W. Anwendung der Impedanzspektroskopie für die Untersuchung von Biogasreformat in Brennstoffzellen. Diplomarbeit, Technische Universität Berlin. 2017 https://doi.org/10.14279/depositonce-1845

Holschemacher K, Klug Y, Dehn F, Wörner JD. Faserbeton. Beton-Kalender, Ernst & Sohn, Berlin. 2006; 1:585-664

Hope BB, Ip AKC, Manning G. Corrosion and electrical impedance in concrete. Cem. Concr. Res. 1985, 15(3):525-534 https://doi.org/10.1016/0008-8846(85)90127-9

Hope BB & Ip AKC. Corrosion of steel in concrete made with slag cement. ACI Mater. J. 1987; 84(6):525-531 https://doi.org/10.14359/2470

Hughes BP, Soleit AKO, Brierley RW. New technique for determining the electrical resistivity of concrete. Mag. Concr. Res. 1985; 37:243-248 https://doi.org/10.1680/macr.1985.37.133.243

Jamil M, Hassan MK, Al-Mattarneh HMA, Zain MFM. Concrete dielectric properties investigation using microwave nondestructive techniques. Mater. Struct. 2013; 46:77-87 https://doi.org/10.1617/s11527-012-9886-2

Juan-García P, Torrents JM, López-Carreño RD, Cavalaro SHP. Influence of fiber properties on the inductive method for the steel-fiber-reinforced concrete characterization. IEEE Trans. Instrum. Meas. 2016; 65(8):1937-1944 https://doi.org/10.1109/TIM.2016.2549678

Jungwirth J. Zum Tragverhalten von zugbeanspruchten Bauteilen aus Ultra-Hochleistungs-Faserbeton, Dissertation, Ecole Polytechnique Federale de Lousanne. 2006 https://doi.org/10.5075/epfl-thesis-3429

Just A, Danckwardt E, Jacobs F. Geoelektrische Tomographie. Prinzip und Anwendungsbeispiele. Universität Leipzig. 2001

Kachouh N, El-Hassan H, El-Maaddawy T. Effect of steel fibers on the performance of concrete made with recycled concrete aggregates and dune sand. Constr. Build. Mater. 2019, 213:348-359 https://doi.org/10.1016/j.conbuildmat.2019.04.087

Kalthoff M & Raupach M. Pull-out behaviour of threaded anchors in fibre reinforced ordinary concrete and UHPC for machine tool constructions. J. Build. Eng. 2021; 33:101842 https://doi.org/10.1016/j.jobe.2020.101842

Karhunen K, Seppänen A, Lehikoinen A, Monteiro PJM, Kaipio JP. Electrical resistance tomography imaging of concrete. Cem. Concr. Res. 2010; 40(1):137-145 https://doi.org/10.1016/j.cemconres.2009.08.023

Karlovšek J, Wagner N, Scheuermann A. Frequency-dependant dielectric parameters of steel fiber reinforced concrete. Paper presented at the 2012 14th International Conference on Ground Penetrating Radar, GPR 2012. 2012; 14:510-516 https://doi.org/10.1109/icgpr.2012.6254918

Kobaka J, Katzer J, Ponikiewski T. A combined electromagnetic induction and radar-based test for quality control of steel fibre reinforced concrete. Materials. 2019; 12(12):3507 https://doi.org/10.3390/ma12213507

Komárková T. Design of methodology for non-destructive testing of steel-reinforced-fiber-concrete. Key Eng. Mater. 2016; 714:179-185 https://doi.org/10.4028/www.scientific.net/kem.714.179

Lataste JF, Behloul M, Breysse D. Characterisation of fibres distribution in a steel fibre reinforced concrete with electrical resistivity measurements. NDT E Int. 2008; 41(8):638-647 https://doi.org/10.1016/j.ndteint.2008.03.008

Lataste JF, Barnett SJ, Parry T, Soutsos MN. Study of fibre distribution and orientations in UHPFRC by electrical resistivity and mechanical tests. Eur. J. Environ. Civ. Eng. 2010; 15(4):533-544 https://doi.org/10.3166/EJECE.15.533-544

Layssi H, Ghods P, Alizadeh A, Salehi M. Electrical resistivity of concrete. Concr. Int. 2015; 37(5):41-46

Lee S, Oh J, Cho J. Fiber orientation factor on rectangular cross-section in concrete members. Int. J. Eng. Technol. 2015; 7(6):470-473 https://doi.org/10.7763/IJET.2015.V7.839

Lehmberg S. Herstellung und Eigenschaften von dünnwandigen, trocken gefügten Bauteilen aus ultrahochfestem faserverstärkten Feinkornbeton. Institut für Baustoffe, Massivbau und Brandschutz, IBMB der Technischen Universität Braunschweig - Materialprüfanstalt für das Bauwesen - MPA Braunschweig. Institut für Baustoffe, Massivbau und Brandschutz IBMB, Braunschweig. 2018 https://doi.org/10.24355/dbbs.084-20180409151

Lehner P, Konečný P, Ponikiewski T. Comparison of material properties of SCC concrete with steel fibres related to ingress of chlorides. Crystals. 2020; 10(3):220 https://doi.org/10.3390/cryst10030220

Lei T, Ottoboni R, Faifer M, Toscani S, Ferrara L. A costeffective method to assess the fiber content and orientation in steel fiber reinforced concrete. Paper presented at the I2MTC 2019-2019 IEEE International Instrumentation and Measurement Technology Conference. 2019; 18974223 https://doi.org/10.1109/I2MTC.2019.8827015

Leone M. Theoretische Elektrotechnik. Elektromagnetische Feldtheorie für Ingenieure. Springer Vieweg, Wiesbaden. 2018; 1 https://doi.org/10.1007/978-3-658-18317-2

Leutbecher T. Rissbildung und Zugtragverhalten von mit Stabstahl und Fasern bewehrtem ultrahochfesten Beton (UHPC). Dissertation. Kassel University. 2007 http://www.urn.fi/urn:nbn:de:hebis:34-2009031226631

Li FY, Li LY, Dang Y, Wu PF. Study of the effect of fibre orientation on artificially directed steel fibre-reinforced concrete. Adv. Mater. Sci. Eng. 2018; 8657083 https://doi.org/10.1155/2018/8657083

Li X, Xue W, Fu C, Yao Z, Liu X. Mechanical properties of high-performance steel-fibre-reinforced concrete and its application in underground mine engineering. Materials. 2019; 12(15):2470 https://doi.org/10.3390/ma12152470

Li L, Xia J, Chin C, Jones S. Fibre distribution characterization of ultra-high performance fibre-reinforced concrete (uhpfrc) plates using magnetic probes. Materials. 2020; 13(22):5064 https://doi.org/10.3390/ma13225064

Li Y, Ruan X, Akiyama M, Zhang M, Xin J, Lim S. Modelling method of fibre distribution in steel fibre reinforced concrete based on X-ray image recognition. Compos. Part B Eng. 2021; 223:109124 https://doi.org/10.1016/j.compositesb.2021.109124

Lin, Y.: Tragverhalten von Stahlfaserbeton. Dissertation, Karlsruher Institute of Technology. 1996

Liu S, Wang L, Gao Y, Yu B, Bai Y. Comparing study on hydration properties of various cementitious systems. J. Therm. Anal. Calorim. 2014; 118:1483-1492 https://doi.org/10.1007/s10973-014-4052-4

Liu Y & Presuel-Moreno F. Effect of elevated temperature curing on compressive strength and electrical resistivity of concrete with fly ash and ground-granulated blast-furnace slag. ACI Mater. J. 2014; 111(5):531-542 https://doi.org/10.14359/51686913

Löfgren I. The wedge splitting test - A test method for assessment of fracture parameters of FRC. Proceedings of the fifth International Conference on "Fracture Mechanics of Concrete Structures" (FRAMCOS-5), Vail Colorado, USA. 2004; 2:1155-1162

Löfgren I. Fibre-reinforced concrete for industrial construction - a fracture mechanics approach to material testing and structural analysis. Dissertation, Chalmers Tekniska Högskola, Göteborg. 2005; 2378

Lübeck A, Gastaldini ALG, Barin DS, Siqueira HC. Compressive strength and electrical properties of concrete with white portland cement and blast-furnace slag. Cem. Concr. Compos. 2012; 34(2):392-399 https://doi.org/10.1016/j.cemconcomp.2011.11.017

Luo T, Zhang C, Sun C, Zheng X, Ji Y, Yuan X. Experimental investigation on the freeze-thaw resistance of steel fibers reinforced rubber concrete. Materials. 2020; 13(5):1260 https://doi.org/10.3390/ma13051260

Lvovich VF. Impedance spectroscopy. Applications to electrochemical and dielectric phenomena. John Wiley & Sons, Hoboken, New Jersey. 2012

Maidl B. Stahlfaserbeton. Ernst & Sohn, Berlin. 1991

Malakooti, A, Thomas RJ, Maguire M. Investigation of concrete electrical resistivity as a performance-based test, Utah State University, Department of Civil & Environmental Engineering, Report No. UT-19.09. 2019 https://rosap.ntl.bts.gov/view/dot/42384

Maldague X & Fernandes HC. Use of infrared thermography to measure fiber orientation on carbon-fiber reinforced composites. 7th Int'l Workshop-NDT Signal Processing, Quebec City, Quebec, Canada (ASPNDE 2013). 2013

Markovic I. High-performance hybrid-fibre concrete. Development and utilisation. Dissertation, Delft University of Technology. 2006 http://resolver.tudelft.nl/uuid:44ed51cd-fc27-4353-ab81-cf8348f52443

Martinelli P, Colombo M, De La Fuente A, Cavalaro S, Pujadas P, Di Prisco M. Characterization tests for predicting the mechanical performance of SFRC floors: Design considerations. Mater. Struct. 2021; 54:2 https://doi.org/10.1617/s11527-020-01598-2

Martinelli P, Colombo M, Pujadas P, De La Fuente A, Cavalaro S, Di Prisco M. Characterization tests for predicting the mechanical performance of SFRC floors: Identification of fibre distribution and orientation effects. Mater. Struct. 2021; 54:3 https://doi.org/10.1617/s11527-020-01593-7

Mason TO, Campo MA, Hixson AD, Woo LY. Impedance spectroscopy of fiber-reinforced cement composites. Cem. Concr. Compos. 2002; 24(5):457-465 https://doi.org/10.1016/S0958-9465(01)00077-4

Matenco G. Stahlfaserprüfung im Frisch- und Festbeton und Mietmodelle zur Kostensenkung. Messtechnik im Bauwesen, Ernst & Sohn, Berlin. 2009; 1:110

Mazloom M, Allahabadi A, Karamloo M. Effect of silica fume and polyepoxide-based polymer on electrical resistivity, mechanical properties, and ultrasonic response of SCLC. Adv. Concr. Constr. 2017; 5(6):587-611 https://doi.org/10.12989/acc.2017.5.6.587

McCarter WJ, & Garvin S. Dependence of electrical impedance of cement-based materials on their moisture condition. Journal of Physics D: Applied Physics. 1989; 22:1773-1777

Mehdipour I, Horst M, Zoughi R, Khayat KH. Use of near-field microwave reflectometry to evaluate steel fiber distribution in cement - based mortars. J. Mater. Civil. Eng. 2017; 29(7):04017029 https://doi.org/10.1061/(ASCE)MT.1943-5533.0001850

Meyer B. Faserbeton. Unterschied zu Bewehrtem Beton. Eigenschaften im Überblick. Cementbulletin, Technische Forschungs- und Beratungsstelle der schweizerischen Zementindustrie. 1991; 59(22) https://doi.org/10.5169/seals-153761

Molins C, Aguado A, Saludes S. Double punch test to control the energy dissipation in tension of FRC (Barcelona test). Mater. Struct. 2009; 42:415-425 https://doi.org/10.1617/s11527-008-9391-9

Molodtsov MV & Molodtsova VE. Electrical resistivity of steel fiber reinforced concrete. IOP Conf Ser: Mater Sci Eng. 2018; 451(1):012079 https://doi.org/10.1088/1757-899X/451/1/012079

Monfore GE. The electrical resistivity of concrete. J. PCA Res. Dev. Lab. 1968; 10:35-48

Montemor MF, Simões AMP, Salta MM. Effect of fly ash on concrete reinforcement corrosion studied by EIS. Cem. Concr. Compos. 2000; 22(3):175-185 https://doi.org/10.1016/S0958-9465(00)00003-2

Morris W, Moreno EI, Sagüés AA. Practical evaluation of resistivity of concrete in test cylinders using a Wenner array probe. Cem. Concr. Res. 1996; 26(12):1779-1787 https://doi.org/10.1016/S0008-8846(96)00175-5

Mouhasseb H. Bestimmung des Wassergehalts bei Beton mittels eines neuen dielektrischen Messverfahrens, Dissertation, Karlsruher Institute of Technology. 2007 https://doi.org/10.5445/IR/1000008175

Müller F. Leitfähigkeitsmessungen an feuchte- und salzbelasteten Bauwerkstoffen mittels Impedanzspektroskopie. Diplomarbeit, Bauhaus Universität Weimar. 2000

Müller T. Untersuchungen zum Biegetragverhalten von Stahlfaserbeton und betonstahlbewehrtem Stahlfaserbeton unter Berücksichtigung des Einflusses von Stahlfaserart und Betonzusammensetzung. Dissertation, Universität Leipzig. 2014 https://nbn-resolving.org/urn:nbn:de:bsz:15-qucosa-159513

Naik TR, Kumar R, Ramme BW, Kraus RN. Effect of high-carbon fly ash on the electrical resistivity of fly ash concrete containing carbon fibers. 2nd Int. Conf. Sustain. Constr. Mater. Technol. 2010; 3:1875-1885

Newlands MD, Jones MR, Kandasami S, Harrison TA. Sensitivity of electrode contact solutions and contact pressure in assessing electrical resistivity of concrete. Mater. Struct. 2008; 41:621-628 https://doi.org/10.1617/s11527-007-9257-6

Nezhentseva A, Sørensen EV, Andersen LV, Schuler F. Distribution and orientation of steel fibres in UHPFRC. Department of Civil Engineering, Aalborg University. DCE Technical Reports No. 151. 2013

Nordon Nordic Innovation Centre: NT Method - Wedge Splitting Test Method (WST): Fracture testing of fibre-reinforced concrete (Mode I). NT BUILD 511. Oslo. 2005

Orazem ME & Tribollet B. Electrochemical impedance spectroscopy. John Wiley & Sons. Hoboken, New Jersey. 2008 https://doi.org/10.1002/9780470381588

Ozyurt N, Mason TO, Shah SP. Non-destructive monitoring of fiber orientation using AC-IS: An industrial-scale application. Cem. Concr. Res. 2006; 36(9):1653-1660 https://doi.org/10.1016/j.cemconres.2006.05.026

Ozyurt N, Woo LY, Mason TO, Shah SP. Monitoring fiber dispersion in fiber-reinforced cementitious materials: Comparison of AC-impedance spectroscopy and image analysis. ACI Mater. J. 2006; 103(5):340-347 https://doi.org/10.14359/18156

Park TH, Her S, Jee H, Yoon S, Cho BY, Hwang S, Bae S. Evaluation of orientation and distribution of steel fibers in highperformance concrete column determined via micro-computed tomography. Construct. Build. Mater. 2021; 270:121473 https://doi.org/10.1016/j.conbuildmat.2020.121473

Pfyl T. Tragverhalten von Stahlfaserbeton. Dissertation, Technische Wissenschaften ETH Zürich, Nr. 15005. 2003. https://doi.org/10.3929/ethz-a-004502831

Pittino G, Geier G, Fritz L, Hadwiger M, Rosc J, Pabel T. Computertomografische Untersuchung von Stahlfaserspritzbeton mit mehrdimensionalen Transferfunktionen. Beton- und Stahlbetonbau. 2011; 106:364-370. https://doi.org/10.1002/best.201100009

Plizzari GA. Fiber reinforced concrete for repairing and strengthening RC structures: Some recent advancements. Proceedings of the MATEC Web of Conferences; EDP Sciences: Les Ulis, France. 2018; 199:01004 https://doi.org/10.1051/matecconf/201819901004

Polder RB & Ketelaars MBG. Electrical resistance of blast furnace slag cement and ordinary portland cement concretes. Blended Cements in Construction, Papers Presented at the International Conference, University of Sheffield, UK, 9-12 September 1991. Elsevier: Essex, England. 1991

Ponikiewski T & Katzer J. X-ray computed tomography of fibre reinforced self-compacting concrete as a tool of assessing its flexural behaviour. Mater. Struct. 2016; 49:2131-2140 https://doi.org/10.1617/s11527-015-0638-y

Presuel-Moreno F & Liu Y. Temperature effect on electrical resistivity measurements on mature saturated concrete. Corrosion, Salt Lake City, Utah. 2012

Rajeshwari BR, Sivakumar MVN, Praneeth PH. Visualization and quantification of aggregate and fiber in self-compacting concrete using computed tomography for wedge splitting test. Archives of civil and mechanical Engineering. 2020; 20:139 https://doi.org/10.1007/s43452-020-00140-z

Ramezanianpour AM, Esmaeili K, Ghahari SA, Ramezanianpour AA. Influence of initial steam curing and different types of mineral additives on mechanical and durability properties of self-compacting concrete. Constr. Build. Mater. 2014; 73:187-194 https://doi.org/10.1016/j.conbuildmat.2014.09.072

Rasch E & Hinrichsen FW. Über eine Beziehung zwischen elektrischer Leitfähigkeit und Temperatur. Zeitschrift für Elektrochemie. 1908; 14:41-48

Raupach M, Dauberschmidt C, Wolff L. Monitoring the moisture distribution in concrete structures. Concrete Repair, Rehabilitation and Retrofitting-Proceedings of the International Conference on Concrete Repair, Rehabilitation and Retrofitting; CRC Press: Boca Raton, FL, USA. 2006; 166-167

Raupach M, Dauberschmidt C, Wolff L, Harnisch J. Monitoring der Feuchteverteilung in Beton. Beton, Verlag Bau + Technik GmbH, Erkrath. 2007; 57(1+2):20-26

Raupach M, Gulikers J, Reichling K. Condition survey with embedded sensors regarding reinforcement corrosion. Mater. Corros. 2013; 64(2):141-146 https://doi.org/10.1002/maco.201206629

Reichling K & Raupach M. Measurement and visualisation of the actual concrete resistivity in consideration of conductive layers and reinforcement bars. Concrete Repair, Rehabilitation and Retrofitting III-Proceedings of the 3rd International Conference on Concrete Repair, Rehabilitation and Retrofitting; Taylor & Francis Group: Abingdon, UK. 2012; 707-714

Reichling K. Bestimmung und Bewertung des Elektrischen Widerstands von Beton mit geophysikalischen Verfahren. Dissertation, Rheinisch Westfälische Technische Hochschule Aachen. 2014 http://nbn-resolving.org/urn:nbn:de:hbz:82-opus-50963

Reichling K, Asgharzadeh A, Raupach M. Neuer Ansatz zur Bestimmung des elektrischen Betonwiderstands bei vorhandener Bewehrung. Bautechnik. 2014; 91(11):822-827 https://doi.org/10.1002/bate.201400067

Reichling K, Raupach M, Klitzsch N. Determination of the distribution of electrical resistivity in reinforced concrete structures using electrical resistivity tomography. Mater. Corros. 2015; 66(8):763-771 https://doi.org/10.1002/maco.201407763

Roqueta G, Jofre L, Romeu J, Blanch S. Microwave timedomain reflection imaging of steel fiber distribution on reinforced concrete. IEEE Trans. Instrum. Meas. 2011; 60(12):3913-3922 https://doi.org/10.1109/TIM.2011.2138330

Rosenbusch J. Einfluß der Faserorientierung auf die Beanspruchbarkeit von Bauteilen aus Stahlfaserbeton. Beton- und Stahlbetonbau. 2004; 99(5):372-377 https://doi.org/10.1002/best.200490044

Rossi B & Wolf S. Steel fibre reinforced concrete for the future of tunnel lining segments—A durable solution. Tunnels and Underground Cities: Engineering and Innovation Meet Archaeology, Architecture and Art, Proceedings of the WTC 2019 ITA-AITES World Tunnel Congress, Naples, Italy, 3-9 May 2019; CRC Press: Boca Raton, FL, USA. 2019; 2978-2985 https://doi.org/10.1201/9780429424441-315

Ruan T & Poursaee A. Fiber-distribution assessment in steel fiber-reinforced UHPC using conventional imaging, X-ray CT scan, and concrete electrical conductivity. J. Mater. Civ. Eng. 2019; 31(8):04019133 https://doi.org/10.1061/(ASCE)MT.1943-5533.0002733

Sauer DU. Impedanzspektroskopie. Eine Methode, viele Anwendungen - Definitionen, physikalische Bedeutungen, Darstellungen. Technische Mitteilungen, Haus der Technik, Essen. 2006; 99:7-11

Schepers R. Aktuelle Entwicklung bei der Anwendung von Stahl- und Kunststofflasern. BetonWerk International. 2008; 6:42-47

Schnell J, Ackermann FP, Rösch R, Sych T. Statistical analysis of fibre distribution in ultra high performance concrete using computer tomography. Kassel: Schriftenreihe Baustoffe und Massivbau. 2008; 10:145-152

Schnell J, Sych T, Schuler F. Analyse der Faserverteilung in Betonen mit Hilfe der Computer-Tomographie. Abschlussbericht des Forschungsprojektes DBV 273, Bauforschung, Technische Universität Kaiserslautern. 2009; 3218

Schnell J, Schladitz K, Schuler F. Richtungsanalyse von Fasern in Betonen auf Basis der Computer-Tomographie. Beton- und Stahlbetonbau, Ernst & Sohn, Berlin. 2010; 105(2):72-77 https://doi.org/10.1002/best.200900055

Schönlin K. Ein Verfahren zur Ermittlung der Orientierung und Menge der Fasern im faserbewehrten Beton. Diplomarbeit, Karlsruher Institute of Technology. 1983

Schönlin K. Ermittlung der Orientierung, Menge und Verteilung der Fasern in faserbewehrtem Beton. Beton- und Stahlbetonbau, Ernst & Sohn, Berlin. 1988; 83(6):168-171 https://doi.org/10.1002/best.198800280

Schuler F, Breit W, Schnell J, Schladitz K. Computertomografie - den Fasern auf der Spur. Bautechnik. 2017; 94(10):689-696 https://doi.org/10.1002/bate.201700050

Schulz M. Stahlfasern: Eigenschaften und Wirkungsweisen. Verlag Bau + Technik GmbH, Erkrath. 2000; 7:382-387

Schulz M. Stahlfasern: Anwendungsgebiete. Beton, Verlag Bau + Technik GmbH, Erkrath. 2000; 8:452-454

Sengul O. Use of electrical resistivity as an indicator for durability. Constr. Build. Mater. 2014; 73:434-441 https://doi.org/10.1016/j.conbuildmat.2014.09.077

Shan L & Zhang L. Experimental study on mechanical properties of steel and polypropylene fiber-reinforced concrete. Appl. Mech. Mater. 2014; 584-586:1355-1361 https://doi.org/10.4028/www.scientific.net/AMM.584-586.1355

Song PS & Hwang S. Mechanical properties of high-strength steel fiber-reinforced concrete. Constr. Build. Mater. 2014; 18(9):669-673 https://doi.org/10.1016/j.conbuildmat.2004.04.027

Spragg R, Jones S, Bu Y, Lu Y, Bentz D, Snyder K, Weiss J. Leaching of conductive species: Implications to measurements of electrical resistivity. Cem. Concr. Compos. 2017; 79:94-105 https://doi.org/10.1016/j.cemconcomp.2017.02.003

Stähli P, Custer R, van Mier JGM. On flow properties, fibre distribution, fibre orientation and flexural behaviour of FRC. Mater. Struct. 2008; 41:189-196 https://doi.org/10.1617/s11527-007-9229-x

Strack M. Modellbildung zum rissbreitenabhängigen Tragverhalten von Stahlfaserbeton unter Biegebeanspruchung. Dissertation. Ruhr-Universität Bochum. 2007 https://nbn-resolving.org/urn:nbn:de:hbz:294-19985

Suuronen J-P, Kallonen A, Eik M, Puttonen J, Serimaa R, Herrmann H. Analysis of short fibres orientation in steel fibre-reinforced concrete (SFRC) by X-ray tomography. J. Mater. Sci. 2013; 48(3):1358-1367 https://doi.org/10.1007/s10853-012-6882-4

Svec O, Zirgulis G, Bolander JE, Stang H. Influence of formwork surface on the orientation of steel fibres within self-compacting concrete and on the mechanical properties of cast structural elements. Cement and Concrete Composites. 2014; 50:60-72 https://doi.org/10.1016/j.cemconcomp.2013.12.002

Tarawneh A, Almasabha G, Alawadi R, Tarawneh M. Innovative and reliable model for shear strength of steel fibers reinforced concrete beams. Structures. 2021; 32:1015-1025 https://doi.org/10.1016/j.istruc.2021.03.081

Teutsch M & Empelmann M. Faserorientierung und Leistungsfähigkeit von Faserbeton. Schriftenreihe des Instituts für Baustoffe, Massivbau und Brandschutz der TU Braunschweig – Materialprüfanstalt für das Bauwesen Braunschweig. 2008

Thannberger SF. Zur Eignung der Impedanzspektroskopie für die Charakterisierung von polymeren Langmuir-Blodgett-Schichten. Dissertation, Technische Universität München. 2002

Thomée B. Physikalisch nichtlineare Berechnung von Stahlfaserbetonkonstruktionen. Dissertation, Technische Universität München. 2005

Topçu IB, Uygunoğlu T, Hocaoğlu I. Electrical conductivity of setting cement paste with different mineral admixtures. Constr. Build. Mater. 2012; 28(1):414-420 https://doi.org/10.1016/j.conbuildmat.2011.08.068

Torrents JM, Mason TO, Garboczi EJ. Impedance spectra of fiber-reinforced cement-based composites: A modeling approach. Cem. Concr. Res. 2000; 30(4):585-592 https://doi.org/10.1016/S0008-8846(00)00211-8

Torrents JM, Juan-García P, Patau O, Aguado A. Surveillance of steel fibre reinforced concrete slabs measured with an open-ended coaxial probe. 19th IMEKO World Congress, Fundamental and Applied Metrology. 2009.

Torrents JM, Blanco A, Pujadas P, Aguado A, Juan-García P, Sánchez-Moragues MA. Inductive method for assessing the amount and orientation of steel fibers in concrete. Mater. Struct. 2012; 45(10):1577-1592 https://doi.org/10.1617/s11527-012-9858-6

Tue NV, Henze S, Küchler M, Schenck G, Wille K. Ein optoanalytisches Verfahren zur Bestimmung der Faserverteilung und -orientierung in stahlfaserverstärktem UHFB. Beton- und Stahlbetonbau. 2008; 102(10):674-680 https://doi.org/10.1002/best.200700568

Tumidajski PJ. Relationship between resistivity, diffusivity and microstructural descriptors for mortars with silica fume. Cem. Concr. Res. 2005; 35(7):1262-1268 https://doi.org/10.1016/j.cemconres.2004.10.007

Uygunoglu T, Topçu IB, Simsek B. Influence of steel-fiber type and content on electrical resistivity of old-concrete. Comput. Concr. 2018; 21(1):1-9 https://doi.org/10.12989/cac.2018.21.1.001

Van Beek A & Stenfert Kroese W. 24 years of experience with the electrical conductivity to determine material properties of concrete. HERON 64. 2019; 64(1/2):3-19

Van Damme S, Franchois A, De Zutter D, Taerwe L. Nondestructive determination of the steel fiber content in concrete slabs with an open-ended coaxial probe. IEEE Trans Geosci Rem Sens. 2004; 42(11):2511-2521 https://doi.org/10.1109/TGRS.2004.837332

Van Damme S, Franchois A, Pauw DP, Taerwe L. Comparison of two coaxial probes for measuring the steel fiber content in fiber reinforced concrete slabs. 9th International Conference on Electromagnetics in Advanced Applications ICEAA '05; 11th European Electromagnetic Structures Conference EESC '05; September 12-16. Torino, Italy. 2005

Van Mier JGM, Nooru-Mohamed MB, Timmers G. An experimental study of shear fracture and aggregate interlock in cementbased composites. Heron. 1991; 36(4) http://resolver.tudelft.nl/uuid:0664e71e-bb1d-4a0c-a145-73be31e63247

Walsh KK, Hicks, NJ, Steinberg EP, Hussein HH, Semendary AA. Fiber orientation in ultra-high-performance concrete shear keys of adjacent-box-beam bridges. ACI Mater. J. 2018; 115(2):227-238 https://doi.org/10.14359/51701097

Weigler H & Karl S. Beton. Arten - Herstellung - Eigenschaften. Ernst & Sohn, Berlin. 1989

Whiting DA & Nagi MA. Electrical resistivity of concrete— A literature review. PCA R&D, Portland Cement Association. Skokie, Illinois. 2003; 2457:57

Wichmann HJ, Budelmann H, Holst A. Non-destructive measurement of steel fiber dosage and orientation in concrete. Nondestructive Testing of Materials and Structures. RILEM Bookseries, Springer, Dordrecht. 2011; 6:239-245 https://doi.org/10.1007/978-94-007-0723-8_35

Wichmann HJ, Holst A, Budelmann H. Zerstörungsfreie Messung des Stahlfasergehalts und der Stahlfaserorientierung im Beton. 2012

Wichmann HJ, Holst A, Budelmann H. Ein praxisgerechtes Messverfahren zur Bestimmung der Fasermenge und -orientierung im Stahlfaserbeton. Beton- und Stahlbetonbau. 2013; 108(12):822-834 https://doi.org/10.1002/best.201300060

Wille K, Tue NV, Parra-Montesinos GJ. Fiber distribution and orientation in UHP-FRC beams and their effect on backward analysis. Mater. Struct. 2014; 47(11):1825-1838 https://doi.org/10.1617/s11527-013-0153-y

Winsauer WO, Shearin HM, Masso PH, Williams M. Resistivity of brine-saturated sands in relation to pore geometry. Bulletin of the American association of petroleum geologists. 1952; 36:253-277

Wedding P, Woelfl G, Lauer K. The electrical resistivity of concrete with emphasis on the use of electrical resistance for measuring moisture content. Cement, Concrete and Aggregates. 1979; 1:64-67

Woo LY, Wansom S, Ozyurt N, Mu B, Shah SP, Mason TO. Characterizing fiber dispersion in cement composites using AC-impedance spectroscopy. Cem. Concr. Compos. 2005; 27(6):627-636 https://doi.org/10.1016/j.cemconcomp.2004.06.003

Woo LY, Kidner NJ, Wansom S, Mason TO. Combined time domain reflectometry and AC-impedance spectroscopy of fiber-reinforced fresh-cement composites. Cem. Concr. Res. 2007; 37(1):89-95 https://doi.org/10.1016/j.cemconres.2006.09.004

Zak G, Park CB, Benhabib B. Estimation of three-dimensional fibre-orientation distribution in short-fibre composites by a two-section method. J. Compos. Mater. 2001; 35(4):316-339 https://doi.org/10.1177/002199801772662190

Zapico LA. Experimental investigation on electrical resistivity of SFRC. Master Thesis, Chalmers University of Technology, Göteborg. 2015 https://hdl.handle.net/20.500.12380/228078

Zhang P, Li Q, Chen Y, Shi Y, Ling Y. Durability of steel fiber-reinforced concrete containing SiO_2 nano-particles. Materials. 2019; 12(13):2184 https://doi.org/10.3390/ma12132184

Zhou B & Uchida Y. Influence of flowability, casting time and formwork geometry on fiber orientation and mechanical properties of UHPFRC. Cem. Concr. Res. 2017; 95:164-77 https://doi.org/10.1016/j.cemconres.2017.02.017

Zimmermann E. Phasengenaue Impedanzspektroskopie und -tomographie für geophysikalische Anwendungen. Dissertation, Rheinische Friedrich-Wilhelms-Universität Bonn. 2011 https://nbn-resolving.org/urn:nbn:de:hbz:5N-24691

X. Annex A – Influence of Fibre Orientation on Single Fibre Pull-Out Strength

i. Test Program

To evaluate the influence of a single fibre's orientation onto the bond strength and thus the mechanical behaviour of SFRC, a series of six sets of single fibre pull-out tests with 30 specimens each was carried out. Thereby the embedding angle of the single fibres was varied between 0 ° and 75 ° in steps of 15 ° and the maximum transmissible force as well as parameters of friction were determined. The test matrix is presented in Table A.1. The number of valid test results, marked with *, only contains results, where the test could have been performed without test setups regarding failures like a breakage of the resin embedment of the free fibre end inside the clamping or a pull-out of the fibre end on the resin side. Such problems especially occurred for series S5 and S6, where a high embedding angle was used.

Table A.1 Test matrix of single fibre pull-out testing

Series	Embedding angle	Valid test results*
S1	0 °	29
S2	15 °	25
S3	30 °	29
S4	45 °	28
S5	60 °	11
S6	75 °	16

The tests were performed by use special specimens where a fibre is embedded half its length into a block of epoxy resin with a bent fibre end to ensure a good bond and other half into a mortar block with varying embedding angle inside the concrete (see Figure A.1). The embedding angle inside the specimen and not directly at the bottom surface was chosen in order to inhibit mechanical spalling of the upper surface. The bending process of the fibres was performed in one single step, so the risk of a mechanical damage of the inflection point was minimized.

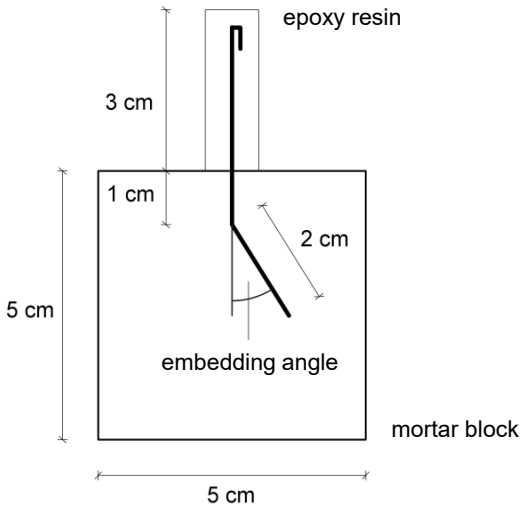

Figure A.1 Specimen dimension for single fibre pull-out testing

The mortar mixture was chosen to show a good bonding behaviour and a sufficient strength in combination with the steel fibres, so a breakage of the mortar could be inhibited. Therefore, the mortar mixture from Table A.2 was used. The mortar was mixed in a Hobart mixer in accordance with DIN EN 196-1, 2016 and the specimens were stored for 7 days under water and afterwards at a temperature of 20 °C and a relative humidity of 65 % until testing in the age of 14 days.

Table A.2 Mortar composition for single fibre pull-out testing

Parameter	Unit	Content
CEM I 42.5 R		470.0
Water	kg/m³	211.5
Aggregates		1624.3
Water/cement ratio		0.45
Grain size distribution	-	C4
Steel fibre type		Macrofibre 60 mm

The pull-out test was performed with a spindle testing machine by displacement control. The testing speed was 5 mm/min, where the mortar block was pulled up in vertical way. The end of testing was determined as fully pull-out of the fibre, which means nearly 30 mm of pull-out distance.

ii. Results

The results of the experiments show clearly that a higher embedding angle leads to an increase in the transmittable tensile strength between concrete and steel fibres (see Figure A.2).

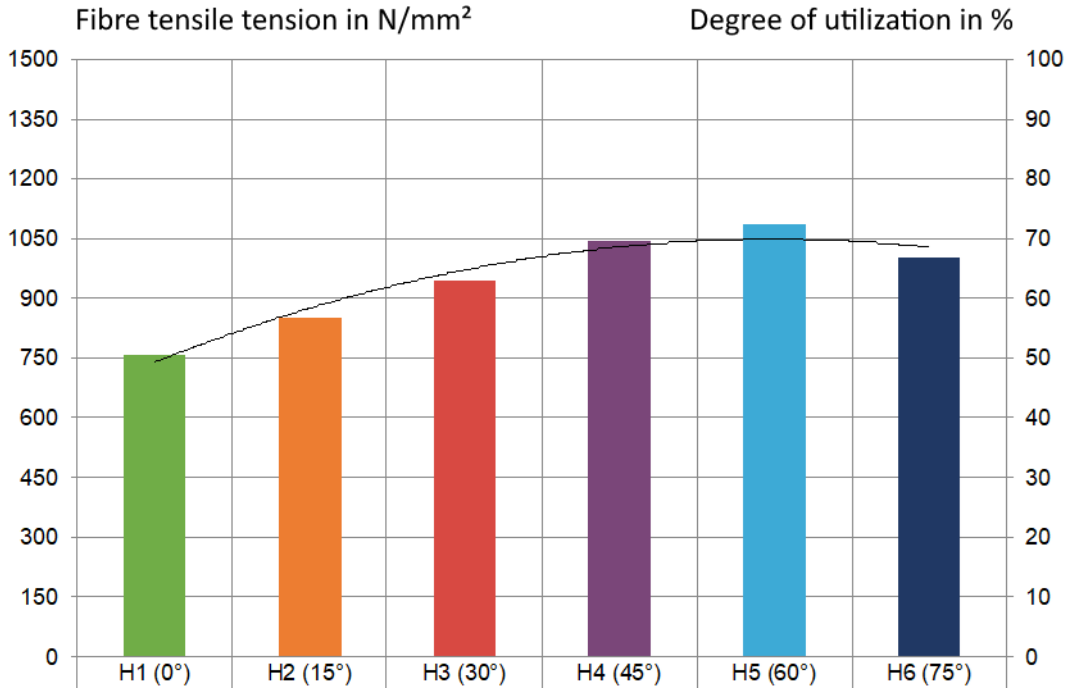

Figure A.2 Maximum transmissible tensile force in dependence of the different embedding angles of the fibres

Analogue to the transmittable strength also the degree of utilization of the fibres gets improved with higher angles. But as can be seen the maximum is reached with an embedding angle of around 60°. As a reason for this behaviour, it can be supposed that the bending of the fibre in case of a tensile load leads to a local failure in the fibre itself and yielding occurs.

XI. Annex B – Influence of Fibre Content on 3-Point Bending Strength

i. Test Program

To identify the effect of different fibre contents on the mechanical behaviour of SFRC a standard test method was used with one concrete composition and fibre contents of 40 kg/m³ and 80 kg/m³. Like for the single fibre pull-out testing, the same macrofibre was used even for this test series. Of both fibre contents four series of each six fibre reinforced concrete beams in accordance with DIN EN 14651, 2007, were produced and tested.

The concrete, used for the tests, was designed based on the mortar for the single fibre pull-out tests and only contained a larger gravel with a maximum grain size of 16 mm. The concrete composition is presented in Table B.1. After the production of the concrete, the specimens were stored for 21 days at a temperature of 20 °C and a relative humidity of > 95 %, until the notch was sawn into a side surface. Afterwards the storage was continued till the day of testing in the age of 28 days. The test was performed with a spindle testing machine under deformation control in accordance with DIN EN 14651, 2007.

Table B.1 Concrete composition for 3-point bending tests

Parameter	Unit	Content
CEM I 42.5 R		470.0
Water	kg/m³	211.5
Aggregates		1624.3
Water/cement ratio		0.45
Grain size distribution	-	C16
Steel fibre type		Macrofibre 60 mm
Steel fibre content	kg/m³	40 and 80

ii. Results

The results of the experiments show a clear correlation between the fibre content and the residual tensile strength, which was determined in the 3-point bending test. As can be seen in Figure B.1, a fibre content of 40 kg/m³ leads to a drop in the strength to CMOD curves after the first crack in concrete occurs, what means a crack mouth opening displacement of 0 mm. The tensile strength decreases by 1.0 to 1.5 N/mm² and for some series of specimens (S1 and S2) the SFRC is able to take higher loads, when a larger CMOD is reached, while for the other two series (S3 and S4) a nearly constant plateau can be observed. In contrast to this, SFRC with a fibre content of 80 kg/m³ after the first crack can increase the transmissible load for all four series of specimens. This means that after an initial crack for a constant load no further displacement respectively CMOD will occur. A simple comparison between both fibre contents can be performed by consideration of the tensile strength for a CMOD of 0.5 mm, that for the lower fibre content range between 3.0 and 4.7 N/mm² and for the higher fibre content between 5.8 and 6.8 N/mm², which means more than 60 % higher values for a doubled fibre content. For larger crack openings the difference clearly decreases to about 30 %.

These series of experiments clearly show the influence of the fibre content on the mechanical properties of SFRC. There is no direct linear correlation between the two parameters,

especially because of other influences in the material system of SFRC like the fibre distribution and fibre orientation, which were not analysed for these investigations. It can be assumed that the influence of the fibre orientation is a crucial factor for lower fibre contents, what can be the reason for the variations, when comparing series S1 and S2 to S3 and S4 for a fibre content of 40 kg/m³. In contrast to this behaviour no analogue phenomenon can be detected for the higher fibre content, what leads to the conclusion that here the fibre content is the decisive parameter, and the orientation is only a subordinated influence.

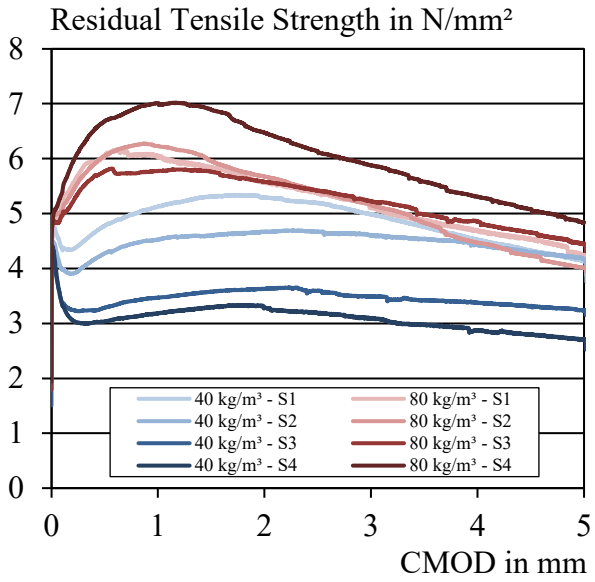

Figure B.1 Strength-CMOD-curves as results of the 3-point bending tests of fibre reinforced concrete beams with fibre contents of 40 kg/m³ and 80 kg/m³ (Cleven et al., 2018)

XII. Annex C – Influence of Fibre Content and Orientation on Mechanical Properties

i. Test Program

Since the behaviour of a single fibre, embedded in concrete under different angles, does not fully represent the composite material behaviour of fibre reinforced concrete, additional tests in a larger scale were performed. Because a smaller embedding angle, that is similar to a fibre oriented in direction of the tensile force, leads to a higher probability of the fibre to cross the opening crack, and thus take part on load bearing, the global fibre orientation of a specimen is even of much interest.

For this reason, tests on cubic specimens with two different fibre contents, 40 kg/m³ and 80 kg/m³, were performed, using the wedge splitting test. The huge advantage of cubic specimens, compared to the beams, described in section XI, is the symmetry and thus the possibility of rotation of the specimens to investigate different testing directions. Therefore, the wedge splitting test, which was presented for SFRC in Löfgren, 2004, in accordance with Nordon, 2005 was performed with specimen dimensions of 150 mm.

For these tests the same concrete and fibres as for the 3-point bending tests (see section XI) was used. After casting of the six batches of concrete with 18 specimens each, the specimens were stored at a temperature of 20 °C and a relative humidity of > 95 % for 21 days. Afterwards a notch of 22 x 30 mm² was sawn into the upper surface as well as a starting notch and two guidance notches into the side surfaces, like presented in Figure C**.1**. The notch was used as admission zone for steel frames with roller bearings and the notches should define the tested specimen section of 100 x 75 mm². The specimens were stored after sawing back in the controlled climate conditions.

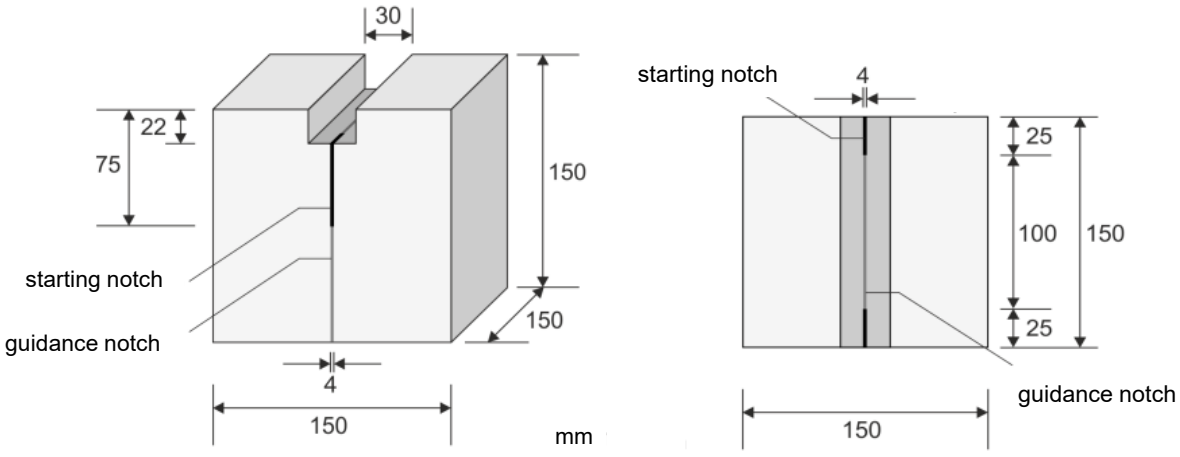

Figure C.1 Prepared specimen for wedge splitting test

To investigate different orientations of the steel fibres inside the specimen and ensure comparable casting conditions, the casting itself was not varied but the specimens, before the preparation, were turned in different directions, like can be seen in Figure C.2. The blue surface represents the upper side of the casting. Based on the literature review it was assumed that fibres generally tend to sink inside the concrete and so a slightly higher fibre content in the bottom zone can be formed. This assumption was checked by rotating the specimens 180 °, so the casting surface afterwards was the bottom of the prepared specimen. The second phenomenon of fibre orientation is an orientation perpendicular to the compaction process and

thus in this case a more horizontal fibre orientation. This was investigated by rotating the specimens 90 °. To ensure that the concrete batch itself has no influence on the results, six specimens of each batch were tested in each direction. The first three mixtures thus contained six specimens, that were tested in casting direction, six specimens tested after turning of 90 ° and six specimens turned by 180 °, each with a fibre content of 40 kg/m³. Mixtures 4 to 6 showed the same set of specimens but with a fibre content of 80 kg/m³.

Figure C.2 Orientation of the wedge splitting test, in casting direction, turned 90 ° and turned 180 °

The test itself was performed at a concrete age of 28 days with a spindle testing machine. A wedge was pushed from the upside between the two roller bearings (see Figure C.3) to create a horizontal splitting force, while the specimen was placed on a rod bearing, to achieve a linear cushion. The test speed was controlled to 0.05 mm until a crack mouth opening displacement (CMOD) of 1 mm was reached. Then it was set to 0.125 mm/min till a CMOD of 2 mm and afterwards to 0.5 mm until a CMOD of 8 mm.

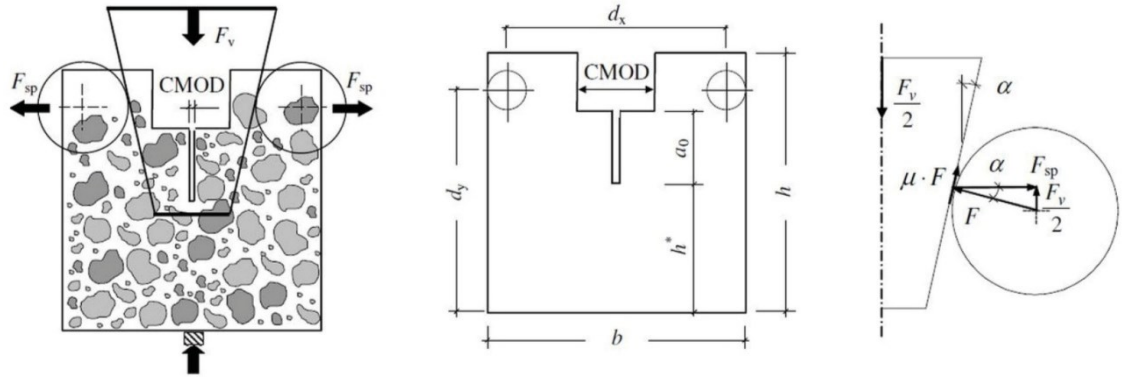

Figure C.3 Schematic load distribution in wedge splitting test (Nordon, 2005)

In accordance with Löfgren, 2005, the horizontal splitting force can be calculated by (eq. XII-*1*).

$$F_{sp} = \frac{F_V}{2 \times tan\,(\alpha)} * \frac{1 - \mu * tan(\alpha)}{1 + \mu * cot(\alpha)} \approx 1{,}866 * F_V \qquad \text{(eq. XII-1)}$$

with:

F_V: vertical force in kN

α: angle of the wedge (α = 15°)

μ: Coefficient of friction of the roller bearings

ii. Results

These investigations were performed to analyse the effect of the fibre distribution and orientation on the mechanical properties of SFRC. Thus, a comparison between specimens of the same fibre content was done, while the specimens itself were oriented differently. The first three series of specimens contained a fibre content of 40 kg/m³ and six specimens each of every testing direction. The tensile splitting force, which can be measured in the wedge splitting test enables a good comparison about the mechanical properties of the SFRC in total. As can be seen in Figure C.4, the specimens, that were tested after 90 ° rotation (violet curves) are the lowest ones for each series and don't show any effect of critical or over critical behaviour. In contrast to this, nearly all other series and orientations at least show a critical behaviour where the load after the first crack can constantly be taken by the fibres until a deflection of 5 mm is reached. Comparing both horizontal orientations, no significant difference is visible for the specimens which are tested with the production surface upwards, and the ones rotated by 180 °. So, it can be concluded that a sinking process of the fibres is not of great influence if the concrete composition and compaction method are suitable for SFRC, but the compaction itself leads to a 2-dimensional orientation of the fibres inside the specimen and thus a much lower load bearing capacity in a 90 ° rotated orientation in reference to the compaction. The specimens of series 3, however, show a slightly lower load bearing capacity which possibly is based on variations in the production process of the concrete.

The specimens which were turned by 90 ° only show a mean tensile splitting load of about 0.8 kN, while the other specimens, which are tested in the horizontal direction of production can withstand a tensile splitting load of about 2.5 kN.

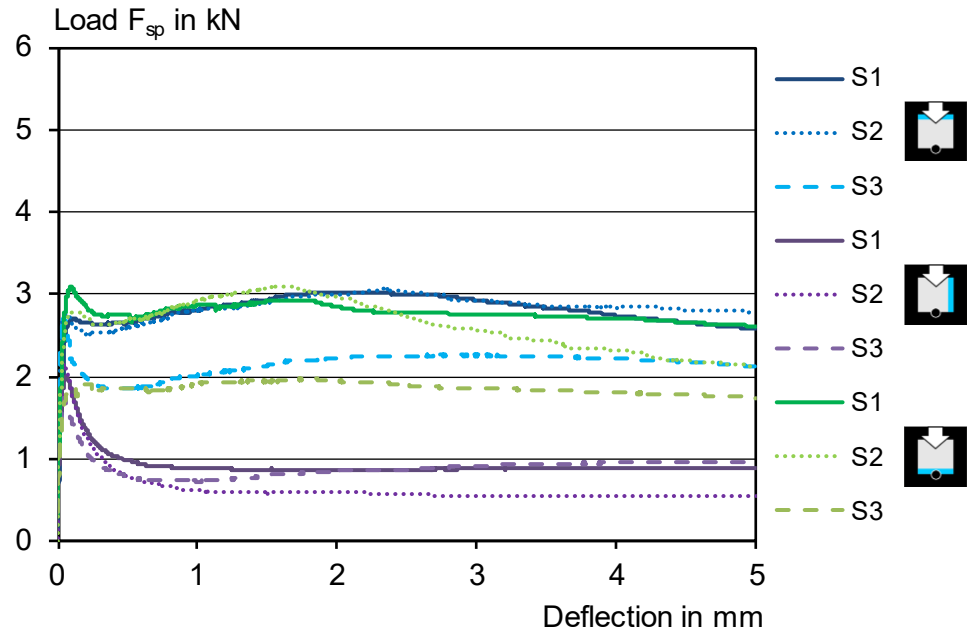

Figure C.4 Load-displacement-curves as result of wedge splitting test on steel fibre reinforced concrete cubes with a fibre content of 40 kg/m³ in dependence of the testing direction

A similar but more significant distinction between the horizontal orientation and the 90 ° rotation of the specimens can be observed with a higher fibre content of 80 kg/m³ (Figure C.5). Like already seen for the lower fibre content a 90 ° rotation leads to an under critical behaviour after

the first crack occurs. Against this, the horizontally tested specimens always show an over critical behaviour, which for those specimens is possible because of the high fibre content of 80 kg/m³. While the specimens of series 3 for the 180 ° rotated specimens show a significantly high load bearing capacity at low deflections under 1.5 mm, the specimens which were tested in direction of production of the same series show the highest results for large deflections. In total, there is no significant distinction between both orientations visible for the tests with a fibre content of 80 kg/m³, analogue to the lower fibre content.

Comparing the tensile splitting loads of the specimens with a fibre content of 80 kg/m³ with the ones with half the fibre content, it is clearly visible that doubling the fibre content leads to a significant increase in mechanical properties. The specimens tested after a 90 ° rotation show average tensile splitting loads of 1.3 kN, what is more than 60 % higher than the ones with a lower fibre content. For the horizontal specimens, in the phase of small deflections the average tensile splitting load is again about 60 % higher with a value of 4.0 kN. Nevertheless, for a higher deflection, the fibres are more and more pulled out of the specimen and thus, the average tensile splitting load decreases to about 3.0 kN to 3.5 kN and thus is only 20 % to 40 % higher than for specimens with half the fibre content. Summarized it is to say that an increase of the fibre content as expected leads to an increase in mechanical properties, but there is no linear correlation between both parameters.

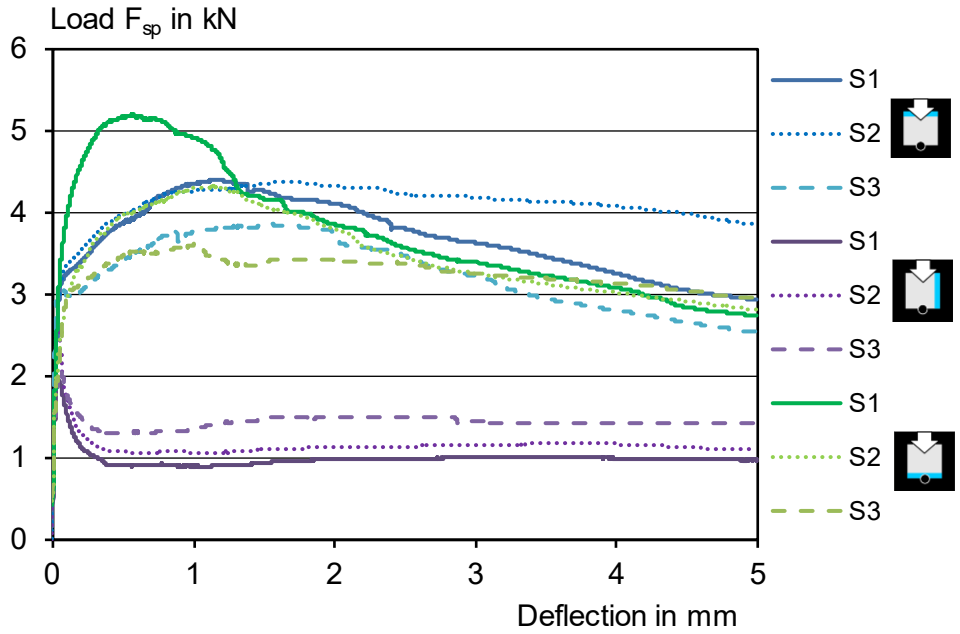

Figure C.5 Load-displacement-curves as result of wedge splitting test on steel fibre reinforced concrete cubes with a fibre content of 80 kg/m³ in dependence of the testing direction

XIII. Annex D – Further Analysis by Use of Computed Tomography

i. Materials

To analyse the influence of the fibre content and fibre dimensions on the orientation of fibres inside SFRC, a basic concrete mixture was produced and two different fibres as well as fibre contents from 10 kg/m³ to 80 kg/m³ were added to this PC. In this way, three series of nine specimens each were produced and tested. The basic concrete mixture is the same than used for most of the scientific papers and can be seen in Table 3.3 (see section 3.3.1.2).

The manufacturing of the concrete always was performed the same way. At the beginning, the solids, such as cement and aggregates, were homogenized for 30 s in a compulsory mixer with a nominal volume of 60 L. Afterwards the water was added, while the mixing process was ongoing. After a mixing phase of two minutes, the mixer was stopped and adhering components were removed from the mixing walls, followed by an additional mixing phase of one minute.

The fibres then, were added to smaller concrete volumes in an additional bucket mixer. Therefore 1.5 L of PC were given into the bucket and the corresponding fibre content was added and mixed for at least one minute. In this way, for each concrete one PC and seven SFRCs with fibre contents from 10 kg/m³ to 70 kg/m³ were produced and one cubic specimen with an edge length of 100 mm was casted. Two series of specimens with macrofibres (S1 and S2) and one series with microfibres (S3) were produced. One series (S2) of macro SFRC was filled into the formworks in one layer and was compacted via an internal vibrator for about five seconds. The other two series of concrete were again filled into the formworks in one layer but were compacted on a vibrating table for five seconds. Detailed information of the fibres is given in section 3.3.1.1 (fibre 1 and fibre 3). The specimens were stored in the formworks for 24 hours. Then, they were demoulded, and the surface was ground down to ensure a good connectivity for the electrical resistivity measurements. After grinding, the specimens were stored in separate storage boxes each, that were filled with on 20 °C tempered water. A water volume of 3.4 L was added to each storage box, so a volume to surface ratio of 5667 L/m² was reached.

ii. Methods

To evaluate the results of the test setup, used in the scientific papers, two additional test methods have been used for some additional specimens. The electrical resistivity measurement was performed in the identical way than presented in the scientific papers for cubic specimens by use of two stainless steel plates and the LCR meter with specimens in the age of 7 days (see e.g., section 3.3.3) with only the difference of smaller specimen dimensions.

In addition to the electrical resistivity measurements two specimens of each concrete series were analysed using CT-scanning afterwards. Those specimens were the ones with fibre contents of 40 kg/m³ and 70 kg/m³ for both series of SFRC, compacted on a vibrating table, where one series contains a macrofibre (S1) and the other one a microfibre (S3). For the series with macrofibres and compaction via internal vibrator (S2), only lower fibre contents with 10 kg/m³ and 30 kg/m³ were analysed because it was expected that this way defects based on the compaction are better visible.

The CT-scans were executed on a tomograph ProCon X-Ray GmbH, model CT-Alpha at the ITA (RWTH Aachen University). The distance between the x-ray source and the middle axis

of the specimens was set to 185 mm and the distance between x-ray source and detector was 200 mm. The electrical voltage was set to 100 kV and the current to 100 mA with an exposure time of 250 ms. In a testing time of 2 hours one specimen was fully rotated in 1600 steps and 15 sectional images per step were generated and combined, to minimize artefacts of distortion because of the missing rotational symmetry of the specimens.

With the software VG Studio MAX 2.2 a 3D-model of each specimen could be generated, and the model could be binarized to fade out the concrete matrix and only leave the fibres inside the model. The macrofibre thereby showed a grey scale of 10500 to 12000 while the microfibres were in a range of 19000 to 20000. Based on this model, it was possible to create sectional images in every direction, which can be compared to results of other test methods. A more detailed analysis of the model unfortunately was not possible due to the lack of an analysation software, so only visual comparisons between the results of the CT-scanning and the electrical resistivity measurements could be done.

After CT-scanning was performed the six specimens were sawn into eight pieces of about 50 x 50 x 50 mm³ to visually analyse the three perpendicular surfaces of the specimens via optoanalytical analysis, which clearly is the more inaccurate measurement method, but also requires less equipment and is much cheaper. All the cross-sectional surfaces to be analysed (see Figure D.1), thus could be investigated as combination of four single specimens. For the macro SFRC, those surfaces in a first step were observed visually and the number of fibres was counted, which for the micro SFRC samples was not possible due to the high amount of fibres. For the micro SFRC samples as well as for one specimen with a fibre content of 70 kg/m³ of the macro SFRC, 3 singular perpendicular surfaces of the small pieces, which were representative for the whole surface, were chosen, saturated with black epoxy resin and ground to generate a smooth surface that could be analysed via incident light microscope. Here, also the number of fibres, the orientation angle of each fibre in relation to the corners of the specimen and the longest and shortest dimension of each fibre, which could be used to calculate the orientation angle in relation to the investigated surface, were analysed.

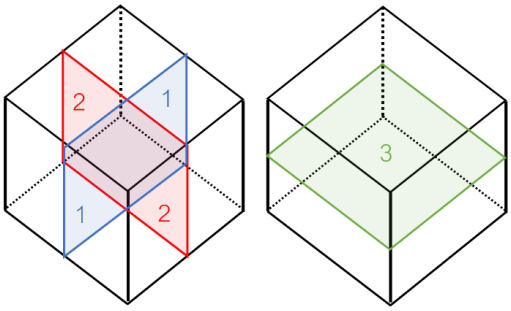

Figure D.1 Surfaces to be analysed via microscopy

The fibre content was determined in accordance with Hilsdorf via the recorded individual areas of the fibres by relating the total area of all fibres inside the section under consideration to the total cross-sectional area of the section (Tue et al., 2008). The expected fibre content of the total sample results from (eq. XIII-2).

$$\phi_F = 25 \cdot \frac{N_F \cdot \pi \cdot d_f^2}{A_p \cdot \eta_F} \qquad \text{(eq. XIII-2)}$$

with:

$\phi_{i,e}$ Fibre content depending on specimen direction in kg/m³
$\eta_{i,e}$ Fibre orientation depending on specimen direction
$N_{f,i,e}$ Number of fibres inside the section under consideration in mm²
d_f Fibre diameter in mm
$A_{p,i,e}$ Cross-sectional area under consideration in mm²

The fibre orientation, which is needed for the calculation is simplified as the number of fibres inside a specific directional section in relation to the summed-up number of fibres inside the sections in all three directions (see (eq. XIII-*3*)).

$$\eta_{i,e} = \frac{N_{f,i,e}}{N_{f,i,1} + N_{f,i,2} + N_{f,i,3}} \qquad \text{(eq. XIII-3)}$$

with:

$N_{f,i,e}$ Number of fibres inside the section under consideration

iii. Results

a. Results of the Electrical Resistivity Measurements

In contrast to the results of the scientific papers, especially section 6.4.1, the prediction of the fibre content based on the cubic specimens by use of the same model than in the paper mentioned above is more inaccurate. The fibre content for macro SFRC, compacted via vibrating table, (S1) is generally underestimated by 10 to 20 % when using specimens with only 100 mm edge length (Figure D.2). A correction using the adjusted aspect ratio (see section 6.4.2.3) also is not of success because that model is based on fibres which are cut by the extraction process of the specimens and thus a real adjustment of the aspect ratio of the fibres. Here, only the dimensions of the specimens in relation to the fibre size are very low, but the aspect ratio of the fibres itself are not influenced.

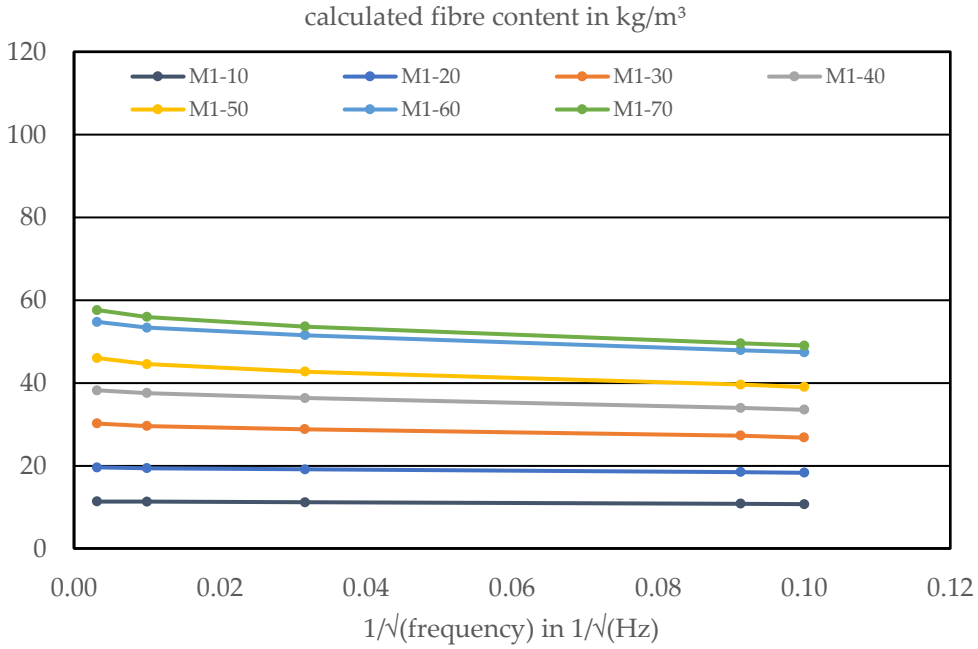

Figure D.2 Electrical resistivity results – S1 (macrofibre – vibrating table)

Even more inaccuracy occurs for the specimens that were compacted by use of an internal vibrator (S2) (Figure D.3). Here, additionally to the small dimensions of the specimens, which

seem too low for a fibre length of 60 mm, the anisotropy of the fibres is expected to badly influence the measurements in only three directions. This can be explained through the measuring principle of the three dimensions of the specimens, which are highly influenced by fibres, which are oriented directly in measuring direction but nearly independent of fibre oriented perpendicular. The vibrating table uses a one-dimensional force for the compaction and thus a two-dimensional orientation results, which can be detected particularly good by the analysis of three measurement directions. In contrast to this, the internal vibrator leads to a very random orientation, which requires a higher number of measuring directions.

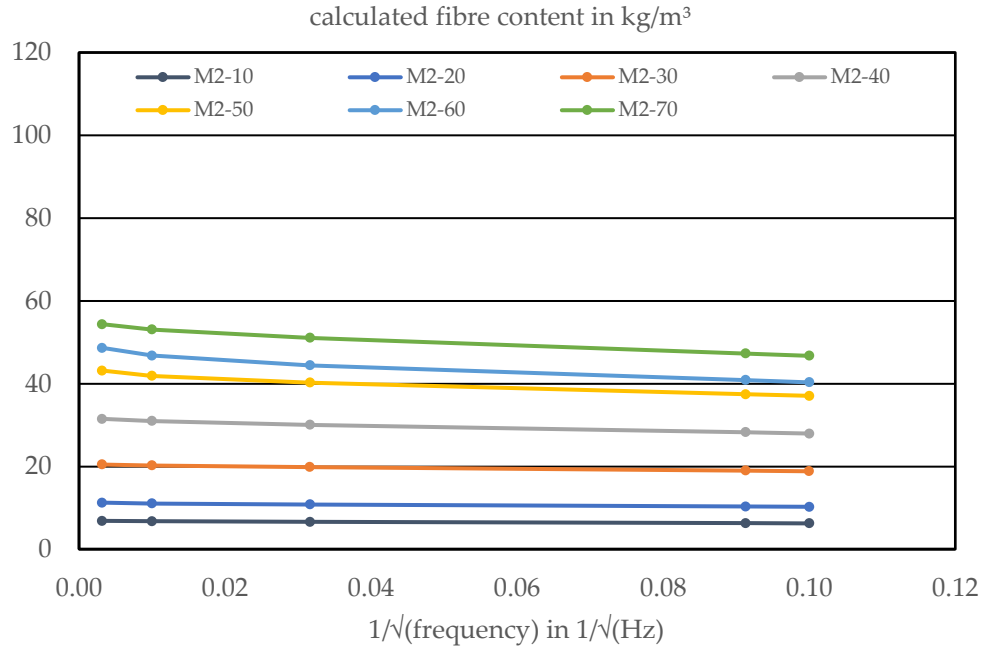

Figure D.3 Electrical resistivity results – S2 (macrofibre – internal vibrator)

For the micro fibres (S3), the size of the specimens seems to fit a good way, while the approximation by use of a logarithmic function doesn't lead to sufficient results. Because of the high number of fibres there is a huge influence of the frequency on the electrical resistivity and thus, a high frequency results in a very low electrical resistivity, more accurate a low active resistance of real part of impedance, of the SFRC and thus to a calculation of very high fibre content (Figure D.4). A more accurate prediction of the fibre content is possible for lower frequencies like 100 Hz, where the calculated results perfectly fit to the produced concrete compositions. Here the easily to measure active resistance nearly corresponds to the impedance.

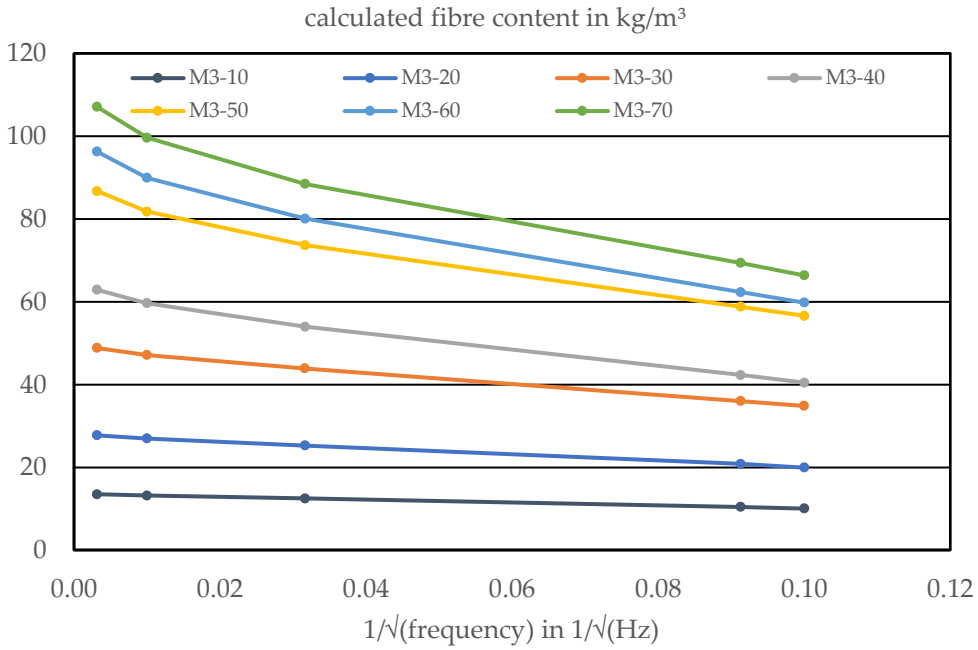

Figure D.4 Electrical resistivity results – S3 (Microfibre)

b. Results of CT-Scanning

After the performance of the electrical resistivity measurements some specimens were analysed additionally by use of CT-scanning. To evaluate differences of the results, one specimen of series S1 with a fibre content of 40 kg/m³ and another one with 70 kg/m³ were analysed. At first sight it is visible that most of the fibres are oriented around the corners and surfaces of the formwork, like stated in the literature review (Figure D.5). Only for the fibres in the middle space an orientation in the horizontal direction can be seen, which can be explained by the compaction method. Because of the lack of an analysing software, the fibre content cannot be determined. Counting of the fibres for such a high number of visible elements seems not a good way, especially because of the blurring artefacts of the corners. With a number of 2600 fibres/kg and a fibre content of 40 kg/m³, there should be 104 inside. For a later discussed specimen, the visual counting of the fibres was done.

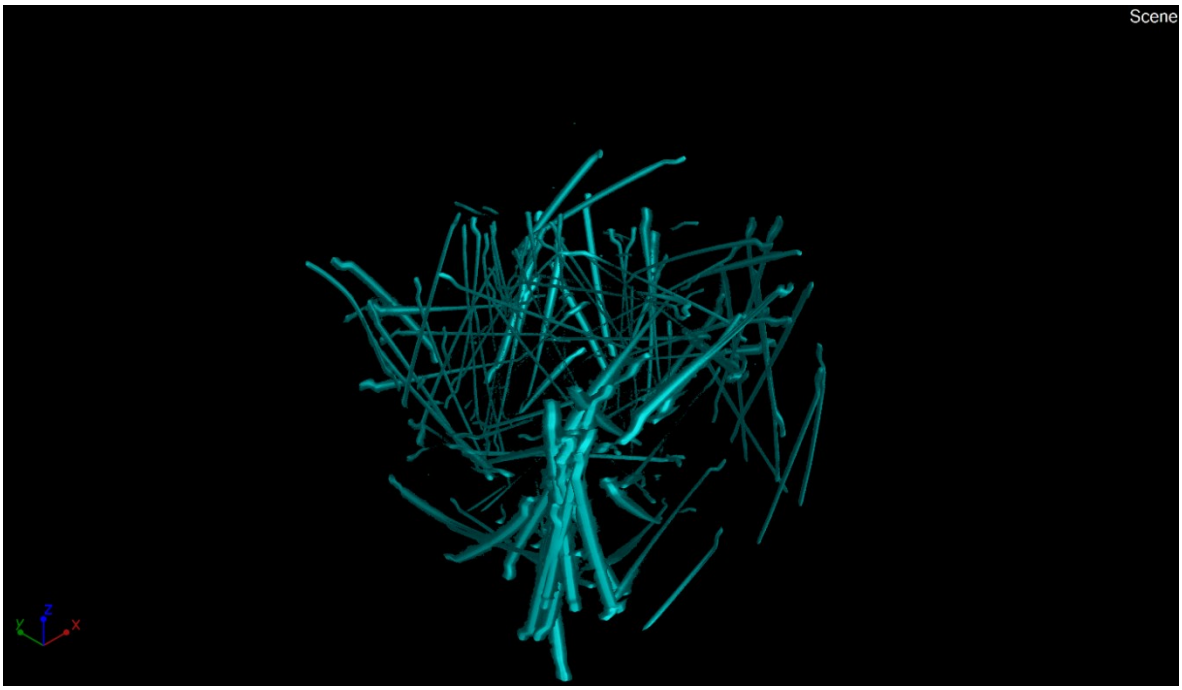

Figure D.5 CT image of specimen S1 – 40 kg/m³

Compared to the specimens discussed above, the one with a fibre content of 70 kg/m³ definitely has a higher number of fibres inside (Figure D.6). Again, a high amount of fibres is located on the surfaces of the formwork, but also fibres in the free space in the centre of the specimen are visible. Analogue to the other specimen, also here the free fibres seem to be oriented in horizontal direction, based on the compaction method.

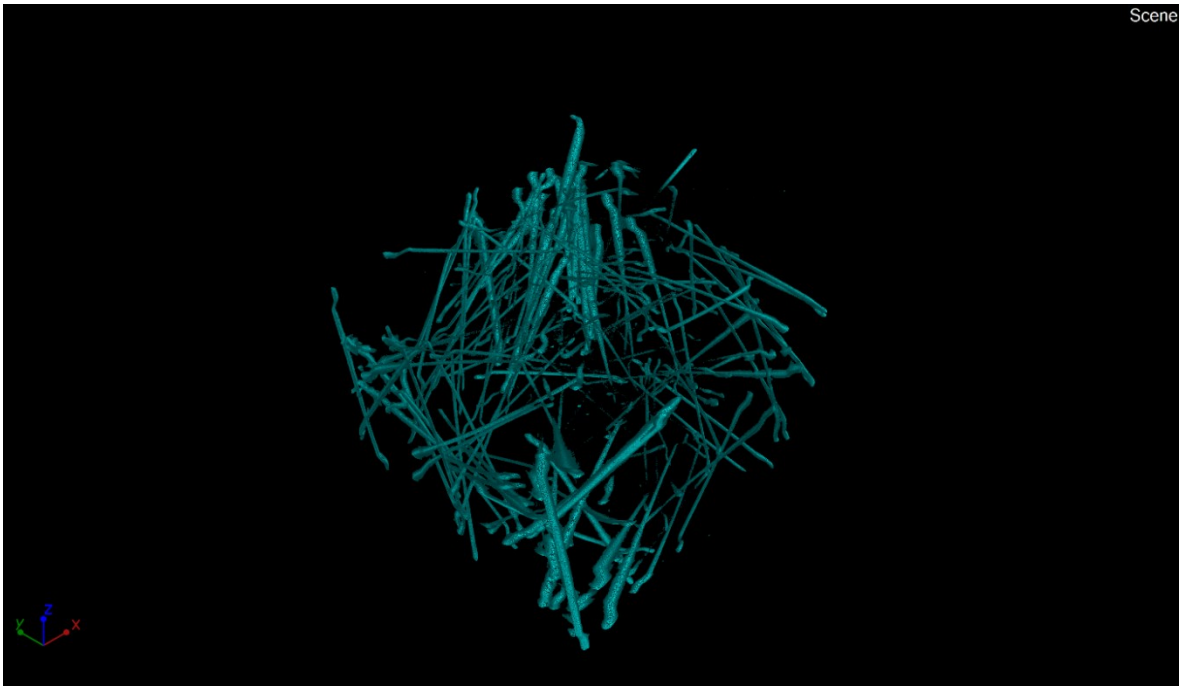

Figure D.6 CT image of specimen S1 – 70 kg/m³

The first specimen of series S2 with macrofibres and compaction via internal vibrator, contained a fibre content of only 10 kg/m³. For this specimen, a nearly free distribution of fibres can be observed via CT-scanning (Figure D.7). Also, no preferred orientation, like the

horizontal one for compaction via vibration table, is visible, but the fibres seem to be various oriented and not directly influenced by the surfaces of the formwork. The only interesting point in the distribution is a small vertical channel right in the middle of the specimen, where no fibres are located. This could be the passage, where the internal vibrator was placed and slowly pulled out of the specimen, while only concrete flew into the free volume and so there is a lack of fibres.

Because of the small fibre content, for this specimen, the manual counting of fibres in the CT-image was possible. As one can see, 26 fibres are visible inside the specimen, what for a fibre quantity of 2600 pieces/kg results in a fibre content of 0.1 g per specimen and in total 10 kg/m³. The small number of fibres additionally makes it easy to observe single fibres very detailed and thus it is clearly visible that in corner areas of the specimens some artificial failures occur through the CT-scanning process. A good example is the point of intersection of the fibres for the fibres on the left or the bottom, where no sharp geometry and bending point is visible but a circular artefact.

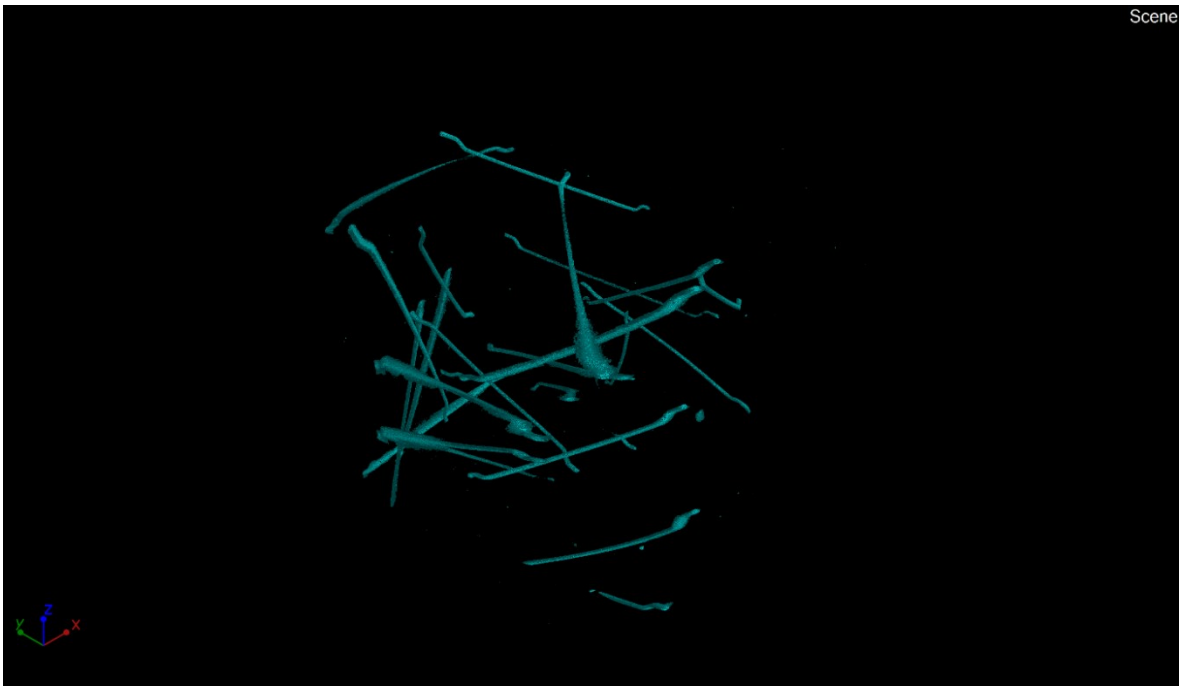

Figure D.7 CT image of specimen S2 – 10 kg/m³

Because of the higher fibre content of the second specimen of series S2, again a manual counting of the fibres based on the 3D image is not precisely possible. As can be seen in Figure D.8 there are both small point elements and thick fibre ends visible, what only can be artefacts of the scanning process. When trying to count the fibres, it can only be found out with certainty that more than 64 fibres are visible in the 3D image, while 78 are to be detected based on the fibre content of 30 kg/m³. Like for the specimens of series S1, many fibres inside of this specimen are oriented on the surfaces of the formwork and only a lower number is freely oriented in the middle area. Additionally one can suppose a small vertical channel in the middle where the internal vibrator was used.

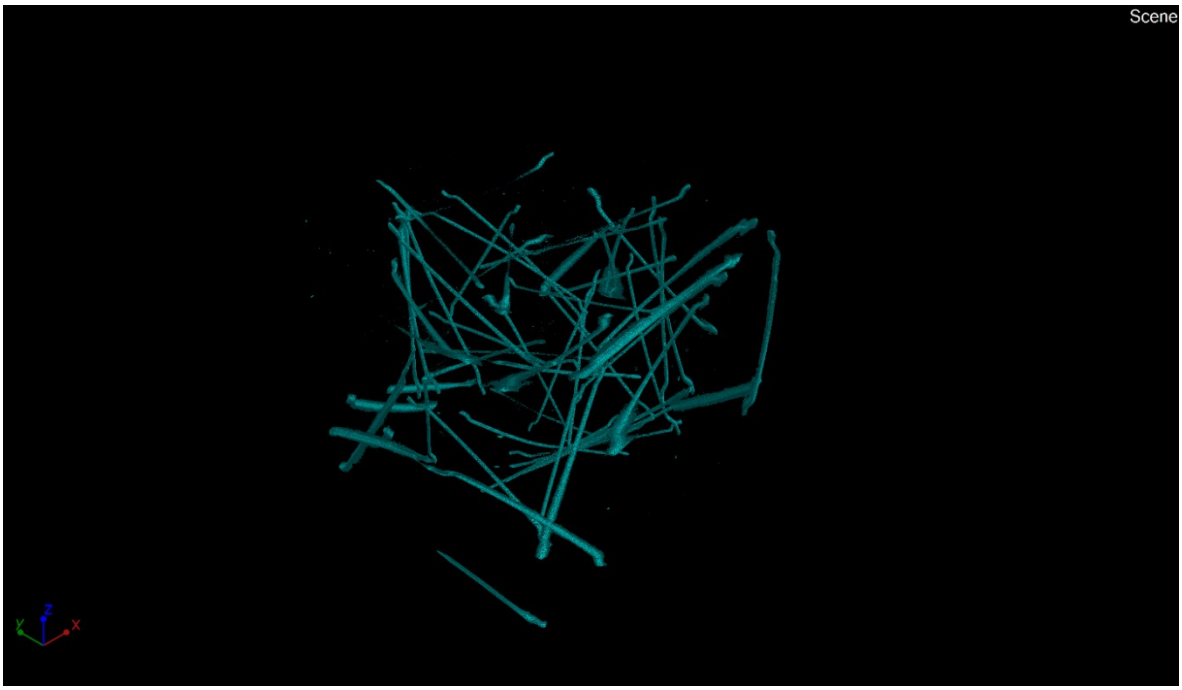

Figure D.8 CT image of specimen S2 – 30 kg/m³

In contrast to the macro SFRC the specimens with microfibres are presented in a very good way via 3D imaging (Figure D.9 and Figure D.10). As already stated for series S1, also here there is no possibility of a manual counting of the fibres, especially as here the number of fibres because of their size should be 662000 pieces/kg and so for a fibre content of 40 kg/m³ there should be about 26480 fibre inside of the specimen. Thus, here only a visual statement about the distribution and orientation again can be drawn. Both specimens show a homogenous distribution of the fibres and the orientation, with except of the surfaces of the formwork looks relatively anisotropic, but tends to be slightly more horizontal, what is explainable trough the direction of compacting.

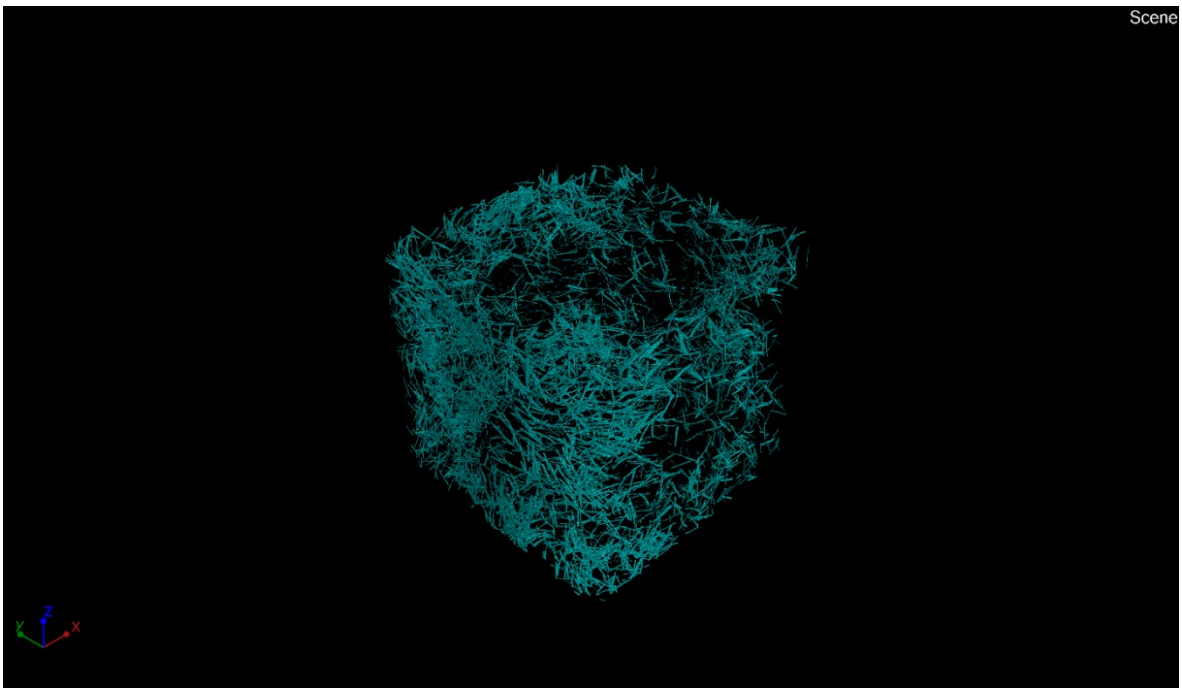

Figure D.9 CT image of specimen S3 – 40 kg/m³

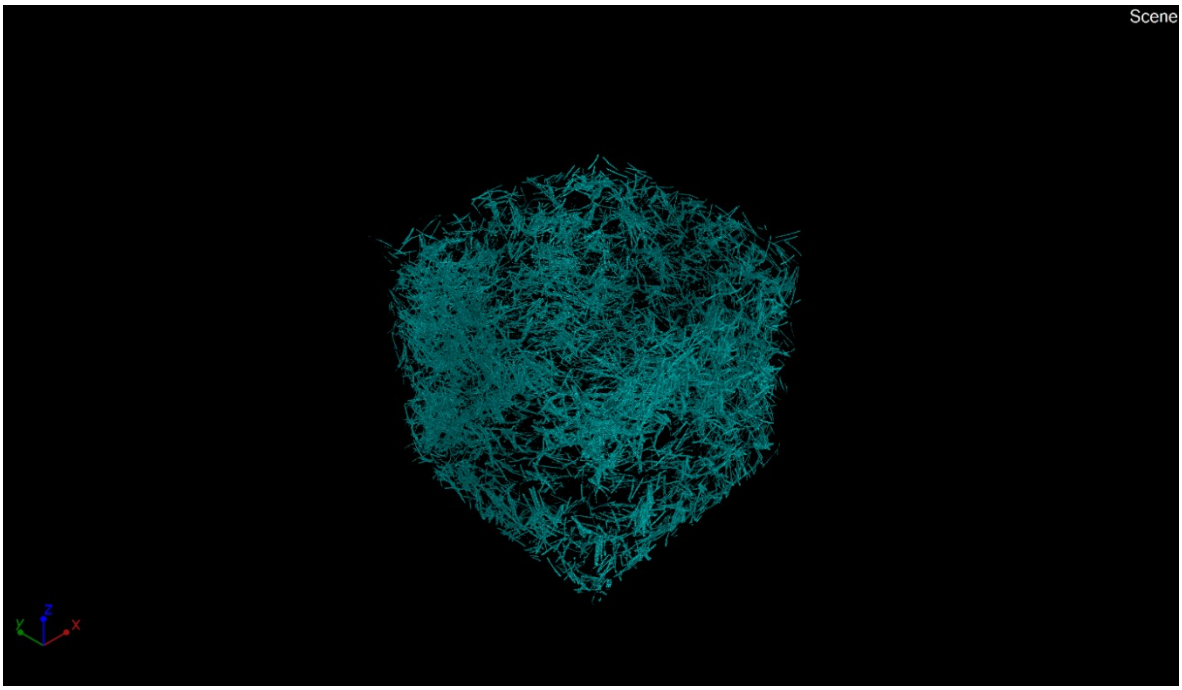

Figure D.10 CT image of specimen S3 – 70 kg/m³

c. Results of the Optoanalytical Investigation

The optoanalytical investigation of the specimens for the micro SFRC only could be performed via microscope. For the macro SFRC additionally manual counting of the fibres on the cut surfaces of about 10 x 10 mm² each direction was done without microscope. Each step was done in all three possible directions and the results were averaged to calculate the fibre content.

For series S1 the manual counting and calculation in accordance with (eq. XIII-2) results in fibre contents of 78 kg/m³ respectively 133 kg/m³ for fibre contents of 40 kg/m³ and 70 kg/m³. Thus, the calculation leads to values that are about 90 % to 100 % higher than expected. For series S2 that was compacted via internal vibrator fibre contents of 15 kg/m³ respectively 45 kg/m³ are calculated, which are about 50 % higher than the actual contents of 10 kg/m³ and 30 kg/m³. In contrast to these results, for the micro SFRC (series S3) the calculated fibre contents with 38 kg/m³ respectively 60 kg/m³ are much more fitting to the actual ones of 40 kg/m³ and 70 kg/m³.

Those results show that a simplified calculation of the fibre content via cross-sectional analysis only is possible if the relation between fibre size and cross-section of concrete to be analysed is small enough. For microfibres with a length of 8 mm it seems that a section of 100 x 100 mm² is enough, while for a fibre length of 60 mm it is much too small.

XIV. Annex E – Tables and Figures

Table E.1 Concrete mix designs for the variation of the water/cement ratio

Parameter	Unit	32-55-300-00	32-65-300-00
CEM I 32.5 R	kg/m³	300.0	300.0
GGBS		-	-
Water		165.0	195.0
Aggregates		1888.9	1810.0
Water/cement ratio		0.55	0.65
Grain size distribution	-	A/B16	A/B16
Steel fibre type		Macrofibre 60 mm	Macrofibre 60 mm
Steel fibre content	kg/m³	0 to 80	0 to 80

Table E.2 Concrete mix designs for the variation of the binder content

Parameter	Unit	32-60-270-00	32-60-330-00
CEM I 32.5 R	kg/m³	270.0	330.0
GGBS		-	-
Water		180.0	180.0
Aggregates		1922.3	1776.7
Water/cement ratio		0.60	0.60
Grain size distribution	-	A/B16	A/B16
Steel fibre type		Macrofibre 60 mm	Macrofibre 60 mm
Steel fibre content	kg/m³	0 to 80	0 to 80

Table E.3 Concrete mix designs for the variation of the cement type

Parameter	Unit	42-60-300-00	52-60-300-00
CEM I 42.5 R	kg/m³	300.0	-
CEM I 52.5 R		-	300.0
GGBS		-	-
Water		180.0	180.0
Aggregates		1849.5	1849.5
Water/cement ratio		0.60	0.60
Grain size distribution	-	A/B16	A/B16
Steel fibre type		Macrofibre 60 mm	Macrofibre 60 mm
Steel fibre content	kg/m³	0 to 80	0 to 80

Table E.4 Concrete mix designs for the variation of the content of GGBS

Parameter	Unit	32-60-300-35	32-60-300-65
CEM I 32.5 R	kg/m^3	195.0	105.0
GGBS		105.0	195.0
Water		180.0	180.0
Aggregates		1843.7	1838.7
Water/cement ratio		0.60	0.60
Grain size distribution	-	A/B16	A/B16
Steel fibre type		Macrofibre 60 mm	Macrofibre 60 mm
Steel fibre content	kg/m^3	0 to 80	0 to 80

Table E.5 Concrete mix designs for the variation of the steel fibre type

Parameter	Unit	32-60-300-00-F2	32-60-300-00-F3
CEM I 32.5 R	kg/m^3	300.0	300.0
GGBS		-	-
Water		180.0	180.0
Aggregates		1849.5	1849.5
Water/cement ratio		0.60	0.60
Grain size distribution	-	A/B16	A/B16
Steel fibre type		Macrofibre 35 mm	Microfibre 8 mm
Steel fibre content	kg/m^3	0 to 80	0 to 80

Table E.6 Concrete mix designs for the multiple parameter variation—part 1

Parameter	Unit	32-55-270-35	32-65-330-65
CEM I 32.5 R	kg/m^3	175.5	115.5
CEM I 42.5 R		-	-
CEM I 52.5 R		-	-
GGBS		94.5	214.5
Water		148.5	214.5
Aggregates		1952.5	1721.4
Water/cement ratio		0.55	0.65
Grain size distribution	-	A/B16	A/B16
Steel fibre type		Macrofibre 60 mm	Macrofibre 60 mm
Steel fibre content	kg/m^3	0 to 80	0 to 80

Table E.7 Concrete mix designs for the multiple parameter variation—part 2

Parameter	Unit	42-55-330-00	42-60-270-65
CEM I 32.5 R	kg/m³	-	-
CEM I 42.5 R		330.0	94.5
CEM I 52.5 R		-	-
GGBS		-	175.5
Water		181.5	162.0
Aggregates		1820.1	1912.6
Water/cement ratio		0.55	0.60
Grain size distribution	-	A/B16	A/B16
Steel fibre type		Macrofibre 60 mm	Macrofibre 60 mm
Steel fibre content	kg/m³	0 to 80	0 to 80

Table E.8 Concrete mix designs for the multiple parameter variation—part 3

Parameter	Unit	42-65-300-35	52-55-300-65
CEM I 32.5 R	kg/m³	-	-
CEM I 42.5 R		195.0	-
CEM I 52.5 R		-	105.0
GGBS		105.0	195.0
Water		195.0	165.0
Aggregates		1804.2	1878.1
Water/cement ratio		0.65	0.55
Grain size distribution	-	A/B16	A/B16
Steel fibre type		Macrofibre 60 mm	Macrofibre 60 mm
Steel fibre content	kg/m³	0 to 80	0 to 80

Table E.9 Concrete mix designs for the multiple parameter variation—part 4

Parameter	Unit	52-60-330-35	52-65-270-00
CEM I 32.5 R	kg/m³	-	-
CEM I 42.5 R		-	-
CEM I 52.5 R		214.5	270.0
GGBS		115.5	-
Water		198.0	175.5
Aggregates		1770.3	1886.8
Water/cement ratio		0.60	0.65
Grain size distribution	-	A/B16	A/B16
Steel fibre type		Macrofibre 60 mm	Macrofibre 60 mm
Steel fibre content	kg/m³	0 to 80	0 to 80

Table E.10 Results of the resistivity measurements of the basic concrete mixture (32-60-300-00)

Fibre content in kg/m³	Global electrical resistivity in Ωm at a frequency of				
	100 Hz	120 Hz	1 kHz	10 kHz	100 kHz
0	44.1	44.0	43.7	43.4	43.0
10	34.2	34.2	33.7	33.3	32.9
20	28.5	28.4	27.8	27.4	27.1
30	24.1	24.0	23.2	22.7	22.3
40	20.9	20.7	19.8	19.3	18.8
50	18.3	18.2	17.4	16.8	16.4
60	16.6	16.5	15.6	15.1	14.7
70	15.2	15.0	14.1	13.5	13.1
80	13.7	13.5	12.5	12.0	11.6

Table E.11 Results of the resistivity measurements of the concrete mixture 32-55-300-00

Fibre content in kg/m³	Global electrical resistivity in Ωm at a frequency of				
	100 Hz	120 Hz	1 kHz	10 kHz	100 kHz
0	50.5	50.6	50.3	49.8	49.2
10	41.1	41.1	40.6	40.2	39.6
20	33.1	32.9	32.3	31.7	31.1
30	27.2	27.0	26.3	25.6	25.1
40	25.6	25.4	24.7	24.1	23.6
50	23.4	23.2	22.4	21.7	21.1
60	20.9	20.7	19.7	19.0	18.3
70	18.1	17.9	16.9	16.1	15.5
80	17.7	17.5	16.7	16.0	15.4

Table E.12 Results of the resistivity measurements of the concrete mixture 32-65-300-00

Fibre content in kg/m³	Global electrical resistivity in Ωm at a frequency of				
	100 Hz	120 Hz	1 kHz	10 kHz	100 kHz
0	40.5	40.6	40.3	40.0	39.6
10	32.2	32.1	31.9	31.5	31.1
20	26.7	26.6	26.0	25.5	25.0
30	24.9	24.7	24.1	23.4	23.0
40	20.8	20.7	20.1	19.5	18.9
50	18.6	18.4	17.7	17.1	16.7
60	17.2	17.0	16.3	15.4	14.8
70	17.1	16.9	16.1	15.2	14.9
80	16.3	16.1	15.3	14.6	14.2

Table E.13 Results of the resistivity measurements of the concrete mixture 32-60-270-00

Fibre content in kg/m³	Global electrical resistivity in Ωm at a frequency of				
	100 Hz	120 Hz	1 kHz	10 kHz	100 kHz
0	50.2	50.1	49.9	49.5	48.8
10	34.2	34.0	33.7	33.3	32.7
20	28.8	28.6	28.1	27.5	27.0
30	26.0	25.8	25.2	24.6	24.0
40	22.5	22.3	21.8	21.0	20.4
50	20.5	20.3	19.7	18.8	18.2
60	19.3	19.1	18.3	17.4	16.8
70	18.1	17.8	17.4	16.7	15.9
80	15.7	15.4	14.9	14.1	13.6

Table E.14 Results of the resistivity measurements of the concrete mixture 32-60-330-00

Fibre content in kg/m³	Global electrical resistivity in Ωm at a frequency of				
	100 Hz	120 Hz	1 kHz	10 kHz	100 kHz
0	36.7	36.7	36.3	36.2	35.9
10	27.7	27.7	27.1	27.0	26.7
20	21.8	21.8	21.1	20.8	20.5
30	19.9	19.7	19.0	18.6	18.3
40	16.5	16.4	15.7	15.2	14.9
50	14.8	14.7	13.9	13.4	13.1
60	13.7	13.5	12.6	12.1	11.8
70	12.2	12.1	11.2	10.6	10.3
80	11.3	11.1	10.3	9.7	9.3

Table E.15 Results of the resistivity measurements of the concrete mixture 42-60-300-00

Fibre content in kg/m³	Global electrical resistivity in Ωm at a frequency of				
	100 Hz	120 Hz	1 kHz	10 kHz	100 kHz
0	55.7	55.6	55.3	54.7	53.8
10	38.8	38.7	38.3	37.9	37.3
20	33.1	33.0	32.5	31.9	31.2
30	29.9	29.7	29.4	28.6	27.9
40	26.1	25.8	25.4	24.8	24.1
50	22.9	22.7	22.1	21.4	20.9
60	21.5	21.3	20.7	20.0	19.4
70	21.3	21.1	20.5	19.8	19.3
80	20.2	20.0	19.3	18.5	17.8

Table E.16 Results of the resistivity measurements of the concrete mixture 52-60-300-00

Fibre content in kg/m³	Global electrical resistivity in Ωm at a frequency of				
	100 Hz	120 Hz	1 kHz	10 kHz	100 kHz
0	39.6	39.5	39.5	38.9	38.4
10	35.4	35.2	35.0	34.3	33.7
20	28.8	28.6	28.0	27.2	26.5
30	27.5	27.3	26.8	26.2	25.5
40	24.4	24.2	23.6	22.7	22.0
50	21.8	21.6	21.0	20.3	19.7
60	20.7	20.5	20.0	19.1	18.5
70	19.6	19.3	18.8	18.0	17.3
80	18.8	18.6	18.1	17.3	16.7

Table E.17 Results of the resistivity measurements of the concrete mixture 32-60-300-35

Fibre content in kg/m³	Global electrical resistivity in Ωm at a frequency of				
	100 Hz	120 Hz	1 kHz	10 kHz	100 kHz
0	40.3	40.3	40.0	39.7	39.3
10	31.0	30.8	30.4	30.0	29.7
20	26.0	25.8	25.3	25.0	24.8
30	23.0	22.9	22.3	21.8	21.5
40	18.5	18.3	17.8	17.4	17.2
50	17.4	17.2	16.6	16.2	15.9
60	16.3	16.2	15.5	15.1	14.7
70	14.0	14.0	13.3	12.8	12.5
80	13.2	13.0	12.3	11.8	11.5

Table E.18 Results of the resistivity measurements of the concrete mixture 32-60-300-65

Fibre content in kg/m³	Global electrical resistivity in Ωm at a frequency of				
	100 Hz	120 Hz	1 kHz	10 kHz	100 kHz
0	54.5	54.3	53.9	53.6	52.8
10	43.3	43.2	42.6	42.1	41.6
20	36.1	35.9	35.3	34.8	34.3
30	28.6	28.5	27.8	27.4	26.9
40	25.0	24.8	23.9	23.4	22.9
50	23.5	23.3	22.4	21.9	21.4
60	20.1	20.0	19.2	18.7	18.2
70	18.9	18.8	18.1	17.7	17.2
80	16.9	16.9	16.1	15.5	15.1

Table E.19 Results of the resistivity measurements of the concrete mixture 32-60-300-00-F2

Fibre content in kg/m³	Global electrical resistivity in Ωm at a frequency of				
	100 Hz	120 Hz	1 kHz	10 kHz	100 kHz
0	43.1	43.0	42.7	42.5	42.1
10	36.4	36.4	35.8	35.4	35.0
20	31.0	30.9	30.2	29.7	29.4
30	25.8	25.7	25.0	24.5	24.0
40	22.8	22.7	21.5	20.8	20.3
50	21.1	20.9	19.7	19.0	18.6
60	19.0	18.8	17.6	16.9	16.5
70	17.5	17.2	15.9	15.2	14.7
80	16.1	15.9	14.6	13.8	13.3

Table E.20 Results of the resistivity measurements of the concrete mixture 32-60-300-00-F3

Fibre content in kg/m³	Global electrical resistivity in Ωm at a frequency of				
	100 Hz	120 Hz	1 kHz	10 kHz	100 kHz
0	44.1	44.0	43.8	43.5	43.1
10	36.4	36.1	34.9	34.4	33.9
20	30.5	30.2	28.4	27.7	27.2
30	26.1	25.6	23.6	22.6	22.1
40	22.6	22.3	20.0	19.0	18.3
50	19.9	19.5	17.2	16.1	15.4
60	17.5	17.1	14.9	13.7	13.1
70	15.8	15.5	13.2	12.0	11.4
80	14.5	14.1	11.9	10.7	10.1

Table E.21 Results of the resistivity measurements of the concrete mixture 32-60-300-00-F1

Fibre content in kg/m³	Electrical resistivity in horizontal direction in Ωm at a frequency of				
	100 Hz	120 Hz	1 kHz	10 kHz	100 kHz
0	43.7	43.7	43.4	43.1	42.7
10	31.7	31.6	31.1	30.7	30.4
20	24.8	24.7	24.1	23.7	23.4
30	20.4	20.3	19.5	19.1	18.7
40	17.4	17.2	16.5	15.9	15.6
50	14.4	14.3	13.6	13.1	12.8
60	13.1	12.9	12.2	11.8	11.5
70	11.8	11.7	10.9	10.5	10.1
80	10.5	10.2	9.5	9.1	8.7

Table E.22 Results of the resistivity measurements of the concrete mixture 32-60-300-00-F2

Fibre content in kg/m³	Electrical resistivity in horizontal direction in Ωm at a frequency of				
	100 Hz	120 Hz	1 kHz	10 kHz	100 kHz
0	43.3	43.3	43.0	42.7	42.3
10	34.4	34.4	33.7	33.3	33.0
20	28.2	28.1	27.3	26.8	26.5
30	22.1	21.9	21.4	21.0	20.4
40	18.9	18.7	17.6	16.9	16.5
50	17.6	17.4	16.3	15.7	15.3
60	15.3	15.1	14.1	13.4	13.1
70	14.0	13.8	12.7	12.0	11.5
80	12.5	12.4	11.3	10.7	10.3

Table E.23 Results of the resistivity measurements of the concrete mixture 32-60-300-00-F3

Fibre content in kg/m³	Electrical resistivity in horizontal direction in Ωm at a frequency of				
	100 Hz	120 Hz	1 kHz	10 kHz	100 kHz
0	44.2	44.1	43.8	43.6	43.1
10	35.5	35.2	33.9	33.4	33.0
20	29.0	28.8	26.9	26.2	25.7
30	24.4	23.9	22.0	21.0	20.5
40	20.7	20.4	18.2	17.2	16.5
50	18.1	17.7	15.6	14.5	13.9
60	15.7	15.2	13.2	12.2	11.6
70	14.2	13.9	11.9	10.7	10.1
80	12.7	12.3	10.4	9.3	8.8

Table E.24 Results of the resistivity measurements of the concrete mixture 32-60-300-00-F1

Fibre content in kg/m³	Electrical resistivity in vertical direction in Ωm at a frequency of				
	100 Hz	120 Hz	1 kHz	10 kHz	100 kHz
0	44.7	44.6	44.3	44.0	43.6
10	39.4	39.4	38.8	38.5	38.1
20	36.0	35.9	35.2	34.9	34.4
30	31.6	31.4	30.5	30.1	29.6
40	27.9	27.7	26.6	25.9	25.3
50	26.1	26.0	24.8	24.2	23.7
60	23.7	23.6	22.3	21.6	21.1
70	21.9	21.7	20.3	19.5	18.9
80	20.2	20.0	18.7	17.8	17.3

Table E.25 Results of the resistivity measurements of the concrete mixture 32-60-300-00-F2

Fibre content in kg/m³	Electrical resistivity in vertical direction in Ωm at a frequency of				
	100 Hz	120 Hz	1 kHz	10 kHz	100 kHz
0	42.6	42.5	42.2	42.0	41.6
10	40.4	40.3	39.8	39.6	39.1
20	36.7	36.6	36.1	35.6	35.2
30	33.4	33.2	32.2	31.6	31.1
40	30.8	30.6	29.2	28.4	28.0
50	28.0	27.8	26.4	25.6	25.1
60	26.5	26.2	24.7	24.0	23.5
70	24.5	24.2	22.5	21.6	21.0
80	23.3	23.0	21.1	20.2	19.5

Table E.26 Results of the resistivity measurements of the concrete mixture 32-60-300-00-F3

Fibre content in kg/m³	Electrical resistivity in vertical direction in Ωm at a frequency of				
	100 Hz	120 Hz	1 kHz	10 kHz	100 kHz
0	44.0	43.9	43.7	43.4	43.0
10	38.2	37.9	36.8	36.3	35.8
20	33.5	33.2	31.5	30.7	30.3
30	29.5	29.1	26.9	25.9	25.4
40	26.5	26.0	23.7	22.5	21.9
50	23.4	22.9	20.4	19.2	18.5
60	21.3	20.9	18.2	16.9	16.2
70	19.1	18.7	16.0	14.6	13.9
80	18.1	17.6	15.0	13.6	12.8

Table E.27 Results of the resistivity measurements of the concrete mixture 32-55-270-35

Fibre content in kg/m³	Global electrical resistivity in Ωm at a frequency of				
	100 Hz	120 Hz	1 kHz	10 kHz	100 kHz
0	48.2	48.1	47.7	47.5	47.0
10	39.4	39.4	38.9	38.5	38.1
20	31.4	31.3	30.7	30.3	29.8
30	25.5	25.3	24.7	24.3	24.0
40	21.4	21.3	20.7	20.2	19.8
50	20.1	19.9	19.3	18.8	18.4
60	17.0	16.9	16.2	15.7	15.3
70	16.2	16.1	15.4	15.0	14.6
80	15.7	15.6	14.9	14.4	14.0

Table E.28 Results of the resistivity measurements of the concrete mixture 32-65-330-65

Fibre content in kg/m³	Global electrical resistivity in Ωm at a frequency of				
	100 Hz	120 Hz	1 kHz	10 kHz	100 kHz
0	46.8	46.7	46.3	46.0	45.5
10	37.6	37.5	37.1	36.8	36.3
20	30.0	29.9	29.3	29.0	28.7
30	26.2	26.1	25.5	25.1	24.7
40	20.3	20.1	19.4	18.9	18.6
50	19.0	18.8	18.1	17.6	17.3
60	17.1	17.0	16.3	15.9	15.5
70	15.5	15.4	14.7	14.3	13.8
80	14.7	14.7	14.1	13.5	13.2

Table E.29 Results of the resistivity measurements of the concrete mixture 42-55-330-00

Fibre content in kg/m³	Global electrical resistivity in Ωm at a frequency of				
	100 Hz	120 Hz	1 kHz	10 kHz	100 kHz
0	42.0	42.0	41.7	41.5	40.9
10	33.3	33.2	32.8	32.5	32.1
20	27.3	27.2	26.7	26.3	26.0
30	22.5	22.3	21.8	21.4	21.0
40	19.7	19.6	19.0	18.7	18.4
50	18.0	17.9	17.4	17.0	16.7
60	14.9	14.8	14.1	13.7	13.4
70	14.2	14.0	13.4	12.9	12.5
80	12.7	12.6	11.9	11.4	11.1

Table E.30 Results of the resistivity measurements of the concrete mixture 42-60-270-65

Fibre content in kg/m³	Global electrical resistivity in Ωm at a frequency of				
	100 Hz	120 Hz	1 kHz	10 kHz	100 kHz
0	68.2	68.1	67.7	67.2	66.2
10	52.6	52.5	51.8	51.3	50.4
20	42.1	42.0	41.3	40.8	40.1
30	35.9	35.8	34.9	34.4	33.7
40	30.2	30.0	29.2	28.8	28.2
50	26.7	26.6	25.8	25.2	24.6
60	23.7	23.5	22.6	22.0	21.5
70	21.3	21.1	20.3	19.7	19.2
80	19.3	19.1	18.2	17.7	17.2

Table E.31 Results of the resistivity measurements of the concrete mixture 42-65-300-35

Fibre content in kg/m³	Global electrical resistivity in Ωm at a frequency of				
	100 Hz	120 Hz	1 kHz	10 kHz	100 kHz
0	33.0	32.9	32.7	32.5	32.2
10	26.3	26.3	25.9	25.6	25.3
20	21.6	21.6	21.2	20.9	20.6
30	18.6	18.5	17.9	17.6	17.3
40	16.5	16.3	15.8	15.5	15.3
50	13.7	13.6	13.0	12.7	12.5
60	12.2	12.1	11.5	11.2	10.9
70	12.2	12.1	11.4	11.4	11.0
80	10.4	10.3	9.8	9.5	9.2

Table E.32 Results of the resistivity measurements of the concrete mixture 52-55-300-65

Fibre content in kg/m³	Global electrical resistivity in Ωm at a frequency of				
	100 Hz	120 Hz	1 kHz	10 kHz	100 kHz
0	36.2	36.2	36.0	35.8	35.5
10	31.0	30.9	30.4	30.2	29.8
20	24.4	24.2	23.7	23.4	23.0
30	20.0	19.9	19.3	18.9	18.7
40	19.4	19.2	18.4	17.8	17.5
50	16.1	16.0	15.3	14.8	14.5
60	13.6	13.5	12.8	12.3	12.1
70	13.3	13.2	12.4	12.0	11.7
80	12.2	12.1	11.5	11.1	10.8

Table E.33 Results of the resistivity measurements of the concrete mixture 52-60-330-35

Fibre content in kg/m³	Global electrical resistivity in Ωm at a frequency of				
	100 Hz	120 Hz	1 kHz	10 kHz	100 kHz
0	24.5	24.4	24.3	24.2	24.0
10	20.8	20.7	20.4	20.2	19.9
20	17.5	17.4	16.9	16.6	16.4
30	15.5	15.4	14.9	14.6	14.3
40	13.8	13.6	13.0	12.7	12.5
50	12.5	12.4	11.8	11.5	11.2
60	11.3	11.2	10.6	10.2	10.0
70	10.2	10.1	9.5	9.2	8.9
80	9.1	9.0	8.4	8.0	7.8

Table E.34 Results of the resistivity measurements of the concrete mixture 52-65-270-00

Fibre content in kg/m³	Global electrical resistivity in Ωm at a frequency of				
	100 Hz	120 Hz	1 kHz	10 kHz	100 kHz
0	36.8	36.8	36.5	36.2	35.9
10	29.4	29.3	28.8	28.5	28.1
20	23.3	23.2	22.5	22.1	21.8
30	20.3	20.1	19.3	18.8	18.5
40	17.3	17.1	16.4	15.9	15.5
50	16.0	15.8	14.9	14.5	14.1
60	14.2	14.0	13.2	12.8	12.4
70	13.2	13.1	12.2	11.7	11.3
80	12.3	12.1	11.3	10.8	10.4

Table E.35 Results of the resistivity measurements of the concrete mixture 32-60-300-00 after storage in H_2O for 7 days for the investigations of possible leaching effects

Fibre content in kg/m³	Global electrical resistivity in Ωm at a frequency of				
	100 Hz	120 Hz	1 kHz	10 kHz	100 kHz
0	40.0	40.0	39.7	39.5	39.1
40	20.1	19.9	19.2	18.8	18.4
80	12.7	12.6	11.9	11.5	11.1

Table E.36 Results of the resistivity measurements of the concrete mixture 32-60-300-00 after storage in H_2O for 14 days for the investigations of possible leaching effects

Fibre content in kg/m³	Global electrical resistivity in Ωm at a frequency of				
	100 Hz	120 Hz	1 kHz	10 kHz	100 kHz
0	46.2	46.1	45.9	45.6	45.1
40	21.4	21.4	20.6	20.1	19.7
80	13.9	13.8	13.1	12.6	12.3

Table E.37 Results of the resistivity measurements of the concrete mixture 32-60-300-00 after storage in H_2O for 28 days for the investigations of possible leaching effects

Fibre content in kg/m³	Global electrical resistivity in Ωm at a frequency of				
	100 Hz	120 Hz	1 kHz	10 kHz	100 kHz
0	50.5	51.4	51.3	51.0	50.5
40	23.8	23.7	22.9	22.3	21.8
80	15.3	15.2	14.4	13.9	13.5

Table E.38 Results of the resistivity measurements of the concrete mixture 32-60-300-00 after storage in H_2O for 56 days for the investigations of possible leaching effects

Fibre content in kg/m³	Global electrical resistivity in Ωm at a frequency of				
	100 Hz	120 Hz	1 kHz	10 kHz	100 kHz
0	57.0	56.9	56.6	56.1	55.0
40	26.5	26.4	25.3	24.5	23.5
80	15.8	15.7	14.9	14.3	13.9

Table E.39 Results of the resistivity measurements of the concrete mixture 32-60-300-00 after storage in H_2O for 91 days for the investigations of possible leaching effects

Fibre content in kg/m³	Global electrical resistivity in Ωm at a frequency of				
	100 Hz	120 Hz	1 kHz	10 kHz	100 kHz
0	63.0	63.0	62.3	61.2	59.2
40	30.1	30.0	28.5	27.0	25.5
80	16.3	16.1	15.2	14.6	14.2

Table E.40 Results of the resistivity measurements of the concrete mixture 32-60-300-00 after storage in H_2O for 185 days for the investigations of possible leaching effects

Fibre content in kg/m³	Global electrical resistivity in Ωm at a frequency of				
	100 Hz	120 Hz	1 kHz	10 kHz	100 kHz
0	78.3	78.2	74.8	70.4	66.3
40	42.7	42.3	38.2	33.3	29.3
80	19.2	19.0	17.7	16.5	15.4

Table E.41 Results of the resistivity measurements of the concrete mixture 32-60-300-00 after storage in $Ca(OH)_2$ for 7 days for the investigations of possible leaching effects

Fibre content in kg/m³	Global electrical resistivity in Ωm at a frequency of				
	100 Hz	120 Hz	1 kHz	10 kHz	100 kHz
0	39.4	39.4	39.1	38.9	38.5
40	18.9	18.8	18.2	17.7	17.4
80	12.6	12.4	11.8	11.4	11.1

Table E.42 Results of the resistivity measurements of the concrete mixture 32-60-300-00 after storage in $Ca(OH)_2$ for 14 days for the investigations of possible leaching effects

Fibre content in kg/m³	Global electrical resistivity in Ωm at a frequency of				
	100 Hz	120 Hz	1 kHz	10 kHz	100 kHz
0	44.8	44.8	44.5	44.2	43.8
40	20.9	20.9	20.2	19.7	19.4
80	13.2	13.1	12.4	12.1	11.8

Table E.43 Results of the resistivity measurements of the concrete mixture 32-60-300-00 after storage in $Ca(OH)_2$ for 28 days for the investigations of possible leaching effects

Fibre content in kg/m³	Global electrical resistivity in Ωm at a frequency of				
	100 Hz	120 Hz	1 kHz	10 kHz	100 kHz
0	49.6	49.6	49.3	49.0	48.4
40	22.2	22.1	21.4	20.9	20.5
80	14.3	14.2	13.5	13.0	12.7

Table E.44 Results of the resistivity measurements of the concrete mixture 32-60-300-00 after storage in $Ca(OH)_2$ for 56 days for the investigations of possible leaching effects

Fibre content in kg/m³	Global electrical resistivity in Ωm at a frequency of				
	100 Hz	120 Hz	1 kHz	10 kHz	100 kHz
0	53.7	53.7	53.3	53.0	52.1
40	23.6	23.5	22.8	22.3	21.8
80	15.8	15.7	14.8	14.0	13.2

Table E.45 Results of the resistivity measurements of the concrete mixture 32-60-300-00 after storage in $Ca(OH)_2$ for 91 days for the investigations of possible leaching effects

Fibre content in kg/m³	Global electrical resistivity in Ωm at a frequency of				
	100 Hz	120 Hz	1 kHz	10 kHz	100 kHz
0	59.2	59.2	58.7	57.7	56.2
40	26.1	25.9	25.1	24.5	24.1
80	18.8	18.6	17.3	15.7	14.4

Table E.46 Results of the resistivity measurements of the concrete mixture 32-60-300-00 after storage in $Ca(OH)_2$ for 185 days for the investigations of possible leaching effects

Fibre content in kg/m³	Global electrical resistivity in Ωm at a frequency of				
	100 Hz	120 Hz	1 kHz	10 kHz	100 kHz
0	68.0	67.9	67.1	65.5	63.1
40	30.3	30.2	29.0	27.9	26.6
80	24.8	24.7	21.9	18.5	15.9

Table E.47 Results of the resistivity measurements of the concrete mixture 32-60-300-00 after storage in synthetical pore solution for 7 days for the investigations of possible leaching effects

Fibre content in kg/m³	Global electrical resistivity in Ωm at a frequency of				
	100 Hz	120 Hz	1 kHz	10 kHz	100 kHz
0	36.6	36.6	36.4	36.1	35.8
40	16.0	15.8	15.2	14.7	14.4
80	9.1	8.9	8.2	7.8	7.6

Table E.48 Results of the resistivity measurements of the concrete mixture 32-60-300-00 after storage in synthetical pore solution for 14 days for the investigations of possible leaching effects

Fibre content in kg/m³	Global electrical resistivity in Ωm at a frequency of				
	100 Hz	120 Hz	1 kHz	10 kHz	100 kHz
0	42.2	42.1	42.0	41.6	41.1
40	17.5	17.5	16.6	16.2	15.8
80	9.7	9.6	8.8	8.3	8.1

Table E.49 Results of the resistivity measurements of the concrete mixture 32-60-300-00 after storage in synthetical pore solution for 28 days for the investigations of possible leaching effects

Fibre content in kg/m³	Global electrical resistivity in Ωm at a frequency of				
	100 Hz	120 Hz	1 kHz	10 kHz	100 kHz
0	48.6	48.5	48.3	48.0	47.3
40	19.7	19.5	18.7	18.2	17.8
80	11.6	11.4	10.6	10.1	9.7

Table E.50 Results of the resistivity measurements of the concrete mixture 32-60-300-00 after storage in synthetical pore solution for 56 days for the investigations of possible leaching effects

Fibre content in kg/m³	Global electrical resistivity in Ωm at a frequency of				
	100 Hz	120 Hz	1 kHz	10 kHz	100 kHz
0	52.3	52.3	52.0	51.6	50.9
40	21.8	21.6	20.7	20.1	19.5
80	12.7	12.6	11.6	11.0	10.4

Table E.51 Results of the resistivity measurements of the concrete mixture 32-60-300-00 after storage in synthetical pore solution for 91 days for the investigations of possible leaching effects

Fibre content in kg/m³	Global electrical resistivity in Ωm at a frequency of				
	100 Hz	120 Hz	1 kHz	10 kHz	100 kHz
0	54.6	54.6	54.3	53.9	52.9
40	23.2	23.1	22.1	21.4	20.6
80	13.5	13.4	12.4	11.6	10.8

Table E.52 Results of the resistivity measurements of the concrete mixture 32-60-300-00 after storage in synthetical pore solution for 185 days for the investigations of possible leaching effects

Fibre content in kg/m³	Global electrical resistivity in Ωm at a frequency of				
	100 Hz	120 Hz	1 kHz	10 kHz	100 kHz
0	62.1	62.0	61.6	60.8	59.4
40	27.2	27.0	25.8	24.9	23.8
80	18.7	18.5	16.5	15.0	13.7

Table E.53 Geometry factors k for the validation tests of the test setup, calculated by Comsol, with an electrode array with angular distances of 180 ° and the electrical conductivity of the electrodes in Comsol model of titanium of 2.5 x 10^6 S/m

Electrode A		Electrode B		k-value
Height level	Angle	Height level	Angle	
all	0°	all	180°	0.073252
1	0°	1	180°	0.026695
3	0°	3	180°	
2	0°	2	180°	0.026986
1	all	2	all	0.051199
2	all	3	all	
1	all	3	all	0.036845
1	0°	2	0°	0.027577
1	180°	2	180°	
2	0°	3	0°	
2	180°	3	180°	
1	0°	3	0°	0.021785
1	180°	3	180°	

Table E.54 Geometry factors k for the validation tests of the test setup, calculated by Comsol, with an electrode array with angular distances of 90 ° and the electrical conductivity of the electrodes in Comsol model of titanium of 2.5 x 10^6 S/m

Electrode A		Electrode B		k-value
Height level	**Angle**	**Height level**	**Angle**	
all	0°	all	180°	0.072101
all	90°	all	270°	
1	0°	1	180°	0.026855
1	90°	1	270°	
3	0°	3	180°	
3	90°	3	270°	
2	0°	2	180°	0.027489
2	90°	2	270°	
1	all	2	all	0.086723
2	all	3	all	
1	all	3	all	0.054244
1	0°	2	0°	0.027987
1	90°	2	90°	
1	180°	2	180°	
1	270°	2	270°	
2	0°	3	0°	
2	90°	3	90°	
2	180°	3	180°	
2	270°	3	270°	
1	0°	3	0°	0.021898
1	90°	3	90°	
1	180°	3	180°	
1	270°	3	270°	

Table E.55 Geometry factors k for the drilling core analysis, calculated by Comsol with an electrode array with angular distances of 90 ° and electrical conductivity of the electrodes in Comsol model of stainless steel: 1.4 x 10^6 S/m

Electrode A		Electrode B		k-value
Height level	**Angle**	**Height level**	**Angle**	
all	0°	all	180°	0.071866
all	90°	all	270°	
1	0°	1	180°	0.026653
1	90°	1	270°	
3	0°	3	180°	
3	90°	3	270°	
2	0°	2	180°	0.027555
2	90°	2	270°	
1	all	2	all	0.086957
2	all	3	all	
1	all	3	all	0.054714

Table E.56 Geometry factors k for the drilling core analysis, calculated by Comsol with an electrode array with angular distances of 90 ° and electrical resistivity of the electrodes in the Comsol model of concrete: 100 Ωm

Electrode A		Electrode B		k-value
Height level	**Angle**	**Height level**	**Angle**	
all	0°	all	180°	0.063497
all	90°	all	270°	
1	0°	1	180°	0.023066
1	90°	1	270°	
3	0°	3	180°	
3	90°	3	270°	
2	0°	2	180°	0.023768
2	90°	2	270°	
1	all	2	all	0.076614
2	all	3	all	
1	all	3	all	0.048069

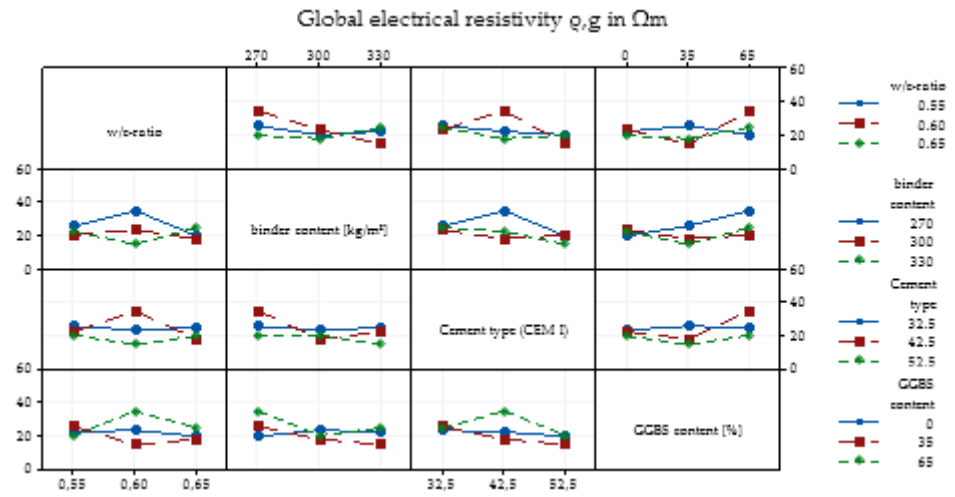

Figure E.1 Interaction plot of the effects of the concrete composition on the global electrical resistivity of SFRC calculated by Minitab based on the mixtures of the multiple parameter variation

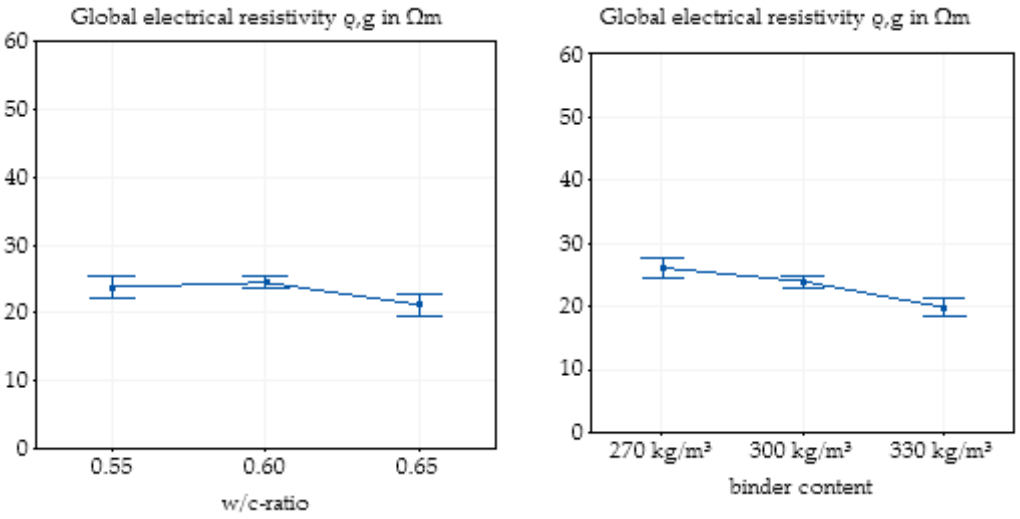

(a) **(b)**

Figure E.2 Main effect plot with 95% confidence interval of the w/c ratio on the global electrical resistivity of SFRC calculated by Minitab based on all experimental data (**a**) and main effect plot with 95% confidence interval of the binder content on the global electrical resistivity of SFRC calculated by Minitab based on all experimental data (**b**)

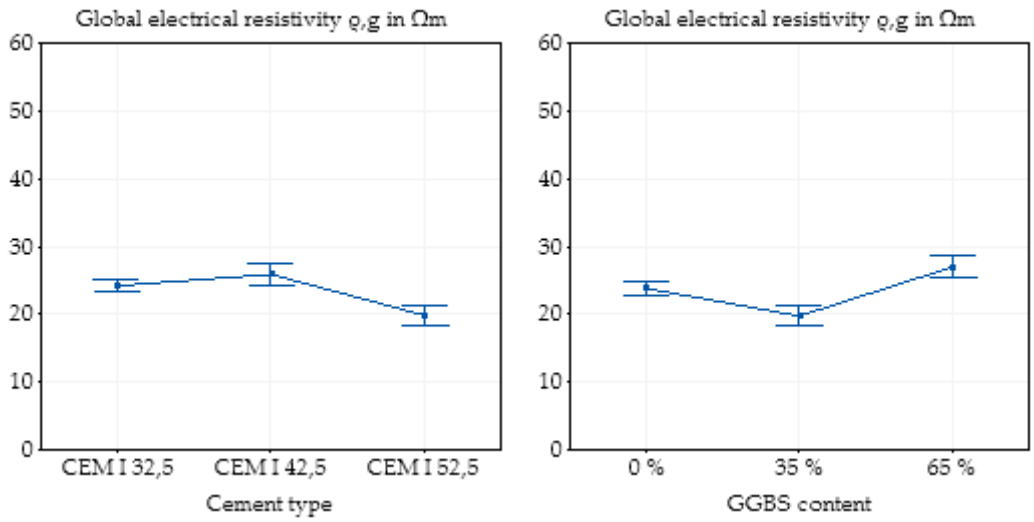

(a) **(b)**

Figure E.3 Main effect plot with 95% confidence interval of the cement type on the global electrical resistivity of SFRC calculated by Minitab based on all experimental data (a) and main effect plot with 95% confidence interval of the GGBS content on the global electrical resistivity of SFRC calculated by Minitab based on all experimental data (**b**)

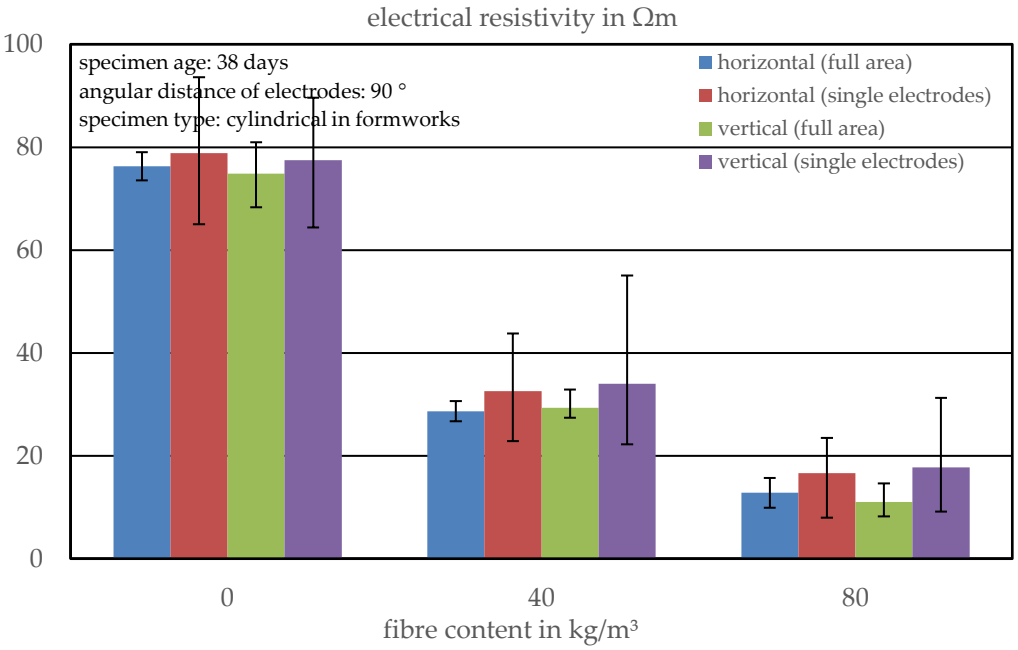

Figure E.4 Electrical resistivity in different directions depending on the fibre content at a specimen age of 38 days and an electrode array with angular distances of 90°

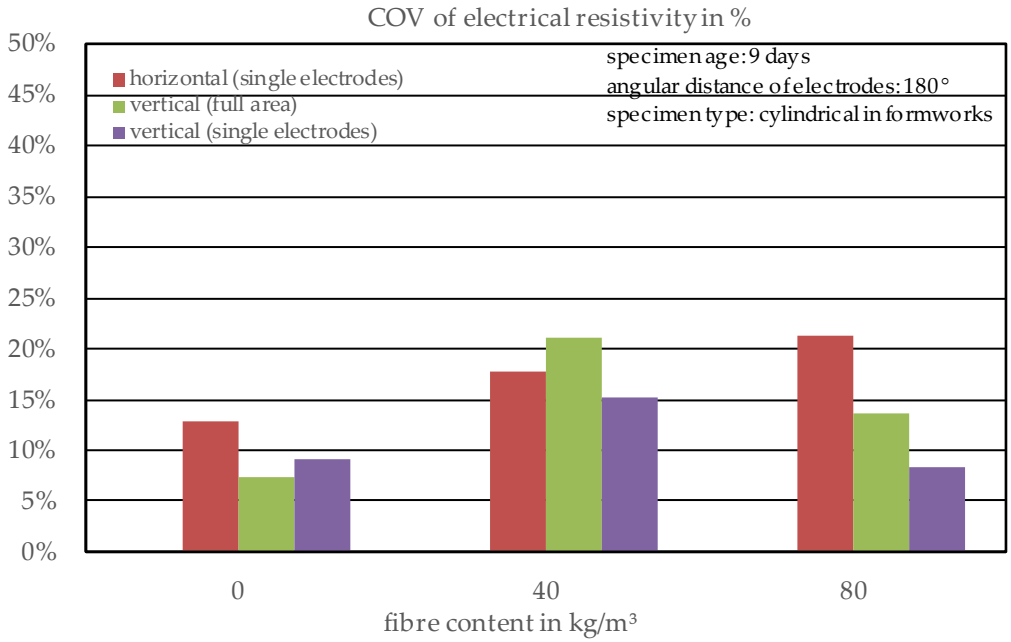

Figure E.5 Coefficient of variation of the electrical resistivity in different directions depending on the fibre content at a specimen age of 9 days and an electrode array with angular distances of 180°

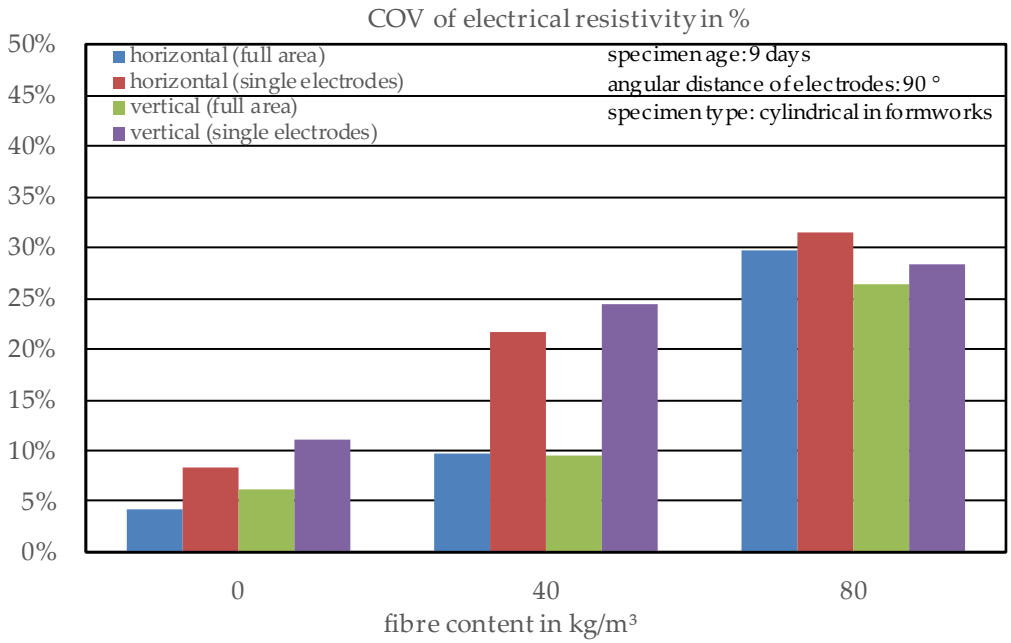

Figure E.6 Coefficient of variation of the electrical resistivity in different directions depending on the fibre content at a specimen age of 9 days and an electrode array with angular distances of 90°

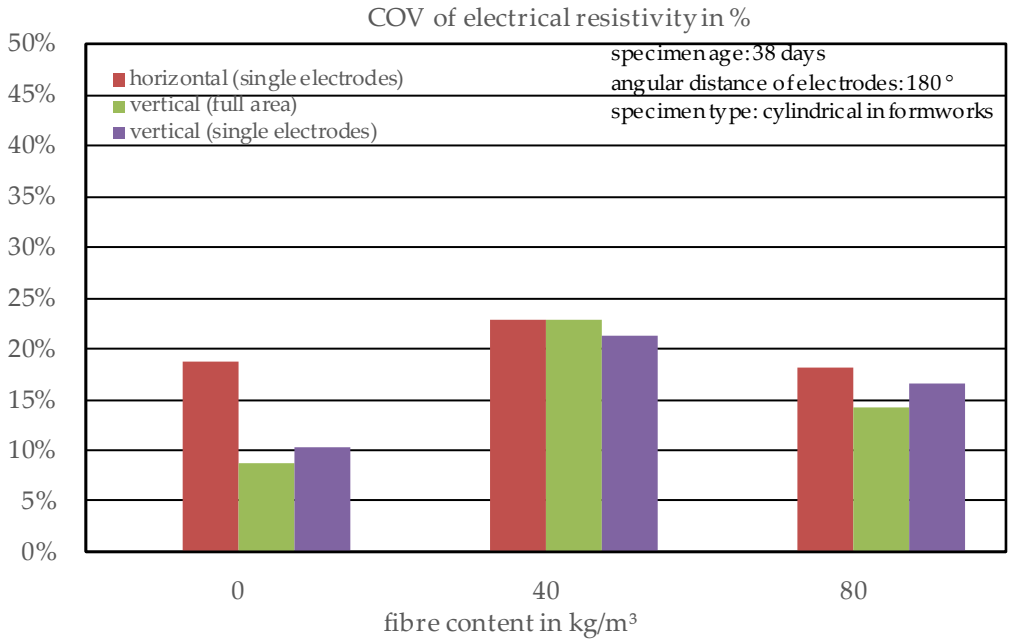

Figure E.7 Coefficient of variation of the electrical resistivity in different directions depending on the fibre content at a specimen age of 38 days and an electrode array with angular distances of 180°

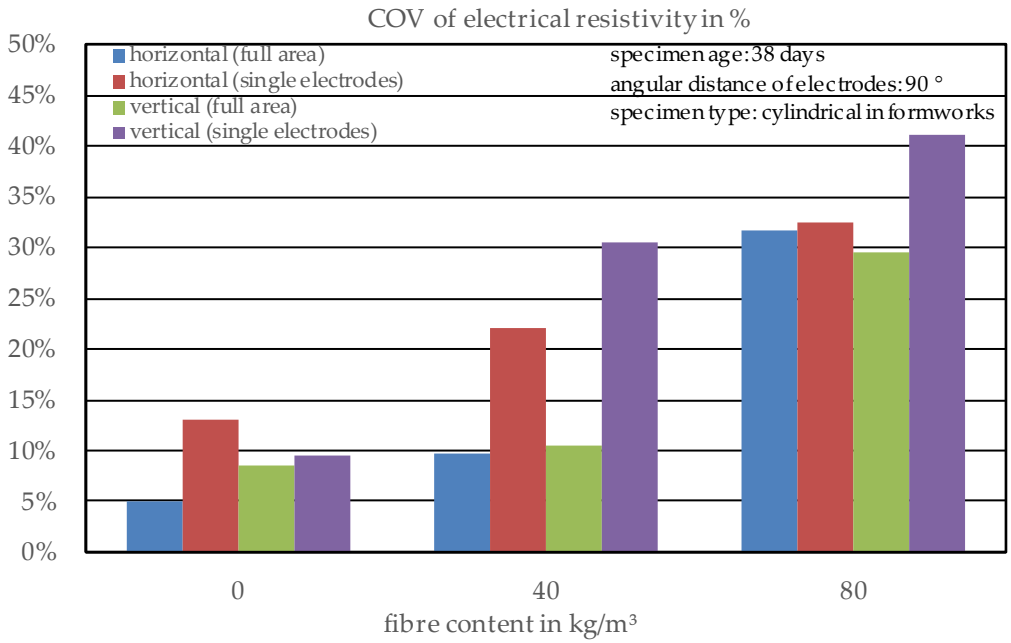

Figure E.8 Coefficient of variation of the electrical resistivity in different directions depending on the fibre content at a specimen age of 38 days and an electrode array with angular distances of 90°

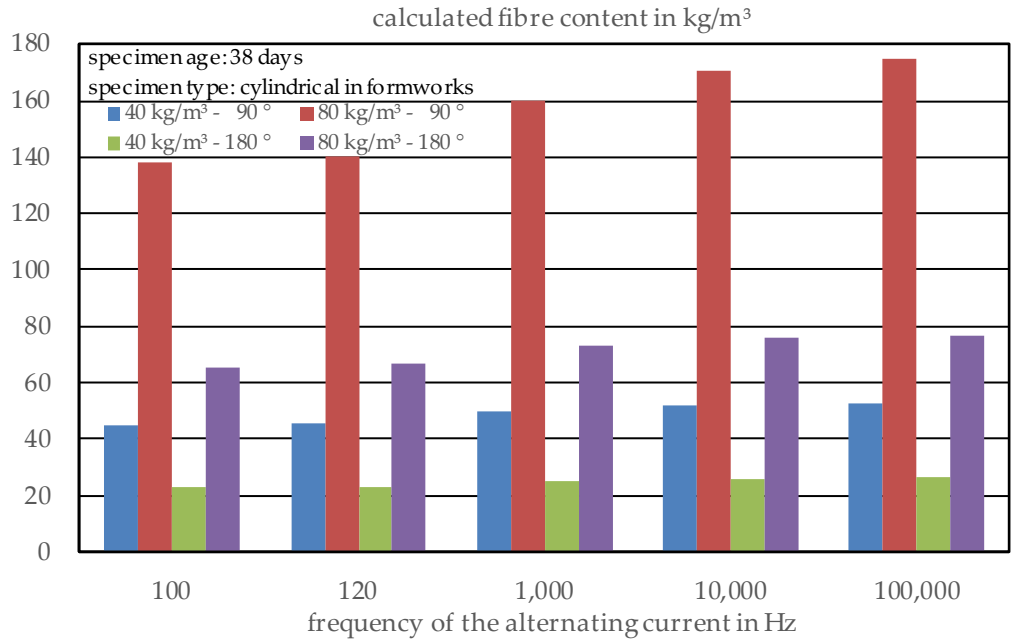

Figure E.9 Calculated fibre content of the concrete specimens with different electrode arrays depending on the fibre content and frequency of the alternating current at a specimen age of 38 days

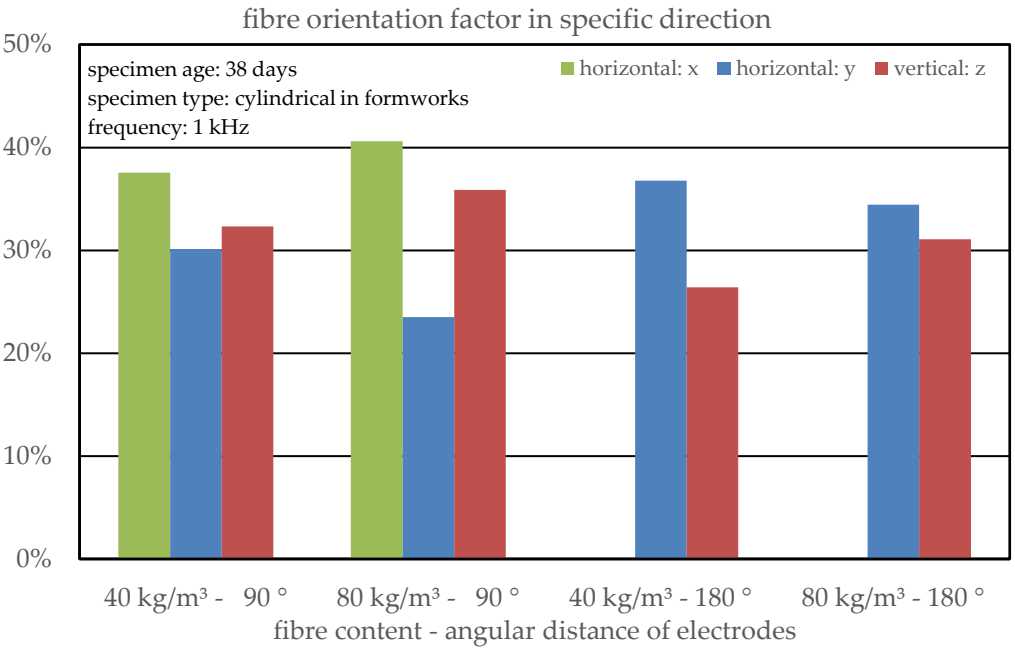

Figure E.10 Calculated fibre orientation of the concrete specimens with different electrode arrays depending on the fibre content at a specimen age of 38 days